2020

Cellular and Developmental Insights into the Early Evolution of Muscle

Jeffrey J. Colgren
University of Denver

Cellular and Developmental Insights into the Early Evolution of Muscle

Abstract

Whereas a great deal has been learned about the molecular underpinnings of morphological evolution in animals, much less is known about the origin of novel cell and tissue types. During the time in which the earliest animal lineages were diversifying, fundamental cell and tissue types, such as muscles, arose. Sponges are one of two animal lineages that lack muscles, yet they undergo coordinated full body contractions. Whereas the signaling processes have been studied, the physical mechanisms of contraction are completely uncharacterized. The main purpose of this work is to understand the primary contractile tissue of the sponge *Ephydatia muelleri*, from a structural, functional, and developmental standpoint. As there is no single unique feature that is shared by all muscle types in animals, a full picture of the contractile tissue of *E. muelleri* is needed to assess its homology with these tissues. Here the focus is on an endothelial-like tissue containing tissue-level organized actin bundles, which shorten during contractions. Additionally, a muscle-specific paralog of type II-Myosin heavy chain (stMyHC) is found exclusively at these structures. Contractions appear to be initiated by release of internal Ca^{2+}stores and are regulated by phosphorylation of myosin regulatory light chain by myosin light chain kinase. From a developmental perspective, formation of contractile bundles depends on myocardin related transcription factor (MRTF), an important myogenic factor in many animals. Comparative studies on the myoepithelial muscles of the cnidarian model *Nematostella vectensis*, found evidence of conserved developmental regulation by MRTF. Taken together, these finding suggest the contractile tissue of *E. muelleri* shares elements of homology with muscles of other animals and can aid in understanding key cellular innovations involved in the evolution of this tissue type.

Document Type

Dissertation

Degree Name

Ph.D.

Department

Biological Sciences

First Advisor

Scott A. Nichols

Second Advisor

J. Todd Blankenship

Third Advisor

Schuyler Van Engelenburg

Keywords

Cell type evolution, Myocyte, Myogenesis, Porifera

Subject Categories

Biochemistry, Biophysics, and Structural Biology | Cell Biology | Developmental Biology | Molecular Biology | Other Ecology and Evolutionary Biology

Cellular and Developmental Insights into the Early Evolution of Muscle

---

A Dissertation

Presented to

the Faculty of the College of Natural Sciences and Mathematics

University of Denver

In Partial Fulfillment

of the Requirements for the Degree

Doctor of Philosophy

---

by

Jeffrey J. Colgren

June 2020

Advisor: Scott A. Nichols, PhD

Author: Jeffrey J. Colgren
Title: Cellular and Developmental Insights into the Early Evolution of Muscle
Advisor: Scott A. Nichols, PhD
Degree Date: June 2020

Abstract

Whereas a great deal has been learned about the molecular underpinnings of morphological evolution in animals, much less is known about the origin of novel cell and tissue types. During the time in which the earliest animal lineages were diversifying, fundamental cell and tissue types, such as muscles, arose. Sponges are one of two animal lineages that lack muscles, yet they undergo coordinated full body contractions. Whereas the signaling processes have been studied, the physical mechanisms of contraction are completely uncharacterized. The main purpose of this work is to understand the primary contractile tissue of the sponge *Ephydatia muelleri*, from a structural, functional, and developmental standpoint. As there is no single unique feature that is shared by all muscle types in animals, a full picture of the contractile tissue of *E. muelleri* is needed to assess its homology with these tissues. Here the focus is on an endothelial-like tissue containing tissue-level organized actin bundles, which shorten during contractions. Additionally, a muscle-specific paralog of type II-Myosin heavy chain (stMyHC) is found exclusively at these structures. Contractions appear to be initiated by release of internal Ca^{2+} stores and are regulated by phosphorylation of myosin regulatory light chain by myosin light chain kinase. From a developmental perspective, formation of contractile bundles depends on myocardin related transcription factor (MRTF), an important myogenic factor in many animals. Comparative studies on the myoepithelial muscles of the cnidarian model *Nematostella vectensis,* found evidence of conserved developmental

regulation by MRTF. Taken together, these finding suggest the contractile tissue of *E. muelleri* shares elements of homology with muscles of other animals and can aid in understanding key cellular innovations involved in the evolution of this tissue type.

Acknowledgements

My sincerest and most grateful thanks to my advisor Dr. Scott Nichols, for his unwavering academic, financial, intellectual, and personal support. A special thanks to my committee members, Dr. Todd Blankenship, Dr. Daniel Mederios, Dr. Schuyler Van Engelenburg for their wonderful guidance, questions, and aid in experimental design. Thank you to my committee chair, Dr. Martin Margittai for his support and suggestions to improve my dissertation. To Dr. Scott Barbee for his assistance with RT-qPCR and initial training on confocal microscopy and to Dr. Matthew Gibson for kindly gifting *Nv*FP-7R *Nematostella vectensis.*

Thank you to Dr. Jennyfer Mitchell for her invaluable help when first started in the lab, and continued support and friendship. For all the members of the Nichol's Lab, past and present, especially Dr. Klaske Schippers for her help with RT-qPCR and *in situ* hybridization protocol development, Bernadette Doyle, Katy Anderson, Shaliegh Smith, and Lindsey Ray. I am endlessly grateful for the general support and kindness I experienced from all the staff and faculty in the Department of Natural Sciences and Mathematics at the University of Denver.

Finally, for the endless help, support, and encouragement from Patti, Walden, and Cassidy, I could not have done this without you.

Table of Contents

Abstract ii
Acknowledgements iv
List of Figures vii

Chapter 1: The Significance of Sponges for Comparative Studies of Developmental Evolution 1
- Introduction 1
- Sponges are Neither Ancient Nor Primitive 3
- Plasticity May Predominate Over Genetic Patterning in Sponge Development 11
- Sponge Can Help Clarify the Origin of Novel Cell and Tissue Types 18
- Origins of Contractile Regulatory Mechanisms 19
- Origin of Myocyte Developmental Specification 23
- Conclusions 27

Chapter 2: Physiology of Contractions in *Ephydatia muelleri* 29
- Introduction 29
- Documentation of Contraction 31
- Depolarizing Agents 42
- Membrane Potential Dye 49
- The Role of Ca^{2+} in Contractile Response 55
- The Role of NO in Signal Propagation and Response 63
- The Role of TRP Channels in Sponge Contractions 67
- Conclusions 70

Chapter 3: Contractile Tissues in *Ephydatia muelleri* 72
- Introduction 72
- Actin Stability 76
- Exopinacocytes 81
- Endopinacocytes 88
- Choanocyte Chambers 92
- Unattached Sponges 96
- Contractions During Development 102
- Transgelins in *Ephydatia muelleri* 107
- Conclusions 116

Chapter 4: *Ephydatia muelleri* Muscle Myosin and Regulation of Contraction 118
- Introduction 118
- Type II-Myosin Heavy Chain Localization in *Ephydatia muelleri* 125
- Regulation of Contraction 137
- Conclusions 149

Chapter 5: Developmental Regulation of Contractile Tissue in *Ephydatia muelleri* 151
Introduction 151
Myocardin Related Transcription Factor Localization in *Ephydatia muelleri* 156
Pharmacological Perturbation of MRTF Pathway 166
Conclusions 189

Chapter 6: Myogenesis in *Nematosetlla vectensis* 191
Introduction 191
Myocardin Related Transcription Factor in *Nematostella vectensis* 194
Functional Evidence for MRTF activity 199
Other Myogenic Factors, HAND, Dach, and FoxL-like 217
Conclusions 228

References 231

Appendices
Appendix I: Supplemental Figures 265
Appendix II: Technique Development 278
Introduction 278
In situ Hybridization in *Ephydatia muelleri* 279
Unsuccessful Antibodies for *Ephydatia muelleri* 293
Injectroporation in *Ephydatia muelleri* 304
Streptolysin O Treatment 309
Osculum Isolation 316
Additional Figures 321
Appendix III: Additional Information 324

List of Figures

Chapter 1: The Significance of Sponges for Comparative Studies of Developmental Evolution 1
Figure 1. A comparative framework for studies of early evolution in animals 2
Figure 2. Competing hypotheses about the evolution of collar cells 4
Figure 3. Sponge migratory cells and body plan plasticity 14
Figure 4. Myosin II heavy chain isoforms and transcription factors associated with different contractile tissues 24
Figure 5. Actin organization in the sponge *Ephydatia muelleri* and the cnidarian *Nematostella vectensis* 26

Chapter 2: Physiology of Contractions in *Ephydatia muelleri* 29
Figure 6. Time lapse series of *E. muelleri* contraction 34
Figure 7. Change in canal size during contraction 35
Figure 8. Induction of contraction with low concentration of ink 36
Figure 9. Changes in canal size following treatment with 80µM glutamate 37
Figure 10. Imaging of contraction from the side 38
Figure 11. Osculum dynamics 39
Figure 12. Lateral view of tissues during contraction 40
Figure 13. Time series of sponge treated with KCl in lake water 45
Figure 14. Time series of sponges treated with arginine 46
Figure 15. Second trial live imaging with FluoVold dye 52
Figure 16. Live imaging with FluoVolt dye using confocal microscopy 54
Figure 17. Ionomycin triggers a contraction in *E. muelleri* 60
Figure 18. Internal Ca^{2+} stores are released during contractions 61
Figure 19. Contractions initiated with thapsigarin do not require external Ca^{2+} 61
Figure 20. L-NAME blocks contractions when induced by ink but not increased Ca^{2+} 66
Figure 21. Activation of TRP channels leads to contraction that propagates from body to osculum 69

Chapter 3: Contractile Tissues in *Ephydatia muelleri* 72
Figure 22. Time series treatment with latrunculin B 80
Figure 23. Work-flow for dual staining experiment 82
Figure 24. Exopinacocytes expand and contract while moving with a contractile wave 85
Figure 25. Dual imaging suggests exopinacocytes do not undergo exocytosis during contractions 86
Figure 26. Actin tracts shorten during a contraction 91
Figure 27. Size of choanocytes significantly decreases 95
Figure 28. Distance between choanocyte chambers did not significantly decrease during a contraction 95
Figure 29. Unattached sponges can still contract their body 100
Figure 30. EmVin1 localizes to apical pinacoderm in unattached sponges 100

Figure 31. Actin organization resembles attached sponge with absence of stress fiber-like structures 102
Figure 32. Tent stage sponges show a response to 80μM glutamate 104
Figure 33. Sponges lacking choanocyte chambers can still contract 105
Figure 34. Immunostaining for EmTAGLN3 shows localization to major actin structures 110
Figure 35. EmTAGLN2 is more restricted to the actin tracts 111
Figure 36. EmTAGLN3 is broadly expressed in pinacocytes and EmTAGLN2 is more restricted to endopinacocytes 112
Figure 37. Cytoplasmic staining of EmTAGLN3 in the endopinacoderm helps to resolve cell morphology 113
Figure 38. EmTAGLN2 reveals endopinacocyte shape and complex actin tract network organization 114
Figure 39. EmTAGLN3 staining at stress fiber-like structures provides insight into protein function 115

Chapter 4: *Ephydatia muelleri* Muscle Myosin and Regulation of Contraction 118
Figure 40. Structure of Type II-Myosin 118
Figure 41. Ultrastructure of different muscle types 119
Figure 42. Tropomyosin/Troponin complex regulation of thin filament 120
Figure 43. Troponin independent regulation of contractions 121
Figure 44. Distribution two myosin II heavy chain types 123
Figure 45. EmstMyHC localizes to structures resembling the actin tracts 132
Figure 46. EmstMyHC intensified at larger structures 133
Figure 47. EmstMyHC appears to be restricted to a layer of tissue 133
Figure 48. Large stMyHC structures are higher in the visual plane 134
Figure 49. Developmental sequence for stMyHC 135
Figure 50. Immunoprecipitation for stMyHC 136
Figure 51. Structure of EmRLC ortholog 139
Figure 52. Contraction assay 142
Figure 53. Immunostaining for pRLC in *E. muelleri* 143
Figure 54. In contracted sponges, strong pRLC is found at short actin tracts 143
Figure 55. Treatment with MLCK inhibitor ML-7 reduces the Ca^{2+} dependent contractile response 144
Figure 56. pRLC staining in ML-7 treated sponges resembles that of uninduced sponges 145
Figure 57. Treatment with ML-7 blocks ability to contract under physiological conditions 146
Figure 58. ROCK inhibition effects ability to contract 147

Chapter 5: Developmental Regulation of Contractile Tissue in *Ephydatia muelleri* 151
Figure 59. Core group of terminal myogenic regulatory factors present in the stem bilaterian. 152
Figure 60. *E. muelleri* has well conserved SRF and Mef2 orthologs 152

Figure 61. Actin dynamics modulates MRTF function 153
Figure 62. Domain structure of EmMRTF.....154
Figure 63. MRTF family underwent expansion in vertebrate lineage 155
Figure 64. Subcellular localization of EmMRTF seems cell type specific.....161
Figure 65. Immunoprecipitation with antibody produces inconsistent results ...162
Figure 66. Actin staining in the pinacoderm is reduced in treated sponges.....175
Figure 67. Inhibition of MRTF during development limits the sponge's ability to contract.....176
Figure 68. EmMRTF has conserved targets.....177
Figure 69. Workflow for aggregation assay.....178
Figure 70. Inhibition of MRTF effects attachment and spreading.....179
Figure 71. Activation of MRTF in aggregates induces development of dense actin network 179
Figure 72. Actin structures along the edge of aggregates resemble actin tracts .180
Figure 73. ISX9 treated aggregates contain pRLC in the area of the actin bundles 180
Figure 74. ISX9 treated aggregates have a contractile phenotype.....181
Figure 75. Inhibition of MRTF during development reduces ability to clear ink from excurrent canals.....183

Chapter 6: Myogenesis in *Nematosetlla vectensis*.....191
Figure 75. Schematic of *N. vectensis* muscles 192
Figure 76. Domain structure of NvMRTF 194
Figure 77. Development expression pattern for NvMRTF shows strong expression in tissues that give rise to muscles 198
Figure 78. NvMRTF morphants do not develop body muscles or tentacles.....206
Figure 79. Knockdown of NvMRTF with shRNA shows similar phenotype to 3morpholinos 207
Figure 80. Knockdown of NvMRTF prevents proper endoderm formation and muscle development.....208
Figure 81. Expression of NvSRF 208
Figure 82. Knockdown of NvSRF prevents proper endoderm formation and muscle development.....209
Figure 83. Pharmacological inhibition of MRTF activity shows a similar but reversable phenotype. 210
Figure 84. Activation of MRTF during regeneration gives strong phenotypes ..211
Figure 85. Ectopic tentacles contain primarily muscles and tissue ruffles contain actin dense cells 212
Figure 86. Disconnected cells are wider and shorter and contain oriented actin bundles 213
Figure 87. Developmental expression of NvHAND proteins 223
Figure 88. Developmental expression of NvDach 224
Figure 89. Expression of NvFoxL-like is highly restricted to the ectoderm of developing tentacles.....224

Figure 90. Knockdown of HAND1 and Dach result in actin disruption and a reduced endoderm 225
Figure 91. Knockdown of NvFoxL-like inhibits tentacle formation 226
Figure 92. Reduction in longitudinal tentacle muscles and retractor muscles is seen following knockdown of NvFoxL-like 226

Appendix II: Technique Development 278
Figure 93. Stellaris probes targeting stMyHC show broad signal that is likely non-specific 287
Figure 94. Cell level staining is difficult to interpret 288
Figure 95. Isolated oscula show some signal 288
Figure 96. Signal in the attachment epithelium 289
Figure 97. Signal is strong in pinacocytes and not choanocytes 290
Figure 98. Immunostaining with anti-EmMef2 298
Figure 99. Western blot with anti-EmMef2 299
Figure 100. Immunostaining with commercial anti-Mef2 antibody 299
Figure 101. Immunostaining with commercial anti-SRF antibody 300
Figure 102. Immunostaining with commercial panMyHC antibody 300
Figure 103. Immunostaining with commercial RLC antibody 301
Figure 104. Immunostaining with nmMyHC antibody 301
Figure 105. Western blot of sponge cell lysates with nmMyHC and RLC antibodies 302
Figure 106. Injectroporation shows evidence of entry into cells 308
Figure 107. Treatment with SLO doesn't allow entry of phalloidin 313
Figure 108. SLO shows some evidence of dye entry in isolated cells 313
Figure 109. SLO appears to be effective in permeabilizing *N. vectensis* embryos 314
Figure 110. SLO treatment facilitates morpholino delivery 315
Figure 111. Actin organization in isolated oscula 318

Chapter 1: The Significance of Sponges for Comparative Studies of Developmental Evolution

Introduction

A central concept of evolutionary-developmental biology is that morphological differences between animals reflect changes to the spatiotemporal expression of patterning genes that are conserved between disparate species (reviewed in Carroll, 2008). Perhaps the greatest caveat to this idea is that it derives from case studies of a limited subset of animal diversity. Essentially, everything that we know about animal development comes from a relative handful of experimental models such as *Drosophila*, *Caenorhabditis, Xenopus, Strongylocentrotus, Danio*, and *Mus* (**Figure 1a**)—all of which have bilaterian body plans, or modifications therefrom (echinoderms). Only recently have genomic and experimental advances enabled mechanistic developmental studies in more divergent animal lineages, including the cnidarians *Hydra*, *Hydractinia*, *Nematostella*, and *Clytia*.

Although this comparative framework is vast, spanning hundreds of millions of years of animal evolution, important lineages are under-sampled. Specifically, ctenophores, sponges, placozoans, and cnidarians bracket the interval of early animal evolution during which fundamental cell and tissue types evolved (epithelia, muscles, neurons), along with the regulatory mechanisms that specify their fate and spatial patterning during development. Aspects of the basic biology of these lineages are so

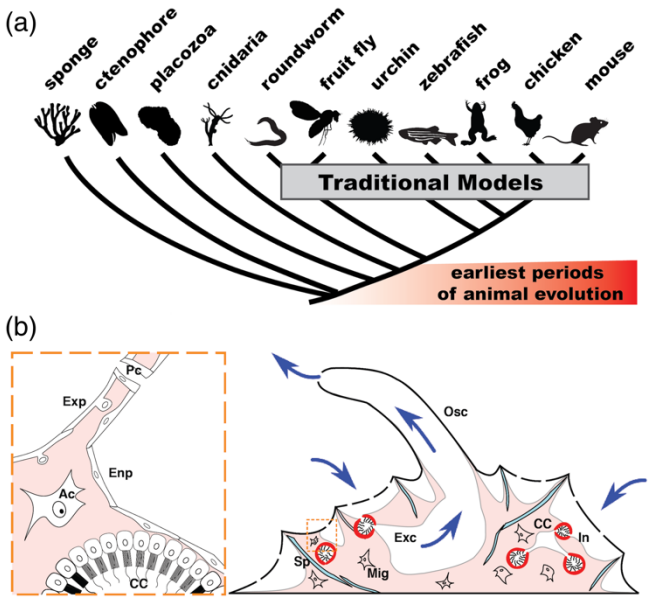

Figure 1. A comparative framework for studies of early evolution in animals. (a) Lineages like sponges, ctenophores, placozoans, and cnidarians bracket the earliest periods of animal evolution, yet we have only begun to study their cell and developmental biology from a mechanistic perspective. These lineages comprise half (or more) of deep phylogenetic diversity within animals. **(b)** The anatomy of sponges diverges considerably from other animals. They are essentially epithelial organisms organized around a network of internal water canals. Water flows (arrows) in through incurrent canals (In), travels through choanocyte chambers (cc; highlighted in red) where bacteria (and other picoplankton) are phagocytosed by choanocytes, then leaves via excurrent canals (Exc) that lead to the exhalant siphon (the osculum; Osc). Migratory cells (Mig) are found in the interior, as are skeletal elements (spicules; Sp). The box (left) shows a higher magnification depiction of the primary sponge tissues including the exopinacoderm (outer layer; Exp), porocytes (specialized cells that regulate incurrent water flow; Pc), endopinacocytes (the inner epithelial lining; Enp), choanocytes of a choanocyte chamber, and archeocytes (migratory stem cells; Ac). (All images in panel **a** are from PhyloPic.org. Artistic credits: Sponge = Mali'o Kodis, photograph by Derek Keats (http://www.flickr.com/photos/dkeats/); Mnemiopsis = Mali'o Kodis, photograph by Aqua-Photos (https://www.flickr.com/people/undervannsfotografen/); Xenopus = Sara Werning; Strongylocentrotus = Frank Förster (based on a picture by Jerry Kirkhart; modified by T. Michael Keesey); Trichoplax = Oliver Voigt; all listed images are available for use under the following license: https://creativecommons.org/licenses/by-sa/3.0/legalcode

divergent as to challenge our very concept of what it means to be an animal. For example, sponges have coordinated behavioral responses, yet they lack neurons and muscles (Ludeman, Farrar, Riesgo, Paps, & Leys, 2014). Some ctenophores can transiently form

both a mouth and an anus, which seal through unknown mechanisms when not in use (Tamm, n.d.; Tamm & Tamm, 1993; Tamm, 1999). Placozoans are asymmetrical animals with oral/aboral patterning, but lack both a mouth and anus (DuBuc, Bobkov, Ryan, & Martindale, n.d.) and instead digest food externally, rather than in a gut (Fortunato & Aktipis, 2019).

The focus of this review is on sponges. We highlight aspects of sponge biology that illustrate their importance for understanding developmental evolution in animals. First, we critique the traditional view that the evolutionary significance of sponges stems from the fact that they are in some way ancient or primitive. Next, we explore fundamental differences between development in sponges compared to other animals. We argue that adult cell fate and tissue identity is not strictly determined during embryogenesis; rather, environmentally induced plasticity is paramount. Finally, we present a case study to illustrate how sponges can be used to clarify the origin of key animal cell and tissue types. Specifically, we examine the hypothesis of homologous contractile properties between epithelia in sponges and muscle tissues in other animals.

Sponges are Neither Ancient nor Primitive

A common misconception about sponges is that they are "living fossils" that serve as surrogates for early animal ancestors (e.g., Müller, 1998; Nielsen, 2008). This misconception derives from several different lines of reasoning. First, sponges are often described in terms of the traits they lack: they have no muscles, neurons, or a gut. They are imagined to reflect what animals may have been like before complex traits evolved. This narrative is reinforced by the possible (but contentious) phylogenetic placement of

sponges as the sister-group to other animals (Feuda et al., 2017; King & Rokas, 2017; Simion et al., 2017); affording the opportunity for complex traits to have evolved in other animal lineages, to the exclusion of sponges. These arguments come perilously close to the mistaken view that evolution is a march toward complexity, and they underplay the fact that sponges have been evolving for as long as any other modern animal lineage.

Perhaps the most persuasive argument supporting the sponge body plan (**Figure 1b**) as representative of the ancestral condition is that it is organized around a water canal system that contains choanocytes—specialized feeding cells notable for their similarity in both form and function to choanoflagellates, the unicellular/colony-forming sister-group to animals (Brunet & King, 2017). In both lineages, these cells (collectively termed "collar cells") are <5 μm in diameter and have a ring of actin-filled microvilli that

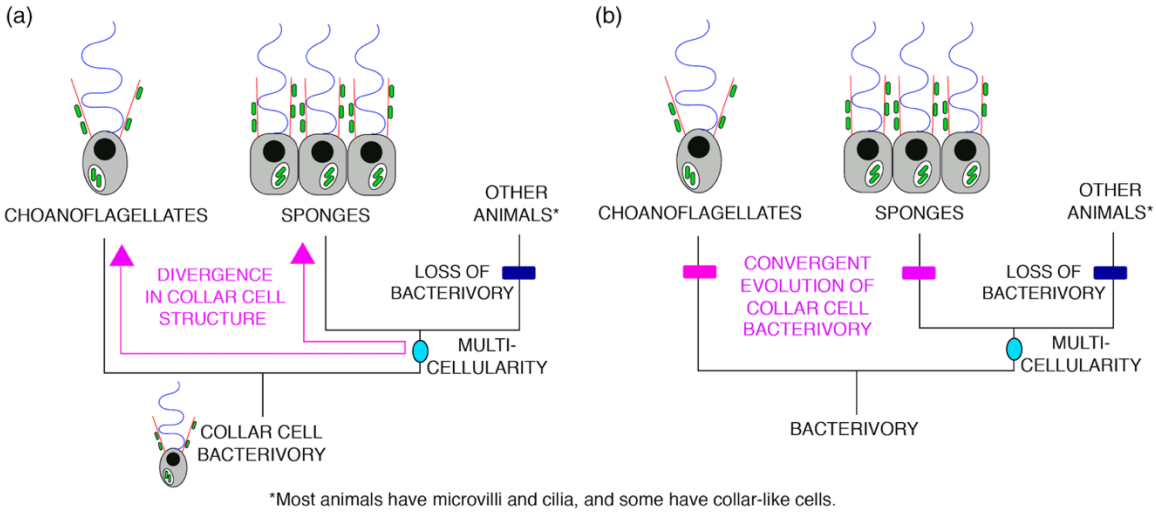

Figure 2. Competing hypotheses about the evolution of collar cells. Choanoflagellates resemble choanocytes, the feeding cells of sponges. **(a)** The traditional perspective is that the similarity between these cell types reflects their descent from a common ancestral cell type, and that detected differences between these cell types result from >600 million years ago of divergent evolution. **(b)** An alternative hypothesis is that the resemblance of choanoflagellates and choanocytes is superficial and reflects convergent evolution for efficient bacterivorous filter-feeding by a collar cell. Collar-like cells are present in non-sponge animals, but have functions other than bacterivory

encircles a single flagellum. Both function to capture and phagocytize bacterial prey. If collar cells are similar due to common ancestry, then collar-cell bacterivory is likely the ancestral animal feeding mode (**Figure 2**). Indeed, animals must have evolved in an environment dominated by bacteria (Alegado & King, 2014); >600 million years ago the oceans were very different and there were fewer large prey to eat. Thus, the first animals almost certainly fed on bacteria (and other picoplankton). How can we test the evolutionary significance of similarity between choanocytes and choanoflagellates? Are they really so similar that we think they retain the structure and function of a common ancestral cell type? Several studies have compared choanoflagellates and choanocytes and concluded that they have both similarities and differences at the ultrastructural level (Laundon, Larson, McDonald, King, & Burkhardt, 2019; Mah, Christensen-Dalsgaard, & Leys, 2014; Maldonado, 2004), and some authors have suggested that detected differences warrant reconsideration of the homology of their similar traits (Mah et al., 2014). Dunn, Leys, and Haddock (2015) re-assert this perspective with the strengthened claim that similarities between choanocytes and choanoflagellates are "largely superficial" and "suggest convergence to an efficient filter-feeding mode." However, as others have already pointed out (Adamska, 2016; Brunet & King, 2017; Laundon et al., 2019), even if choanocytes and choanoflagellates have homologous feeding structures/modes, differences should be expected because they have been evolving independently for hundreds of millions of years in very different contexts (choanoflagellates are free-living, whereas choanocytes form a specialized epithelial tissue within sponges).

Testing the hypothesis of homology between choanocyte/choanoflagellate feeding structures is no less fraught with difficulty when using gene expression data. A recent study (Sogabe et al., 2019) compares the expression profile of three sponge cell types to choanoflagellates and finds no particular similarity with choanocytes. Rather, 43% of the upregulated genes in choanocytes are restricted to the sponge lineage (46% of all genes in the genome are sponge-exclusive). An implicit assumption of this study is that older cell types are expected to express more ancient genes, and that choanocytes and choanoflagellates should express a common battery of ancient genes if their similarities are due to common ancestry rather than convergence. Another implicit assumption is that, if choanoflagellates and choanocytes have retained the ancestral animal feeding mode, the overall expression profile of choanoflagellates should be more similar to choanocytes than other sponge cells; instead choanoflagellates are found to be marginally more similar to archeocytes (a sponge stem cell) in this respect. Thus, the authors conclude that cell-type expression data do not support the hypothesis that similarities between choanoflagellates and choanocytes reflect homology.

While technically correct that these data do not affirmatively support this hypothesis, it is also not clear that this is a robust test of homology between choanocyte/choanoflagellate feeding structures (see Liang, Musser, Cloutier, Prum, & Wagner, 2018). Certainly flagella and microvilli are homologous between these cell types (and these are their defining features) (Brunet & King, 2017; Peña et al., 2016; Sebé-Pedrós et al., 2013), but these similarities are not captured when averaging overall gene expression levels. It could very well be that these physical features of collar cells are controlled by a relatively small subset of genes. This is underscored by the expression

similarities between choanoflagellates and archeocytes (Sogabe et al., 2019), despite that archeocytes have neither microvilli nor a flagellum.

At this point in time there is little precedent to justify predictions about how overall expression patterns should align between a free-living organism (choanoflagellate) and any animal cell type, even if aspects of their structure and function are homologous. After all, if choanoflagellates and animals share a unicellular ancestor, then all animal cell types can be traced back to this ancestor and each has likely retained some aspects of its structure and function. The assumption that ancient genes should be expressed in ancient cell types is also open to debate. Estimation of gene age has been shown to be error prone (Casola, 2018; Elhaik, Sabath, & Graur, 2006; Moyers & Zhang, 2017; Smith & Pease, 2017), and ancient genes are constantly repurposed for new functions. For example, recent molecular phylogenies support that the polyp stage of the cnidarian life cycle is more ancient than the medusa (jellyfish) stage (Kayal et al., 2018; Leclère et al., 2019; Zapata et al., 2015). Nevertheless, expression data from the hydrozoan jellyfish, Clytia hemisphaerica, show that more ancient transcription factors—those that were present in the last common ancestor with bilaterian animals—are more highly expressed in the medusa stage than in polyps (Leclère et al., 2019).

The argument for homology between the feeding structures of choanoflagellates and choanocytes simply predicts that these cells descended from an ancestral cell type that also had a collar/flagellum as specialized structure for feeding on bacteria. No other aspect of their cell biology, including their overall gene expression patterns, must be particularly conserved for this hypothesis to stand. For example, at the very least they can be expected to differ in their handling of captured bacterial prey. The multicellular

context of sponge choanocytes must require that they have elevated levels of exocytosis at the basolateral cell surface, as partially digested bacterial prey must be distributed to other cells and tissues through choanocyte interactions with migratory cells (Imsiecke, 1993; Leys & Hill, 2012). In contrast, choanoflagellates presumably retain the ancestral state, in which cells retain captured prey for themselves.

If gross comparisons of ultrastructure and gene expression averages fall short as metrics to compare choanocytes and choanoflagellates, what is the path forward? There is a rich literature on the criteria used to determine homology, which includes consideration of the phylogenetic distribution of the trait, the fossil record, and detailed similarity in fine structure and developmental origin (e.g., Achim & Arendt, 2014; Arendt et al., 2016; Wagner, 2014; Wake, 1999). In our opinion, a strong argument for the hypothesis of homology of the feeding apparatus between choanocytes and choanoflagellates is that it has already proven to be predictive (Nichols, Dayel, & King, 2009). More than 100 years before the phylogenetic position of either choanoflagellates or sponges was known, James Clark noticed the similarity between choanoflagellates and choanocytes (Clark, 1866). This observation provided a morphological link between choanoflagellates and animals long before that link was independently confirmed via genomics (Burger, Forget, Zhu, Gray, & Lang, 2003; King et al., 2008) and molecular phylogenetics (Steenkamp, Wright, & Baldauf, 2006; Wainright, Hinkle, Sogin, & Stickel, 1993). The strength of any hypothesis ultimately rests in its predictive power.

Irrespective of how the question of collar-cell homology is ultimately resolved, it remains important to remember that sponges are neither simple nor primitive, nor are they merely the leftovers after derived traits are stripped from more complex animals.

Rather, they have their own unique mixture of derived and ancestral traits, shaped by hundreds of millions of years of evolution; as do all animals. The extent to which they appear to be simple is a reflection of the bias in our understanding of animal biology toward traditional research models (Dunn et al., 2015). Had sponges been the focus of large international research communities for decades past, we may have a very different view of the scope and nature of animal biology.

So, if sponges are not valid surrogates for early animal ancestors, then what is their evolutionary significance? It is simply their phylogenetic placement—they offer a critical comparative point for triangulation, through phylogenetic comparative methods, to the earliest periods in animal evolution. Traits that they share with other animals are most parsimoniously inferred to have been present in early animal ancestors. The ways in which they differ from other animals create opportunities to test our generalizations and challenge our understanding of what it means to be an animal.

Finally, it is important to note that sponges are diverse and that traits of any single species should not be uncritically generalized to the entire clade. There are four major groups: demosponges, hexactinellids, calcareous sponges, and homoscleromorphs. Species within these groups differ in size, habitat preference, and basic body organization. For example, all sponge groups can produce skeletal elements, but the structure and composition of these elements varies considerably. Some demosponges and homoscleromorphs, and all hexactinellids produce internal skeletal elements (spicules) composed of silica. Other demosponges and homoscleromorphs lack spicules altogether. Demosponges, both with and without spicules, all produce a fiber skeleton composed of spongin—a short-chain collagen (Fidler et al., 2017); this is very pronounced in some

species, such as commercial bath sponges. Calcareous sponges all produce spicules, but they are composed of calcium carbonate.

Species with unique adaptations can be found in environments ranging from the intertidal zone to the deep sea, freshwater lakes, streams and seasonal pools, and can range in size from millimeters to meters. Some species harbor dense populations of bacterial symbionts (Thomas et al., 2016), others have few (Sipkema, Holmes, Nichols, & Blanch, 2009). At least one demosponge lineage has lost the ability to filter feed and has independently evolved carnivory, in which animal prey are snared by specialized spicules and then encased by phagocytic cells that migrate to the point of capture (Godefroy et al., 2019). Most sponges are cellular, whereas hexactinellids are syncytial—permitting the organism-wide propagation of electrical signals and coordinated behaviors without the benefit of neurons or gap junctions (Leys & Mackie, 1997; Leys, Mackie, & Meech, 1999).

The extent of sponge diversity is also reflected in the size and content of their genomes (Renard, Leys, Wörheide, & Borchiellini, 2018; Schuster et al., 2018). Comparisons within demosponges alone have revealed genome sizes ranging from ~40 to 614 Mbp (Jeffery, Jardine, & Gregory, 2013). An example of differences in their genome content comes from examination of the diversity of their Wnt genes. Animals as disparate as cnidarians and vertebrates have conserved orthologs belonging to the same 11 Wnt subfamilies (Kusserow et al., 2005), whereas sponge Wnts do not clearly align with identified subfamilies in other animals. The genome of the demosponge Amphimedon queenslandica encodes three Wnt ligands (Adamska et al., 2010), *Sycon ciliatum* has 21 (Leininger et al., 2014), and hexactinellids appear to lack Wnts altogether— probably

because they are syncytial and have little need for secreted, morphogen-based signaling (Riesgo, Farrar, Windsor, Giribet, & Leys, 2014; Schenkelaars et al., 2017).

In the remainder of this review, we discuss the extent and significance of developmental plasticity in sponges, and we consider how studies of their contractile epithelia may be used to illuminate the evolution of muscle tissues. The extent to which we generalize reflects that developmental plasticity and contractile epithelia are features common to all major sponge lineages, and are thought to be ancestral properties of the clade (albeit, there are surely differences between species).

Plasticity May Predominate Over Genetic Patterning in Sponge Development

An initially surprising finding from early genome and transcriptome sequencing of sponges was that, despite having vast morphological differences with other animals, they also have highly conserved homologs of most developmental regulatory genes (Nichols, Dirks, Pearse, & King, 2006; Renard et al., 2018; Srivastava et al., 2010). Furthermore, it has been shown that these genes have spatiotemporal expression patterns consistent with conserved roles in developmental patterning. For example, in the calcareous sponge *Sycon ciliatum*, both Wnt and TGF-β show polarized expression in the larva and in the adult (Leininger et al., 2014). This was interpreted as evidence for the homology of the primary sponge body axis with that of other animals (cnidarians, in particular). Furthermore, ciliated larval cells are thought to give rise to choanocytes in the adult of this species, and both were found to express endomesodermal markers. This was interpreted as evidence that the choanoderm of sponges is homologous to the gut of cnidarians, and that adult tissues are specified during embryonic germ layer formation.

Collectively, these data support a scenario in which developmental patterning of sponges is substantially more like other animals than anticipated based upon consideration of their divergent anatomy. However, a recent lineage-tracing study offers a different perspective. *A. queenslandica* exhibits nested, polarized patterns of developmental gene expression in the larval stage (Adamska et al., 2007) similar to *Sycon*. But, when Nakanishi, Sogabe, and Degnan (2014) labeled individual cells and with a fluorescent dye and tracked their fate throughout development, no evidence was found for the hypothesis that sponges have discrete germ layers that give rise to specific adult cell or tissue types with fidelity. Instead, cell fate was found to be highly labile and indeterminate. This conclusion fits well with single-cell sequencing data from the same species, which found that archeocytes were the only cells with similar gene expression profiles in adult and larval tissues (Sebé-Pedrós et al., 2018).

Although it is premature to draw conclusions about developmental patterning mechanisms in sponges compared to other animals, they clearly have conserved developmental regulatory genes, and there is evidence that these function in embryonic patterning. However, sponges also exhibit extraordinarily high levels of developmental plasticity in response to environmental conditions, and they can completely regenerate from adult stem cell populations. It is intriguing to imagine a transition during early animal evolution in which upstream genetic controls over developmental patterning superseded more ancient, environmental feedback mechanisms. However, it is also possible that extensive developmental plasticity evolved in the stem-lineage leading to modern sponges; a derived, not ancestral trait.

A classic experiment that highlights the plasticity and regenerative capacity of sponges is that their tissues can be dissociated into single cells, and yet the cells can reaggregate to form a functional individual (Lavrov & Kosevich, 2014; Wilson, 1907). Sponges also lack discrete body parts of stereotypical number and position. Instead they can remodel their body in response to environmental conditions (Wilkinson & Vacelet, 1979). Many sponge cell types are thought to be pluripotent and they contain dense populations of migratory stem cells throughout their lifespan (Funayama, 2010).

The plasticity of the sponge body plan has likely been shaped by selective pressures associated with their dependence upon water flow through their body (discussed in Leys & Hill, 2012). They have an internal network of water canals that are connected to choanocyte chambers which generate directional water flow for filter feeding, gas exchange, and waste removal (**Figure 1**). Because their growth form and canal system is responsive to environmental conditions (Hill & Hill, 2002; Palumbi, 1986; Wilkinson & Vacelet, 1979), the same species can form thin encrustations in high energy environments, and massive, branching, or columnar structures in low energy environments (Kaandorp, 1991; Wilkinson & Vacelet, 1979). Concomitant with environmentally induced changes in gross morphology are changes to the diameter of water canals and density of skeletal elements (Hill & Hill, 2002; Palumbi, 1986). **Figure 3** illustrates water canal dynamics in a demosponge over the course of a single day in the laboratory; individual branches can split into two, merge, or be pruned. These dynamics allow canals to reorganize and scale with growth and in response to environmental stimuli (Gaino & Burlando, 1990; Palumbi, 1986). From a developmental perspective, it is hypothesized that the water canal system is patterned from the outside-

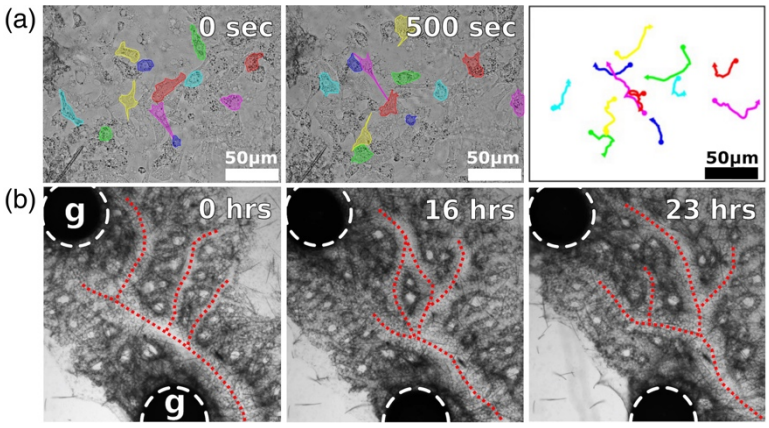

Figure 3. Sponge migratory cells and body plan plasticity. (a) In the freshwater sponge model, Ephydatia muelleri, time-lapse video illustrates cell motility over a 500-s time span. Location of tracked cells at time 0 s (left panel) and time 500 s (middle panel). Right panel shows tracers of tracked cells, circles mark position at T = 0 s and arrowheads mark position at T = 500 s. **(b)** Time series illustrating the rearrangement of excurrent canal system (traced in red) over a 23-hr time frame. g, gemmule

in; excurrent canals form first, to which choanocyte chambers and incurrent canals subsequently connect (Leys & Hill, 2012). This developmental sequence is experimentally reproducible, as transplanted oscula (exhalant siphons) induce rearrangement of internal canals around the ectopically positioned osculum (Windsor & Leys, 2010).

Plasticity in the water canal system of sponges resembles tissue/organ plasticity in other animals. The trachaeole system of insects is also a tubular network that reorganizes in response to oxygen levels and scales with volume (Harrison et al., 2018). Also, in the vascular and lymphatic systems of vertebrates, directional fluid flow is constantly sensed by the endothelium and alterations to fluid shear stress induce tissue remodeling (Baeyens & Schwartz, 2016). The cell and developmental mechanisms by which sponges reorganize their bodies are largely unknown. In other animals, luminal networks of tubes have been shown to form new branches via collective cell migration, patterned cell

proliferation/deformation, and cell rearrangement (Larsen, Wei, & Yamada, 2006). In addition to these possible mechanisms, remodeling of water canals in sponges may also involve apoptosis (Wiens, Krasko, Perovic, & Müller, 2003, Wiens, Krasko, Müller, & Müller, 2000) and/or tissue shedding. It has been reported that choanocytes in the tropical sponge *Halisarca caerulea* have a rapid cell cycle and high turnover rate, with extensive cell shedding (Alexander et al., 2014; De Goeij et al., 2009). These cells form the primary tissues of the water vascular system, and the possibility of their constant renewal creates the opportunity for rapid canal reorganization in response to environmental inputs. Furthermore, lineage tracing indicates that individual choanocytes turnover as frequently as every 2 hr, and that turnover can partly be attributed to transdifferentiation back to archeocytes (Sogabe et al., 2019).

Sponge tissue remodeling is presumably guided by the local action of physical forces on tissues. At least one plausible mechanism has been proposed for how sponges sense and respond to flow. Ludeman et al. (2014) found that the excurrent canals of diverse sponges are lined by epithelia with what appear to be non-motile, flow-sensing cilia. Sponges may use these cilia to coordinate a behavioral response (cycles of inflation and contraction of the canal system) that functions to clear debris from the canal system. However, it is possible that they also serve to provide signaling inputs into processes of developmental plasticity and tissue remodeling. Indeed, the role of sensory cilia in bilaterian development is widely appreciated (Anvarian, Mykytyn, Mukhopadhyay, Pedersen, & Christensen, 2019; Dasgupta & Amack, 2016; Ezratty et al., 2011; Goetz & Anderson, 2010; Ko, 2012; Mariani & Caspary, 2013; Sun, Wu, & Zhong, 2016; Tasouri, Willaredt, & Tucker, 2013). For example, it is tempting to see similarities in the plasticity

of the sponge body plan with, for example, vascular remodeling through sensory cilia-based signaling in vertebrates (Chen, Gays, Milia, & Santoro, 2017). The evolutionary gulf separating these phenomena is immense, and the specific mechanisms involved are likely independently derived, but it is at least plausible that the role of sensory cilia in animal development extends to the earliest animal ancestors.

Cell death, tissue shedding and flow-sensing cilia notwithstanding, the cornerstone of developmental plasticity in sponges is almost certainly their dense populations of migratory stem cells (archeocytes; **Figure 3**). A compelling piece of evidence for archeocyte pluripotency comes from freshwater sponges grown in the laboratory from gemmules. Gemmules are small capsules that form when environmental conditions become unfavorable. They each contain ~10^4 yolk-laden cells (thesocytes) and can resist freezing, high temperatures, and desiccation. When favorable conditions return, thesocytes (which are binucleate) undergo cytokinesis to produce archeocytes (Simpson, 1984). Archeocytes migrate from the developing gemmule, divide and differentiate to produce somatic tissues of the juvenile (Funayama, 2010). In further support of this view, in dissociation studies archeocyte-enriched cell fractions are the most regenerative. When depleted, cell aggregates form but do not reattach to the substrate and are not viable (De Sutter & Van de Vyver, 1977; Funayama, 2010).

From a genetic perspective, archeocytes (and choanocytes) have been found to express Piwi (Funayama, Nakatsukasa, Mohri, Masuda, & Agata, 2010), a marker of pluripotent stem cells in cnidarians and planarians. More recently, transcriptomics of isolated archeocytes revealed enrichment of RNA regulatory genes involved in germline multipotency, and RNA-binding proteins that regulate mammalian embryonic stem cells

(Alié et al., 2015). Wnt/β-catenin signaling has also been implicated in stem cell maintenance and renewal in other animals (Clevers & Nusse, 2012), and nuclear populations of β-catenin are detected in archeocytes of the sponge *Ephydatia muelleri* (Schippers & Nichols, 2018).

The abundance of pluripotent cells in sponges is also evident in a recent single-cell sequencing study. Sebé-Pedrós et al. (2018) dissociated larval and adult sponge tissues, quantitatively sequenced their expressed genes, and clustered cells based upon similarities in their overall expression profile. In most animals, this technique results in fairly discrete clusters corresponding to terminally differentiated cell types. In sponges, discrete clusters were detected, but cells with intermediate expression profiles were abundant and distributed along a continuum between clusters. This is also seen in single-cell sequencing data from the cnidarian *Hydra*, which also has abundant stem-cell populations (Siebert et al., n.d.). This result likely reflects that many cells (plausibly archeocytes and choanocytes) were sampled in the process of interconversion and differentiation.

The high degree of plasticity in sponges has implications for our understanding of developmental evolution. General principles of developmental evolution are derived from animals whose adult body plans are determined by tightly regulated embryonic patterning mechanisms. In contrast, the connection between embryogenesis and adult body morphology in sponges appears to be more tenuous; environmental feedback mechanisms and plasticity may play a greater role. Consequently, the evolutionary forces shaping morphological evolution in sponges may depart considerably from expectations calibrated by studies of other animals.

Sponges Can Help Clarify the Origin of Novel Cell and Tissue Types

The field of evolutionary developmental biology has made considerable progress toward understanding how changes to development lead to changes in form. In contrast, the question of how the component parts of modern animals—diverse cell and tissue types—first evolved remains largely unanswered. From what antecedents, and through what sequence did muscles, neurons, sensory cells, epithelial cells, excretory cells, and myriad other cell types originate and diversify? As a case study, here we consider how sponges may help to illuminate the cellular foundations of myocyte evolution—the cell type that forms muscle, which sponges lack.

Sponge tissues mostly resemble epithelia in that they comprise planar sheets of polarized cells that line the body, separating the inside from the outside. The exopinacoderm lines the outer surface of the sponge, the endopinacoderm lines internal cavities, the choanoderm functions in filter feeding, and the basopinacoderm serves as the attachment interface with the substrate. There is some debate about whether these tissues meet the strictest definition of an epithelium as defined in bilaterian animal models (Fahey & Degnan, 2010; Leys, Nichols, & Adams, 2009; Nickel, Scheer, Hammel, Herzen, & Beckmann, 2011); they typically lack obvious cell junctions and an underlying basal lamina. However, some sponge species do have these features (Boute et al., 1996; Fidler et al., 2017), whereas cell junctions in other species are only evident when examined by immunostaining for adhesion proteins rather than by electron microscopy. For example, the cell junction protein vinculin was found to localize to cell–cell and cell–extracellular matrix contacts in the homoscleromorph sponge *Oscarella pearsei* (Miller et al., 2018). Likewise, the cell junction protein β-catenin was found to co-precipitate with

expected binding partners, α-catenin and cadherin, and to localize to cell contacts in the freshwater sponge *E. muelleri* (Schippers & Nichols, 2018). There is also evidence that freshwater sponge tissues exhibit transepithelial resistance, a fundamental property of barrier-forming epithelia (Adams, Goss, & Leys, 2010).

Although sponges lack muscle tissues, their epithelia undergo coordinated, organism-wide contractions that likely function to clear debris from the water canal system and maintain water flow (Elliott & Leys, 2007; Leys & Hill, 2012; Ludeman et al., 2014). Understanding how sponge epithelia contract may offer clues to how muscles evolved; it is hypothesized that muscle tissues may have even evolved from ancient contractile epithelia (Nickel et al., 2011). Although the mechanisms of contraction in sponge epithelia are largely uncharacterized, they do have conserved homologs of proteins of the contractile apparatus of myocytes, proteins that regulate muscle contraction, and developmental regulatory proteins that specify myocyte fate. Understanding how these proteins function in contractile epithelia of sponges will help illustrate how they functioned ancestrally, and how they may have been recruited to function in muscle tissues of other animals.

Origins of Contractile Regulatory Mechanisms

The molecular motor for muscle contraction is the myosin II molecule: a complex of two myosin heavy chains (MyHC), which contain the motor domains and long tails that form the so-called "thick filament," as well as two regulatory light chains and two essential light chains, proteins involved in modulating the activity of the motor. Myosin II interacts with actin filaments to generate contractile force in muscle, but also during

cytokinesis, cell motility, and apical constriction. In each of these contexts, the basic mechanism of contraction is the same: thick filaments exert force on actin-based "thin" filaments, which is converted into mechanical stress through anchor points in the cell.

An historical contingency with consequences for myocyte evolution was the duplication of MyHC in the holozoan stem-lineage, which led to two paralogs, non-muscle myosin II (nmMyHC) and striated muscle myosin II (stMyHC), distinguished by a 29aa-coiled-coil domain in the stMyHC tail (Sebé-Pedrós, Grau-Bové, Richards, & Ruiz-Trillo, 2014). In bilaterians, nmMyHC serves all non-muscle contractile functions, but also has a derived role in vertebrate smooth muscle (**Figure 4**). In contrast, stMyHC is essentially restricted to muscle: striated (Schiaffino & Reggiani, 1994) and cardiac muscle (d'Albis, Anger, & Lompré, 1993; Weiss & Leinwand, 1996) in vertebrates, and smooth and striated muscle in invertebrates (Hooper, Hobbs, & Thuma, 2008; Hooper & Thuma, 2005). The most parsimonious interpretation is that nmMyHC retains many of the ancestral functions of MyHC, whereas stMyHC was restricted to muscle contractility in the last common ancestor of Bilateria, or earlier.

These myosin paralogs have different functional properties, and recent work has predicted that they were likely associated with two predominant myocyte types in the last common ancestor of bilaterians: a fast contracting myocyte that used stMyHC and a slow contracting myocyte that used nmMyHC (Brunet et al., 2016). It is reasonable to predict that, in non-bilaterians, cells that express stMyHC have homology with fast contracting myocytes in bilaterians. What we know so far is that in cnidarians stMyHC is indeed expressed in fast contracting myocytes but, in a departure from bilaterians, it may also be expressed at low levels in some non-muscle cells. Conversely, cnidarian nmMyHC is

broadly expressed in non-muscle epithelia, but is also expressed in smooth muscles of the gastrovascular system (Steinmetz et al., 2012; Sulbarán et al., 2015). In the ctenophore *Peurobrachi pileus*, the stMyHC is expressed in all muscle types, which have a smooth-muscle ultrastructural phenotype, whereas nmMyHC is not expressed in any muscle type (Dayraud et al., 2012; Steinmetz et al., 2012).

Characterization of the role of MyHC paralogs in sponges is of particular interest because they have contractile epithelia, but apparently lack bona fide muscle tissue (reviewed in Elliott & Leys, 2007; Nickel et al., 2011). One hypothesis is that muscle tissues evolved from contractile epithelia (Nickel et al., 2011). The cleanest evidence in support of this hypothesis would be if contractile epithelia in sponges express stMyHC. If they express nmMyHC, it is possible that their contractile properties have homology with non-muscle contractile cells/tissues.

To date, there are limited, contradictory data on MyHC expression in sponge tissues. A study of MyHC expression in the demosponge *Tethya wilhelmia* indicates that nmMyHC and stMyHC have non-overlapping expression patterns, with nmMyHC expressed in the pinacoderm—the putative contractile epithelium (Nickel et al., 2011; Steinmetz et al., 2012). However, single-cell sequencing data from the demosponge *A. queenslandica* indicate that stMyHC is specifically expressed in this tissue (Sebé-Pedrós et al., 2018). Thus, the role of different myosin paralogs in epithelial contraction of sponges has not been unambiguously determined.

Another important consideration for assessing the homology of sponge contractile tissues with muscle is the question of how sponge contractions are regulated. There is no easy way to talk about the mechanisms that regulate muscle contraction without

oversimplification because the mechanisms are complex, incompletely characterized and vary by phylogenetic lineage. One widespread mechanism is tropomyosin/troponin regulation of the actin filament; found in striated and cardiac muscles of vertebrates (Farah & Reinach, 1995; Gordon, Homsher, & Regnier, 2000; Kobayashi, Jin, & de Tombe, 2008; Spudich & Watt, 1971), and in striated and smooth muscles of invertebrate bilaterians (Hooper et al., 2008; Hooper & Thuma, 2005). This protein complex sterically hinders stMyHC from binding to actin, but is released in the presence of Ca^{2+}, allowing for a rapid contraction in fast contracting myocytes (Farah & Reinach, 1995). But, troponin C is restricted to bilaterians, and so this mechanism is thought to have evolved in the bilaterian stem lineage (Steinmetz et al., 2012).

A potentially more ancient strategy for regulating contractions is to disrupt the autoinhibitory interactions of MyHC in the thick filament. MyHC undergoes asymmetric head–head interactions in which the two heads of the homodimer interact, thereby blocking actin-binding on one head and the ATPase activity on the other (Jung, Komatsu, Ikebe, & Craig, 2008). MyHC also undergoes head–tail interactions in which the heads interact with the coiled-coil tail, preventing filament assembly and stabilizing head–head interactions in assembled filaments (Himmel, Mui, O'Neall-Hennessey, Szent-Györgyi, & Cohen, 2009; Jung et al., 2008). Both head–head and head–tail interactions appear to be ancient within the animal lineage, found in vertebrate smooth and striated muscles (Nogara et al., 2016; Woodhead, Zhao, & Craig, 2013), and in muscles of invertebrate bilaterians (Alamo et al., 2015; Himmel et al., 2009; Jung et al., 2008). Moreover, there is in vitro evidence for the presence of these interactions in MyHC of non-bilaterians, as well as in the social amoeba Dictyostelium (Lee et al., 2016, 2018; Liu, Shu, Yamashita,

Xu, & Korn, 2000) suggesting that MyHC autoinhibition predates animals and the origin of myocytes, altogether. How MyHC autoinhibition is disrupted in activated myosin has not been fully determined and may differ between animal lineages, but appears to function in association with regulatory light chain or essential light chain regulation. Non-bilaterian lineages all have conserved orthologs of myosin light chain kinase, which in vertebrates functions to regulate contractions by phosphorylation of the thick filament. Thus, this may be the ancestral mechanism for regulating muscle contractility in animals (Steinmetz et al., 2012). However, there is limited functional evidence from non-bilaterians with which to evaluate this hypothesis. There could also be alternative mechanisms for thin-filament regulation that are not yet characterized.

Origins of Myocyte Developmental Specification

A final consideration for understanding myocyte evolution and for testing the homology between contractile tissues in different phylogenetic lineages is whether there are conserved developmental regulatory mechanisms involved in myocyte differentiation. In bilaterians, myogenic regulatory factors such as MyoD play a prominent role in the expression of contractile machinery and in differentiation of fast contracting myocytes (Tapscott, 2005). In contrast, in slow-contracting myocytes these roles are served by interactions between the MADS-box transcription factors, Mef-2 and serum response factor (SRF) and their co-activators, myocardin and myocardin-related transcription factor (MRTF; Long, Creemers, Wang, Olson, & Miano, 2007; Wang, Wang, Pipes, & Olson, 2003; **Figure 4**).

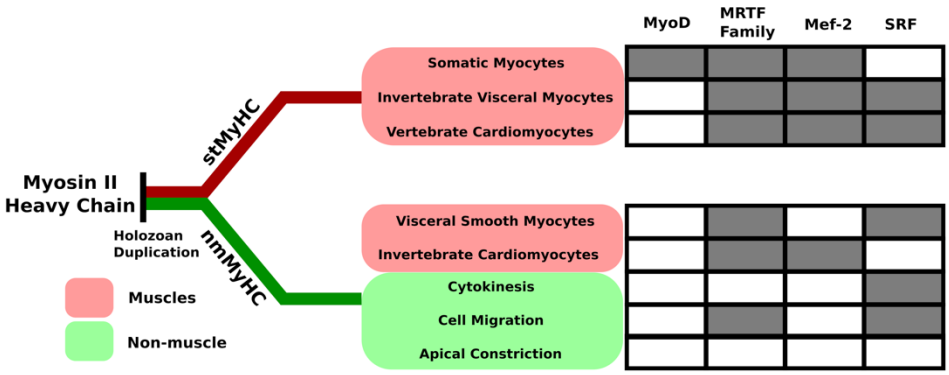

Figure 4. Myosin II heavy chain isoforms and transcription factors associated with different contractile tissues. The pre-animal duplication of myosin II heavy chain (MyHC) has resulted in a separation of function of the two isoforms (stMyHC and nmMyHC) in all studied animals. The highlighted areas show highly generalized cellular context in which these have been shown to function. Red highlighting represents a muscle context and green highlighting represents a non-muscle context. On the right, filled boxes signify that the transcription has been shown to play an important role in cell fate determination, or in the specified contractile context. If sponge contractile tissues are homologous to bilaterian muscle, the clearest expectation would be that they contain stMyHC and their differentiation is dependent on MRTF/Mef-2 interactions

Ctenophores, cnidarians and sponges lack MyoD, but have highly conserved SRF, Mef-2, and MRTF orthologs (Martindale, 2004; Ryan et al., 2013; Steinmetz et al., 2012) (MRTF paralogs in invertebrates are often referred to as myocardin, but myocardin is an MRTF paralog that is restricted to vertebrates). To understand the possible mechanisms of myocyte differentiation in these lineages, it is necessary to understand the details of MRTF regulation: the N-terminus of MRTF contains as series of RPEL repeats (RPxxEL) which bind to G-actin, thereby blocking a nuclear localization signal (NLS; Miralles, Posern, Zaromytidou, & Treisman, 2003; Sotiropoulos, Gineitis, Copeland, & Treisman, 1999). Changes in actin dynamics (often in response to mechanical force on the cell) leads to an increase in the F-actin/G-actin ratio, dissociating MRTF from G-actin and exposing the NLS. The result is that when cells experience mechanical stress, MRTF translocates to the nucleus where it interacts with Mef-2 or SRF, activating myocyte

differentiation and the expression of contractile genes (Miano, Long, & Fujiwara, 2007; Vartiainen, Guettler, Larijani, & Treisman, 2007).

Mechanical stress-mediated activation of cellular processes is well-appreciated in bilaterians and serves a variety of important physiological roles both in muscles and other tissues (Cui et al., 2015; Finch-Edmondson & Sudol, 2016; Zhao et al., 2007). In vertebrate cardiac and smooth muscles, tissue stress leads to MRTF-dependent growth and differentiation of myocytes; essentially, muscle plasticity. In non-muscle contexts, mechanical stress from injury leads to myofibroblast differentiation and contraction-dependent wound healing (Velasquez et al., 2013). Also, localized assembly and contraction of actomyosin networks are involved in single cell puncture wound repair (Bement, Mandato, & Kirsch, 1999).

The developmental roles of mechanical tissue stress have not been well characterized in non-bilaterians, but it has been shown that Mef-2 is expressed in myocyte precursors of the cnidarian, *Nematostella vectensis*. Moreover, Mef-2 morphants failed to develop muscle, but this effect could not be separated from more general effects on endoderm development (Genikhovich & Technau, 2011; Martindale, 2004). SRF/Mef-2/MRTF interactions and functions remain entirely unexamined in sponges.

A hypothesis that takes into account the tremendous plasticity of the sponge body plan is that the contractile tissues of sponges are homologous to myocytes at the level of development specification, and rely upon MRTF-mediated environmental response rather than upstream genetic factors to initiate differentiation. Through this mechanism, sponges may develop contractile tissues in areas that experience mechanical stress in response to water flow. If so, one would expect sponge contractile tissues to be somewhat irregularly

dispersed throughout the tissue, and indeed, **Figure 5** illustrates that the putative actomyosin tracts in sponge epithelial tissues are irregular in both number and, to a lesser degree, orientation. This organization may be indicative of highly localized environmental stimuli. Thus, it is plausible that their differentiation depends upon the activation of MRTF in response to environmentally induced actin dynamics.

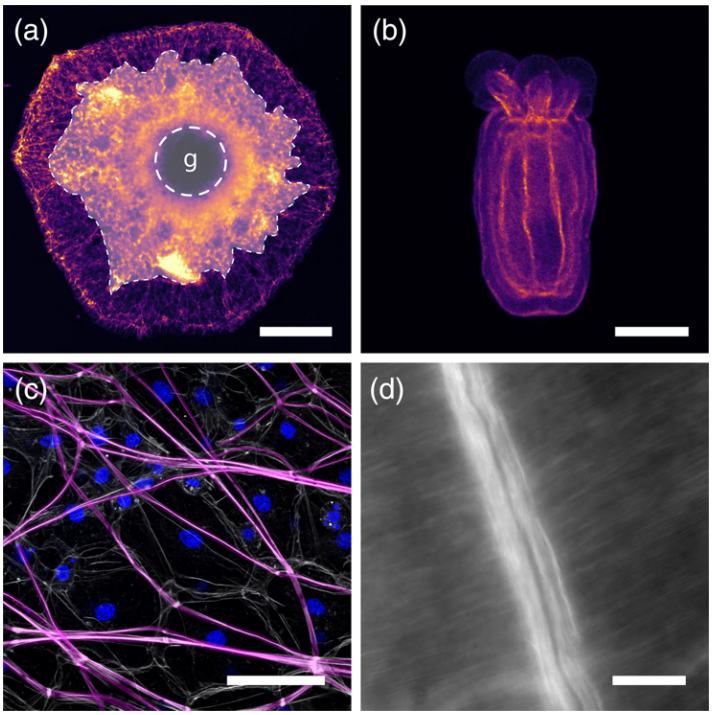

Figure 5. Actin organization in the sponge *Ephydatia muelleri* and the cnidarian *Nematostella vectensis*. (a) Whole-mount F-actin staining in an *E. muelleri* juvenile. White overlay marks the choanoderm, containing brightly stained choanocyte chambers and the empty gemmule capsule in the middle. Image is intensity shaded, revealing actin organization in contractile tissues in the area outside the choanoderm. **(b)** Whole-mount F-actin staining in a *N. vectensis* polyp, a cnidarian model with muscles. Vertical bundles of high intensity staining through the body and in the tentacles correspond to the large retractor muscle and longitudinal tentacle muscles. **(c)** High resolution confocal image of the pinacoderm of the *E. muelleri* showing irregular organization of F-actin bundles (highlighted in magenta). These bundles are aligned between neighboring cells, and dense actin plaques represent points of cell–cell contact. **(d)** High resolution confocal image of a retractor muscle in *N. vectensis*. The large vertical actin bundles belong to the retractor muscle, while the thin bundles running perpendicular constitute the circular body musculature. Scale bars **(a, b)** 200 µm and **(c, d)** 30 µm

Environmentally induced differentiation of contractile tissues in sponges could certainly reflect the ancestral condition, but it is difficult to polarize this transition without more information from sponges and other non-bilaterian lineages. For example, placozoans also lack muscles and have recently been shown to have epithelial cells that undergo rapid contractions that appear to be more analogous to apical constriction (Armon & Prakash, 2018).

Clearly, the challenge of reconstructing cell-type evolution is tremendous. One must consider the molecular mechanisms that contribute to the cellular phenotype of interest, the developmental factors regulating differentiation of the cell type, and then disentangle a web of phylogenetic uncertainty, incomplete information, and divergent/convergent evolution. Contractile tissues in sponges may offer clues to the origin of myocytes. If they have homology to muscle we predict that cell fate is developmentally specified by interactions between MRTF with Mef-2, and that their contractions are dependent on regulation of stMyHC. This example illustrates how comparative study of sponge cell biology and development can clarify the origin of ancient, fundamental cell types; even those that sponges lack.

Conclusions

If we are to make progress toward understanding the cellular foundations of animal body plan evolution, more attention must be devoted to non-bilaterian animals, including sponges. However, the outdated narrative that sponges have persisted, unchanged since the origin of animals, is unjustified. Instead, the value of sponges for

studies of early animal evolution will come from comparative research with other animal lineages and animal outgroups such as choanoflagellates, filasterians, and icthyosporeans.

A critical bottleneck that limits progress in sponge research is the development of experimental techniques for functional studies. Both overexpression and knockdown methods have been reported (Pfannkuchen & Brümmer, 2009; Revillai-Domingo, Schmidt, Zifko, & Raible, 2018; Rivera et al., 2011), but are currently inefficient and have not been widely adopted or applied. The most experimentally tractable animal models are amenable to injection of oocytes/zygotes so that molecular cargo can have organism-wide effects throughout development. However, most sponges cannot be cultivated and so far none can be experimentally induced to spawn. Researchers therefore tend to work on species that are accessible in their geographic region, or on freshwater sponges which can be grown from gemmules (overwintering spores that contain stem cells). Future investment in technique development will be absolutely critical for realizing the full scientific potential of sponges (and other non-bilaterian animals). Studies of animal origins are inextricably linked to these organisms, which reprezsent hundreds of millions of years of understudied evolutionary experimentation and have immense potential for enabling new discoveries.

This chapter is a slightly modified version of Colgren, J. & Nichols, SA. The significance of sponges for comparative studies of developmental evolution published in WIREs Developmental Biology (DOI:10.1002/wdev.359) and has been reproduced with permission of copyright holder under license number 4838430405336.

Chapter 2: Physiology of Contractions in *Ephydatia muelleri*

Introduction

The contractile response of sponges has been documented for over 100 years (Parker 1919; McNAIR 1923) and is observed in all four classes of sponges (Simpson 1984; Bond 2013; Nickel 2010), suggesting presence in the ancestral sponge. Despite this timespan, there is still little known about the cellular nature of these contractions as well as what tissue is contracting to generate the primary force (focus of next chapter). The basic behavior likely arose as a means of maintaining water flow through the sponges aquiferous system. As sessile filter feeders, it is essential that sponges maintain adequate flow in order to expose choanocytes to bacterial prey. Debris or sediment entering their canal system can aggregate in the excurrent canals disrupting flow, and by contracting the sponge is able to generate force, which translates to increased water pressure through the osculum (main excurrent canal) sufficient to clear obstructions. These contractions are seen as parastatic-like waves, propagating across the body in a coordinated manner (Elliott & Leys, 2007; Nickel, 2004). Changes in flow rate are thought to be detected by non-motile cilia lining the inside of the osculum, which functions as a sensory organ in a Ca^{2+} dependent manner (Ludeman et al., 2014). Various molecules that function in neuronal signaling of other animals, such as NO, glutamate, and GABA, have been implicated in the propagation of the signal (Elliott & Leys, 2010; Ramoino et al., 2007;

Ellwanger et al., 2007). These waves of contractions consist of two primary phases, first and inflation of the excurrent canals as an increased volume of water enters, followed by a decrease in canal diameter in the direction of the osculum (Elliott & Leys, 2007). The work described in this chapter was performed in order to build on these previous studies in order to better understand the physiology of the contractions.

Simplified, the process of contraction is thought to originate with detection at the osculum, followed by production and release of NO which diffuses through the body (Ludeman et al., 2014; Elliott & Leys, 2010). This is followed by release of a signaling molecule, such as glutamate, which then propagates the signal to contract towards the osculum (Elliott & Leys, 2010). Early studies found that, in contrast to neuro-muscular coupling of other animals, contractions could be initiated by mechanical stimuli but not electrical stimuli, and action potentials could not be detected (Prosser et al., 1962; Leys et al., 1999). However, the more recent findings, coupled with genomic data, suggest that there are components of neuron type signaling present in sponges (Tompkins-MacDonald et al., 2009; Srivastava et al., 2010; Leys, 2015). My work does not focus strongly on the signaling aspect, but rather the contractile response. However, I did want to see if there was evidence for cellular excitation/depolymerization coupled with the contractile response. I first wanted to focus on general documentation of contractions in our lab using *Ephydatia muelleri* grown from gemmules. I then looked for evidence of the role of cellular depolarization in the contractions. This was followed by looking for evidence of the role of calcium in the behavior as well as identifying whether or not the influx comes from internal or external pools. Finally, I wanted to see if I could disrupt the NO pathway to identify its role coordination of the behavior.

Documentation of contractions

Background

The first goal was to establish a method to consistently document contractions in *E. muelleri* in our laboratory. Physiological contractions occur due to flow disruption (i.e. blockage or agitation), while contractions can be induced with bath application of glutamate (Elliott & Leys, 2010). These were used to take time-lapse videos of sponges during contractions in order to show repeated control over the behavior.

Methods

Sponge collection and culturing

Pieces of *Ephydatia muelleri*, consisting of the spicule scaffold containing gemmules, were collected from an unnamed lake above Red Rock Lake in the Brainard Lake Recreation Area in the Colorado Rocky Mountains (coordinates) and were transferred to the laboratory, where they were stored in autoclaved lake water (LW) at 4^{o}C until use. Gemmules were separated from the spicules and surrounding tissue using tweezers and a soft brush. Species was confirmed based on the appearance of the spicules in the gemmule (Barton & Addis, 1997). Separated gemmules were then treated with 1% H_2O_2 for 5 minutes and washed thoroughly with autoclaved lake water. Cleaned gemmules were then stored at 4^{o}C until use. Gemmules were plated in a solution of autoclaved lake water and 100µg/mL Ampicillin. They were plated in either 6 well culture plates (CellTreat #229106) or glass bottomed dishes (MatTek Corporation #P35G-1.5-10-C). Using a 1000µL pipette with a cut tip, 5-6 gemmules were added to the six well plates and 2-3 were added to the bottom well of the glass bottom dishes.

Plates/dishes were then placed in a dark cabinet and left at room temperature. Gemmules were allowed to hatch and attach (approx. 3 days) and then water was replaced with fresh autoclaved LW (no antibiotic). Water was changed each day following hatching. Sponges were grown for 5 days following hatching and were examined to confirm the presence of canals and choanocyte chambers.

Imaging

Sponges were imaged using an inverted scope. The transparent nature of *E. muelleri* means that the major incurrent and excurrent canals are clearly visible with this setup. The microscope was fitted with a monochromatic camera and associated imaging software. Focus and exposure were set to minimize the amount of focused light on the tissue and time-lapse video was taken generally using a 30 second duration between images over 181 images. Videos were processed using Fiji (Schindelin et al., 2012).

Treatments

Agitation was performed by placing the plate or dish containing sponges on a vigorous rocking platform for 3 minutes and then transferring them to the microscope for imaging. Imaging was started approximately 5 minutes after initial stimuli. Canal blockage was performed using bath application of Sumi Ink (Yasutoma #KY6). Ink was pre-diluted in LW water and the concentrations tested were 1/2 stock, 1/10 stock ,1/100 stock, and 1/1000 stock. LW was replaced with ink solution and the sponges were incubated for 10 minutes. Following the incubation, the water was quickly changed 3-5 times (until it was visibly clear) and the sponges were imaged. Glutamate was applied

following the basic protocol found in Elliot & Leys, 2010. A 20mM stock solution was prepared using L-glutamate (Sigma-Aldrich #G1501) in dH_2O and pH was adjusted to 7.4. The stock was diluted to 160μM in LW water prior to treatment. Sponges in 6 well plates were placed in 3mL of LW and sponges in glass bottom dishes were in 2mL of LW. These were placed on the microscope and brought into focus, and then were left for ~1 hour in order to relax without agitation. Following the relaxation period, the time-lapse was started and allowed to progress for 10 frames. In the time between frame 10 and 11, one half of the volume of LW was removed and the same volume of 160μM glutamate was added. This was done in order to balance the concentration added with minimizing the amount of mechanical stimulus from mixing flow.

Alternative imaging strategies

In order to image sponges from the side using the same microscope setup above, sponges were grown on 4mm clear cube beads. Beads were first washed in 1% H_2O_2 in LW for 5 minutes at room temperature and then were rinsed several times with fresh LW. The beads were placed in the middle of the well in 6 well plates and 5 mL of LW was added to the well. Using a cut tip, gemmules were pipetted onto the cube. The easiest way to perform this was to draw one or two gemmules into the pipette tip and position it directly above the well containing the cube. Light pressure is used to expel ~25μL volume from the tip so that the droplet is held in place at the tip through surface tension. When the gemmule was seen to have drifted into the droplet, the tip is lowered into the well directly above the bead, allowing the gemmule to sink down onto it. Once the gemmule had settled on the bead, care was taken not to move it until it hatched, around 3

days later. Once the sponge had attached to the cube and began to develop, the cube was then rotated in the well in order to image the side of the sponge.

Results

Agitation

Vigorously rocking or shaking the dishes containing sponges efficiently trigger contractions in both the 6 well plates and the glass bottom dishes, with no evident difference based on the differences in volumes surrounding the sponges. Contractions were judged as some inflation followed by constriction of the canals occurred ~70% of the time. The dynamics of these contractions were consistent with previously published data for *E. muelleri*. Incurrent canals can be seen to contract over the course of around 20 minutes, which is coupled with an inflation of the major excurrent canals. This is followed by a steady constriction of the excurrent canals over the next 20 minutes during which time the incurrent canals expand (**Figure 6**). Over the course of the next 40 minutes the canals returned to the resting size, with random fluctuations in size (**Figure 7**). Following different incurrent canals

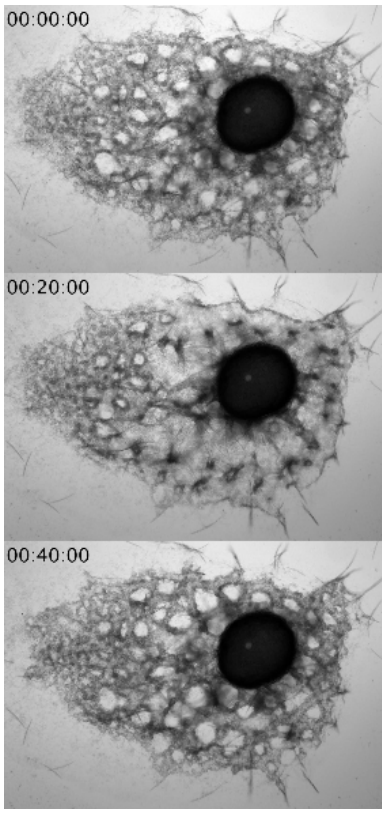

Figure 6. Time lapse series of *E. muelleri* contraction. A contraction was induced using vigorous agitation of the samples dish prior to imaging and time point 0 represents the first frame of imaging. At 20 minutes incurrent canals (green arrows) of the body have contracted and excurrent canals (red arrows) are fully inflated. Over the next 20 minutes excurrent canals contract as incurrent canals relax to their original state. Scale bar 500μm.

showed some variation in the size of the contraction, but a general coordination during the behavior, primarily during the initial constriction period for canals in the same general body region **(Figure 7A)**. Canals in more distal regions of the body (green and dark blue traces in figure 2a) showed a delayed constriction. The inflation and subsequent constriction of the excurrent canals overlapped with the constriction and relaxation of the incurrent canals, and was regionally coordinated (**Figure 7B)**. A distal canal (shown in gray in figure 2b) showed a delayed inflation and contraction that overlapped with the constriction of the distal incurrent canals. The return to a resting size, similar to what was measured at time 0 at approximately 80 minutes was seen for all of the canals in the body area around the gemmule, which constitutes the majority of body mass. There is a good amount of variation in the size of the canals during this return to the resting size (**Figure**

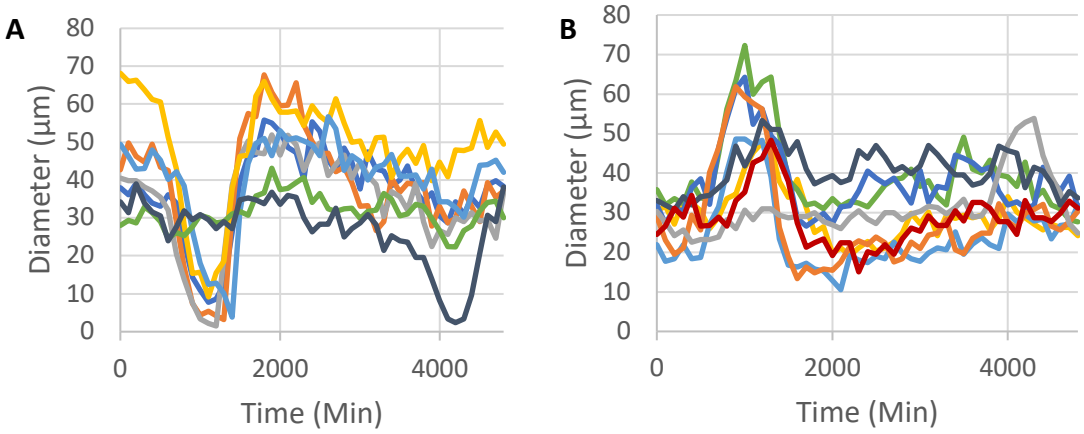

Figure 7. Change in canal size during contraction. **(a)** Each trace represents the diameter of an incurrent canal measured over the course of the contraction. Green and dark blue lines are distal canals, while the other were in the same region near the gemmule and show a synchronized dramatic reduction in size, followed by expansion and return to resting size. **(b)** Traces of diameter for major excurrent canals which show a dramatic expansion that overlaps with the contraction of the incurrent canals. This is followed by a reduction in diameter to a point below the size at time 0 seconds and a subsequent return to initial size. Gray trace represents a distal canal and shows a late inflation and contraction cycle.

7). Similar fluctuations in localized canal size are seen in sponges not induced to contract (**Figure S1)**. The primary distinguishing factors between coordinated contractions and local movement is the overlapping of movement between adjacent canals as well as that of incurrent contraction and excurrent inflation.

Ink

High concentrations of ink (1/2 stock and 1/10 stock) appeared to be lethal to the sponges, which were characterized by large amounts of tissue damage and disruption of flow. Both 1:100 stock and 1:1000 stock concentrations were effective in producing contractions following every treatment. The 1:1000 showed a clear contraction of the

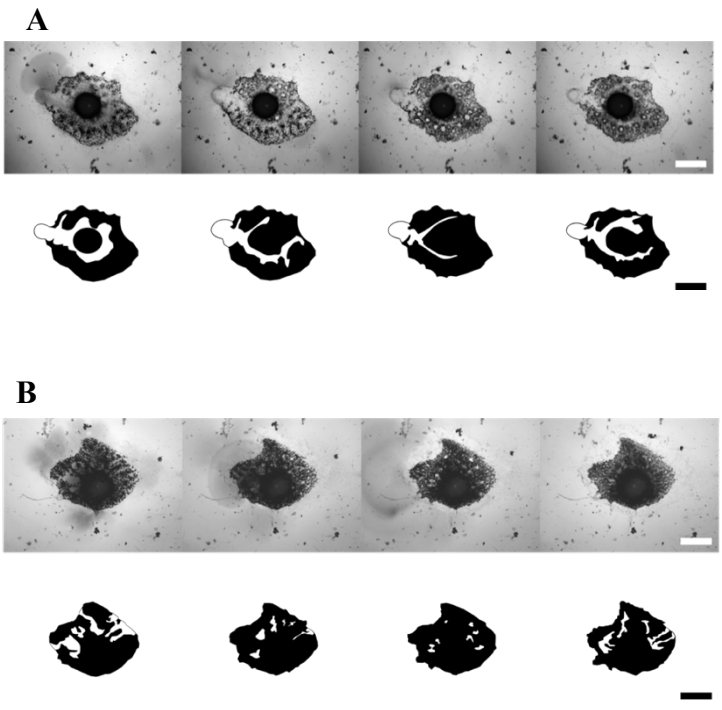

Figure 8. Induction of contraction with low concentration of ink. **(a)** Sponge was treated with 1:1000 dilution of sumi ink for 10 minutes and then wash with lake water prior to imaging. **(b)** Sponge was treated with 1:100 dilution of sumi ink for 10 minutes and the washed with lake water prior to imagining. Panels represent time points 0, 20, 40, and 80 minutes. Bottom panel shows outline of major excurrent canals. At the beginning of the series, the excurrent canals can be seen to be inflated, suggesting a contraction had initiated during the staging process. Over the next 40 minutes these are seen to dramatically reduce in size and then return to a resting state. Scale bars 500μm.

incurrent canals coupled with an inflation of the excurrent canals. As the excurrent canals contracted, incurrent canals relaxed again, followed by a return to the resting state. During this ink could be seen exiting the osculum, suggesting clearing from the aquiferous system (**figure 8a).** Treatment with 1:100 dilution of ink showed similar dynamics with an initial inflation of the excurrent canals, followed by constriction, which was then followed by a slight relaxation (**Figure 8b**).

Glutamate

80µM Glutamate effectively triggered contractions (around) 50% of the time. When contractions were triggered, they followed the dynamics observed in the previous studies (Elliott & Leys 2007, 2010) as well as those seen with both ink and agitation. Incurrent canals initially contracted to over half of their original diameter while excurrent

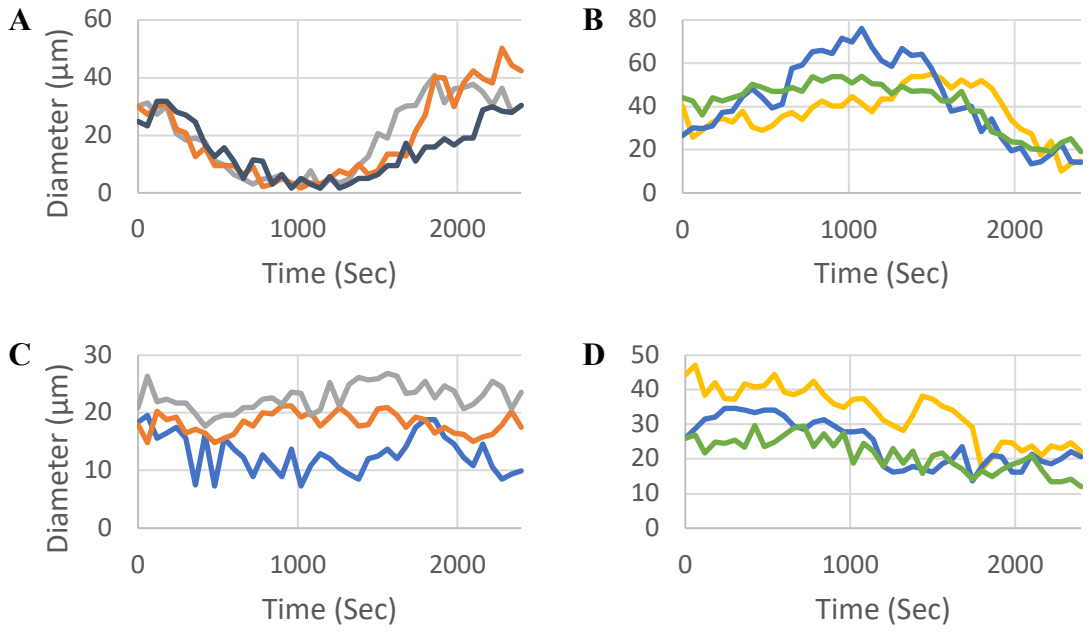

Figure 9. Changes in canal size following treatment with 80µM glutamate. **(a&c)** Traces for individual incurrent canals. **(b&d)** Traces for individual excurrent canals. **(a&b)** Show individual that had full inflation-contraction response and **(c&d)** show and individual without full response.

canals showed a similar respective inflation (**Figure 9a&b**). In cases that were judged to have not contracted, there was movement and generally a decrease in the diameter of excurrent canals though no inflation was seen (**Figure 9c&d**).

Alternative Imaging

Imaging of the side of sponges on beads was effective in giving insight into the tissue that was contracting as well as a clear view of the osculum. Lighting and shadowing issues did arise which made it difficult to image at low magnification while observing both the osculum and the body of the sponge (**Figure 10**). This method did allow for increased magnification while imaging the osculum (**Figure 11**). During the contraction, the osculum can completely contract within 5-15minutes which is more rapid than is seen in the other canals, both incurrent and excurrent (**Figure 7**). These contractions appear to consist of local pinching (green arrows) concurrent with adjacent expansion (red arrows). The regions of pinching seem to contain tissue ruffling which suggests a ring type constriction through the tissue. Imaging of the sponges from the side also allowed for visualization of the different tissue layers in the body during contractions. During the contraction of the apical pinacoderm, the region between two

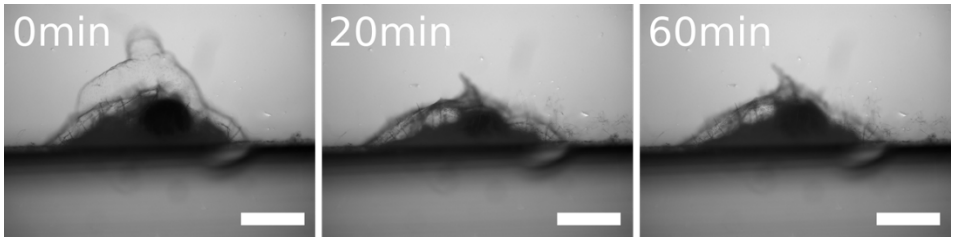

Figure 10. Imaging of contraction from the side. Sponge was grown on a square bead which was rotated to allow imaging on an inverted scope. Contraction was induced by the addition of 80μM glutamate and time lapse series shows a strong contraction of the osculum followed by contraction through the body between 20 and 60 minutes. Scale bars 500μm.

spicules can be seen depressing in the middle of the expanse, with no observable movement of the spicules themselves. At the site of spicule attachment, there appears to be an expansion in the upper layer of tissue whereas the lower layer decreases (**Figure 12a**). This could represent a constriction of the endopinacoderm (layer lining the internal canal) with an expansion of the exopinacoderm (outside layer of the sponge). Inside the body of the sponge, changes in the choanoderm and mesohyl demonstrate the contractions through the excurrent canals (**Figure 12b&c**). During this, incurrent canals begin to contract (black arrows in fig 13) as the subdermal cavity swells with volume (magenta arrows in fig 13), which is seen as general expansion between 12-20minutes. Following this expansion, the choanoderm can be seen moving downward between 20-28 minutes (red arrows fig 13) without additional expansion in the subdermal cavity. This movement likely represents the constriction of the excurrent canals which run through this tissue, pulling it down around them.

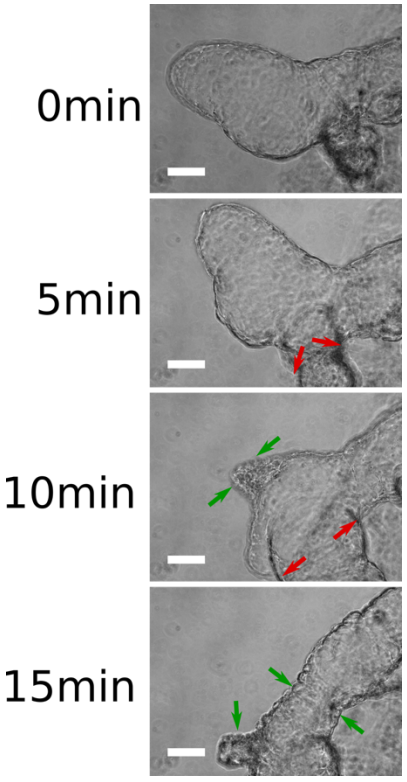

Figure 11. Osculum dynamics. Sponge was grown on a square bead which was rotated so that the osculum was in the field of view. Time lapse imaging was then performed using a higher powered objective and higher temporal resolution. The osculum shows a series of localized constrictions (red arrows) and expansions (green arrows). Scale bars 20µm.

Discussion

Both agitation and addition of ink are solid methods for triggering reproducible physiological contractions. It appeared that the timing for the

start of the contraction was more consistent with the addition of ink, whereas it varied some with the agitation. This makes it a slightly better method for showing a contraction under physiological conditions. However, the ink that remains in the choanocytes as well as in moving through the canals could cause some imaging problems, so both methods are useful. Triggering a contraction with glutamate was not as consistent as the other methods, but is useful to have. Based on the inconsistency of triggering contractions, negative results should be repeated a sufficient number of times in order to convincingly say that contractions are blocks under some condition. Imaging sponges grown on cubes

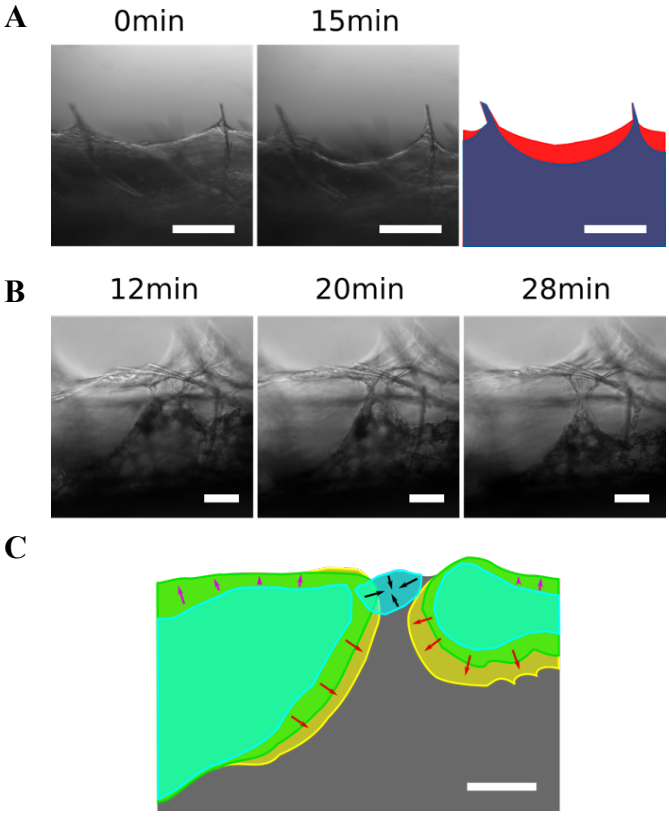

Figure 12. Lateral view of tissues during contraction. Stills from a time lapse taken following induction of a contraction with 80µM glutamate. **(a)** Apical pinacoderm movement over the course of 15 minutes. The third panel is an overlay of the two panels with time 0 minutes in red and time 15 minutes in blue. **(b)** Imaging through mesohyl and choanoderm. **(c)** The bottom panel is an overlay of the three time points with subdermal cavity from 12 minutes in cyan, 20 minutes in green and 28 minutes in yellow. Black arrows show pinching of a canal just below the apical pinacoderm between 12 and 20 minutes. Magenta arrows show inflation of subdermal cavity during this time span and red arrows show movement of the choanoderm boundary between 12 minutes and 28 minutes. Scale bars 50µm.

is a promising method for describing tissue dynamics with high resolution and from an angle not normally available, but presents some technical challenges. The plating of the gemmules is difficult and highly inconsistent as to where the gemmule actually attaches on the cubes, which affects the depth of focus needed to image them. Since sponges do not have defined body plans, how the sponge grows from the gemmule is also inconsistent, making it difficult to know how a tissue of interest will be oriented in the imaging space. The technique does provide some insight into the mechanics of contractions which are not visible from whole body imaging. The contractions of the osculum show a good deal of tissue ruffling in areas of strong contraction. This suggests that the force of the constriction is occurring along contractile rings through the tissue, which generates a pinching force. This is consistent with the dense rings of actin that have been documented to run through this tissue in a variety of sponges (Prosser et al., 1962; reviewed in Simpson, 1984). High magnification lateral imaging of the sponges also provides additional insight into the tissues involved in the contractions through the body of the sponge. Looking at the apical pinacoderm, spicules remain stationary during the contraction appearing as solid support. Conceptually, if exopinacocytes were contracting along these to attachment points, then this would result in a raising and straightening of the tissue as it shortened. The opposite is seen, suggesting this is not what is occurring. The alternative is that either the whole tissue is relaxing and being pulled down by reduced or negative pressure below it, or that the endopinacoderm is contracting which is coupled with the expansion of the exopinacoderm to allow for the movement. There is some evidence for the latter in that the lower layer of tissue attached to the spicule is seen to move downward during the contraction, while the upper layer

does not, but further work needs to be done to resolve this. Viewing the choanoderm during a contraction, the main takeaways is that the tissue in the choanoderm begins to contract prior to a noticeable change in the size of the choanocyte chambers (visible as small circles in the tissue). An influx of water can be observed prior to the tissue contracting, which likely correlates with the inflation and subsequent contraction of the excurrent canals which run through this tissue.

Depolarizing Agents

Background

Sponges are traditionally thought to be one of the few phylum of multicellular eukaryotes that do not transmit action potentials. The exception to this is seen in the class Hexactinellida, which transmit electrical signals through their trabecular syncytium (Leys et al., 1999). There is no strong evidence for a similar tissue in members of the other classes, nor the cellular machinery for establishing low-resistance pathways, such as gap junctions seen in other animals (Adams et al., 2010). Studies on contractions in demosponges (to which *E. muelleri* belongs), have not found evidence for electrical coupling of the contractile response nor have they found evidence for a change in the transmembrane potential during contraction (Leys & Meech, 2006). However, there have been studies that show electrical coupling in aggregated sponge cells (Dunham et al., 1983) as well as depolarization coupled exocytosis of GABA in dissociated sponge cells (Ramoino et al., 2007). Genomic and biochemical data has also found functional inward rectifying potassium channels (Kir) in the demosponge Amphimedon queenslandica (Tompkins-MacDonald et al., 2009), suggesting a physiological role for membrane

depolarization in sponges. My primary question for this section is if there is evidence for localized depolarization coupled with contractions, similar to what is seen in excitable animal cell types (such as neurons, muscles, astrocytes, and β-cells). In-order to address this I first looked at the ability of depolarizing molecules (potassium and arginine) to trigger a contraction and second utilized a voltage sensitive membrane dye in order to see how membrane potential varied during a contractile wave.

K^+ and Arginine Treatment

Searching of the *E. muelleri* transcriptome revealed that they have Kir channels similar to those studied in *A. queenslandica*. The role of these channels in regulating membrane potential and whether this functions in the contractions in *E. muelleri* has not been explored. Voltage-gated potassium channels appear to be absent in *E. muelleri,* based on a lack of clear voltage sensor domains (Kenny et al., n.d.). These channels are generally responsible for the rapid return to resting potential in depolarized cells and provide the outward current in action potentials. The slow nature of sponge contractions at the cellular level compared to other excitable cells could speak to a different mechanism for return to resting potential, not excluding depolarization as a physiological response. In many excitable cells found in other animals, treatment with high concentrations of K^+ ions leads to depolarization and the resulting response (Adrian, 1956). *E. muelleri* live in freshwater lakes and are highly sensitive to increased ions. Because of this, I tested a range of K^+ concentrations ranging from 30μM to 30mM.

The positively charged amino acid arginine has also been shown to depolarize excitable cells and is used to trigger exocytosis in pancreatic β-cells (Smith et al., 1997).

Arginine is also a substrate NO signaling (Wiesinger, 2001), which sponges appear to utilize for propagation of the signal involved in the contractile response (Elliott & Leys, 2010). Searching the *E. muelleri* transcriptome also shows the presence of putative orthologs of cationic amino acid transporters which generally serve in arginine uptake (Closs et al., 2004). Based on this, it was hypothesized that, following bath application of arginine, sponges would take up a sufficient quantity to alter the membrane potential. If the contractile behavior is coupled with depolarization, then this should trigger a contraction.

Methods

Sponge gemmules were separated and washed as described earlier and were plated in LW+100µg/mL Ampicillin. These were left at room temperature in the dark for 3 days and checked to confirm the gemmules had hatched. Following hatching, the water was replaced with fresh LW and the sponges were placed back in the dark at room temperature. Once sponges had developed choanocytes and canals (~3dph) water was changed and they were prepared for imaging. Prior to imaging, an exact volume of LW was added to each well (2mL for 24-well plates) and the sponges were left to relax on the microscope stage for at least 1 hour. 1M stock solutions of KCl, L-Arginine, and NaCl were made in MilliQ H_2O. 2x Solutions were then prepared by diluting stock solutions in LW. After the relaxation period, time-lapse images were taken at a rate of 30sec per frame for 161 frames. After the initial 20 frames, 1 mL of LW was removed from the well and 1 mL of the 2x solution was added. Removing 1 mL of LW and adding 1 mL of fresh lake water was used as a control. Working concentrations tested were;

KCl – 30µM, 500µM, 5mM, and 30mM

Arginine – 500µM, 2mM, 20mM

NaCl – 30mM*

*NaCl was tested only in higher concentrations because *E. muelleri* is known to be highly sensitive to increased NaCl.

Results

The control sponges showed some localized movement through the tissue (termed 'twitching') but did not show a clear contraction. The low concentrations of KCl (30µM and 500µM) did not appear to be any different from the control. 5mM KCl did show what appeared to be a clear contraction of the canals followed by a relaxation to the original

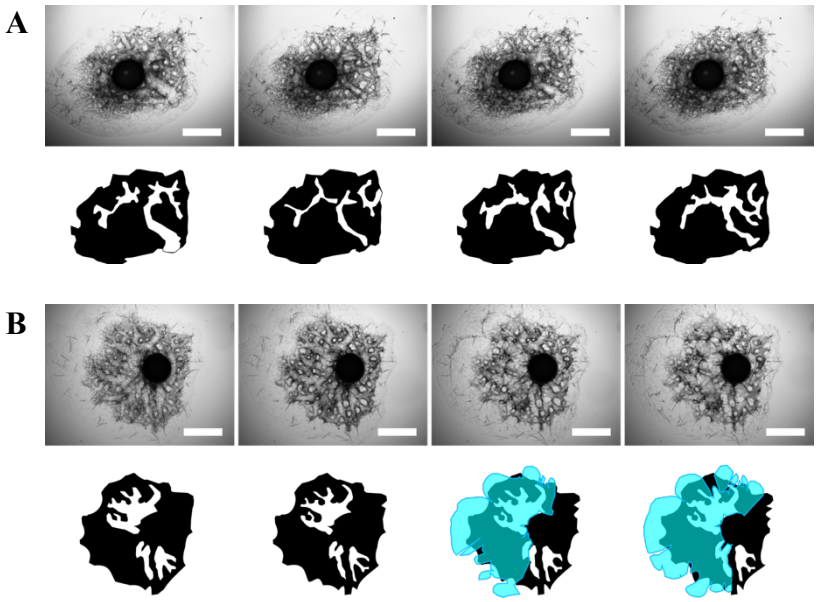

Figure 13. Time series of sponge treated with KCl in lake water. **(a)** Sponge was staged and treated with 5mM KCl in lake water. Frames represent time points 0, 9, 30, and 80 minutes. Bottom panel shows outlines of major excurrent canals, which can be seen quickly contracting and then relaxing. **(b)** Sponge treated with 30mM KCl in lake water. Frames represent time points 0, 8, 25, and 40 minutes following treatment. Bottom panels show outlines of major excurrent canals in white and areas of pinacoderm rupture in cyan. Scale bars 500µm.

state (**Figure 13a**). Treatment with 30mM KCl appeared to trigger both contractions of incurrent and excurrent canals, which was followed by large amounts of tissue damage in the apical pinacoderm (**Figure 13b**). An initial contraction of the incurrent canals and inflation of the excurrent canals can be seen, at which point the pinacoderm begins to lose integrity (damaged pinacoderm in cyan in fig 13). Following the damage, the excurrent canals appear to remain inflated. One possibility is that this is the result of osmotic stress, and could result from arrest of flow and cell shrinking due to dehydration. In order to test this, a sponge was treated with the same concentration of NaCl, which is known to be above the lethal concentration. In this case, the sponge did not noticeably respond over the same time course (**Figure S2**). The 500μM Arginine treatment did not appear to differ

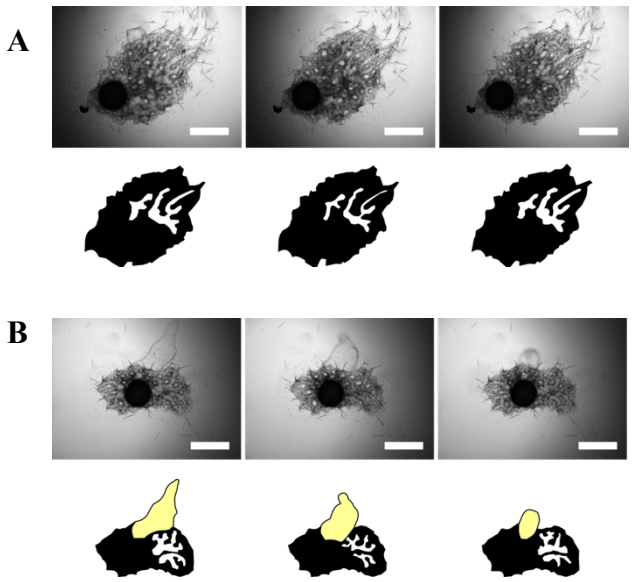

Figure 14. Time series of sponges treated with arginine. **(a)** 2mM treatment, frames represent time points 0, 20, and 40 minutes. Bottom panel shows outline of major excurrent canals. A slight decrease in diameter can be seen over the first 20 minutes which relaxes over the next 20 minutes. **(b)** 20mM treatment, frames represent time points 0, 20, and 40 minutes. Bottom panel shows outline of major excurrent canals in white and osculum, which is visible, in yellow. Over the first 20 minutes a contraction of the excurrent canals is coupled with an expansion of the osculum. Scale bars 500μm.

from the control sponge. 2mM arginine showed what appeared to be a slight contraction, in which the excurrent canals can be seen slightly inflated, then contracted and finally relaxing again (**Figure 14a**). 20mM arginine treatment showed a stronger response (**Figure 14b**). The incurrent canals can be seen constricted in the first panel, which is followed by a constriction of the excurrent canals and inflation of the osculum (highlighted in yellow) in the second panel. The osculum is then seen to contract as the excurrent canals re-inflate and then return to a resting size in the next two panels.

Discussion

Based on these results, there is evidence that depolarizing molecules can trigger a contraction in *E. muelleri.* The lower concentrations of both KCl and arginine did not have a strong effect. There are a few basic possibilities for the effects of these treatments and accompanying expectations. First the treatment could lead to arrest of flagellar beating, which in turn would disrupt flow into the canal system. This would likely show as a thinning of the canals as water is expelled but not replenished, which would likely not be followed by a return to normal size. Next, the treatment may activate sensory cells, which originate or propagate the contraction signal. If this occurred, then the expectation would be to a full inflation-contraction response as if the sponge was treated with ink. Finally, the treatment could be acting on the effector cells, which contract to generate mechanical force. In this case, it would be expected that the canals would contract across the whole sponge (as opposed to a contractile wave), and then would relax to their original size following contraction. Based on the images of these treatments, it appears that the canals ubiquitously contract followed by a relaxation. This suggests that the

treatment is activating the effector cells (what contracts) in the 5mM KCl and 2mM and 20mM arginine treatments. This appears to also be the case in the osculum, which first increases in diameter, as water is pumped into it from the body, followed by a full contraction, as this water is expelled. If the contraction was due in part to tissue collapse (as suggested in the 30mM KCl treatment) then it would be expected there would be no inflation of the osculum and the contraction/collapse would not move from the base towards the tip, as reverse flow would be possible and less obstructed. It was surprising that a strong response was not seen following treatment with 30mM NaCl as this is known to be well above the lethal concentration for *E. muelleri.* However, it is possible that they are tolerant to NaCl in lake water over these time periods, whereas they are susceptible to equivalent concentrations in diluted PBS, due to the presence of phosphate ions. This is supported by the lack of growth in and sensitivity to phosphate buffers (unpublished data). Given the strong response to KCl and not NaCl, suggests that it isn't just osmotic stress or the Cl^- ions in the solution, but the K^+ that is eliciting a response. As seen in the lateral imaging of contractions, regions of the apical pinacoderm need to expand during contractions near spicule attachments. It is possible that the strong uncoordinated contraction of the endopinacoderm generated sufficient force on the exopinacoderm to lead to loss of tissue integrity. Overall, based on these findings, it does seem that depolarization is coupled to the contractile response in the effector cells/tissues of *E. muelleri.*

Membrane Potential Dye

Background

Sponge contractions are slow processes taking anywhere from 30-90 minutes to propagate across the body in juvenile *E. muelleri*. Based on the earlier findings, it does seem that depolarization of the effector cells functions in the contractile response, which is normally a very rapid event. With the slow propagation of the contraction across the body, it is not clear whether the depolarization events are prolonged at the cellular level or whether they are rapid but followed by a slow physical response and/or propagation. Because of this FluoVolt™ Membrane Potential Kit (Molecular Probes #F10488) was chosen as a sensitive membrane potential dye able to detect both rapid and slow depolarization events. It was thought that staining live sponges with this dye could provide *in vivo* evidence for the physiological relevance of depolarization during contractions, as well as help to identify the primary tissue that is contracting (based on earlier evidence that depolarization function in effector cells). Staining does present a methodological challenge though. First, delivery of the dye is difficult, as bath application of membrane dyes tends to strongly stain the choanocyte chambers as they are an area of concentrated flow. Disproportionate staining of the choanocytes makes visualization of tissues, such as the pinacoderm, difficult, while cells in the mesohyl may not be stained at all. Imaging also presents a problem, primarily due to the length of time the contractions take and the temporal resolution needed to visual a depolarization event. Sponges are sensitive to prolonged exposure to laser light, which leads to extensive tissue damage. Taking rapid video (50ms acquisition) means that the sponge must be consistently exposed to high amounts of energy in order to excite the dye sufficiently to

visualize staining, and lowering the laser power means lengthening exposure time per frame and therefore limiting temporal resolution. Apart from this, since these are three dimensional organisms, keeping the tissue in the focal plane during a contraction is difficult. Because of these challenges, imaging was performed on both our traditional inverted epifluorescence scope using a low powered objective as well as using confocal microscopy.

Methods

Sponge Staining

Gemmules were plated in glass bottom dishes in LW+100µg/mL ampicillin and left at room temperature in the dark until they hatched. After hatching water was changed each day with fresh LW. Care was taken to minimize movement of the dishes prior to staining to prevent contractions prior to treatment. Sponges were washed twice prior to treatment by carefully removing most (but not all) of the liquid around the sponge, then gently pipetting 2mL of fresh LW into the dish (using care to prevent turbulent flow, which could trigger a contraction). Prior to treatment, 100x PowerLoad concentrate and 1000x FluoVolt™ dye were diluted to 1x concentrations in autoclaved LW. The water around the sponge was carefully pipetted off, leaving approximately 50µL around the sponge. 1mL of the working dye solution was then added and sponges were incubated at room temperature for 15 minutes in the dark. After incubation, 1mL was carefully pipetted off and 1mL of LW containing 1:100 v/v sumi ink was added and incubated at 5 minutes at room temperature in the dark. The sponges were then washed 3 times in fresh LW and placed on the microscope for imaging.

Imaging

First trials were performed on our inverted epifluorescence scope using a standard FITC filter set and a 10x/0.28 N.A. objective. The laser was set to the lowest power setting and exposure was increased until dye became visible (500ms exposure time). Acquisition was set to the fastest frame rate possible for 400 frames. The second trials were performed under the same initial conditions, but using a 4x/0.10 N.A. objective and frame rate was increased to 60 second intervals for 81 frames. The laser shutter was manually closed between images. Confocal imaging was performed on an Olympus Fluoview FV3000 confocal laser scanning microscope using a 20x/0.45 N.A. objective and a standard FITC filter combination for peak excitation at 494nm and emission at 518nm. Laser level was set to a minimum setting for detection and frames consisted of ten 1μm Z-sections. Maximum intensity projections of each frame were generated and compiled into a stack in Fiji (Schindelin et al., 2012) for analysis. For signal intensity measurement, lines were drawn across specific regions of the sponge and average pixel intensity along this line was measured for each frame.

Results

The first trial showed good staining of the tissue, though the choanocyte chambers were much brighter than the pinacocytes (**Figure S3**). In the first video, which took images as fast as possible, the sponge tissue lost integrity very quickly leading to balling up of the pinacoderm and the choanocyte chambers. There appeared to be a wave of decrease in fluorescence followed by a rapid increase, which was followed by a steady decline as the tissue collapsed. The decrease is difficult to interpret, but overall it does

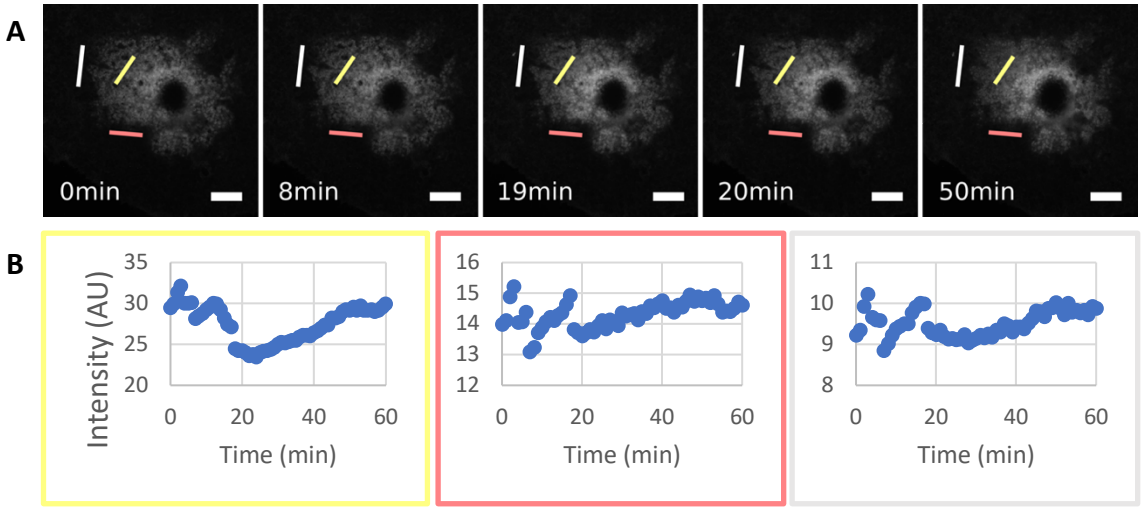

Figure 15. Second trial live imaging with FluoVolt™ dye. Samples were stained as before and induced to contract using 1:1000 sumi ink in lake water. Imaging was performed under lower magnification on an inverted epifluorescent scope. Images were taken at 1 minute intervals with the shutter being manually closed between frames to limit laser exposure. **(a)** Still images display a general increase in signal over the first 19 minutes at which there is an apparent decrease between 19 and 20 minutes. Lines represent regions where fluorescent intensity was measured for each frame. **(b)** Graphs of mean pixel intensity along line scan at each time point during the contraction. Border color corresponds with color of line in **(a)**. All three regions appear to show the same general trend. Scale bars 500µm.

seem that the sponge was exposed to toxic levels of energy. It is unclear if any portion of the physiological contraction was captured or if the changes in potential were the result of loss of membrane integrity as a result of cell or tissue damage.

The second trial was performed using low magnification and 60 second intervals. Following induction, there was some evidence of changes in membrane potential during the contraction (**Figure 15)**. During the first 20 minutes intensity was more variable, with periods of increase followed by rapid loss and repeated increase (**Figure 15b**). During this time the relative increase in signal is consistent with the expectations based on the manufacturer's protocol. After the peak in signal, between 15 and 20 minutes depending on the body location, there was a rapid decrease in signal followed by a period of little

change and then gradual increase over the following approximately 20 minute and then leveling off. There is a slight difference in the timing of the final peak and drop to minimum between the different regions measured, with the peak arriving latest in the tissue further from the gemmule (gray line) and earliest in the region closest to it (yellow line). This could represent propagation time across the body.

For the third trial, slightly higher magnification confocal microscopy was used, with temporal resolution of 30 seconds per frame. During the contraction there was some visible change in the amount of signal in the choanocytes, while signal in the pinacoderm was difficult to detect due to uneven staining between the two tissues (**Figure 16**). The changes in signal using this method were much less pronounced and did not show the rapid increases and decreases seen in the previous trial (**Figure 16b)**. The large excurrent canal near the gemmule (gray line) showed a steady increase for the first 20 minutes followed by an even reading for the following 20 minutes. The region of the distal pinacoderm (red line) showed similar kinetics with the previous trial, in that there was a steady increase for 16 minutes followed by a decrease for the next 11 minutes, with steady readings for the remainder of the contraction. A similar pattern was seen for the region through the choanoderm, in which there was a steady increase for the first 9 minutes followed by a decrease in signal for the next 9 minutes, followed by a more subtle increase and decrease before leveling off. The difference in the timing of peak signal between these two regions is consistent with their position relative to the gemmule as seen in the previous trial.

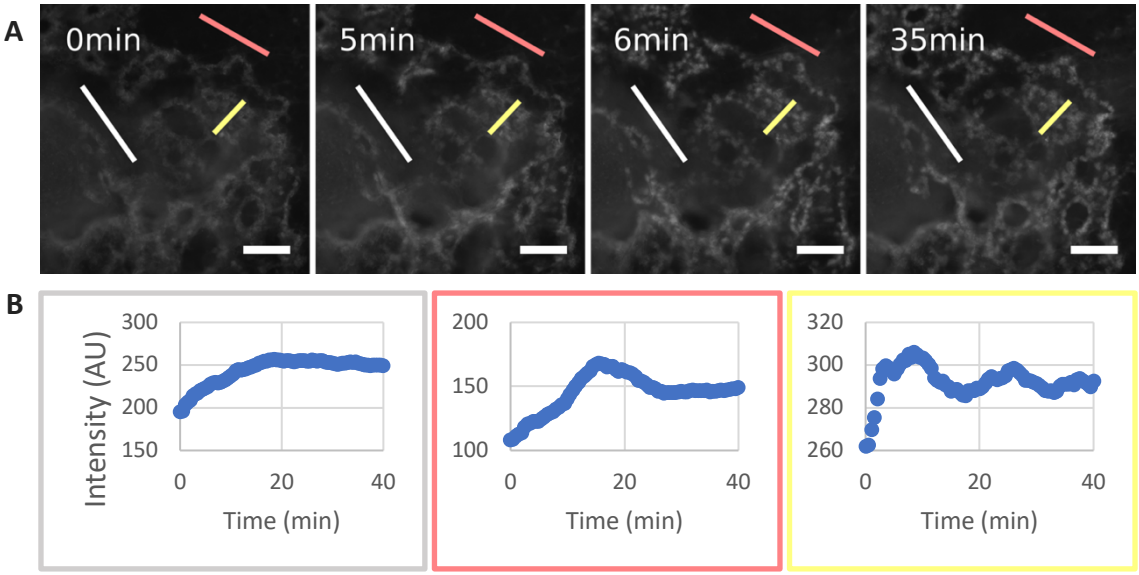

Figure 16. Live imaging with FluoVolt™ dye using confocal microscopy. Sponge was labeled as above and induced to contract using 1:1000 sumi ink in lake water. **(a)** Images from time series movement of the incurrent canals and apparent increased signal in the choanoderm over the first 6 minutes which is followed by a contraction in the excurrent canals **(b)** Mean pixel intensity along each line shown in **(a)** over the course of imaging. Color of outline corresponds with color of line. Measuring through the excurrent canal shows limited change in signal, with a steady increase over the first 20 minutes. The choanoderm and pinacoderm showed early increases followed by rapid decrease before leveling off, as was seen with the previous trial. Scale bar 200µm.

Discussion

A fundamental technical challenge in recording possible depolarization-contraction coupling in sponges is how rapidly depolarization events occur at the cellular level compared to the slow rate at which the sponge contractions propagate across their body. The first attempts to visualize membrane potential changes during a contraction using high temporal resolution resulting in rapid tissue rupturing, likely due to the large amount of laser energy the sponges were subjected to. Subsequent trials limited the continuous exposure time, by lowering the laser levels and increasing the time between frames. However, this may have resulted in rapid localized potential changes to have

been missed in the time between frames. By looking at signal levels in specific regions of the sponge, there did seem to be a pattern of localized increase in signal followed by a decrease. This could be the result of the summation of local depolarization events occurring as the contraction wave moves through the region (increasing the signal) followed by a return to resting potential as the contraction propagates away. This is supported by the apparent correlation between the timing of the signal peak and the position of the region relative to the gemmule. The bulk of the sponge body and generally the osculum (which is thought to be the source of the contractile signal) are located near the gemmule in laboratory hatched sponges of this age. As a result of this, contractions can appear to originate in the tissue proximal to the gemmule and progress out towards the edge of the sponge. When using FluoVolt™ dye, tissues close to the gemmule showed peak signal earlier than tissues that were further away. This adds support to the idea that the increase in signal is a result of the sponge undergoing a contraction. Overall, these results do not definitively suggest that depolarization-contraction coupling is present in *E. muelleri*, but they do not suggest that it is absent either.

The role of Ca^{2+} in contractile response

Background

Ca^{2+} is an important signaling molecule in all domains of life. In animals, excitable cells, such as muscles and neurons, undergo rapid increases in cytoplasmic calcium levels following activation, which triggers the cellular response (contraction or neurotransmitter release respectively). Within the diversity of muscle types found in animals, Ca^{2+} signaling plays a consistent role. There are two primary mechanisms by

which this regulation occurs, either through direct action on the myosin bundles (thick filament regulation) or through affecting the ability of the myosin head to bind to actin (thin filament regulation). In thick filament regulation, the basic pathway follows; increased Ca^{2+} binds to calmodulin, which then binds to myosin light chain kinase (MLCK), which in turn phosphorylates the myosin regulatory light chain (RLC) activating the ATPase activity of the myosin head, leading to contraction (Johnson et al. 1981). In thin filament regulation, myosin binding to actin and ATPase activity are prevented by the troponin complex which associates with the actin filament through tropomyosin. Increased Ca^{2+} binds to the troponin C, which leads to a conformational shift in the full complex, freeing up the myosin binding sites on the actin filament (Spudich & Watt, 1971; Spudich et al., 1972; Hooper et al., 2008). Though there are a lot of variations and some unique exceptions, these two mechanisms are found throughout bilaterian animals (Webb, 2003; Butler et al., 1998; Szent-Györgyi, 1996; Gordon, 1992; Schulz & Triggle, 1994; Hooper & Thuma, 2005). However, a functional troponin complex has not been identified outside of bilaterians and sponges do not appear to have orthologs for key components (Steinmetz et al., 2012). The main components of thick filament regulation, on the other hand, are present in non-bilaterians, including sponges (Steinmetz et al., 2012). Based on this, it is likely that this is the ancestral mechanism of regulation in muscle contractions and if sponge contractile tissue shares homology with muscle tissue of other animals, it will likely utilize this basic mechanism for initiating a contraction.

The rapid increase in Ca^{2+} generally comes from release from internal stores in the sarcoplasmic or endoplasmic reticulum, either through ryanodine receptors or IP3

receptors in the membrane (Kuo & Ehrlich, 2015). In order to maintain these concentrated stores Ca^{2+} is consistently shuttled into the organelle from the cytoplasm by sarco/endoplasmic reticulum Ca^{2+}-ATPase (SERCA) pumps, which are highly conserved across animals (Altshuler et al., 2012).

Previous studies have demonstrated the necessity of extracellular Ca^{2+} during sponge contractions (Prosser, 1967; Prosser et al., 1962; Leys, 2015). However, this could be due to its role in signal initiation and propagation (disrupted flow activates surface Ca^{2+}channels which initiates contraction signaling or Ca^{2+} entry leads to exocytosis of molecules involved in signal propagation). If the effector cells are utilizing Ca^{2+} to regulate the on-off of physical shortening, then it is possible that the increased Ca^{2+} concentration results from an influx of extracellular Ca^{2+}. If this is the case, then even if contraction is occurring through a conserved MLCK dependent actomyosin shortening, it would present a difference from muscles of other animals and would not strengthen an argument for homology. There are also possibilities in which cell shortening (contraction) of the effector cells is uncoupled from Ca^{2+}signaling. This could be either in a myosin II dependent or independent way. Though commonly Ca^{2+}dependent, especially in muscles, actomyosin contractility can rely on or be modulated by various enzymes in a Ca^{2+} independent manner. Two well studied examples of this are through the phosphorylation of myosin light chain phosphatase (MLCP) by rho-associated protein kinase (ROCK) or through direct phosphorylation of the RLC by p21-activated kinase (PAK) (Amano et al., 2010; Chu et al., 2013; Kaneko-Kawano et al., 2012; Zhang et al., 2018). These mechanisms of regulation have been shown to extensively function in the context of non-muscle cell contractility, such as

during cell migration (Ridley, 2001; Mikami et al., 2015; Kiosses et al., 1999) or apical constriction during tissue morphogenesis (Sawyer et al., 2010; Butler et al., 2019). If this is shown to be the primary mechanism of regulating actomyosin contractility in sponge tissue, it would again not strengthen the hypothesis for homology with muscles of other animals. Based on the slow rate of progression of the contraction across the body of the sponge, it is also possible that this behavior does not rely on actomyosin contractility, but rather simply changes in the cytoskeleton. This could be thought of as shortening through actin depolymerization which is also seen in tissue morphogenesis and cell migration (Svitkina, 2018; Hilfer & Searls, 1986).

In order to first investigate the role of Ca^{2+} in sponge contractions, cytoplasmic Ca^{2+} were increased using bath treatment of the Ca^{2+} ionophore, ionomycin of varying concentrations. Hypothetically, if this increase in cytoplasmic Ca^{2+} triggers the effector cells to contract, then we would expect a global contraction in a concentration dependent fashion. By this, I mean, at low concentrations, the incurrent canals should only contract as these are the first cells to come into contract with the chemical. In high concentrations, both incurrent and excurrent canals will be affected and therefore both are expected to contract. This should mirror the strong contraction followed by tissue disruption seen following treatment with high concentrations of K^{+}. This on its own would not clarify whether the Ca^{2+} increase is triggering release of signal or acting directly on the effector cells that are contracting. In order to better get at this question, the same assays will be performed, in Ca^{2+} free medium. Previous work has shown that extracellular Ca^{2+} is necessary for physiological contractions (Leys, 2015; Prosser, 1967). Ionomycin is able

to shuttle Ca^{2+} across internal membranes as well, so if intercellular stores are sufficient, there should not be a difference between the two treatments.

To further confirm that contractions utilize internal stores of Ca^{2+}, the SERCA pump inhibitor thapsigargin will be used. The basic mechanism of action for this drug is to lock the channel in an inactive state, which creates an outward leaking of Ca^{2+} coupled with store depletion and increase in cytosolic levels due to lack of sequestering in the ER (Wictome et al., 1992). Analysis of the SERCA pump sequence in *E. muelleri* suggests the binding site for thapsigargin is conserved and therefore presents an option for increasing cytosolic Ca^{2+} from internal stores. In order to better understand the sequence of events occurring during a contraction, this treatment can be coupled with treatment of L-NAME.

Method

Gemmules were plated in LW+100µg/mL ampicillin and incubated at room temperature in the dark until hatched. Following hatching, water was refreshed daily with autoclaved LW. At 3 days post hatching, sponges were examined for the presence of canals and choanocyte chambers prior to treatment. Before imaging, sponges were placed in 2mL of fresh LW and left on the microscope stage for 1 hour. Imaging was setup as described before with a 30 second frame rate for 181 frames. Between frames 10 and 11, 1mL of water was removed from the dish and replaced with 1mL of 2x treatment solution. Concentrations of ionomycin tested were 30nM, 300nM, 3µM, 10µM, and 100µM. Concentrations of thapsigargin tested were 500pM, 1nM, 100nM, 1µM, 10µM. In order to inhibit NO production sponges were treated with 50µg/mL L-NAME

overnight which was refreshed and throughout the washes and treatments. In order to assay sponges in Ca^{2+} free water, sponges were washed 3x with and then treated in either LW+0.1mM EDTA or MilliQ H_2O.

Results

Treatment with ionomycin results in strong global contractions (as opposed to contractile waves). The patterned followed the hypothesis, as concentration decreased the contraction seemed to be disproportionately strong in the incurrent canals, which gave the appearance of an inflation-contraction cycle in the excurrent canals (**Figure 17)**.

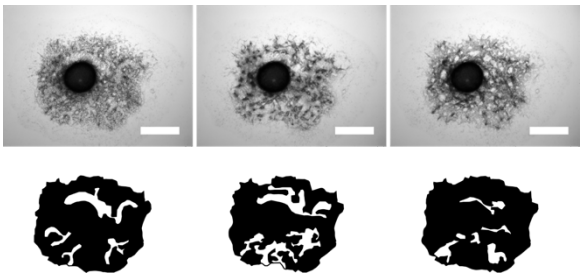

Figure 17. Ionomycin triggers a contraction in *E. muelleri*. Time lapse series of a sponge treated with 300nM of the Ca^{2+} ionophore, ionomycin. Frames represent time points 0, 20, and 40 minutes. Bottom panel shows the outline of major excurrent canals. Scale bars 500μm.

At higher concentrations, it appears that both incurrent and excurrent canals contract simultaneously, resulting in the possible loss of tissue integrity, as is seen with high concentrations of K^+ (**Figure S4a).** However, following washout and overnight incubation some of these sponges appeared to be normal (**Figure S4b)**. Treatment with ionomycin in Ca^{2+} free medium followed the same trend and was indistinguishable from normal LW (**Figure S5**).

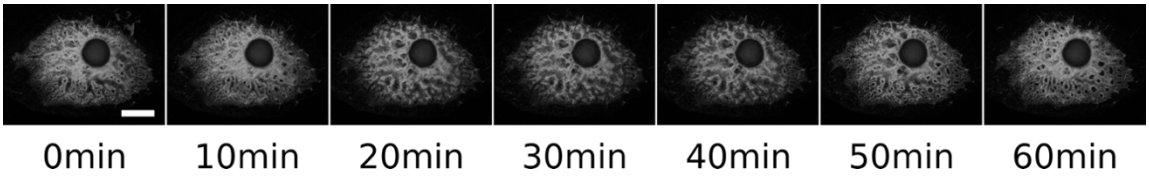

Figure 18. Internal Ca^{2+} stores are released during contractions. Time lapse series of a sponge treated with 500nM of the SERCA pump inhibitor thapsigarin. Sponge is seen to undergo strong inflation-contraction cycle seen in physiological contractions. Sponge was imaged using phase contrast microscopy to better visualize the canals. Scale bars 500μm.

Strong contractions were also observed when sponges were treated with thapsigargin, with very low concentrations eliciting a physiological type contraction, consisting of incurrent contraction-excurrent inflation followed by excurrent contraction (**Figure 18**).

Slightly higher concentrations mirrored treatment with ionomycin, in which rapid strong contraction of the incurrent canals was followed by opposing contraction of the excurrent canals, while incurrent ones were still slightly contracted (**Figure 19)**. This was also seen in absence of extracellular Ca^{2+}.

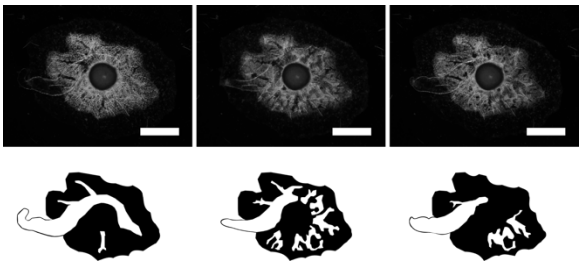

Figure 19. Contractions initiated with thapsigarin do not require external Ca^{2+}. Time lapse series of a sponge maintained in CFM which is treated with 500nM thapsigarin. Frames represent time points 0, 20, and 40 minutes. The bottom panel shows outline of major excurrent canals. Scale bars 500μm.

Discussion

Treatment with both ionomycin and thapsigargin lead to strong and rapid contractions independent of the presence of extracellular Ca^{2+}. The major takeaway from these findings are that sponge contractions are Ca^{2+} dependent, which is released from

internal stores, presumably in the ER (based on the activity of SERCA pumps). This doesn't clarify whether the increased Ca^{2+} is directly causing the contraction (through MLCK for example) or if it is acting in cells which propagate the signal. However, based on the rapid and global effect, it is likely that the increase is occurring in the effector cells. This is also consistent with the findings for low concentrations of either ionomycin or thapsigargin. The rapid contraction in the incurrent canals should lead to rapid flow through the choanocyte chambers and into the excurrent canal systems. This results in the apparent inflation of the canals, which should cause localized turbulent flow. This should result in a physiological contraction of the excurrent canal system in a delayed fashion. This secondary contraction of the excurrent system is not seen in the L-NAME treated sponges.

Taken together with the findings from the depolarizing agents, this suggests that depolarization coupled with Ca^{2+} release from internal stores plays a role in sponge contractions. Although this has been found in non-excitable cells (Mahaut-Smith et al., 1999), it points to the possibility that excitable cells play a role in the contractile response. If excitable cells are found to be the primary contractile cells involved in the contraction, this would strengthen the argument for homology with myocytes of other animals. Electrophysiological studies performed directly with the contracting cells would be highly informative. However, as explained in the next chapter, the putative contractile cells comprise a tissue that is not easily accessible in live sponges, making this highly technically challenging. However, recent work has suggested that isolated sponge cells could be maintained in culture (Conkling et al., 2019). If this could be adapted, cultured cells could potentially be pharmacologically (as discussed in the development chapter) or

genetically forced to differentiate into contractile cells, and then be studied as a monolayer.

The Role of NO in Signal Propagation and Response

Background

Previous studies on contractions in *E. muelleri* have identified NO as a potential molecule in propagating the contraction signal. This was done by indirectly visualizing nitric oxide synthase (NOS) as well as the accumulation of cGMP in the osculum and pinacocytes (Elliott & Leys, 2010). They also reported that contractions, more pronounced in the osculum, could be triggered with the NO donor S-Nitroso-N-acetyl-DL-penicillmine. Strong labeling for NOS in the osculum as well as the rapid contractile response suggest that this is the primary source of NO released during the contraction. A later study found that the osculum acts as a sensory organ, in which changes in flow are detected by non-motile cilia on the epithelial lining (Ludeman et al., 2014). Taken together, these data suggest that NO is likely released as the initial signaling molecule for the sponge to contract. This is consistent with the evidence for a diffusible molecule (migration halts) (Elliott & Leys 2010) as well as the initial contracting of the osculum tip, which allows for the inflation of the canal system prior to the contraction. Arginine-based inhibitors of NOS have been widely used, both *in vitro* and *in vivo* to regulate NO production in a variety of organisms (Víteček et al., 2012). L-N$^{\omega}$-Nitroarginine Methyl Ester (L-NAME) is a water soluble, cell permeable molecule, which once in a cell is cleaved by endogenous esterases, to produce L-N$^{\omega}$-Nitroarginine (L-NNA), a potent inhibitor of NOS (Miilsch & Busse, 1990). Previous studies on sponges have shown

weak esterase activity in their cells (Schoots et al., 1977), however, it is unclear if this is a property of the enzymes or a result of some type of compartmentalization of foreign molecules in the cells. Regardless, a high concentration of L-NAME was tested under the assumption that efficiency would be low compared to other *in vivo* treatments. The hypothesis of this assay was that by disrupting NO production, specifically in the osculum, then contractions would be blocked under physiological conditions (shaking or ink treatment).

Methods

A kill curve was first performed in order to identify the minimal lethal dose of L-NAME (Cayman Chemical #80210). Concentrations tested were; 1µg/mL, 5µg/mL, 20µg/mL, 50µg/mL, 100µg/mL, and 500µg/mL. Gemmules were plated in a 24-well culture dish, with 3 replicates at each and 3 LW controls, in LW+ampicillin (100µg/mL) and hatched as described previously. L-NAME stock was diluted in LW to treatment concentration and was used to replace the water in each well. The sponges were then incubated for 1 hour at room temperature in the dark. At 1 hour, the sponges were views for gross morphology and one of the three replicates was treated with 1:100 (v/v) sumi ink to verify choanocyte labeling. This was repeated at 5 hours post treatment and then again at 18 hours post treatment. Based on the results of this assay the working concentration of L-NAME was determined to be 50µg/mL for bath treatment of *E. muelleri.*

In order to test the effect of L-NAME treatment on the sponge's ability to contract, gemmules were plated in LW+100µg/mL ampicillin in glass bottom dishes as

described earlier. Water was changed each day following hatching. Sponges were treated with the working concentration of L-NAME in LW 2 hours prior to induction of a contraction. In-order to maintain treatment timing while initiating contractions with ink, sumi ink was diluted 1:100 (v/v) in LW containing 50µg/mL L-NAME. Water was replaced with ink solution and the sponge was incubated for 10 minutes at room temperature. The sponge was then washed 3x with fresh LW and then placed back in LW containing working concentration of L-NAME during imaging. Following ink treatment, imaging was performed on our stereoscope as described above, with 30 second frame rate for 181 images. This same basic procedure was also used for contractions initiated with agitation. For these sponges, instead of the addition of ink, after 2hours of treatment, the water was replaced with fresh LW+50µg/mL L-NAME and the dishes were placed on a vigorous rocker for 3mins prior to imaging.

In order to test the sponge's effective ability to contract in the presence of L-NAME contractions were induced using the SERCA pump inhibitor thapsigargin (Tocris # 1138) (described in detail in next section). Sponges were treated with 50µg/mL L-NAME in LW for 1 hour. After 1 hour, the solution was refreshed with 2mL of fresh LW+L-NAME and the dish was placed on the microscope stand and left to incubate for an additional hour. This was done to prevent any accidental triggering of a contraction as well as allow time for the sponge to fully relax if one had been triggered. After the 2-hour L-NAME treatment, time lapse imaging was started (30sec frames, 181 frames). Between frames 10 and 11, 1mL of the solution was removed and 1mL of 1µM thapsigargin in LW+50µg/mL L-NAME was added.

Results

Treatment with 500µg/mL L-NAME showed a strong effect after 1 hour and there was no staining in the choanocytes following treatment with ink. This continued through the other time points, suggesting this is a toxic concentration. The sponges treated with 100µg/mL L-NAME still showed ink staining in the choanocyte chambers after 1 hour, but not at later time points. Sponges treated with 50µg/mL and lower concentrations, maintained staining with ink throughout the treatment period and gross morphology appeared normal. Treatment with 50µg/mL L-NAME did appear to prevent a contraction from occurring when triggered by either ink or agitation. In both cases there is little change in both incurrent and excurrent canal diameters over the 90 minutes of imaging, with just normal random twitching visible (**Figure 20a)**. For the sponges treated L-NAME that were induced to contract with thapsigargin, there was a clear contractile response (**Figure 20b**). The incurrent canals can be seen contracting between panels 1 and 2 as the excurrent canals inflate. This is followed by a contraction through the excurrent canals visible in panel 3.

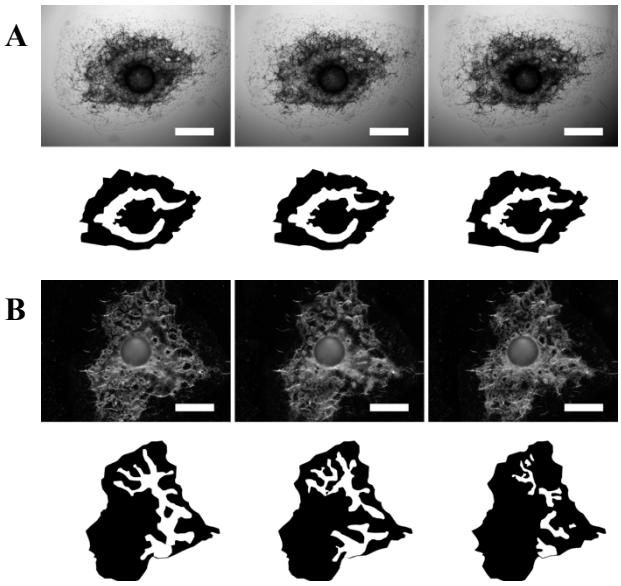

Figure 20. L-NAME blocks contractions when induced by ink but not increased Ca^{2+}. Sponges treated with 50µg/mL of L-NAME were then treated with **(a)** 1:1000 sumi ink or **(b)** 500nM thapsigargin to increase cytoplasmic Ca^{2+}. Frames represent time 0, 30, and 60 minutes. Bottom panels show outline of major excurrent canal. Scale bars 500µm.

Discussion

There are two important takeaways from this experiment. First, it further confirms the role of NOS in *E. muelleri* contractions and demonstrates our ability to gain control of physiological contractions by disrupting the NOS pathway. Second, it suggests that the Ca^{2+} dependent contractile response acts downstream of NO release. For this, seeing no contractile response to disruption of flow or agitation in L-NAME treated sponges, but still being able to trigger a contraction with thapsigargin, strongly suggests that NO production and release occurs early following stimulus, which may act directly on the contractile effector cells or other signaling cells which could release different messengers, such as glutamate. A loss of some of the coordination of the contraction suggests that this is a complicated behavior, in which NO likely helps modulate local activity across the body. Based on previous studies (Ludeman et al., 2014; Elliott & Leys, 2010) it is likely that NO is originally released from the osculum following the stimulus of disrupted flow. However, following this event, NO is likely produced and released in cells throughout the body, in responses to localized forces, which allows for production of a smooth contractile wave through the body.

The Role of TRP Channels in Sponge Contractions

Background

Previous studies have shown the necessity for extracellular Ca^{2+} in initiation of the contraction signal. This coupled with the presence of non-motile cilia lining the osculum suggest that a Ca^{2+} channel is likely involved in signal origination (Leys, 2015; Ludeman et al., 2014). A likely candidate for this is a member of the transient receptor

potential (TRP) channel family member. These compose a large family of Ca^{2+} channels, some of which have known mechanosensitive activity and which function in flow sensing on non-motile cilia (TRPP-type channels) (Basten & Giles, 2013; Kotsis et al., 2013). There are a variety of these channels in sponge genomes and transcriptomes (Srivastava et al., 2010; Kenny et al., n.d.), and previous physiological work on sponges have used known inhibitors to block contractions (Ludeman et al., 2014). The dietary flavonoid, naringenin has been shown to selectively activate TRPP2 (also known as pkd2) channels in a variety of organisms (Holzer & Izzo, 2014; Waheed et al., 2014). In vertebrate renal and endothelial tissues, these channels, along with TRPP1, localize to non-motile cilia which have flow sensing capabilities (Mohieldin et al., 2016; Retailleau & Duprat, 2014). If this basic mechanism is conserved in sponges, then treatment with naringenin should trigger a normal contraction.

Methods

Sponges were grown and prepared for imaging as described before. Sponges were left to relax on the microscope stage for 1 hour prior to treatment, as were treated by the addition of 1mL of 2x naringenin (Sigma-Aldrich #N5893) solution as described for other treatments. Concentrations of naringenin tested where 1μM,10μM, and 100μM, with DMSO treatments serving as a control. In order to image both the osculum and pinacoderm at the same time, sponges were grown on beads as described earlier and then imaged from the side during treatment with 100μM naringenin.

Results

Treatment with DMSO did not show any signs of contraction as observed in prior assays. Treatment with 1μM naringenin also did not show a strong effect, while treatment with 10μM and 100μM appeared to trigger a contraction. These contractions did appear to originate in the incurrent canals and then propagate through the body (**Figure 21a**). Imaging of the side of the sponge seems to confirm this and, though difficult to resolve cellular detail in the pinacoderm, shows a body contraction that propagates to the osculum. The body of the sponge and osculum remained contracted at the end of the 90 minutes of imaging time. Following removal of the surrounding media and thorough washing with fresh lake water the sponges did return to a relaxed state (**Figure 21b**).

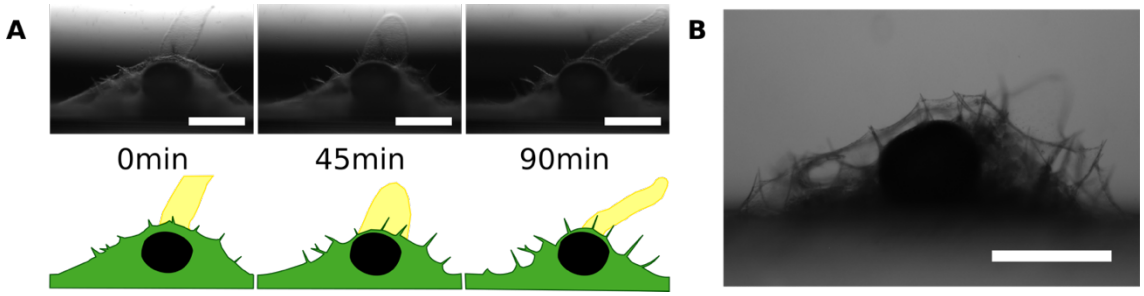

Figure 21. Activation of TRP channels leads to contraction that propagates from body to osculum. (a) Lateral imaging time series of a sponge treated with the TRP channel activating chemical naringenin. Bottom panel shows outlines of the body in green and osculum in yellow to show differential dynamics. The gemmule shown in black. **(b)** The same sponge after thorough washing and incubated overnight in lake water. Scale bars 500μm.

Discussion

Naringenin does appear to induce contractions in the sponge, which suggests that TRPP-type channels are functioning in the detection of changes of flow through the canal system. The dynamics of the contraction appear to differ slightly from normal

physiological ones. This is interpreted as a difference in the cells from which the signal is originating. Ludeman *et al.* 2014, show that the osculum is lined with non-motile cilia which appear to function in flow detection. However, staining for acetylated tubulin in *E. muelleri* has shown evidence for ciliated cells throughout the canal system (unpublished data). This could explain the unique dynamics for contractions in sponges treated with naringenin. Channels on cilia lining the incurrent canals or near the outlet of choanocyte chambers in the excurrent canals would be activated first, as water is drawn through the body. Overall, the treatment provides further evidence that flow sensitive Ca^{2+} channels function in initial signaling for contractions.

Conclusions

The most significant finding for understanding the contractile response of *E. muelleri* is that it appears to be dependent on the release of internal stores of Ca^{2+}. The dependence on Ca^{2+} for sponge contractions has been well documented (Elliott & Leys, 2007, 2010; Ludeman et al., 2014; C. L. Prosser et al., 1962; C. Ladd Prosser, 1967). However, these have primarily been done in the context of removal of external Ca^{2+} followed mechanical induction of contraction. Here, it is shown that internal Ca^{2+} stores are sufficient to physically contract, and based on the effectiveness of thapsigargin, likely originate from the ER. If activation of TRP channels or other mechanosensory channels initiates the signal to contract, then it is expected that external Ca^{2+} is required for this. Being able to block ink induced contractions with L-NAME is consistent with the role of NO production during the contraction. Inducing contractions in L-NAME treated sponges with thapsigargin suggests that Ca^{2+} release occurs downstream of NO production. This

is consistent with the osculum being a sensory structure as well as the source of the signal to contract. The reliance on internal Ca^{2+} stores for a cellular response is in no way unique to muscles, and the treatment doesn't tell us if the release is occurring in the contracting cells or ones involved in a secondary signal release. However, that contractions involve increased cytosolic Ca^{2+} levels from an internal source is consistent with homology with muscle.

Chapter 3: Contractile Tissues in *Ephydatia muelleri*

Introduction

One of the fundamental unresolved questions on sponge contractions is the identity of the tissue or tissues that provide the primary force during this behavior. Though there is, no doubt, a large amount of variation amongst the diversity of sponges my hope is that by comparing my findings in *E. muelleri* with the literature on a variety of sponge species some general principles will emerge. There are a few basic possibilities for how these contractions occur that warrant considerations; 1) The pinacoderm is comprised of a contractile epithelium, which constricts and dilates the canal system, 2) isolated cells contracting in the mesohyl could pull on the surrounding tissues, resulting changes in pressure in the canal system, or 3) the aquiferous system is inflated by the flow of water into it, and changes in flagellar beating in the choanocytes could alter the pressure on it, resulting in constriction or dilation. Using a combination of live imaging with various vital stains and descriptive imaging of sponges that are fixed in a relaxed or contracted state, I hope to better understand the structures in *E. muelleri* which are actually contracting.

Two competing hypotheses for the mechanism of contraction in sponges are contractions of the pinacocytes directly results in the contraction of the pinacoderm or contraction of the mesohyl results in the contraction of the pinacoderm through cells that

have been termed myocytes (Bagby, 1966) or actinocytes (Thacker et al., 2014; reviewed in Simpson, 1984). There are well-organized actin networks in both of these cell types (Leys, 2015; Bagby, 1966; Matsuno et al., 1988) as well as evidence for the presence of myosin (Lorenz et al., 1996). The level of organization of the putative actomyosin structures in the actinocytes of the mesohyl resulted in the hypothesis that this was the primary contractile cell in sponges (de Ceccatty, 1974). However, the contractile nature of the cells was never directly observed or measured. Studies performed using the rhythmic contractions of the demosponge *Tethya wilhelma* provided evidence that it was direct contractions of the pinacocytes which mediated the movement of the pinacoderm (Nickel, 2004; Nickel et al., 2011). This was done by performing 3D reconstructions of the contracting sponges and looking at volume change in the canal system versus the mesohyl. In this the mesohyl did not contract sufficiently in volume to mediate the change seen in the aquiferous system (Nickel et al., 2011). This does not directly rule out the role of actinocytes in regulating contractions but does provide strong evidence that the pinacoderm is a type of contractile epithelium. The actinocytes could still play an important role in regulating the force of the contraction though. This could be done through the antagonist interaction of contracting in order to provide pressure to dilate the canals. The coupling of contraction in the pinacoderm with the relaxation of the actinocytes and vice versa could function to regulate the constriction and dilation of the canals in a manner that prevents the collapse of the aquiferous system while maintaining non-turbulent flow. However, based on the evidence to date, it does seem that the primary contractile tissue in *T. wilhelma* is the pinacoderm. The pinacoderm of *E. muelleri* shows some similarities and differences with *T. wilhelma*. In the case of *E.*

muelleri it is important to make the distinction between exopinacocytes, which form the outer layer of the sponge pinacoderm and endopinacocytes, which line the canal system. Scanning electron microscopy (SEM) images of *E. muelleri* suggests that these tissues are tightly sandwiched together along much of the outside of the sponge, separated by ECM, with some transient migratory cells moving through (Elliott & Leys, 2007). Visualization of actin networks shows what appears to be large amounts of cortical actin in the exopinacocytes, whereas the endopinacocytes appear to contain linear, tissue spanning actin bundles, termed 'actin tracts', with some cortical actin visible and dense actin plaques where actin tracts align with neighboring cells (Elliott & Leys, 2007). Because of the extremely delicate nature of the pinacoderm, and the tight proximity of the exopinacocytes and endopinacocytes it is difficult to tell if the endopinacocytes comprise an intact epithelium or if they are solely adherent at the actin plaques between the actin tracts. SEM images and phalloidin staining seem to suggest that they do form an intact epithelium with the actin tracts running through each cell. It is important to note that these actin structures are only well documented in the juvenile stage of *E. muelleri* and closely related demosponges. However, transmission electron microscopy (TEM) images of members of the genus *Haliclona* have shown what appear to be organized actin filaments in endopinacocytes, which were postulated to be contractile (reviewed in Simpson, 1984).

There is also the possibility that contractions are regulated by changes in flow rate originating from the choanoderm. There is evidence that in hexactinellid sponges will arrest flagellar beating of choanocytes following stimulation (Leys et al., 2007). Asynchronous flagellar beating has also been reported for cellular sponges (Weissenfels,

1992; Asadzadeh et al., 2019; Becerro, 2012) as well as arrest of feeding current (Reiswig, 1971). There is evidence in demosponges that during strong contractions, choanocyte chambers become so condensed that flagella extend out of the chamber (Leys, 2015). Descriptive studies have also identified sphincter like cell types near the choanocyte chamber, which may function in regulating flow rate through the canal system (Hammel & Nickel, 2014). As sessile filter feeders, sponges are supported in part by the water flowing through their aquiferous system. The primary distinction to make with this proposed type of contraction, is that it would not necessarily require direct regulation by actomyosin contractility. In this, the canal system could be under constant stress, supported by the actin network, either with or without myosin II activity. The pressure of the water flowing into the body could be the primary force leading to inflation. In this case, the disruption of flow would result in the collapse of the canals. There is evidence that this may be the case, based on a few lines of evidence. There is strong staining for a vinculin homolog at the actin plaques connecting actin tracts between adjacent cells (Miller et al., 2018), which are presumed to be sites of cell-cell contacts. In other animals, vinculin localizes to adherences junctions (cell-cell contracts) under the condition of tissue stress (Bays & DeMali, 2017). In this scenario, stable attachment to the substrate and tissue stress through the pinacoderm are necessary to allow the internal pressure of water moving through the sponge to inflate the aquiferous system.

Actin Stability

Background

Actin based structures in cells are highly dynamic due to the turnover of actin monomers (G-actin). There are a variety of regulators which alter the rate at G-actin is added to actin filaments (F-actin), the rate at which G-actin is removed, and the general stability of F-actin. F-actin in the contractile bundles of muscles is fairly stable (i.e. slow turnover rate) due to the presence of capping proteins which slow the off rate of actin monomers as well as general stabilizing proteins like tropomyosin (Ono, 2010; Yu & Ono, 2006; Gokhin & Fowler, 2011). We currently do not have a way to monitor actin dynamics in living sponges (SiR-Actin (Cytoskeleton, Inc #CY-SC001) has been tried but did not show promise), so we must rely on staining fixed sponges. Latrunculin B is a cell permeable drug which disrupts actin dynamics by binding to actin monomers, preventing polymerization (Wakatsuki et al., 2001). All actin based structures in the cell have some rate of treadmilling which will vary based on a number of factors (Chandrasekaran et al., 2019). By disrupting the addition of G-actin with latrunculin B, we can gain insight into the rate at which F-actin degrades in sponge cells. There is a great deal of variation in the rate at which F-actin structures are lost in different cell types of different animals following treatment with latrunculin B. Therefore, direct measurements of concentration and time will not be very informative. However, under the assumption that structures that contain capping and stabilizing proteins will be more resistant to severing and depolymerization, structures that persist longer following treatment can be considered more stable. Studies of actin dynamics in muscles have shown that a combination of enhancers of actin dynamics and stabilizers are essential for

maintenance of sarcomeric actin organization (Gautel & Djinović-Carugo, 2016). Based on this, it is hypothesized that the contractile bundles in sponges should show a relatively high amount of stability due the resistance to severing but will likely not be the most stable structures in the animal, due to increased treadmilling.

Methods

Concentration gradient 1

Gemmules were plated and hatched as described before in a 24 well plates, with approximately 3 gemmule per well. Sponges were then washed twice with fresh LW and then treated with a specific concentration of latrunculin B (abcam #ab144291) in LW. Concentrations tested were; 29µM, 10µM, 2µM, 500nM, and 50nM, with 1µL of DMSO in 1mL of LW serving as the control. Four replicates were performed for each concentration tested. Sponges were incubated for 10 minutes and then quickly fixed in 3.7% formaldehyde in EtOH. Sponges were washed 3x with 1x PBS + 0.1% Tween-20 (PBST) pH 7.4. Sponges were then blocked in 3% BSA in PBST for 1 hour at room temperature. Actin staining was performed with Alexa Fluor™ 488 Phalloidin (ThermoFisher Scientific #A12379) diluted 1:120 in blocking solution, overnight at 4^{o}C. Sponges samples were then washed 3x in PBST and imaged.

Concentration gradient 2

Based on the finding of the first assay, lower concentrations of latrunculin B were tested. Gemmules were plated and hatched as described before in glass bottom dishes. Concentrations tested were; 50nM, 25nM, 10nM, 5nM, 2nM, and 500pM. Sponges were

treated for 20 minutes and then quickly fixed in 3.7% formaldehyde in EtOH. Staining was performed as described earlier with the addition of 1:100 Hoechst 33342 dye to the staining solution. After washing steps, sponges were mounted in mounting media. Confocal Images were acquired on an Olympus Fluoview FV3000 confocal laser scanning microscope using either a 60×/1.4 NA or 100×/1.4 NA objectives. Laser levels and acquisition setting were not adjusted for imaging controls. Images were processed in FIJI (Schindelin et al. 2012).

Time Series

Gemmules were plated and hatched as described before in glass bottom dishes. 6 dishes of sponges were treated as described above with 25nM latrunculin B. At specific time points, the sponges were quickly fixed with 3.7% formaldehyde in EtOH and stained as described above. The times tested were 3 minutes, 5 minutes, 10 minutes, 15 minutes, 20 minutes, and 25 minutes post treatment. Confocal Images were acquired on an Olympus Fluoview FV3000 confocal laser scanning microscope using either a 60×/1.4 NA or 100×/1.4 NA objectives. Laser levels and acquisition setting were not adjusted for imaging controls. Images were processed in FIJI (Schindelin et al., 2012).

Results

Following the first concentration gradient tested, only the 50nM treatment contained intact tissue. For concentrations higher than this the sponge no longer had a continuous pinacoderm or visible choanocyte chambers. For the second round of concentrations tested, most of the tissue appeared to be disrupted following 20 minutes

treatment with 5nM latrunculin B (**Figure S6**). The choanocyte chambers were still viable in the 25nM treated sponges, but most of the other tissue and cells appeared to be disrupted. Lower concentrations still showed intact pinacoderm, with clear staining of cortical actin. The actin tracts were still visible up to 10nM treatment (**Figure S7**). The time series showed that the actin-based protrusions in the cells in the mesohyl were gone after 3 minutes of treatment and there appeared to be a reduction in the number of stress fibers in the basopinacoderm. These structures were completely absent following 5 minutes of treatment. At 10 minutes the actin tracts appear to diminish, while cortical actin of the exopinacocytes and basopinacocytes is clear and microvilli collars of the choanocytes are still present. This trend continued until 25 minutes, when choanocytes appeared to start losing F-actin in their collars. At 15 minutes, the endopinacoderm appears to have lost integrity and the cells of the exopinacoderm, though still intact, became irregular in size and shape (**Figure 22**).

Discussion

The time series treatment provides valuable insight into the relative stability of various actin structures in E. muelleri. The rapid loss of actin-based protrusions of the cells in the mesohyl is not surprising if these structures are used in cell migration, as we would expect rapid turnover (Schaks et al., 2019). The actin tracts do appear to be more stable than the stress fibers seen in the basopinacoderm, but not as stable as the cortical actin in the exopinacocytes or the microvilli collars of the choanocytes. This fits the hypothesis that, if these are contractile bundles similar to what is found in muscles, they will be stable in their resistance to severing, but degrade due to increased treadmilling.

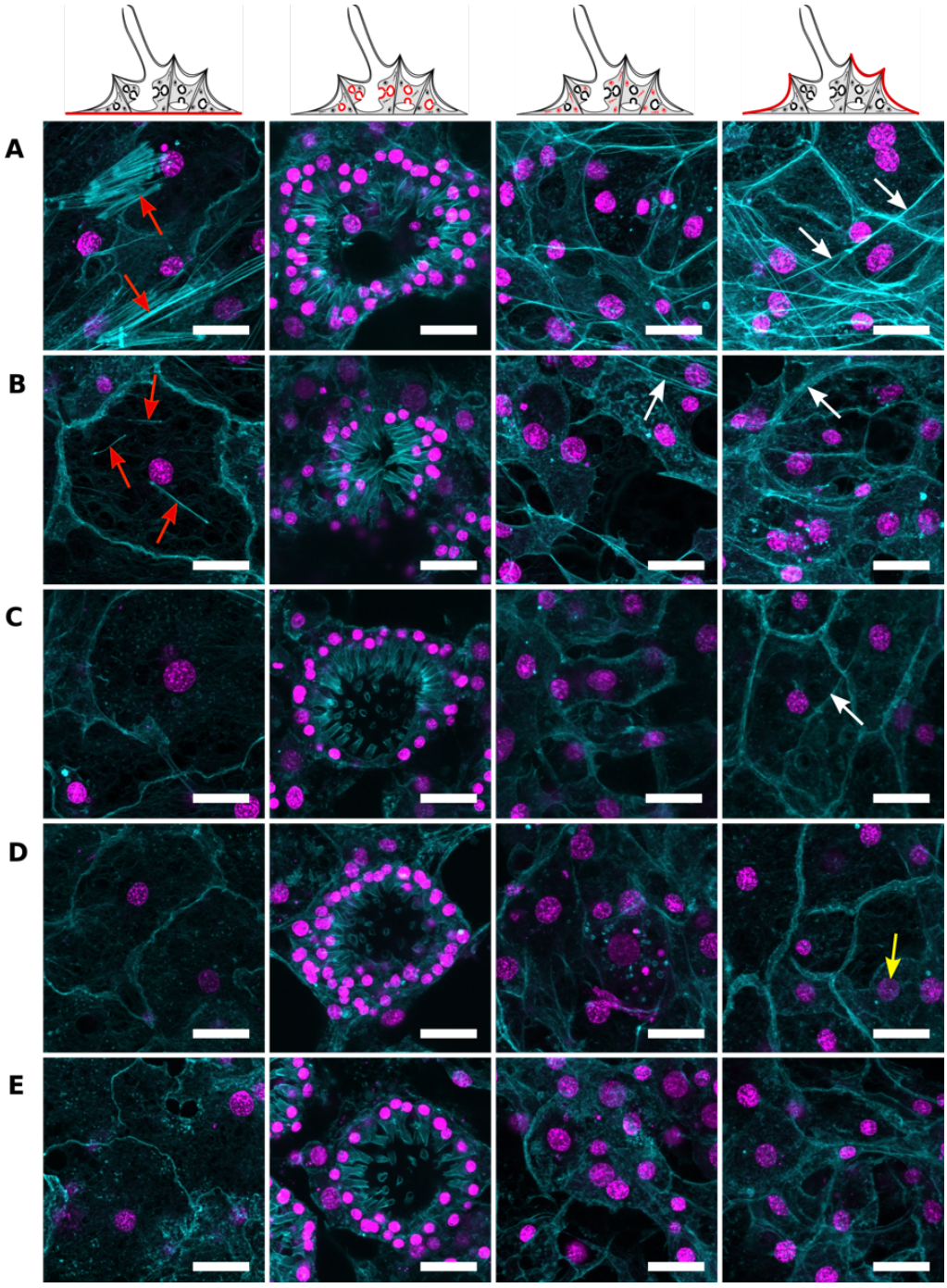

Figure 22. Time series treatment with latrunculin B. Confocal images of phalloidin labeled sponges (cyan), following treatment with 25nM for 3 minutes **(a)**, 5 minutes **(b)**, 10 minutes **(c)**, 15 minutes **(d)**, or 25 minutes **(e).** Red arrows show the reduction and loss of stress-fiber like structures in the basopinacocytes. White arrows show the reduction of the actin tracts over the first 10 minutes of treatment. Yellow arrow shows an endopinacocyte which has lost its shape in the absence of the actin tracts. This seems to correlate with highly inconsistent sizing for the exopinacocytes.. Scale bars 10μm.

Exopinacocytes

Background

Exopinacocytes constitute the outer epithelium of E. muelleri. Based on SEM and TEM imaging these cells seem to form a t-shaped morphology, in which the cytoplasm forms a large flat upper layer with a hanging nucleus in the middle (Leys & Hill, 2012; and reviewed in Simpson, 1984). Studies of small molecule movement have shown that this forms a strong barrier (Adams et al., 2010; Leys et al., 2009). There is no strong evidence that the actin tracts observed running through the pinacoderm are located in these cells, though. Rather, the actin organization appears to be large amounts of cortical actin with some overlapping of the cell contact areas. Since this is the tissue layer in direct contact with the water outside of the sponge, and it forms a tight barrier, it stains nicely with membrane dyes, which allows for live imaging of the tissue during contractions. This can be coupled with dual membrane staining with the vital stain FM™1-43 (ThermoFisher Scientific #T3163) which can be used to track vesicle release during signaling events. Prior studies have shown that treatment with FM™1-43 prevents contractions by blocking Ca^{2+} channel activity on the non-motile cilia of the osculum (Ludeman et al., 2014). However, treatment with thapsigargin has been shown to circumvent this step in the behavior, which means that this dye can be used to better understand which cells are undergoing exocytosis during a contraction. The basic setup of this experiment is to label the cells with the sponge with FM™1-43 dye and then trigger a contraction with thapsigargin. The dye is then washed away, and the sponge is counter stained with the membrane dye CellMask™ Orange Plasma membrane Stain (ThermoFisher catalog# C10045). Live imaging of the sponge will then allow tracking of

cells that have taken in FM™1-43, suggesting they underwent exocytosis during the contraction. Recycling of vesicles should then be seen as a decrease in signal during a subsequent contraction (**Figure 23**).

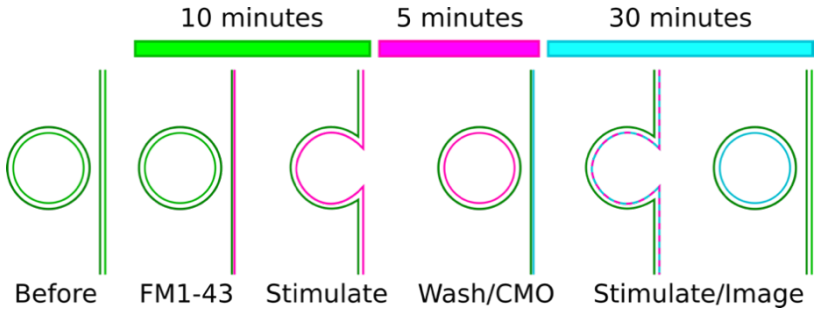

Figure 23. Workflow for dual staining experiment. Samples are first labeled with FM™1-43 dye and then a contraction is triggered in order to induce exocytosis of signaling molecules. Membrane recycling brings dye into vesicles, which protects it from thorough washing which removes general staining. Cells are then co-stained with CMO to visualize the outer membrane. This first step should identify cells which took up dye during a contraction event, suggesting an exocytosis event following induction. Duel labeled sponges are then induced to contract again, which should result in a decrease in signal as recycled vesicle release FM™1-43 dye.

Methods

Live imaging

Gemmules were plated and hatched in LW+100µg/mL ampicillin in glass bottom dishes as described before. Prior to imaging, sponges were washed with fresh LW. A working solution of CellMask™ Orange Plasma membrane Stain (CMO) (ThermoFisher catalog# C10045) was prepared by diluting stock dye 1:1000 in LW. Water was removed from the area around the sponge and replaced with 100µL of 1x CMO solution. This was incubated at room temperature for 10 minutes. In order to induce a contraction, 1mL of 1:100 sumi ink in LW was added to the dish and incubated for an additional 5 minutes at room temperature. The sponges were then washed 3x with fresh LW prior to imaging.

For control sponges, ink was omitted from the LW. Contractions were imaged using Olympus Fluoview FV3000 confocal microscope using a TRITC filter settings. Ten 0.4µm Z-sections focused on the exopinacoderm. Image stacks were taken every 60 seconds on a 1024x1024 pixel area for 30 minutes. For analysis, maximum intensity projections were made for each frame in Fiji (Schindelin et al., 2012), and measurements of cell area and position were made for time in which the contractile wave passed through the imaged area.

Dual Imaging

Gemmules were plated and hatched as described above in glass bottom dishes. A working solution of 5µg/mL of FM™1-43 dye was prepared in autoclaved LW. Sponges were washed with fresh LW and then 100µL of dye solution was added to the well containing the sponge. Sponges were incubated in dye for 1 minute at room temperature and then 1mL of 550nM thapsigargin was added to the dish without removing the dye solution. Sponges were then incubated for 10 minutes for initial contraction to occur and dye to be taken up. Solution was then removed and 100µL of 1x CMO solution (above) was added and sponges were incubated at room temperature for 5 minutes. Sponges were washed 3x with fresh LW and prepared for imaging. Contractions were imaged on Olympus Fluoview FV3000 confocal microscope, using a FITC filter setting for FM™1-43 dye and TRITC filter setting for CMO. Ten 4µm Z-sections focused on the exopinacoderm. Image stacks were taken every 60 seconds on a 1024x1024 pixel area for 30 minutes. Imaging was started prior to induction of the second contraction. After 10 minutes, 1mL of LW was removed and replaced with 1µM thapsigargin in LW. For

analysis, maximum intensity projections were made for each frame in Fii (Schindelin et al., 2012), and measurements of cell area and position were made for time in which the contractile wave passed through the imaged area.

Results

Sponges stained with CMO mainly showed staining of the exopinacocytes, with some labeling of the cells in the mesohyl, and possibly the endopinacocytes but this is difficult to resolve. The strongest staining was in the choanocytes, which prevented concurrent imaging of the choanocytes and the pinacocytes. For the first round of imaging, there appeared to be a good amount of tissue damage, likely caused by the extensive washing and the addition of the ink. This made it difficult to track individual cells, but it was obvious that in areas where the exopinacoderm was damaged, the tissue would ball up during the contraction, either because of the cells contracting or being pulled by contracting endopinacocytes, or a combination of this. In the second round, individual exopinacocytes could be tracked during the contraction. During this time, cells showed a trend of increasing in area followed by a decrease in area (**Figure 24**). During this increase-decrease cycle, the centroid of the cell moved in across the frame at a fairly constant rate in the direction of the contraction in the tissue (**Figure 24c**). During this, the initial increase is cell size is in the direction of the contraction as well (**Figure 24a**).

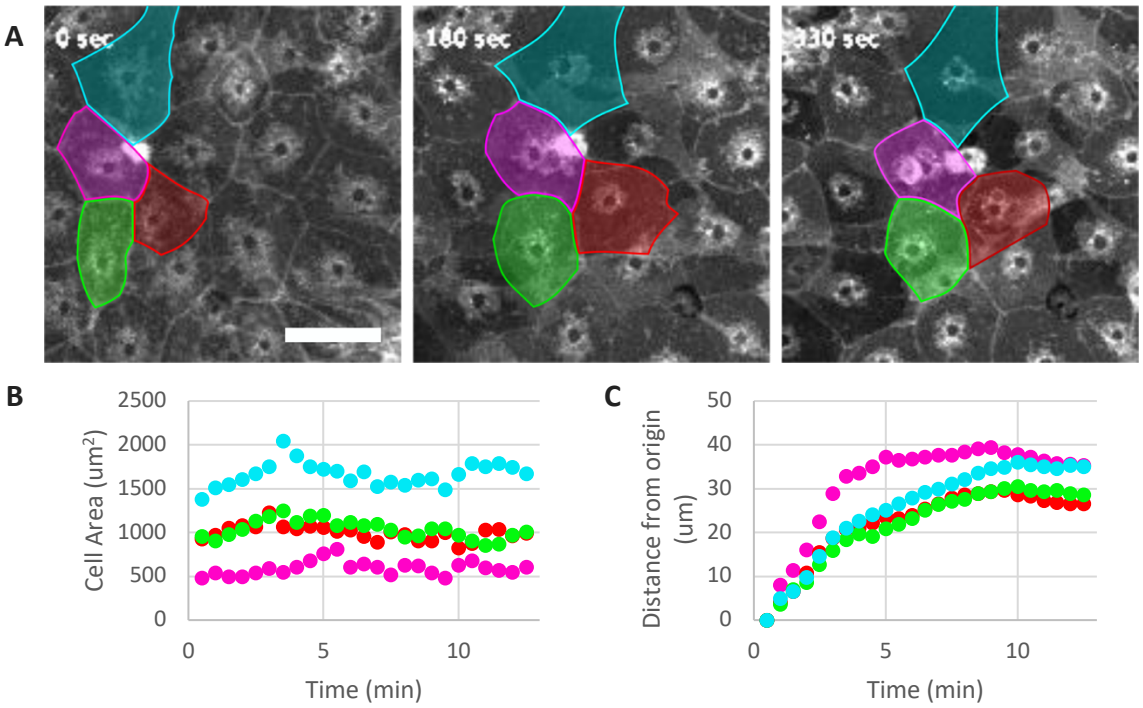

Figure 24. Exopinacocytes expand and contract while moving with a contractile wave. (a) CMO labeled cells can be identified by peripheral membrane staining and can be track as a contractile wave moves through the tissue. **(b)** Cell area measurement of single cells over the course of a contractile event shows expansion and contraction events, colors of points match outlined cells in **(a)**. **(c)** Distance traveled by the cells during the contractile event was measured based on the centroid of the cells in each frame. Colors of points correspond with cell outline in **(a)**. Scale bar 20µm.

Dual imaging

For the dual imaging experiments, it appeared that FM™1-43 and CMO primarily stained different cells. The cells that stained with FM™1-43 were located below the CMO stained exopinacocytes in the visual plane (**Figure 25a**) which could be differentiated by the presence of vesicles spanning cell boundaries of CMO positive cells.

During the contraction, there is a strong decrease in signal between 5 and 15 minutes which is followed by a period of leveling off (**Figure 25b&c**).

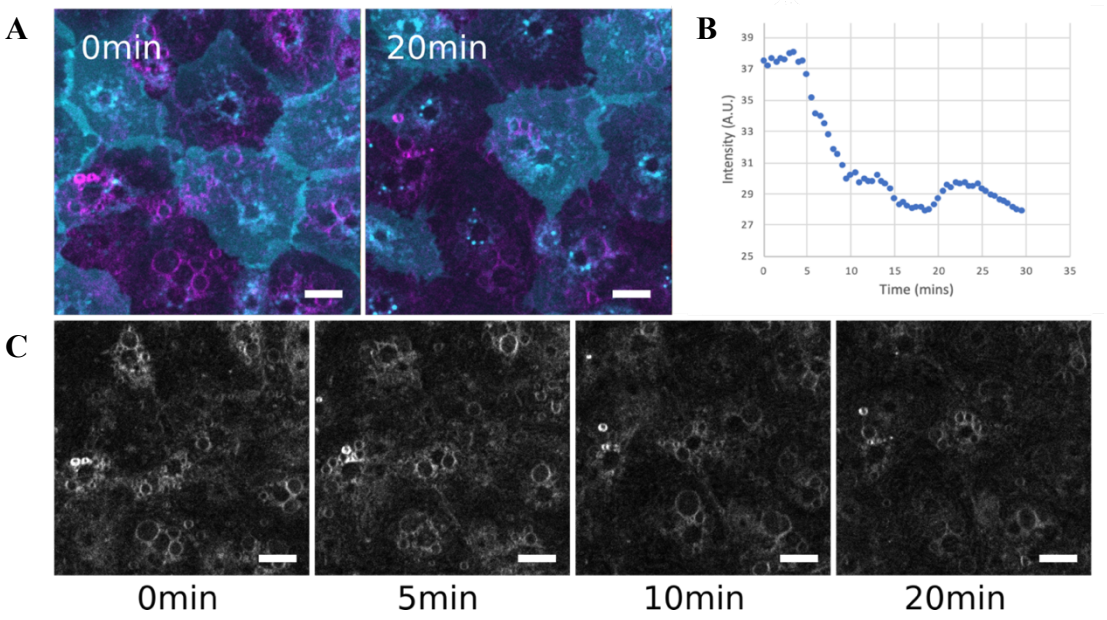

Figure 25. Dual imaging suggests exopinacocytes do not undergo exocytosis during contractions. (a) Exopinacocytes show strong staining with CMO dye (cyan) which does not overlap with FM™1-43 staining (magenta). FM™1-43 signal decreases between time point 0 and 20 minutes. **(b)** Signal intensity for FM™1-43 is steady for the first 5 minutes but then decreases dramatically over the next 10 minutes. **(c)** Time series for FM™1-43 channel shows a decreases in signal between 5 minutes and 10 minutes which correlates with the apparent movement of the FM™1-43 + cells, suggesting the passage of the contractile wave. Scale bars 10μm.

Discussion

Based on the results of the disrupted tissue, it does seem that the exopinacocytes are contractile, and will ball up when the integrity of the epithelium is compromised. However, their behavior during contraction as an intact tissue suggests that this is not the driving force for the contraction. As the wave of contraction moves through the tissue,

the cells expand in size before returning to resting size, without a noticeable decrease in area. This suggests that the contractile nature of these cells is primarily as a means of maintaining tissue integrity in the face of localized forces. This would be similar to what is seen in the dorsal epithelium of *Trichoplax adhaerens*, in which local rapid contractions are coupled with expansions of near-by cells, mediated through cortical actomyosin bundles (Armon & Prakash, 2018). The directional movement of the individual cells with respect to their position coupled with the directional expansions of the cell shape, leads to the idea that this tissue is being pulled during the contraction. These findings support the idea that the primary contractile force does not come from the exopinacocytes, but their dynamic nature helps to counteract the force experienced by the tissue.

For the dual imaging experiment, the presence of differential staining between FM™1-43 and CMO suggests that the exopinacocytes, which strongly stain with CMO, are not undergoing exocytosis during contractions, but a cell type in close proximity is. The lack of co-staining with CMO makes it difficult to understand the morphology of the FM™1-43+ cells, but based on their movement during the contraction and the regions of signal decrease (which are presumably at the plasma membrane), the cells appear to compose an epithelial sheet as opposed to being the migratory cells in the mesohyl below the exopinacoderm. If this is the case, then it is likely the endopinacocytes that are initially taking up FM™1-43 dye during a contraction and then releasing it during a subsequent one. This would suggest that these cells are undergoing exocytosis during a contraction. This could serve as a means of paracrine signaling in which signaling molecules are locally released, acting on adjacent cells, triggering a response which

involves further release of signaling molecules, allowing for propagation of the signal across the tissue. Overall, these finding suggest that the endopinacocytes are likely involved in propagation of the signal during contractions through exocytosis of a signaling molecule.

Endopinacocytes

Background

Endopinacocytes are an endothelial-like tissue that line the canals of the sponge. Previous studies have suggested that the tissue spanning actin tracts of *E. muelleri* run through the endopinacoderm (Elliot & Leys, 2007). TEM images of other sponges have also shown what appears to be organized actin bundles in the endopinacoderm (reviewed in Simpson, 1984). Based on staining for the cell adhesion marker vinculin in *E. muelleri*, these actin tracts appear to connect at points of cell-cell contact (Mitchell & Nichols, 2019). However, the cortical actin in these cells is less pronounced than the exopinacocytes making it difficult to discern whether or not these constitute a continuous epithelium or if they are composed of sickle shaped projections that extend through extracellular matrix (ECM). Based on the dual imaging data above, it does appear that these cells have a signaling role during contractions, and based on latrunculin B treatment, the actin tracts do appear to be fairly stable structures. A fundamental unanswered question of these actin tracts is whether there is direct evidence that they are contractile, i.e. if they shorten during a contraction.

Methods

Gemmules were plated and hatched as described earlier in glass bottom dishes. Six dishes containing 3 gemmules each were used. After hatching sponges were washed with LW and examined for presence of a canal system and choanocyte chambers. Three of the dishes (labeled 'relaxed') were treated with 50µg/mL of L-NAME in LW and incubated overnight at room temperature, with on refresh in the morning. Untreated sponges (labeled 'contracted') were treated with 500pM thapsigargin in LW just prior to fixing. After treatment, one of the contracted dishes was monitored by time lapse video to watch for signs of contraction. Once the sponge was completely contracted (approximately 20 minutes) all sponges were fixed in 3.7% formaldehyde in EtOH. Sponges were then washed 3x in 1x PBST and then blocked in 3% BSA in PBST for 1 hour at room temperature. Sponges were then treated with 1:1000 anti-EmVin1 in blocking solution for 1 hour at room temperature. Sponges were then washed 3x in PBST and secondary solution of 1:500 anti-rabbit AF™488 (abcam #ab150081), 1:120 Alexa Fluor™ 568 phalloidin (Life Technologies #A12380), and 1µg/mL Hoechst 33,342 dye in blocking solution. Sponges were incubated for 45 minutes in the dark at room temperature. Sponges were then washed 3x with PBST and mounted with mounting media. Samples were imaged with Olympus Fluoview FV3000 confocal microscopy with z-stacked through the pinacoderm using a 40x/1.25 N.A. objective, focusing on the same body region of each sponge. Each sponge in each dish was imaged. Images were then processed in Fiji (Schindelin et al., 2012) and then distance along the actin tract between two vinculin plaques was measured. An ANOVA was performed between biological and technical replicates to see if there was any significant variation in the measurements and

then a one-tailed T-test was used to compare pooled samples of relaxed and contracted sponges.

Results

The results of the ANOVA suggest that there is no significant difference between technical or biological replicates for both relaxed (**Table 1**) and contracted sponges (**Table 2**).

Table 1. ANOVA results for biological and technical replicates of relaxed sponges

Source	Df	Sum of Squares	Mean Square	F-Stat	P-Value
Between Groups	8	85239.8501	10654.9813	1.1147	0.3569
Within Groups	141	1347776.0976	9558.6957		
Total:	149	1433015.9477			

Table 2 . ANOVA results for biological and technical replicates of contracted sponges

Source	Df	Sum of Squares	Mean Square	F-Stat	P-Value
Between Groups	8	81110.9225	10138.8653	1.5854	0.1342
Within Groups	141	901734.6854	6395.2815		
Total:	149	982845.6079			

Based on this, all measurements for each treatment were pooled. A one-tailed T-test revealed that the mean value for the actin tracts in the contracted sponges is significantly lower than that of the actin tracts in the relaxed sponges ($t(288)=4.44$, $p<<0.001$). The mean for contracted actin tracts is 80.32% of the mean for relaxed sponges (**Figure 26**).

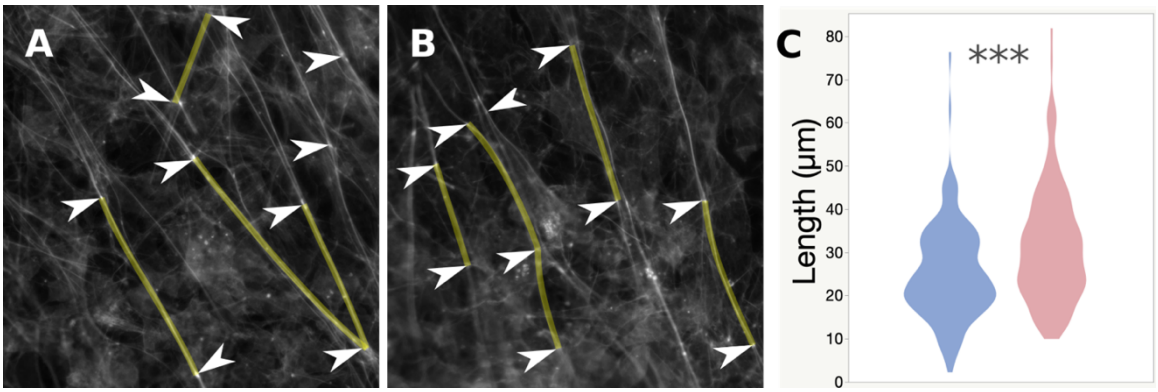

Figure 26. Actin tracts shorten during a contraction. Sponges were fixed and stained with phalloidin in either relaxed or contracted states. **(a)** Example of a relaxed sponge, white arrows show adhesion plaques along actin tracts. Measurements were taken of highlighted regions between two adhesion site on a single tract. **(b)** Example of a contracted sample. Images were taken and measurements were made in analogous regions of the body of each sponge. **(c)** Plot of measurements made for contracted (blue) and relaxed (red) sponges show a significant decrease in contracted sponge ($n=120$, $p<<0.001$).

Discussion

The actin tracts of the endopinacoderm clear shorten during the contractions. This is strong evidence that they are contractile structures. However, because of the slow rate of decrease (~20% of length in 20 minutes) this does not rule out shortening due to changes in actin dynamics. Based on the latrunculin B treatments, this time is sufficient for actin filament shortening through increased depolymerization, severing, or decreased polymerization to explain the difference in length. Because of this, it is important to look

for the presence of myosin in these filaments. If myosin II is present then a similar experiment can be performed, utilizing an inhibitor of myosin activity, such as blebbistatin (Farman et al., 2008). This should help clarify whether the shortening is due to contraction. The finding that these structures shorten also does not clarify whether the tissue is under constant stress, and contracts due to decreased pressure from flow, or if the shortening actively generates the force to propel water out of the aquiferous system. Further experiments are needed to clear this up, but the length of the shortening of the actin tracts compared to the size changes in the exopinacocytes strongly suggests that the shortening of the first pulls the second along. Another possible mechanism that had been suggested is that the pinacoderm is under stress between points of adhesion to the spicules. For this, the actin tracts would contract to create negative pressure though the body, which helps to inflate it. In this mechanism, relaxation of the contracted bundles, would be coupled with changes in flow rate to allow for the canals/body to contract. The shortening of the actin tracts suggests that this is an unlikely mechanism and that the lengthening of tissue between the spicules is likely through the exopinacoderm.

Choanocyte Chambers

Background

There is only direct evidence that hexactinellid sponges arrest flagellar beating (Leys & Meech, 2006; Leys et al., 1999), but this is evidence that choanocyte chambers of other sponges do contract as well as alter the synchronicity of their beating (Weissenfels, 1992; Becerro, 2012; Reiswig, 1971). There have also been sphincter-like cells identified in association with the choanocyte chambers, which could contract or

relax to regulate flow independent of flagellar beating (Hammel & Nickel, 2014). These factors could play a role in the contractions by either changing the pressure within the canal system and/or simply generating the direct force by contracting. For the first possibility, the force of the water through the aquiferous system would be generating force that inflates the canals. For this hypothesis, the canal system would be under constant stress and the slowing in incurrent flow, would result in constriction of the canal system. The constriction of the canal system, either through or resulting in the shortening of the actin bundles in the endopinacocytes, could occur in a myosin independent fashion, though this is not necessary. So, if actomyosin contractility is shown to be necessary for contraction it doesn't directly rule out this possibility, however, if contractions are actomyosin independent, then this would be the most likely mechanism by which they occur. For the second possibility, in which direct contraction of the choanocyte chambers is coupled with contraction through the mesohyl, it is expected that the choanocyte chambers would reduce size as well as move closer together during a contraction. This mechanism would also result in changes in flow rate, due to a point of constriction, but the primary contractile force would come through the choanoderm. Apart from documented contractions of choanocyte chambers in a variety of sponges, colonial choanoflagellates have been shown to undergo orientation flips and shape change through collective contraction of apical actomyosin bundles (Brunet et al., 2019). The adhesion mechanism between these cells appears unique, which suggests an independent origin, but tightly regulated constriction of the apical region of the cell could be a fundamental trait of choanoflagellate-like cells and may be retained in choanocytes. If this is the case,

then it would strengthen the argument for homology between these cell types and would provide a possible mechanism for body movement in the stem animal lineage.

Methods

Gemmules were plated and hatched as described above in glass bottom dishes. In order to induce strong contractions, sponges were treated with 1μM thapsigargin in LW as described earlier. Time lapse images were taken to monitor progression of contraction, and when sponges appeared to be at the point of maximum contraction through the choanoderm, they were fixed in 3.7% FA in EtOH as described earlier and stained with phalloidin AF™488 (Life Technologies, 1:120) and Hoechst dye (33,342 1μg/mL) using the standard protocol. Images of comparative regions of the choanoderm in relaxed and contracted sponges were taken and measurements of the area of choanocyte chambers were made using Fiji (Schindelin et al., 2012). Measurements of intra-choanocyte chamber movement were made by measuring the distance of the centroid of the choanocyte chamber to that of its nearest neighbors that were located on the same side of an excurrent canal (minimum 3). Statistics were performed in R.

Results

During strong contractions the area of individual choanocyte chambers significantly decreases ($t(60)=1.67$, $p<<0.001$) (**Figure 27**). The mean area of contracted choanocyte chambers was 253.1μm^2 while the mean area of relaxed choanocyte chambers was 299.3μm^2, representing a 15.43% decrease in size. This decrease in size

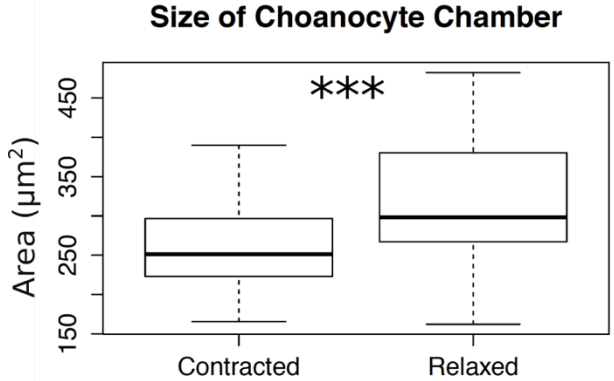

Figure 27. Size of choanocytes significantly decreases. The area of choanocyte chambers of either relaxed or contracted sponges were measured based on phalloidin and Hoechst staining. Contracted sponges contained significantly smaller choanocyte chambers compared with relaxed ones (n=62, p<<0.001).

would account for an average of a 1.57µm decrease in the diameter of each choanocyte chamber.

The distance between the chambers did not significantly change though (T(70)=1.67, p=0.052) (**Figure 28**). The average distance between the center of contracted choanocyte chambers was 21.1µm while the average distance between the center of relaxed choanocyte chambers was 22.6µm. Given the number of chambers in a linear orientation relative to the movement of the contraction, this amount of change is insufficient to generate the rate of bulk movement observed in the exopinacocytes, which are displaced between 30-40µm (data above).

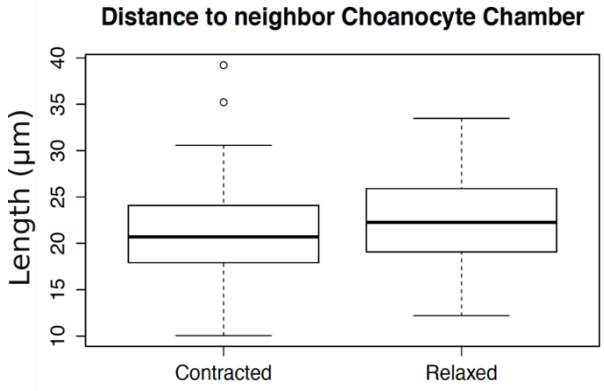

Figure 28. Distance between choanocyte chambers did not significantly decrease during a contraction. The distance between the centroid of a choanocyte chamber and that of at least 3 adjacent chambers, without crossing a canal, was measured in contracted and relaxed sponges. The centers of the contracted chambers were not significantly closer together (n=72, p=0.052).

Discussion

Based on these findings, the choanocyte chambers clearly constitute a contractile tissue. However, the mixture of the insufficient size change, especially under physiological conditions, and the lack of significant change in the distance separating them, strongly suggests that they do not generate the primary force during sponge contractions. This does not rule out that changes in flow are responsible for the contractions, but the source of the contraction is not likely to be a result of the physical movements in the choanocyte chambers and mesohyl. This adds further weight to the idea that the actin tracts shortening is pulling on the canals to constrict them. This could be through actomyosin contractility or via actin dynamics, which changes in flow leading to the shortening. If it is actomyosin contractility that is providing the force to constrict the tissue, this could either be activated upon sensation of a contractile cue or it could be continual activation which is normally counteracted by the force of flow through the system. These two things do not need to be mutually exclusive, i.e. increased activity results in constriction of the canal and relaxation leads to dilation, but whether in-flow rate or myosin activity is the driving force remains unclear.

Unattached Sponges

Background

Sponges are sessile filter feeders which means that they attach to a substrate and actively draw water through their body. *E. muelleri* forms large actin bundles, which resemble stress fibers at focal adhesions, in their basopinacoderm (Leys et al., 2009; Schippers & Nichols, 2018; Mitchell & Nichols, 2019). These increase in number when

grown in a rocking environment and form at the organism substrate interface (Mitchell & Nichols, 2019) which both suggest that these function in stable attachment. In terms of contraction, these likely provide traction force, to oppose the contracting tissue and prevent collapse of the aquiferous system. In order to better understand the mechanism of contraction, it would be beneficial to disrupt this adhesion. During processing of gemmules, we routinely washed them in hydrogen peroxide in order to remove surface bacteria prior to plating. The result of this is that some gemmules would float to the surface, which were usually discarded. While plating a very large number of cleaned gemmules it was observed that some of these floating gemmules hatched and developed at the air-water interface. This is likely the result of produced O_2 gas getting caught in grooves on the gemmule casing, increasing buoyancy. Interestingly the surface tension of the water appears sufficient for development of the sponges, which take on an inverted orientation (osculum is oriented towards the bottom of the dish). These sponges develop to juvenile stage, just as attached ones (similar size, clear canal system and osculum, and choanocyte chambers). At juvenile stage, these sponges can be seen slowly moving around the dish, which also suggests that there is flow through the body with excurrent flow propelling them. Because of the unique way these sponges grow, they are beneficial for 1) seeing if they develop a clear apical and basal pinacoderm, 2) do the basopinacocytes contain stress fiber-like structures, and 3) Do these sponges contract normally when stimulated?

\

Methods

Approximately 100 gemmules were isolated and treated with 1% H_2O_2 in LW for 3 minutes at room temperature and were then rinsed several times with fresh LW in a 40μm cell strainer. All gemmules were then placed in ~20mL LW in a petri dish. After hatching, floating sponges were carefully transferred to a fresh petri dish, avoiding inadvertent attachment to any substrate.

Contraction imaging

For live imaging, sponges were carefully transferred to glass bottom dishes which contain an ~100uL well at the bottom. Under the dissecting scope, water was removed from the upper part of the dish until the sponge was floating in the well at the bottom (care was taken to avoid it contacting any surface during liquid removal). On the inverted microscope, additional liquid was removed, making sure that the sponge osculum did not contact the bottom of the well, and the sponge was centered by gently pipetting the solution around it. For induction of the contraction, 1.5μM thapsigargin was prepared in LW. A 50μL drop was then placed outside of the well on the far end from the sponge. A sterile needle was then used to drag the drop to make contact with the well. This was done to avoid a rapid increase in volume in the well moving the sponge laterally and vertically out of the frame. Time lapse video was taken at 30 second per frame for 81 frames with extended exposure time per frame so that the lamp could be set as low as possible. This was done to prevent drying of the small volume of liquid that the sponge was in.

Immunostaining

Sponges were carefully transferred into 3mL of 3.7% formaldehyde in EtOH and were fixed for 1 hour at room temperature. Sponges were then washed 3x with 1x PBST and blocked for 1 hour at room temperature in 3% BSA in PBST. Sponges were then treated with anti-EmVin1 (1:500) in blocking solution and incubated at room temperature for 1 hour. Sponges were washed 3x with PBST and secondary was added containing; anti-rabbit AF™488 (Life Technologies, 1:500), Alexa Fluor™ 568 Phalloidin (Life Technologies, 1:120), and Hoechst dye (33,342, 1μg/mL) in blocking solution. Sponges were incubated for 45 minutes at room temperature in the dark. Sponges were then washed 3x with PBST and mounted with mounting media in glass bottom dishes to maintain three-dimensional structure. Sponges were also stained for just DNA and actin using the same method described without the addition of primary or secondary antibodies.

Results

Contraction

Unattached sponges treated with thapsigargin visibly contracted. Due to technical limitations imposed in imaging these sponges, it is difficult to resolve the detail necessary to make comparative measurements of canal dynamics as seen in attached sponges. However, it is clear that the tissue draws into the body (**Figure 29**). However, over the timescale of 90 minutes the tissue did not relax and return to the original shape. This suggests that the contraction could have resulted in collapse of the aquiferous system.

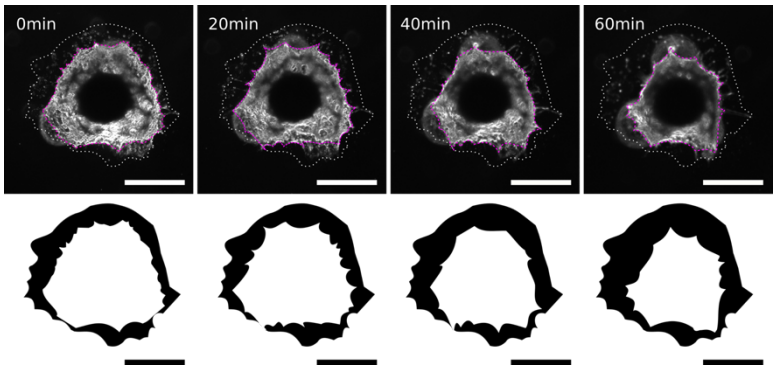

Figure 29. Unattached sponges can still contract their body. Time lapse series of an unattached sponge induced to contract by the addition of ~500nM thapsigarin. Outline of sponge established by the spicules is outline with white dotted line while the body tissue of the choanoderm is outlined in magenta. Bottom panel is an overlay of the two showing contraction of the body tissue. Scale bars 500μm.

Immunostaining

Staining for vinculin reveals localization to the pinacoderm in the floating sponges. This can be resolved as colocalization with actin in the tissue between spicules (**Figure 30**). The tissue opposite the gemmule is where the osculum extends (faintly visible in bottom right corner), suggesting this is the region representing the apical pinacoderm. There is very strong staining for EmVin1 along this tissue. Looking at both actin staining and vinculin staining reveals that there is no evidence for the actin bundles in the tissue opposite the osculum. Actin staining shows cells that have the morphology of basopinacocytes in this tissue but there is no evidence of stress fiber-like structures

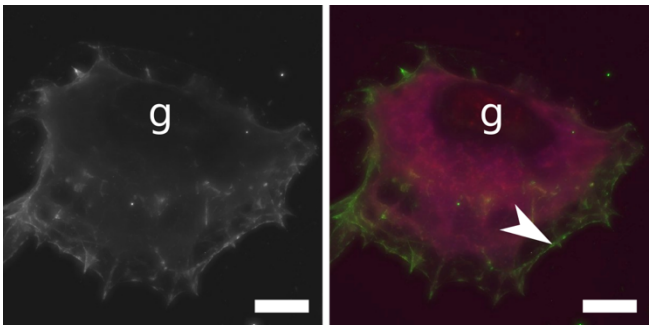

Figure 30. EmVin1 localizes to apical pinacoderm in unattached sponges. Immunostaining of unattached sponge for EmVin1 (green) with phalloidin (red) as a counterstain. Strong staining is seen along the tissue opposite the gemmule (g). Scale bars 200μm.

(**Figure 31**). The actin tracts are clearly visible through the body of the sponge though (Figure 31B – orange arrowheads).

Discussion

One hypothesis for the mechanism of contraction for *E. muelleri* is that constant contraction of the pinacoderm leads to negative pressure through the aquiferous system, which is supported by the incurrent flow of water through the body. For this mechanism to work, there would need to be opposing traction forces at the attachment to the substrate coupled with cementing of the spicules in order to prevent collapse of the canals. The finding that there is no evidence for the large adhesion structures in the basopinacocytes coupled with the ability of the sponge to considerably reduce its size when induced to contract, suggests that this is not the primary mechanism by which *E. muelleri* contracts. This can be coupled with the finding that EmVin1 staining along the pinacoderm is present in unattached sponges, suggesting that it is a constitutive part of these adhesion structures rather than one that is recruited when the tissue is under stress (Bays & DeMali, 2017). That the sponges remained contracted for the duration of imaging suggests that induction of the contraction caused collapse of the aquiferous system. Combining this with the finding that actin tracts shorten during the contraction suggests that the force of contraction is coming from the endopinacoderm, which contains these structures. Under normal, attached, conditions the contraction of the body would be restricted by opposing force from the attachment to the substrate and the stability of the spicule skeleton. Taken together with the previous findings, it is likely that the

endopinacoderm is the primary contractile tissue responsible for this behavior in *E. muelleri*.

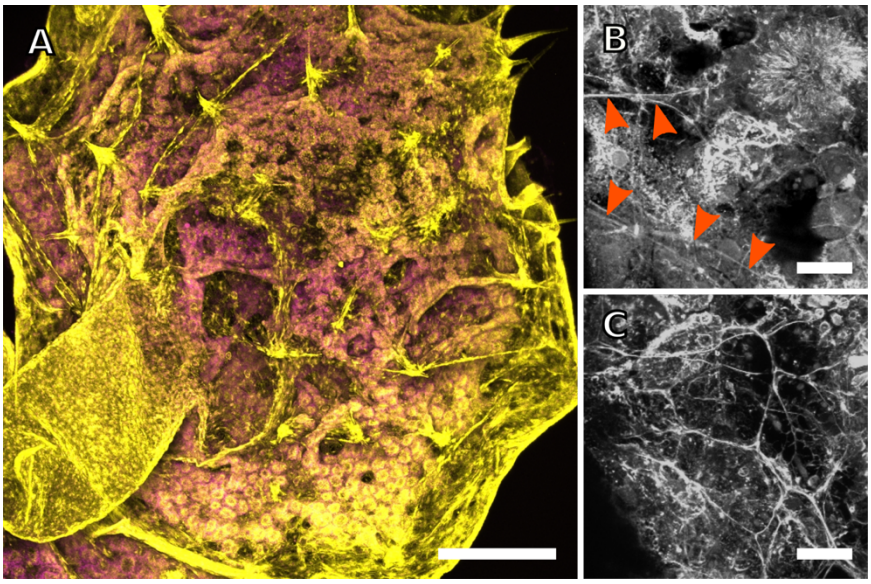

Figure 31. Actin organization resembles attached sponge with absence of stress fiber-like structures. Unattached sponge was stained with phalloidin (yellow) and Hoechst (magenta) to visualize the actin and nuclei respectively. **(a)** Full body image of the apical pinacoderm, with osculum visible in the center. Organized actin bundles can be seen running through the tissue around the body. **(b)** Higher magnification image of actin structures, showing actin bundles (orange arrowheads) which run between dense actin plaques, resembling the actin tracts. **(c)** Actin staining of the tissue opposite the osculum shows cortical actin and cell morphology similar to basopinacocytes, but no stress fiber-like structures are visible. Scale bars 200µm **(a)** 10µm **(b&c)**.

Contractions During Development

Background

Based on these findings, both the choanocytes and endopinacocytes significantly contract during contractions. This coupled with the floating sponges and movement of exopinacocytes suggest that the contractions are the result of actin constriction rather than passive movement resulting from decreased force on the tissue. In order to better understand which of these tissues generates the primary force of contraction it is valuable

to view them in the absence of the other's influence. The pinacoderm, including the actin tracts, develop prior to the development of choanocyte chambers. Based on this, it is possible to see if sponges are able to contract prior to the development of choanocyte chambers. However, the actin tracts are not fully developed, and canals have not formed at this time, which means that there is likely limited contractile tissue present. In order to progress development of this tissue, while inhibiting development of choanocyte chambers, sponges can be treated with hydroxyurea. Treatment of *E. muelleri* with hydroxyurea prior to the formation of choanocyte chambers has been shown to prevent them from forming, without greatly affecting the development or maturation of other tissues (Peña et al., 2016; Rozenfeld & Rasmont, 1977). This should provide insight into the ability of the pinacoderm to contract the body of the sponge, without the influence of choanocyte chambers.

Methods

Early tent-stage contractions

Gemmules were plated on clear beads and hatched in 6-well format in LW+100µg/mL ampicillin as described earlier. Gemmules were monitored daily for hatching and attachment to the bead. As soon as this occurred, the beads were rotated in the well so the tent-stage sponge could be viewed from the side on an inverted microscope. Contractions were induced using 80µM glutamate in LW, and time lapse images were taken with a 30 second frame rate for 181 frames.

HU treated sponges

Gemmules were plated and grown in 6-well format in LW+100µg/mL ampicillin as described earlier with 8 hour staging. Following hatching, sponges were monitored closely for spreading of tissue from the gemmule and early development of choanocyte chambers. As soon as the first plate of sponges showed choanocytes, the second plate was treated with 100µg/mL hydroxyurea in LW, which was refreshed daily. Following 2 days further development sponges were prepared for induction of contraction by washing and staging on the microscope. Contractions were induced with 80µM glutamate in LW. Time lapse images were taken with a 30 second frame rate for 181 frames.

Results

Early tent-stage contractions

Tent stage sponges did show a response to treatment with glutamate which should trigger a contraction. This was seen as what appeared to be a swelling of the apical pinacoderm which was not seen in LW treated controls (**Figure 32**). There does appear to

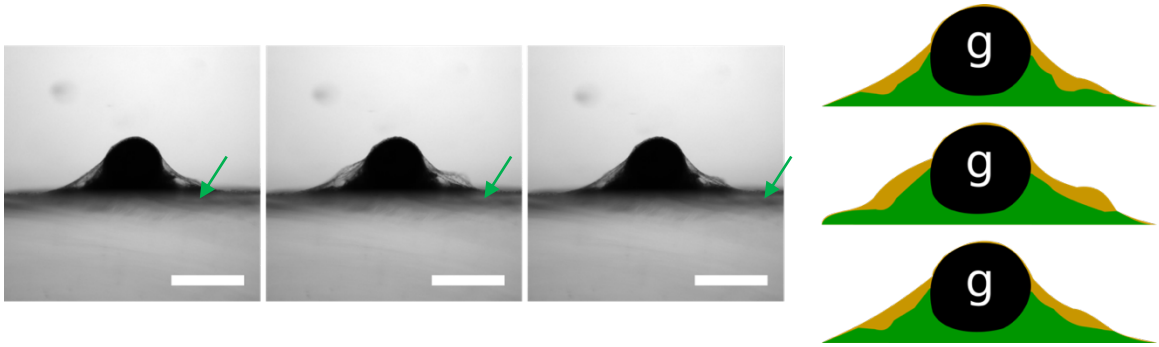

Figure 32. Tent stage sponges show a response to 80µM glutamate. Time series of a tent stage sponge treated with glutamate to induce a contraction. Frames represent time points 0, 45, and 90 minutes. Right panel shows outlined of apical tent (yellow) and internal tissue (green) with the gemmule in black. The internal tissue can be seen straightening between the attachment point and gemmule, which corresponds with extension of the apical tissue. Scale bar 500µm.

be a straightening of the lower tissue layer which runs up to the gemmule. This straightening seems to correspond with the region of inflation. During this developmental stage, there are no spicules that create anchor points for the sponge tissue. In this, the apical pinacoderm appears to wrap around the gemmule, while the lining of the cavity below it is attached to the gemmule. This internal lining likely develops into the endopinacoderm as canals form through the body. The straightening of this tissue suggests that it is contracting, which would generate pressure on the apical pinacoderm, through the water in the cavity. This is likely what leads to the swelling.

HU treated sponges

Sponges treated with hydroxyurea contained reduced canals and no visible choanocyte chambers, but still contained a small osculum. Hydroxyurea crystals precipitated out of solution during treatment and appeared to be taken up by the sponge (either intracellularly or within the mesohyl) creating dark puncta throughout the body.

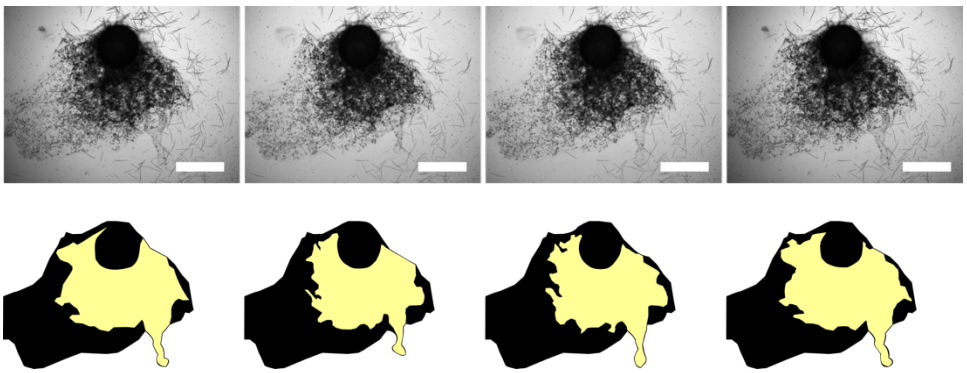

Figure 33. Sponges lacking choanocyte chambers can still contract. A sponge was treated with hydroxyurea prior to formation of choanocyte chambers to prevent their development. Contraction was induced with 80μM glutamate and frames represent time points 0, 25, 30, and 90 minutes. The middle two panels represent the transition from contraction to relation. As fully developed canals are absent, bottom panel represents the outline of the primary body of the sponge. Scale bars 500μm.

These regions were used to identify the bulk of the body tissue, in which changes in size could be monitored. Following treatment with glutamate, this body region reduced in size and then returned to normal over the same timespan observed in normal contractions (**Figure 33**). During this time, the osculum was also seen to slightly constrict and move.

Discussion

In both cases in which choanocytes are absent, treatment with glutamate appears to have elicited a response. In the early tent-stage sponges, this initially appears to be contradictory to the expectation, in that the apical pinacoderm swells out. However, as explained above, the structure of the sponge tissue at this stage is consistent with this being a contractile response. The lack of excurrent canals and an osculum means that a contraction through the body is not able to expel water from the sponge. Since the sponge tissue is still supported by water at this stage, constriction of the tissue that will give rise to the canals inside the sponge will generate force on this water, resulting in swelling. The sponges that were treated with hydroxyurea prior to choanocyte development also showed what appeared to be a contractile response in that the primary body area constricted and then returned to the original size. The absence of choanocytes means that there is no active incurrent flow through the sponge. Therefore, the reduction in size followed by the return to normal size suggests that the tissue is actively contracting during the reduction which must be creating counter stress on other tissues sufficient to generate negative pressure during the relaxation in order to refill the tissue with water. This is consistent with the model in which the endopinacoderm actively contracts while the exopinacocytes reactively expand and contract in order to maintain tissue integrity.

Transgelins in Ephydatia muelleri

Background

In order to get a better understanding of structure of the contractile tissue in *E. muelleri*, the transcriptome (Peña et al., 2016) was searched for orthologs for various structural proteins involved in the contractile apparatus of muscles from a variety of animals. Transgelins are actin bundling and gelling proteins that are abundant in muscles in a variety of animals, though they are not restricted to them (Shapland et al., 1988; Prinjha et al., 1994; Camoretti-Mercado et al., 1998; Dvorakova et al., 2014). Within the family there are proteins that appear to be restricted to muscles such as, SM22alpha (Lees-Miller et al., 1987; Li, Miano, et al., 1996; Li, et al., 1996), MP-20 (Ayme-Southgate et al., 1989), unc-87 (Goetinck & Waterston, 1994), and myophillin (Martin et al., 1995). The basic structure of these proteins is consistent in that the N-terminus contains a CH domain and the C-terminus contains a single calponin family repeat (Assinder et al., 2009). *E. muelleri* has three transgelin like proteins in its transcriptome, all of which have this domain structure. Aligning these with other transgelin proteins from a variety of animal, these all cluster together suggesting lineage specific expansion (**Figure S8**).

These were arbitrarily named EmTAGLN1, EmTAGLN2, and EmTAGLN3. Based on the transcriptome data, EmTAGLN1 showed the lowest expression levels, while EmTAGLN3 showed the highest. EmTAGLN2 and EmTAGLN3 recombinant proteins expressed well in *E. coli* and were soluble, whereas EmTAGLN1 did not. For this reason, custom antibodies were raised for these two proteins. As transgelins tend to be found at contractile actin structures in other animals, the first question is, do these

orthologs show the same pattern in E. muelleri? If they do associate with specific actin structures, are there specific structures that each associate with, or cell types in which they are expressed, or is there overlap between them?

Methods

Cloning, Expression, and Purification

EmTAGLN2 and EmTAGLN3 were cloned into the pET His6 GST TEV LIC cloning vector (Addgene, plasmid #29655) from the E. muelleri cDNA library using the following primers;

EmTAGLN2

Forward - TACTTCCAATCCAATGCAGAAGTGCAGCAAAAGCTAGCAG

Reverse - TTATCCACTTCCAATGTTATTAGACCACAAGGCATGCACTAA

EmTAGLN3

Forward – TACTTCCAATCCAATGCAAAGGGATATGGCATGACTGC

Reverse - TTATCCACTTCCAATGTTATTAAGGTCCGTGAGATGCCTAA

This plasmid was the used to transform NEB 5-alpha Competent *E .coli* (High efficiency) (New England Biolabs #C2987). Transformed cultures were grown for plasmid extraction and establishing a freezer stock. Purified plasmid was sequenced off the pGEX site to confirm proper insertion and then transformed into Rosetta strain *E. coli* for expression. 2L of each culture was grown to an optical density of 0.4 and then expression was induced with addition of 250µM IPTG. Expression was carried out for 3 hours at 30^{o}C and purification was performed with Pierce Glutathione resin (ThermoFisher Scientific #16101) following the manufacturer's protocol. Purified

recombinant proteins were sent to Pacific Immunology for injection into chickens. IgY was purified from egg yolk using a standard ammonium sulfate precipitation protocol (Wallman et al., 1990) and then affinity purified against recombinant protein bound to AminoLink Coupling Resin (ThermoFisher Scientific #20381).

Western Blot

Western blots were performed using sponge whole cell lysates prepared by the scraping of approximately 50 individual juveniles directly into SDS PAGE loading dye (1 M Tris, pH 7.0, 20% SDS, 20% Glycerol, 0.02% bromophenol blue and 2.5% β-mercaptoethanol), followed by hand homogenizing and boiling for 10 minutes. Proteins were run out by SDS PAGE on a 10% tris-glycine acrylamide gel at 200V for approximately 40 minutes and then transferred to a PVDF membrane at 350mA for 25 minutes. The membrane was washed with 1xPBST and blocked in 5% Milk in 1xPBST for 1 hour at room temperature. The membrane was cut in strips and blotting was performed using a small dilution series for each antibody as well as competing each blot with recombinant protein.

Immunostainings

Gemmules were plated and hatched in glass bottom wells in LW+100μg/mL ampicillin as described earlier. At day 4 post hatching, sponges were fixed in 3.7% formaldehyde in EtOH for 50 minutes at room temperature. These were then washed in 1xPBST and blocked with 3% BSA in 1xPBST for 1 hour at room temperature. Primary was applied in blocking solution, with a dilution of 1:250 for anti-EmTAGLN2 and 1:500 for anti-EmTAGLN3, and samples were incubated for 1 hour at room temperature.

Secondary, Goat anti-Chicken IgY AF™ 647 (Invitrogen #A32933) was applied in a 1:1000 dilution, with 1:120 phalloidin AF™ 568 (ThermoFIsher Scientific #A12380), and 1:100 Hoechst dye in blocking solution. Samples were then incubated for 45 minutes at room temperature in the dark and then thoroughly washed and mounted in mounting media. Competition stainings were also performed with the addition of recombinant EmTAGLN2 and EmTAGLN3 for each antibody.

Results

The western blot showed bands of the correct size for both proteins as well as a few extra higher molecular weight bands (**Figure S9**). The highest bands on each membrane do appear to occur at around twice the size of the proteins and may represent dimerization that was not disrupted by the SDS PAGE. The predicted size for EmTAGLN2 is 20.8kD and for EmTAGLN3 it is 21.1kD. The lowest bands are

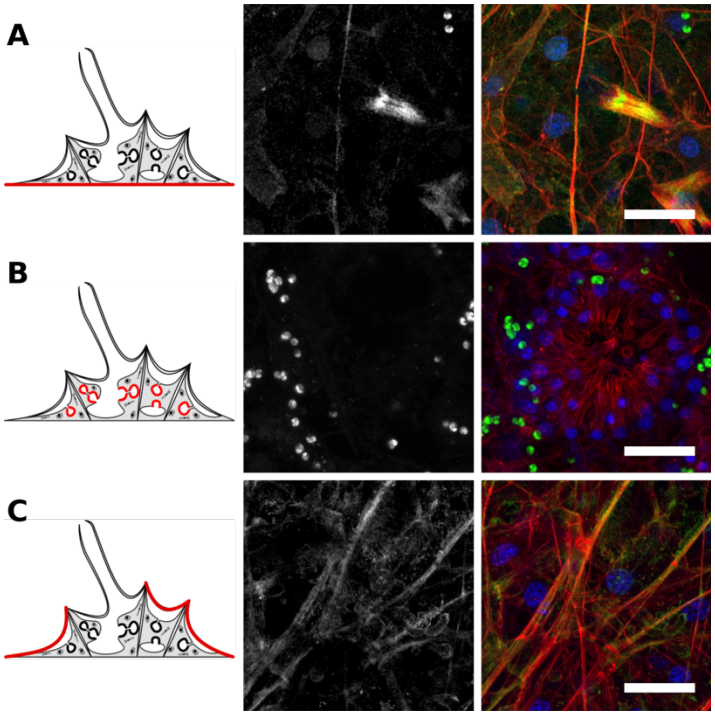

Figure 34. Immunostaining for EmTAGLN3 shows localization to major actin structures. Confocal images through sponges stained for EmTAGLN3 (green), actin (red), and DNA (blue). Green channel alone in gray. **(a)** The attachment epithelium shows strong EmTAGLN3 staining present at the stress fiber-like structures. **(b)** Choanocyte chambers show no EmTAGLN3 signal in choanocytes. **(c)** Apical pinacoderm shows staining along the actin tracts as well as cortical actin of the exopinacocytes. Scale bars 10µm.

consistent with the size of both of these proteins, and in both cases the band goes away with incubation with recombinant protein.

For immunostainings, both antibodies label actin structures in the sponge. EmTAGLN3 shows strong staining at a variety of structures such as the stress fiber-like structures in the basopinacoderm, the actin tracts of the endopinacocytes, and the cortical actin of the exopinacocytes (**Figure 34**). There is no obvious staining in the choanocyte chambers. For EmTAGLN2, there is strong staining along the actin tracts in the endopinacoderm, with light cell boundary staining in the basopinacocytes (**Figure 35**). There is no detectable staining at the stress fiber-like structures or in the exopinacoderm, as well as in choanocyte chambers. For both proteins, these staining patterns were lost when incubated with the matching recombinant proteins (ex. anti-EmTAGLN3 w/EmTAGLN3), but persisted when incubated with the other recombinant protein (ex. anti-EmTAGLN2 w/EmTAGLN3). The only structures that both antibodies stained were

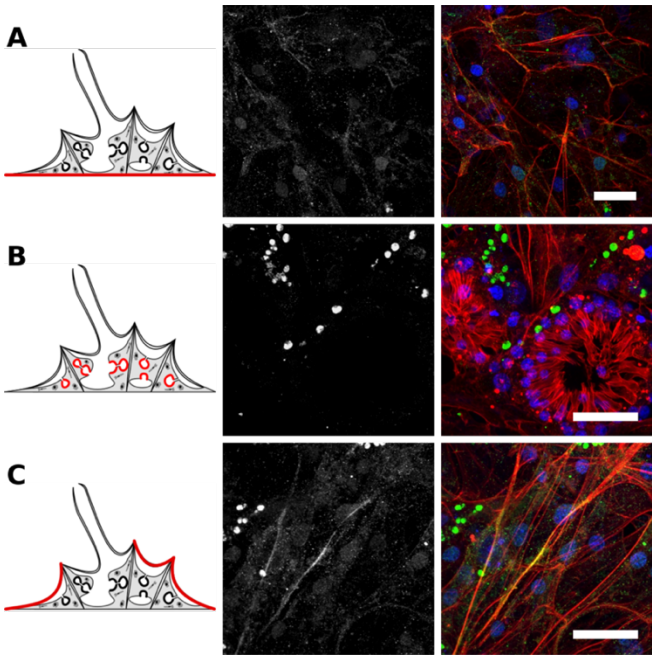

Figure 35. EmTAGLN2 is more restricted to the actin tracts. Confocal images through sponges stained for EmTAGLN2 (green), actin (red), and DNA (blue). Green channel alone in gray. **(a)** The attachment epithelium shows limited EmTAGLN2 staining with some signal at the boundaries of basopinacocytes. **(b)** Choanocyte chambers show no evidence of EmTAGLN2 in choanocytes. **(c)** The apical pinacoderm shows EmTAGLN2 localization to the actin tracts, with no clear staining in the exopinacocytes. Scale bars 10μm.

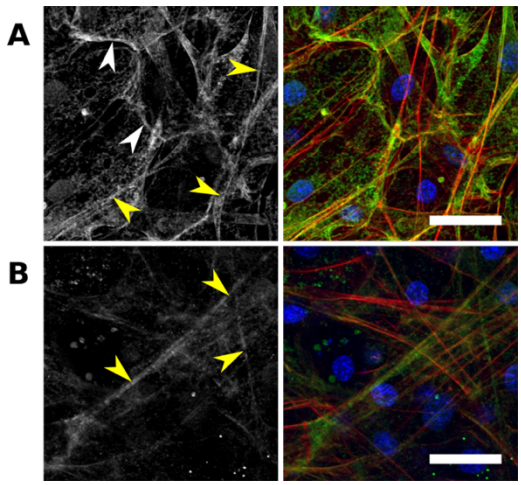

Figure 36. EmTAGLN3 is broadly expressed in pinacocytes and EmTAGLN2 is more restricted to endopinacocytes. Confocal images of the apical pinacoderm of sponges stained for **(a)** EmTAGLN3 and **(b)** EmTAGLN2. Merge images show secondary in green, actin in red, and DNA in blue. EmTAGLN3 localizes to both the actin tracts of endopinacocytes (yellow arrowheads) and the cortical actin of exopinacocytes (white arrowheads). EmTAGLN2 appears to only localize to the actin tracts, with some diffuse signal in the cytoplasm of the endopinacocytes. Scale bars 10μm.

the actin tracts that run through the endopinacoderm. For these, EmTAGLN3 seemed to label a large number of the structures, whereas EmTAGLN2 was found at larger structures (**Figure 36**). Both proteins appear to be highly expressed in the endopinacoderm relative to other tissues. As a result of this, they can help to visualize the shape of these cells, which is normally difficult to do with actin staining alone. EmTAGLN3 does a good job of revealing cell boundaries in this tissue and gives an idea of the organization of the tissue in different regions of the sponge (**Figure 37**). As imaging is performed closer to the body of the sponge, the cells appear to form a cohesive epithelium with the actin tracts running between points of adhesion (**Figure 37a**). Towards the edge of the sponge, where the apical pinacoderm connects to the basopinacoderm, this tissue becomes much more variable, consisting of cells that contain large actin dense protrusions (**Figure 37b**). EmTAGLN2 staining in the endopinacoderm

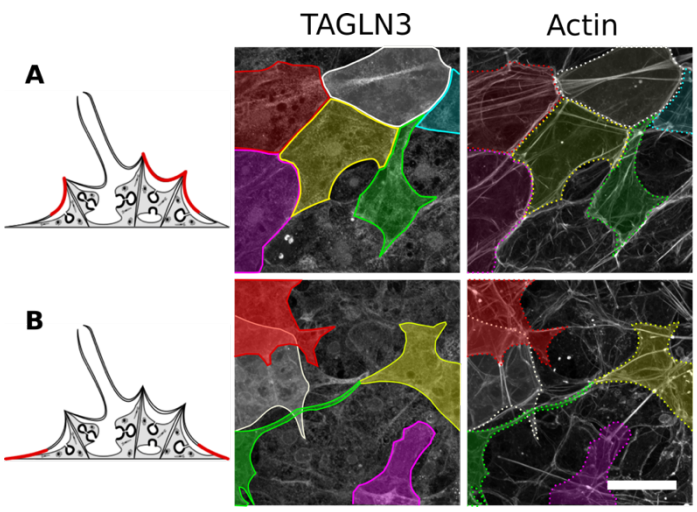

Figure 37. Cytoplasmic staining of EmTAGLN3 in the endopinacoderm helps to resolve cell morphology. Confocal images of the pinacoderm of sponges stained for EmTAGLN3 and actin. Cell bodies were traced based on the EmTAGLN3 staining pattern and then overlaid on the actin channel, where they consistently lined up with adhesion plaques for the actin tracts. **(a)** In tissue near the body of the sponge, this tissue forms a cohesive epithelial sheet. **(b)** In tissue towards the edge of the sponge, where the apical pinacoderm connects with the basopinacoderm, the tissue becomes less evenly spaced and contains cells with long actin dense protrusions. Scale bars 10µm.

is associated with large actin structures. It is normally difficult to tell if these structures are thin cellular extensions or if they are running through body of cells that compose an intact epithelial layer. EmTAGLN2 staining suggests that the latter is true and that single cells can contain multiple actin bundles in different regions (**Figure 38**). The cell in the middle of the panel contains a large actin bundle in the top region of the cell, with a smaller bundle on the opposite side, each contacting a different cell. This organization gives the tissue a web like structure to the contractile network, which should allow for more complex dynamics than the simple linear belt.

EmTAGLN3 gave strong signal at the stress fiber-like structures that are seen in the basopinacocytes. These structures are diverse and appear to attach to a variety of adhesion structures (Mitchell & Nichols, 2019), but there are some general patterns that can be seen in the EmTAGLN3 immunostainings (**Figure 39**). First of all, EmTAGLN3

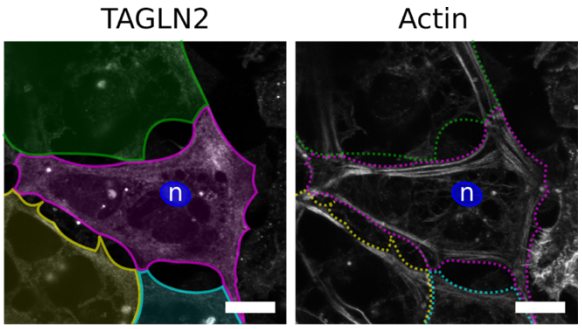

Figure 38. EmTAGLN2 reveals endopinacocyte shape and complex actin tract network organization. Confocal images of sponges stained for EmTAGLN2 and actin. Cell shape is identified based on cytoplasmic staining for EmTAGLN2 and then overlaid on actin channel image. Nucleus added (n) to aid in orientation of cell based on DNA staining (not show). Scale bars 5µm.

does not localize to any of the actin dense plaques that are thought to be adhesion sites. Rather, the strongest staining runs along the length of the actin bundle and is absent at the ends (yellow arrows). In a given structure, the strongest signal in the EmTAGLN3 channel seems to be in regions of lower signal in the actin channel (white arrows). Strong signal can also be seen for small dispersed actin bundles (cyan arrows). These could be a result of higher epitope availability in smaller actin structures or they could represent a biologically relevant function of the protein. As an actin bundling protein, EmTAGLN3 could function to link smaller actin structures together to form the large dense fibers. As these fibers mature, the protein then dissociates from it, reducing the signal.

Discussion

The immunostainings show both proteins strongly localizing to actin structures, which is consistent with the predicted function of these proteins. The western blot results were less convincing but did show bands at the predicted protein size. The competitions with recombinant protein suggest that these antibodies are very specific to the protein they were raised against. That staining persisted following incubation with the other recombinant protein suggests that there is no cross reactivity, despite the similarity

between these two proteins. Attempts were made to perform immunoprecipitation with these antibodies in order to validate them by mass spectrometry, but these were unsuccessful thus far.

The staining patterns for these two proteins show broad association with actin structures for EmTAGLN3 while EmTAGLN2 appears to be highly specific to the actin tracts. Based on the patterning of EmTAGLN3 with respect to the stress fiber-like structures of the basopinacoderm, it is compelling to think that this protein serves in the formation of large actin structures, by linking together smaller units. If this role is expanded to other cell types, then EmTAGLN3 may serve in early organization of the actin tracts in the endopinacoderm. As these mature and get larger, it may dissociate and be replaced by EmTAGLN2, which is consistent with the restricted staining at large actin tracts.

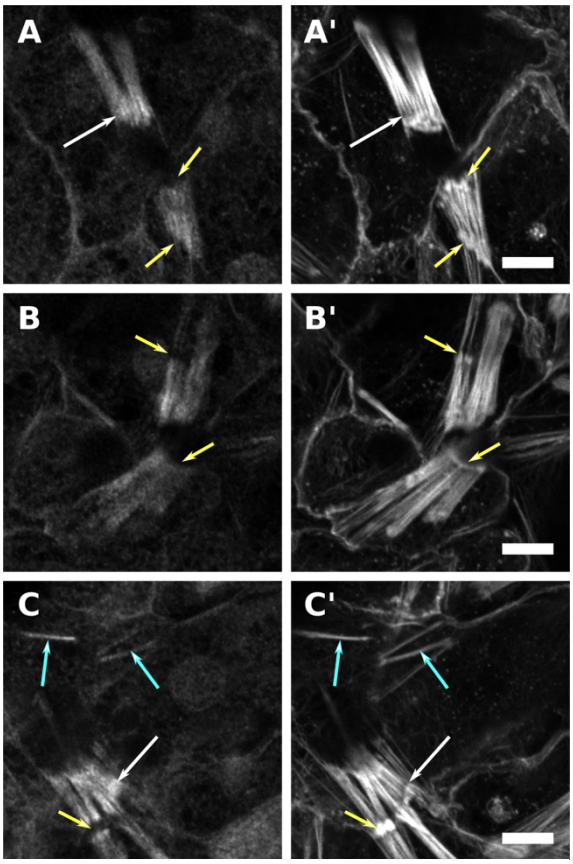

Figure 39. EmTAGLN3 staining at stress fiber-like structures provides insight into protein function. (a) Large bundles show strong EmTAGLN3 signal at regions of weaker actin staining (white arrows). **(b)** Sites of adhesion (yellow arrows) do not show any signal from EmTAGLN2. This occurs with ventral adhesions **(a)**, bacterial adhesions – visible by curved plaque **(b)**, and dorsal adhesions **(c)**. **(c)** Relatively strong signal can also be seen in small isolated actin bundles (cyan arrows). Scale bars 5μm.

The restricted localization of EmTAGLN2 does suggest that this protein can serve as a marker for the contractile actin

tracts. The high expression levels of both proteins in the endopinacocytes helps in understanding these cells apart from just the actin tracts. This is consistent with published scRNA-seq data, which showed upregulation of the transgelins in a specific group of pinacocytes which showed strong expression of other contractile proteins (Musser et al., 2019). Because of strong relative actin staining along the actin tracts and limited amounts of cortical actin, it is generally difficult to visualize the boundaries or body of these cells. Because of this it is not generally not clear whether the endopinacoderm is a continuous epithelial layer or if the cells are connected by long protrusions that the actin tracts run through. Based on the findings from these antibodies, it appears that both of these scenarios are occurring. In the body of the sponge, the endopinacoderm appears to be a continuous epithelial sheet, with the actin tracts running through the cells in discrete regions. Out near the edge of the sponge, this tissue appeared less organized, with long protrusions extending out and over different cells. These extensions appear to attach to the basopinacoderm area and may represent a method of anchoring the tissue to the attachment epithelium.

Conclusions

A fundamental, yet unknown aspect of sponge contractions is the identity of the cells or tissue that contributes the primary force during contractions. There are many dynamic tissues in the sponge as well as processes that could lead to whole body movements. The overall findings of this section suggest that the contraction of the actin tracts, which run through the endopinacoderm, is responsible for the primary generation of force during the contractions. This tissue forms a continuous epithelium in the body of

the sponge, where it lines the canals. Towards the edge of the sponge it forms a looser network of cells, with actin dense protrusions that integrate into other tissues which likely serve as anchoring points as well as to transmit force through the body. The most compelling finding is the significant shortening of these structures during a contraction. This is also seen in the choanocyte chambers, but the lack of significant movement between the chambers suggests that their change in size is absorbed in the mesohyl, and therefore does not exert direct force on the canals. The exopinacocytes are suitable for live imaging and can be seen expanding and contracting during a body contraction. Collective movement in the direction of the contraction is more synchronized than their local expansion and contractions, suggesting the tissue is being moved and the individual cells are reacting to dissipate the force at adhesion sites and maintain integrity.

The findings that *E. muelleri* can move its body prior to the establishment of choanocyte chambers as well as in their absence, suggests that this behavior is not entirely dependent on the opposing force produced by incurrent flow. Likewise, the ability of unattached sponges to fully contract their body suggests that this is an active contraction, which is normally balanced by traction forces at the attachment to the substrate. Finally, the restricted expression of EmTAGLN2 to endopinacocytes, as well as its localization to the actin tracts, suggests that these structures have a distinct molecular composition, which likely points to a specific function.

Chapter 4: *Ephydatia muelleri* Muscle Myosin and Regulation of Contraction

Introduction

Through interactions with actin, type II myosin heavy chain (MyHC; **Figure 40**) is the nearly universal motor for cellular contraction in all contexts, including cytokinesis, cell motility, apical constriction, and of course -- in myocytes. In each of these contexts, the basic mechanism of contraction is the same: 'Thick' filaments, primarily composed of hundreds of myosins, exert force on actin-based 'thin' filaments, which is converted into mechanical stress through anchor points in the cell (**Figure 41**). Contractions can be regulated in two general ways; either at the thick filament (generally through modifications to light chains) or at the thin filament (e.g., troponin/tropomyosin complex).

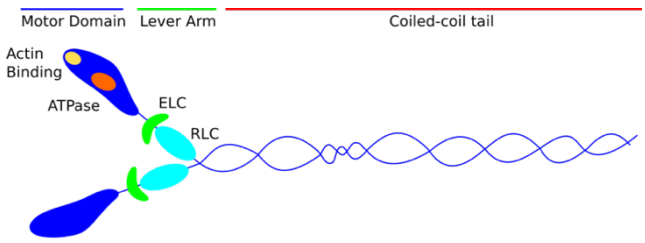

Figure 40. Structure of Type II-Myosin. Myosin II contains a motor domain, lever arm, and long coiled-coil trail. Each assembled myosin contains two heavy chains (MyHC), which make up the motor domain, containing the actin binding and ATPase sites, and the tail, two essential light chains (ELC), and two regulatory light chains (RLC) at the lever arm.

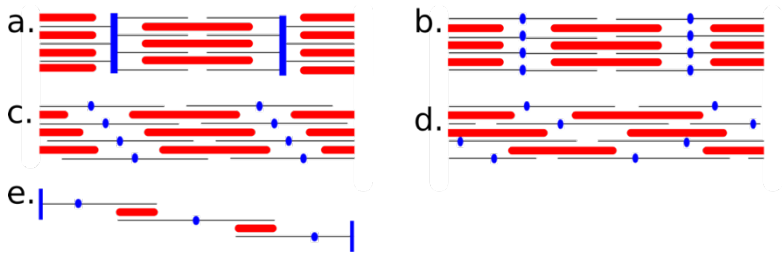

Figure 41. Ultrastructure of different muscle types. The general ultrastructure of different muscle types are shown; (A) transverse striated with continuous Z-discs, (B) transverse striated with discontinuous Z-elements, (C) obliquely striated, (D) smooth, (E) vertebrate smooth with side polar thick filaments. Black bars represent thin filaments, red bars represent thick filament, and blue structures represent dense bodies/thin filament anchors.

There is no easy way to talk about the mechanisms that regulate myocyte contraction without oversimplification because the mechanisms are complex, incompletely characterized and vary by phylogenetic lineage. One widespread mechanism that is found in the striated and cardiac muscles of vertebrates (Farah & Reinach, 1995; Gordon et al., 2000; Kobayashi et al., 2008), and in the striated and smooth muscles of invertebrate bilaterians (Hooper & Thuma, 2005; Hooper et al., 2008), is tropomyosin/troponin regulation of the actin thin filament. This protein complex sterically hinders MyHC from binding to actin, but is released in the presence of Ca^{2+}, allowing for a rapid contraction in response to Ca^{2+} influxes characteristic of fast contracting myocytes (Farah & Reinach, 1995) (**Figure 42**). Troponin C is restricted to bilaterians, and so this mechanism is thought to have evolved in the bilaterian stem lineage (Steinmetz et al., 2012). Increased cytosolic Ca^{2+} levels can also trigger enzymatic cascade resulting in phosphorylation of the myosin regulatory light chain (RLC), which has been well characterized in vertebrate smooth muscles **(Figure 43)**. The majority of components of this pathway predate bilaterians.

A potentially more ancient strategy for regulating contractions is to disrupt the autoinhibitory interactions of MyHC in the thick filament. MyHC undergoes asymmetric head-head interactions in which the two heads of the homodimer interact, thereby blocking actin-binding on one head and the ATPase activity on the other (Jung et al., 2008). MyHC also undergoes head-tail interactions in which the heads interact with the coiled-coil tail of the myosin, thereby preventing filament assembly and stabilizing head-head interactions in assembled filaments (Jung et al., 2008; Himmel et al., 2009). Both head-head and head-tail interactions appear to be ancient within the animal lineage, found in vertebrate smooth and striated muscles (Woodhead et al., 2013; Nogara et al., 2016), and in muscles of invertebrate bilaterians (Jung et al., 2008; Himmel et al., 2009; Alamo et al., 2015). Moreover, there is evidence for the presence of these interactions in *Dictyostelium* (Liu et al., 2000; Lee et al., 2016) suggesting that MyHC autoinhibition predates animals and the origin of myocytes, altogether.

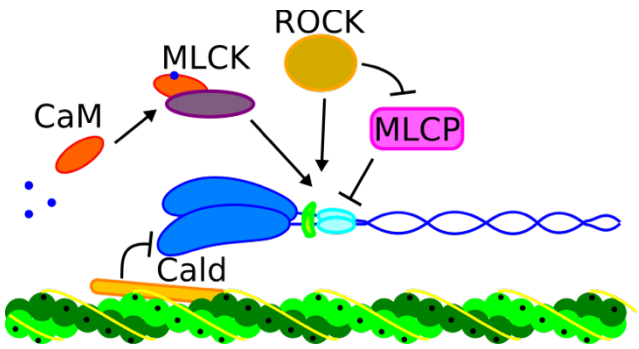

Figure 43. Troponin independent regulation of contractions. The primary Ca^{2+} dependent enzymatic pathway consists of increased Ca^{2+} levels (blue circles) bind to calmodulin (CaM), which then activates myosin light chain kinases (MLCK) which phosphorylates the RLC of a myosin filament, activating the motor activity. Removal of this phosphate is performed by myosin light chain phosphatase (MLCP) which inactivates the motor. MLCP activity is regulated by rho-associated protein kinases (ROCK) activity, which can also act directly on the RLC. Thin filament regulation by the protein caldesmon (Cald), which directly inhibits myosin ATPase activity. Cald has only been described in vertebrates, while all other components are found throughout animals.

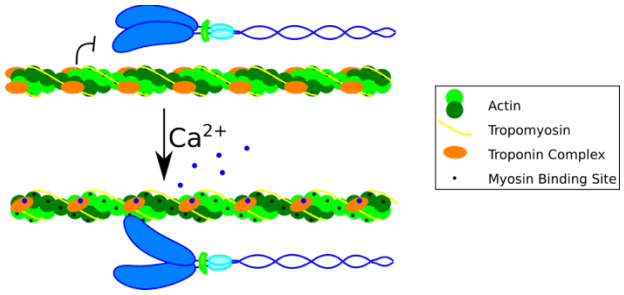

Figure 42. Tropomyosin/Troponin complex regulation of thin filament. The troponin complex binds to both actin and tropomyosin, sterically hindering the binding of MyHC. Increases in cytoplasmic Ca^{2+} concentrations results in Ca^{2+} binding to the troponin complex leading to the shifting of tropomyosin, exposing the MyHC binding sites.

In a recent review, Brunet and Arendt (Brunet & Arendt, 2016), make an argument for the evolution of Ca^{2+} activation of actomyosin contractile machinery in ancient eukaryotes being driven by response to membrane damage. This becomes even more compelling when considering the roles of the RLC and essential light chain (ELC) in modulating the head-head and head-tail interactions. Both RLC and ELC are members of the canonical EF-hand superfamily of proteins, although they have largely lost their affinity for directly binding Ca^{2+} in extant animals (Nakayama & Kretsinger, 1994). In early eukaryotes, binding of Ca^{2+} to RLC/ELC precursors likely functioned to disrupt the head-tail interactions, allowing for the assembly of thick filaments in a manner that was spatially and temporally coupled to the influx of external Ca^{2+}. The disruption of autoinhibitory headhead interactions, also via Ca^{2+} binding, would then drive contraction of the cortical actinomyosin ring until the damage was sealed and Ca^{2+} concentrations dropped (Brunet & Arendt, 2016; Nakayama & Kretsinger, 1994; Murrell et al., 2015). Once this general mechanism appeared, specialization of the MyHC regulatory switch would have allowed for tighter control over contractions, for example, in response to the stimulus induced release of internal Ca^{2+} stores in myocytes.

A gene duplication in the stem holozoan lineage gave rise to two type-II myosin heavy chain (MyHC) isoforms, each with unique motor dynamics and tail structures (Steinmetz et al., 2012; Kollmar & Mühlhausen, 2017). There have been later expansions in different lineages, but type-II MyHC can be separated into two distinct families, referred to hereafter as non-muscle (nmMyHC) and a muscle (stMyHC). Sponges, including *E. muelleri,* have orthologs that fit clearly into each of these types (Steinmetz et al., 2012; Srivastava et al., 2010). In bilaterians, nmMyHC shows broad function, in a variety of cell types and different contexts, including muscles. In contrast, stMyHC is restricted to muscles (Brunet et al., 2016). Outside bilaterians, there is a clear separation of function of the two in cnidarians. The anthozoan model, *Nematostella vectensis,* shows broad expression of nmMyHC, in both non-muscle cells as well as in slow contracting circular body muscles (Steinmetz et al., 2012; Sebé-Pedrós et al., 2018). On the other hand, stMyHC is expressed specifically in the longitudinal tentacle muscles as well as in the retractor muscles that run through the body (Steinmetz et al., 2012; Sebé-Pedrós et al., 2018; Renfer et al., 2010). Both of these muscles are involved in fast movement and contain the largest contractile bundles of *N. vectensis* muscle types (Jahnel et al., 2014). Although these fast muscle types have smooth ultrastructure, these findings suggest that the separation of function between the two MyHCs into fast and slow contracting muscle types predates bilaterians (**Figure 44**). Striated muscles are also present in some cnidarians, which also contain stMyHC, though these appear to have been independently derived in the cnidarian lineage (Steinmetz et al., 2012). Interestingly, there was a lineage specific duplication of stMyHC in ctenophores. In the ctenophore, *Pleurobrachia pileus,* there is a separation of function between these two paralogs, with one specific to muscles

and the other in a variety of cell types, providing a non-muscle function. The ortholog of nmMyHC is restricted to proliferative cells and likely serves a core function in cytokinesis (Dayraud et al., 2012). This demonstrates that there is nothing intrinsic about the muscle function of stMyHC or the non-muscle functions of nmMyHC, and that a separation of function may not have predated animals. Previous studies of sponges have shown differential expression of nmMyHC and stMyHC in two different demosponges. *Amphimedon queenslandica* shows expresson of stMyHC during embryo and larval development, while *Tethya wilhelma* shows strong expression of stMyHC in sieve-like apopyle cells at the exit of choanocyte chambers (Steinmetz et al., 2012). These sieve-like cells also have large linear bundles running between the pores, which are thought to be contractile actin structures (Steinmetz et al., 2012; Hammel & Nickel, 2014). It is thought that these may be fast contracting cells, which rapidly regulate the rate of flow out of the choanocyte chambers. These findings of differential expression between nmMyHC and stMyHC in sponges suggests that the separation of function between the two isoforms predates the last common ancestor of sponges and other animals.

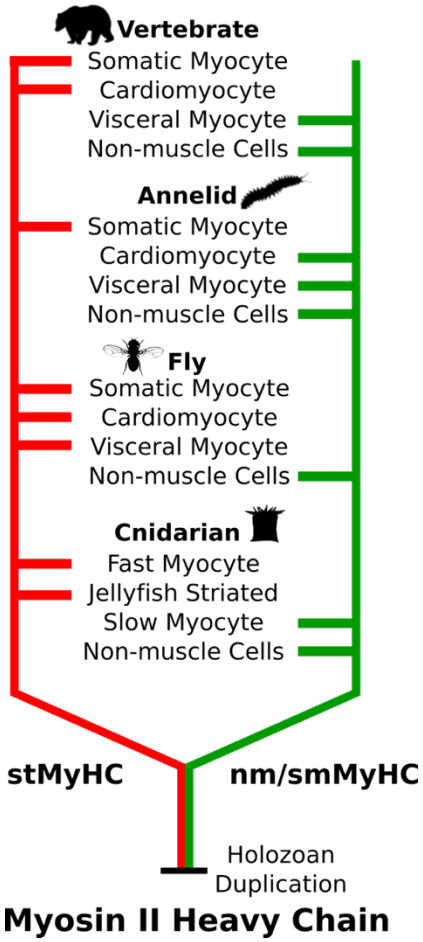

Figure 44. Distribution two myosin II heavy chain types. A pre-animal duplication of myosin II heavy chain gave rise to stMyHC and nm/smMyHC. In well studied animal groups, stMyHC is restricted to muscles, while nm/smMyHC is found in both muscles and non-muscle cells. All images from PhyloPic.org.

However, these findings are based on expression data, and does not resolve the subcellular structures that the protein is localizing too as well as the type of filaments that the protein forms.

Apart from the basic components and structure of the contractile machinery, it is important to consider regulation of contraction when judging homology. As said earlier, there is no evidence for a functional troponin complex in non-bilaterian animals. In vertebrate smooth muscles, the predominant mechanism of regulation is through phosphorylation of the RLC by myosin light chain kinase (MLCK) in a Ca^{2+} dependent manner. This alters the interaction with the ELC leading to increased movement of the MyHC which allows the motor to act on actin (Taylor et al., 2014). Phosphorylation of the RLC as a regulatory mechanism is seen in a variety of muscles as well as in non-muscle context (Sellers, 1985; Wu et al., 1999; Sellers, 1991), though in non-muscle context it is not always in a Ca^{2+} dependent manner or through MLCK (Chen et al., 2014). MLCK appears to be an animal innovation (Steinmetz et al., 2012), and is well conserved in sponges and other non-bilaterians. Because of this, it is assumed to be the primary regulatory mechanism for contractions in these animals, though direct evidence for this is limited. Proteomics performed on the striated muscles of the cnidarian *Aurelia sp.* found a MLCK-like protein associated with muscle fibers, but could not definitely identify it (Tanaka et al., 2018). Because of the nature of the RLC and ELC and the ancient mechanism of head-tail interaction regulating MyHC activity, MLCK does not have function in contractile tissues of sponges for them to share homology with muscles of other animals, as this could have been co-opted for this function later. Sponges could also be utilizing a derivative of a mechanism that gave rise to the troponin complex in

bilaterians as well. However, if sponges are utilizing phosphorylation of the RLC by MLCK in a specific context of regulating body contractions, this would strengthen the argument for homology.

Type II-Myosin Heavy Chain Localization in Ephydatia muelleri

Background

A fundamental part of understanding the structure of the contractile tissue of *E. muelleri* is to look at the distribution of the two type II-MyHCs. Transcriptomic data shows that both nmMyHC and stMyHC are expressed in the juvenile stage of *E. muelleri* (Peña et al., 2016) (**Figure S10**). The spatiotemporal expression patterns and how they compare to other studied demosponges would provide valuable initial insight, but *in situ* hybridization methods have shown limited success in this system (see technique development section). For this reason, custom polyclonal antibodies were designed to target the two proteins. Putative *E. muelleri* sequences were aligned with the assembled reference set using MUSCLE v3.8 (Edgar, 2004) and molecular phylogenetic analysis was performed using MEGA 7 (Kumar et al., 2016). Secondary and tertiary structure of the motor domains were predicted using Phyre v.2 (Kelley et al., 2015) and the coiled-coil domain structure of the tails were predicted using COILS server (Lupas et al., 1991). This structural information was used to identify variable regions in the head and tail domains of the two proteins as viable targets for raising isoform specific antibodies. The *E. muelleri* stMyHC and nmMyHC orthologues were then aligned with 19 other myosin family proteins found in the transcriptome in order to verify the uniqueness of the variable regions and limit the possibility for cross reactivity with other myosin family

members. The amino acid sequences for the identified targets were codon optimized for expression in *Escherichia coli*. Custom gBlocks Gene Fragments for the target regions were ordered from Integrated DNA Technologies with LIC adapter sequences on each end and were cloned into pET His6 GST TEV LIC vectors (Addgene plasmid #29655). Vectors were transformed into Rosetta (DE3) competent cells (Novagen) and proteins were expressed and purified and sent to Syd Labs (https://www.sydlabs.com) for rabbit injection. A unique region of the N-terminus of stMyHC was identified and used to generate anti-stMyHC-N serum, while unique regions of the C-terminus of both stMyHC and nmMyHC were identified and used to generate anti-stMyHC-C and anti-nmMyHC-C serum. These were then affinity purified to generate stocks of each antibody. Fragments inserted for recombinant expression are;

stMyHC - N

ACCACCGACATACCGAACAGATGCGTATGTTCGACGCGAAAAATGGCTGTGG
CTGAACGACGAAGAAGAATGCTTCAAAGCGGCGTTCGTT

stMyHC - C

CGTTCTGCGCTGGACGAATCTGAAGAAGAAAAAGCGGGTCTGCAGGCGCAGC
TGTCTAAAGCGCGTACCACCACCACCACCTCTGCGCGTAAAGGTAAACCGGC
GCCGGTTGACGCG

nmMyHC

GGTGCGGGTGCGGGTGGTGCGGGTTCTCGTCGTTCTACCTTCACCGGTGGTTC
TAAAGGTTCTACCGCGGGTGTTGGTCGTAAAACCTCTACCCGTCACGACCGTC
AGACCGGTCACGGT ACCGACGACTCTCTGCCG

Methods

Affinity purification

Recombinant protein from each sample was expressed and dialyzed into 0.1M sodium citrate, 0.05M sodium carbonate buffer, pH 10 (pH10 coupling buffer). 1mL of AminoLink coupling resin (Thermo Scientific #20318) was washed thoroughly with pH10 coupling buffer and then recombinant protein was added and incubated on a rotisserie for 4 hours at room temperature. Unbound protein was drained and 1mL of 1x PBS pH7.2 containing 20µL of sodium cyanoborohydride was added. This was then incubated on the rotisserie overnight at 4^{o}C. The columns were then drained and washed with 1M Tris-HCL, 0.05% sodium azide, pH7.4 (Quenching buffer) and then incubated with 20µL sodium cyanoborohydride in quenching buffer for 30 minutes at room temperature on the rotisserie. Samples were then washed thoroughly with 1M NaCl, 0.05% sodium azide and then 1x PBS, sodium azide, pH 7.2. Columns containing whole *E. coli* proteins were also prepared in this manner.

For each serum, 2mL was cleared through an *E. coli* column, by incubating for 1 hour at room temperature on a rotisserie. This was then transferred to the column containing the specific antigen and incubated for 1 hour at room temperature on a rotisserie. After incubation, serum was drained, and the columns were washed extensively with 1x PBS pH 7.4 prior to elution. Antibody was eluted using IgG Elution Buffer (Thermo Scientific #21004). 1mL samples were eluted into 100µL of 1M Tris pH 9 to neutralize. Antibodies were then concentrated and transferred into 1x PBS pH 7.2 using Amicon® Ultra-4 10K centrifugal filters (Millipore #R7PA80988)

Immunostaining

Gemmules were plated and hatched as described before. Initial stainings were performed using the standard fixation protocol described earlier; using 3.7% formaldehyde in EtOH. A range of concentrations was tested for each antibody, from 1:100 to 1:1000. Since none of these showed consistent or predicted staining patterns different fixation methods were used. For stMyHC-N, samples were fixed in Carnoy's solution (60% EtOH, 30% chloroform, 10% acetic acid) for 3 minutes at room temperature. Sample were then gently washed into 100% EtOH for 10 minutes at room temperature. Samples were washed 3x with 1x PBST pH 7.4, and blocked for 1 hour in 3% BSA in 1x PBST. Primary antibody was diluted 1:500 in blocking solution and added to the sample. Samples were incubated overnight at 4ºC. The following day, sponges were washed 3x with 1x PBST and then stained with anti-rabbit AF™488 (Life Technologies, 1:500) secondary, and Hoechst dye (33,342, 1µg/mL) in blocking solution for 45 minutes at room temperature in the dark. Sponges were then washed 3x with 1x PBST and mounted in mounting media. Confocal Images were acquired on an Olympus Fluoview FV3000 confocal laser scanning microscope using either a 60×/1.4 NA or 100×/1.4 NA objectives. Laser levels and acquisition setting were not adjusted for imaging controls. Images were processed in FIJI (Schindelin et al., 2012).

. In order to understand the developmental dynamics of stMyHC, time series stainings were performed. Gemmules were plated in 8 hour stacked timing and monitors for the last plated sponge to attach to the dish. These samples were then fixed and stained for stMyHC following the established protocol. The only change was that initial fixation was performed with a 6:3 ratio of EtOH and chloroform and one volume of acetic acid

was added dropwise during the first minute of fixation. This appeared to help maintain the very delicate structure of the newly hatched tissue.

Since co-staining for F-actin was not possible using the fixation protocol necessary for this antibody, a time series of treatment with latrunculin B was performed. Gemmules were plated and hatched in glass bottom dishes and grown until canals and choanocytes were clearly visible. Sponges were then treated with 20μM latrunculin B in LW for either 1, 5, 10, or 30 minutes, and were rapidly fixed using the Carnoy's solution protocol. Immunostaining were performed as described above.

Confocal Images were acquired on an Olympus Fluoview FV3000 confocal laser scanning microscope using either a 60×/1.4 NA or 100×/1.4 NA objectives. Laser levels and acquisition setting were not adjusted for imaging controls. Images were processed in FIJI (Schindelin et al., 2012).

Western Blot

Approximately 50 gemmules were plated and hatched in LW+100μg/mL ampicillin in a petri dish as described earlier. Water was refreshed with LW each day following hatching. At 5dph sponges were harvested by scraping with a sterile razor blade directly into SDS PAGE loading buffer (1 M Tris, pH 7.0, 20% SDS, 20% Glycerol, 0.02% bromophenol blue and 2.5% β-mercaptoethanol). The sample was then boiled for 8 minutes and then half was diluted 1:1 (v/v) in SDS PAGE loading buffer. Samples were then separated by SDS PAGE on an 8% tris-glycine SDS gel. Proteins were transferred to a PVDF membrane at 40mA overnight in tris-glycine transfer buffer containing 2% MeOH and 0.1% SDS. Membrane was washed with 1xPBST and blocked

in 5% milk (wt/v) in 1xPBST for 1 hour at room temperature. Membrane was then cut in half and incubated in either 1:500 (v/v) dilution of anti-stMyHC-N in blocking solution or 1:500 (v/v) dilution of anti-stMyHC-N and 5µg recombinant MyHC N-term in blocking solution. Membranes were incubated overnight at 4ºC and then were washed and secondary, anti-rabbit AF™488 (Life Technologiesm, 1:2000) in blocking solution for 45 minutes at room temperature.

Immunoprecipitation

Immunoprecipitation was performed using anti-stMyHC-N as this was the only antibody to give interpretable and reproducible staining patterns. The goal was to validate the antibody's ability to recognize endogenous stMyHC through mass spectrometry as well as possibly identify other proteins that localize to the structures associated with stMyHC. Approximately 300 gemmules were plated in three petri dishes (~100 per dish) containing LW+100µg/mL ampicillin and incubated for 3 days to hatch and attach. The water was then changed daily with just LW. On the 6th day, sponges from each dish were harvested by scraping into a 1.5mL Eppendorf tube with a razor blade and water was removed. In an attempt to free stMyHC from the cytoskeleton in hopes to increase the soluble concentration cells were then dissociated in LW+1mM EDTA for 10 minutes at room temperature with gentle agitation. Solution was passed through a 70µm cell strainer (CellTreat #NCS002) and the solution was removed. 700µL of cold triton lysis buffer (TLB - 25mM HEPES, 100mM NaCl, 1mM EDTA, 1mM PMSF, 10mM DTT, 10ng/mL leupeptin, 1ng/mL aprotinin, 10% (v/v) glycerol, and 1% (v/v) Triton X-100) was added to each tube and samples were vortexed thoroughly and then homogenized using a hand

homogenizer. Cellular debris was spun out and the three soluble fractions were combined in a clean tube. Immunoprecipitation columns were prepared using the Pierce crosslink CoIP kit (Thermo Scientific #26147) omitting the crosslinking steps. The recipes were scaled up for an 85µL volume of beads and coupling was done in a 500µL volume. Two columns were prepared, one with 125µg of anti-EmstMyHC-N and one with 125µg of anti-Rabbit IgG (as a control). For the immunoprecipitation, 700µL of cell lysates were added to each column and they were incubated on a rotisserie overnight at 4°C. The columns were then washed and eluted following the published protocol, with the addition of a 1M LiCl wash just prior to the conditioning step. Protein was eluted in 65µL volume for the first two elutions, and 55µL volume for the second two. 12µL of each sample were run out on an 8% SDS-PAGE gel and then transferred to a nitrocellulose membrane for blotting. Transfer was done using 25mM Tris, 192mM Glycine, 1% MeOH, and 0.1% SDS transfer buffer and was performed at 40mA at 4°C overnight. Membrane was then washed with PBST and blocked with 5% milk in PBST. Primary antibody (anti-EmstMyHC-N) was diluted 1:300 in blocking solution and added to the membrane which was incubated for 1 hour at room temperature. Secondary, anti-rabbit AF™488 (Life Technologies) was diluted 1:5000 in blocking solution. Imaging was performed on a BioRad Molecular Imager FX (BioRad #170-9450).

Results

The purification yielded a good amount of antibody, but there was no clear staining pattern with any of the antibodies on the first attempts. There was a good amount of signal, especially from the anti-stMyHC but it did not clearly localize to any structures

(mainly broad cytosolic staining) (**Figure S11**). The western blot on sponge whole cell lysates shows the antibodies showed little staining, though overexposing the region between 250kD and 150kD did show some signal, which is likely actual signal. Troubleshooting was performed using the stMyHC-N antibody, as this showed the most promise for stainings. Optimized transfer parameters did result in high molecular bands, which disappeared when competed with recombinant protein (**Figure S12)**. Stainings with stMyHC-N using Carnoy's solution fixation did show very clear staining at structures that resemble the actin tracts (**Figure 45**). Co-staining with phalloidin to visualize actin gave no signal, suggesting that the F-actin had been destroyed during fixation. Based on the proximity of the antigen region to the actin binding site, it is likely that F-actin was masking the epitope in the formaldehyde fixed samples. Unfortunately lack of co-staining prevents direct observation of colocalization. The structures seen in the stMyHC stainings do appear to be organized in a manner consistent with the actin tracts as well as of a size and length that is consistent with these structures (**Figure S13**). Both antibodies targeting the C-terminus did not show clear staining patterns in the

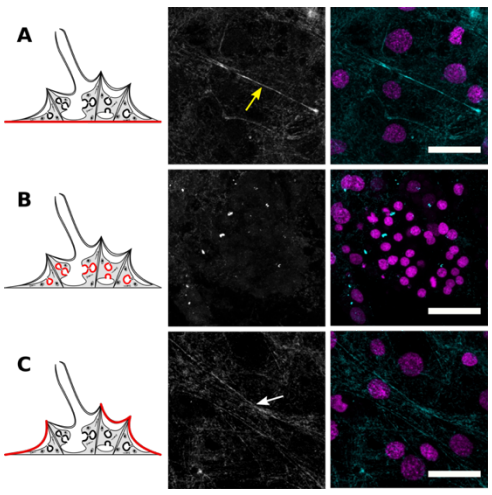

Figure 45. EmstMyHC localizes to structures resembling the actin tracts. Staining with anti-stMyHC N-term (cyan) following fixation with Carnoy's solution and counter stained for DNA (magenta). **(a)** Attachment epithelium shows little signal in the basopinacocytes, though filaments extending down towards the tissue are visible (yellow arrow). These resemble the actin structures at the junction between apical and basopinacoderm. **(b)** The choanocyte chambers show no clear staining pattern for stMyHC. **(c)** The apical pinacoderm shows staining of linear filaments running through the tissue (white arrow), which resemble the actin tracts. Scale bars 10µm.

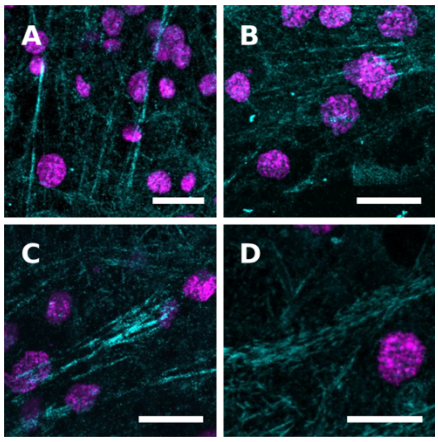

Figure 46. EmstMyHC intensified at larger structures. Representative images of various structures seen in sponges stained for stMyHC (cyan) and DNA (magenta). **(a)** Linear filaments of stMyHC can be seen running above the nuclei in the visual plane. **(b)** Filaments branching from a putative site of cell-cell adhesion resembles structures seen in actin staining suggesting tissue level organization for these structures. **(c)** Dense staining of a structure appears to reduce as it branches off. **(d)** lighter stained structures have a striated appearance, suggesting they are composed of many discrete units. Scale bars **(a)** 10μm, **(b-d)** 5μm.

Carnoy's solution fixed samples either. The staining for stMyHC shows clearly organized structures and increases in intensity in larger structures (**Figure 46**). Taking thin optical sections through the sponge tissue reveals that the staining is restricted to a thin layer of tissue, which is likely the pinacoderm (**Figure 47**). The faint staining surrounding the linear bundles also appears to be restricted to this tissue layer, which suggests that it is not background staining, but a resting pool of myosin in the cells. Combining intensity with depth in field, reveals that the organized structures (higher intensity) are higher than the diffuse staining that surrounds them (**Figure 48**). If these structures are in the endopinacocytes, then this would mean they are oriented towards the mesohyl in the

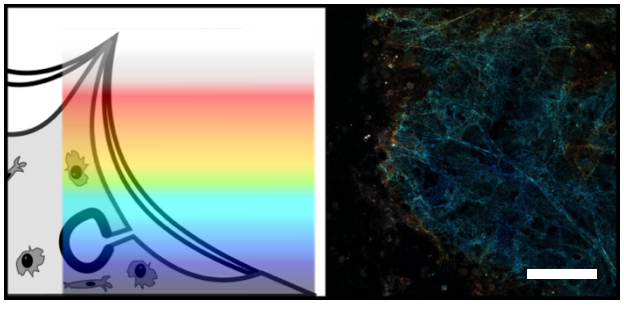

Figure 47. EmstMyHC appears to be restricted to a layer of tissue. Confocal Z-sections of 0.4μm were taken through the tissue of a sponge stained for stMyHC. Signal in right image is colored based on the position in the optical plane, following the diagram on the left. Pattern suggest that stMyHC signal is present in a thin optical section that raises towards the body of the sponge. Scale bar 50μm.

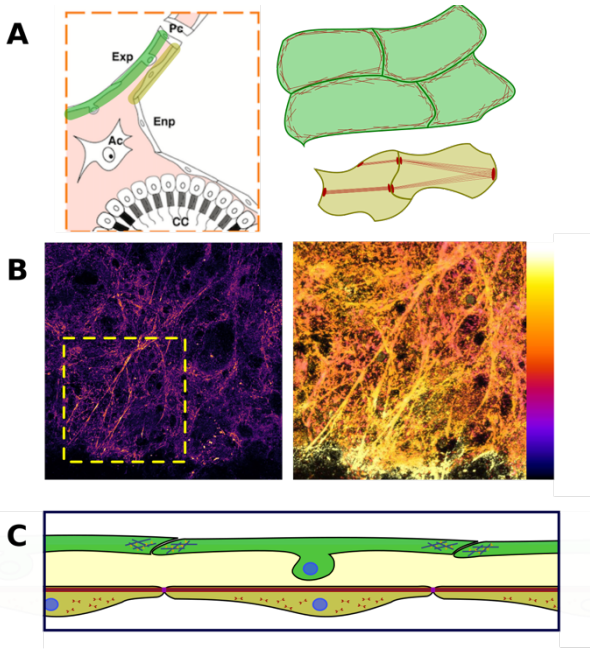

Figure 48. Large stMyHC structures are higher in the visual plane. (a) Schematic of the regions imaged with exopinacocytes in green and endopinacocytes in yellow. General actin organization is shown in red. **(b)** Intensity colored images of stMyHC stained tissue shows areas of strongest signal in warmer colors. Right panel is depth colored image of square region in left panel, with warm color high and cool colors low. Areas of higher intensity staining also appear higher in the visual plane relative the staining surrounding them. **(c)** Schematic of the organization of this tissue layer, in which the stMyHC+ contractile bundles run along the basal region of the endopinacocytes, positioned along the mesohyl. Within the cell body is a pool of stMyHC that is not associated with the structures.

basal region of the cell (**Figure 48c**). This is consistent with the organization seen in the myoepithelial cells of cnidarians (Jahnel et al., 2014).

For the developmental series, expression and cell level organization appears to occur shortly after hatching. Large puncta appear to begin forming as the sponge continues to develop. These appear to start aligning within the tissue, and then begin to form linear bundles with a highly striated appearance (**Figure 49**). This development follows the development of the actin tracts, suggesting that they serve as a guide for building the myosin filaments. Likewise, treatment with latrunculin B leads to loss of organization following similar dynamics to the loss of actin tracts following treatment (**Figure S14**). This provides further evidence that stMyHC is associated with the actin tracts.

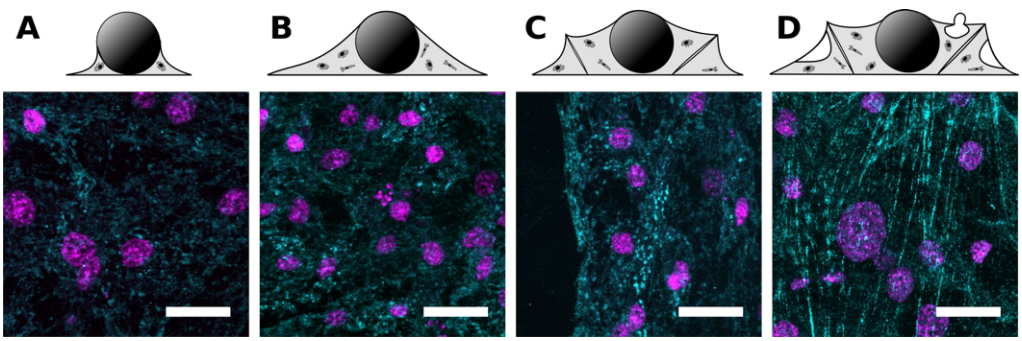

Figure 49. Developmental sequence for stMyHC. Sponges staged at specific times following hatching from gemmule and stained for stMyHC (cyan) and DNA (magenta). Developmental timings diplayed are **(a)** Shortly after hatching, **(b)** 8 hours post hatching, **(c)** 16 hours post hatching, and **(d)** 24 hours post hatching. Weak and diffuse signal is seen during early spreading **(a&b)**, which is followed by strong, unorganized signal in specific cells near the edge of the sponge **(c)**. As the sponge continues to develop, linear bundles appear, which have a strongly striated appearance **(d)**. Scale bars 5µm.

The immunoprecipitation showed a faint band in precipitates 2,3, and 4 with the strongest band in precipitate 2 (**Figure 50**). This is likely a mix of low protein concentration mixed with low efficiency of transfer, which is supported by the lack of signal in the raw cell lysates. The samples were pooled and sent for mass spec in a gel slice of the region above the IgG bands. There was a very low abundance of protein in the sample, but EmstMyHC did come back while nmMyHC was not seen in the sample (**Figure 50c**).

Because of the very small amount of protein in the samples, the signal was dampened by normal contaminates, such as keratins and other human proteins. There were no other strong hits for *E. muelleri* predicted proteins in the sample. It does appear that the antibody is specific to the stMyHC isoform in sponge tissue.

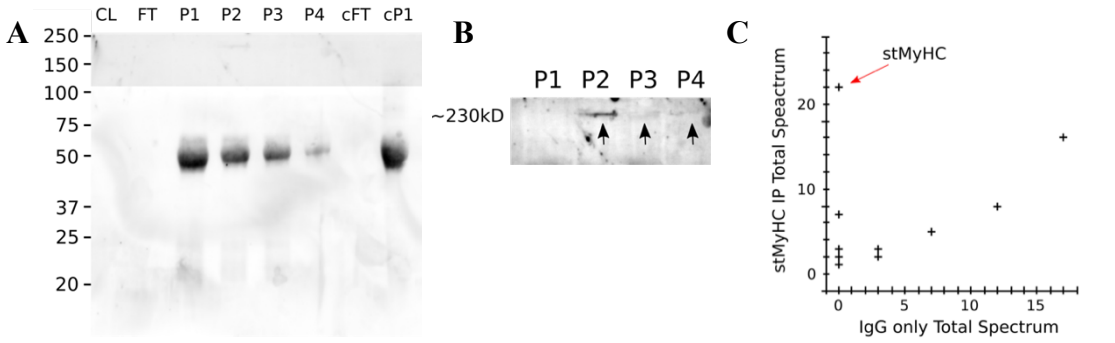

Figure 50. Immunoprecipitation for stMyHC. (a) Full image of membrane with higher exposure on top to help visualize any bands. Dark staining can be seen for the IgG heavy chain at around 50kD. Loading are raw cell lysates (CL), flow-through following precipitation (FT), precipitates 1-4 (P1-4), IgG control flow-through (cFT) and control precipitate (cP1). **(b)** Shows higher exposure of the stMyHC precipitates, which contain a faint band in P2-4, which is consistent with the size of EmstMyHC. This band is not seen in the raw cell lysates, which may be reflective of an increase in concentration in the precipitates. **(c)** Results of mass spectrometry performed on stMyHC precipitates and IgG precipitates.

Discussion

There is strong evidence that stMyHC expression in *E. muelleri* is restricted to the endopinacocytes and it localizes to the actin tracts that run through this tissue. It is unfortunate that co-localization with F-actin could not be directly confirmed, but the loss of signal following latrunculin B treatment strongly supports the interaction of the two. From a developmental side, it does appear that the actin begins to organize prior to the formation of large thick filaments of stMyHC. As development progresses, filaments become larger and denser with myosin molecules. This suggests that the F-actin serves as a scaffold which recruits stMyHC containing myosin II molecules. It is tempting to interpret the increase in size as these contractile bundles develop a result of increased stability in the interactions of the stMyHC tails allowing for larger and more stable thick filaments to support the structure. A large amount of biochemical work with the sponge proteins would be needed to confirm this, though. The appearance of striations during

development is also an interesting feature, that supports the idea of recruitment of myosin to the actin structures. The actin tracts in *E. muelleri* are smooth in ultrastructure, in that they do not contain regularly spaced regions of different density following actin staining. This is likely the result of uneven overlap of actin fibers as seen in smooth muscle (**Figure 41d**). As a result of this, the thick filaments are also expected to be unevenly spaced and to appear continuous when fully developed, as is seen (**Figure 45c)** The striated appearance in developing structures at first give the appearance of an organization like that seen in striated muscles. However, the spacing between the striations is much too large to be the result of this. More likely, that is some actin bundling protein which is helping to guide the initial organization of the F-actin which is being replaced by newly formed thick filaments as the structures mature. A good candidate for this would be nmMyHC containing myosin II. Myosin II is most often considered for its motor function, but in the absence of motor activity its bipolar orientation makes it a strong actin bundler. This mechanism for recruitment of stMyHC+ thick filaments has been observed in muscle fiber development (Sanger et al., 2005; Van Der Ven et al., 1999). Overall, the finding that stMyHC appears to be highly restricted to the contractile actin tracts of the endopinacocytes strongly supports the homology of this tissue with muscles of other animals.

Regulation of contractions

Background

A fundamental part of tissue level contractility is regulation of the myosin motor activity. In muscles this can be done in two general ways, either at the thin filament, by

regulating the interaction between actin and the myosin motor, or at the thick filament, by regulating the activity of myosin directly. Mechanisms of thin filament regulation; the troponin complex in bilaterian striated muscles (Farah & Reinach, 1995) or caldesmon and calponin in vertebrate smooth muscles (Gerthoffer & Pohl, 1994; Wang, 2008; Winder & Walsh, 1993), are absent in non-bilaterians (Steinmetz et al., 2012). Thick filament regulation is most commonly through phosphorylation of the RLC, though direct Ca^{2+} binding to it or the ELC has been observed (Szent-Györgyi, 1996). This function is not restricted to muscles though.

Phosphorylation/dephosphorylation occurs in either Ca^{2+} dependent or independent ways. Very generalized mechanisms are; increased cytoplasmic Ca^{2+} binds to calmodulin, which activates MLCK, which phosphorylates the RLC, turning on the myosin motor and RhoA activates ROCK which phosphorylates myosin light chain phosphatase (MLCP) inactivating it, which prevents the dephosphorylation of the RLC and the turning off of the motor (Kaneko-Kawano et al., 2012; Webb, 2003). Sponges have a single gene for both the RLC and ELC so the same proteins are associated with both stMyHC and nmMyHC. As demonstrated earlier, *E. muelleri* appears to release Ca^{2+} from internal stores to trigger a contraction. Based on this, if the endopinacoderm shares homology with muscles, it would be expected that the MLCK pathway functions as the primary regulatory mechanism for contractility of the tissue. However, it is also possible that regulation is through thin filament regulation utilizing a mechanism that was either derived in the sponge lineage or lost/replaced by the troponin complex prior to the stem bilaterian. In order to understand the mechanism by which *E. muelleri* is regulating actomyosin contractility during contraction, it is important to see if there are changes in

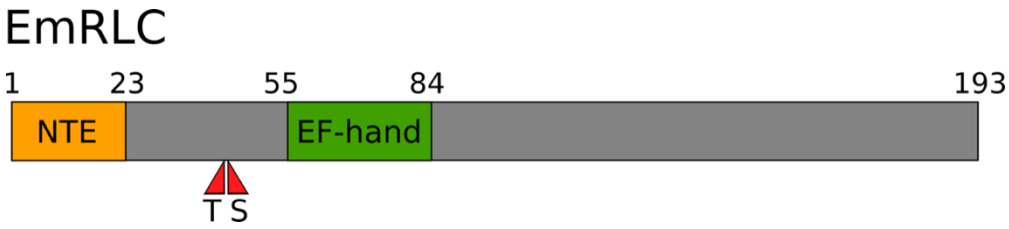

Figure 51. Structure of EmRLC ortholog. Predicted domain structure of RLC ortholog in *E. muelleri,* based on pfam domain predictions. NTE – N-terminal extension, which is found in various invertebrate RLCs. Putative phosphorylation sites shown in red. Numbers correspond to amino acid position.

the amount of phosphorylated RLC during this behavior. A recent study of actomyosin based collective contraction in a newly discovered colonial choanoflagellate was able to utilize a commercially available phosphor-specific RLC antibody (Brunet et al., 2019). Sponge RLC is well conserved and contains putative phosphorylation sites (**Figure 51**), so it is hypothesized that this should also be recognized by the antibody, allowing for visualization of where RLC is phosphorylated. Based on the shortening of the stMyHC+ actin tracts during contraction, it is likely that increased myosin activity is actively contracting the tissue. If this is regulated by phosphorylation of the RLC, then it should either be governed primarily by the active phosphorylation or suppression of dephosphorylation. This does not mean that only one pathway is functioning, as there is quite a bit of overlap in muscles. Vertebrate vascular smooth muscle uses a combination of MLCK and ROCK signaling to maintain tension (Zhou et al., 2017; Hong et al., 2011). Contractility of striated muscles, primarily regulated by the troponin complex, is also modulated by MLCK activity (Yu et al., 2016; Ryder et al., 2007). However, inhibition of MLCK and ROCK should provide insight into the basic mechanism functioning in sponge tissue. If Ca^{2+} release leads to active phosphorylation of RLC by MLCK, which is turned off by MLCP, then inhibition of MLCK should block contractions. On the other

hand, there is likely a steady rate of phosphorylation and dephosphorylation which maintains resting tension in the tissue. Modulation of MLCP could result in an increase in phosphorylated RLC through a decrease in dephosphorylation. In this case, inhibiting ROCK would result in a blocking of contractions. There are well established pharmacological inhibitors of MLCK, such as MLCK inhibitor peptide 18 and ML-7 (Cheng et al., 2015; Foster et al., 1990). ROCK can be inhibited through treatment with the drug Y-27632 (Peh et al., 2015), and there is a study suggesting that it is effective in *E. muelleri*, though this was looked at in a developmental context (Schenkelaars et al., 2016).

Methods

pRLC immunostaining

Gemmules were plated and hatched as described earlier in glass bottom dishes. Initial stainings were performed using standard 3.7% formaldehyde in EtOH protocol. A 1:100 dilution of anti-pRLC (Cell Signaling Technology #3671T) was used, and primary was visualized with anti-rabbit AF™488 (Life Technologies, 1:500) and samples were co-stained with phalloidin AF™568 (Life Technologies, 1:120) and Hoechst dye (33,342, 1µg/mL). Relaxed and contracted stainings were performed following the same protocol used for measurement of the actin tracts. Samples were either treated with L-NAME prior to fixation (relaxed) or were induced to contract using 500pM thapsigargin in LW (contracted). These sponges were fixed in 3.7% formaldehyde in EtOH and stained using 1:100 dilution of primary anti-pRLC. Proteins were visualized with 1:500 dilution of anti-rabbit AF™488, 1:100 Hoechst, and 1:120 phalloidin AF569. Samples were imaged

on an Olympus Fluoview FV3000 confocal laser scanning microscope using either a 60×/1.4 NA or 100×/1.4 NA objectives. Laser levels and acquisition setting were not adjusted for imaging controls. 10 image stacks were taken through comparative regions of the pinacoderm using the exact same setting for both samples. Maximum intensity projections of the images were made in Fiji (Schindelin et al., 2012) and the actin and pRLC images were stacked. Lines were drawn on the actin images connecting adhesion plaques. These were then placed over the pRLC images and length and average pixel intensity were taken.

MLCK and ROCK inhibition

Gemmules were plated and hatched as described earlier in 6-well format. After hatching samples were washed daily in fresh LW. For ROCK inhibition, samples were treated with 5μM Y-27632 for 48 hours beginning at tent stage or 10μM Y-27632 for 2 hours just prior to inducing a contraction. Contractions were induced with sumi ink as described earlier. For MLCK inhibition, sponges were treated with 2μM MLCK inhibitor Peptide 18 or 1μM ML-7 for 2 hours prior to inducing a contraction. Contractions were induced with treatment of 500nM thapsigargin. For induced contractions, time lapse images were taken with 30 second frame rate for 181 frames. Sponges that had been treated with MLCK inhibitors were fixed and stained for pRLC following at ~20 minutes following induction as described earlier.

Contraction assays

Gemmules were plated and hatched in LW+100µg/mL ampicillin in 24-well format as described earlier. Water was refreshed each day following hatching. Sponge were treated with 1µM ML-7 or 50µM blebbistatin in LW 2 hours prior to assay. Sponges were then treated with 1:20 (v/v) sumi ink in LW (control) or treatment solution for 10 minutes. Samples were very carefully washed several times with LW and then incubated for 3 hours. Samples were then treated with 1:1000 (v/v) DiI (ThermoFisher Scientific #D282) in LW for 10 minutes. Samples were washed with LW prior to imaging. The basic idea of the assay is samples that showed ink staining in the choanocyte chambers verified that the treatment doesn't disrupt incurrent flow. Following treatment with ink, if the sponge is able to successfully clear it, the DiI will brightly stain the choanocyte chamber. However, if the sponge is not able to clear the ink, then flow will be disrupted and DiI staining in the choanocyte chambers will be limited **(Figure 52)**.

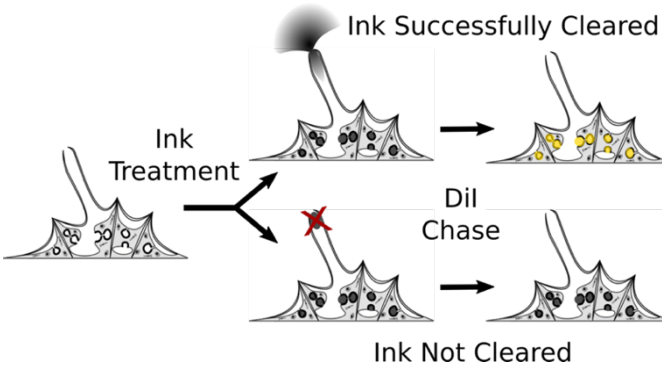

Figure 52. Contraction assay. Sponges are treated with ink, which stains the choanocytes if brought into the sponge. If this is effectively cleared then treatment with DiI will stain the chambers as well. If not cleared, only ink staining will show.

Results

Staining for pRLC showed strong localization to the actin tracts with faint signal at the stress fiber-like structures in the basopinacocytes (**Figure 53**). This is evident in some but not all structures and varied in intensity which is consistent with this serving as

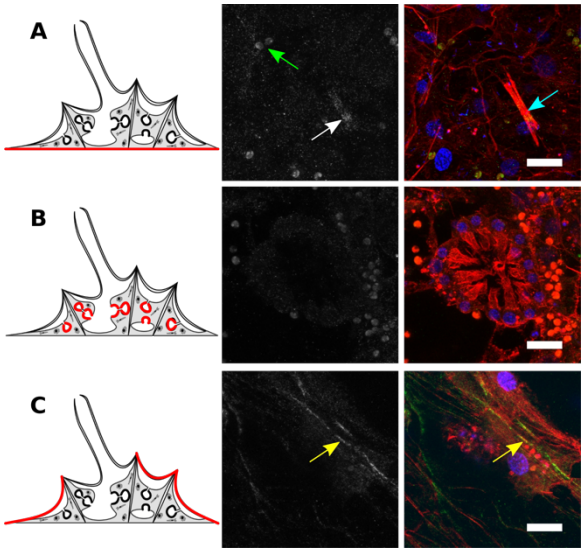

Figure 53. Immunostaining for pRLC in *E. muelleri.* Confocal images of sponges stained for pRLC (green), actin (red), and DNA (blue). Gray scale raw images of pRLC staining on the left. **(a)** Staining in the attachment epithelium shows some signal along the stress fiber-like structures, pRLC (white arrow) and actin structures (cyan arrow). Autofluorescent associated algae labeled with green arrow for reference. **(b)** There is no specific pRLC signal in choanocyte chambers. **(c)** Strong signal can be seen along the actin tracts in the apical pinacoderm (yellow arrows). Scale bars 5µm.

an on-off method of regulation (**Figure S15**). In the relaxed and contracted sponges, contracted sponges show brighter staining in more puncta like structures. This seems to suggest that increased phosphorylation is associated with shorter actin bundles. Measurement of staining intensity along actin tracts does reveal correlation between the

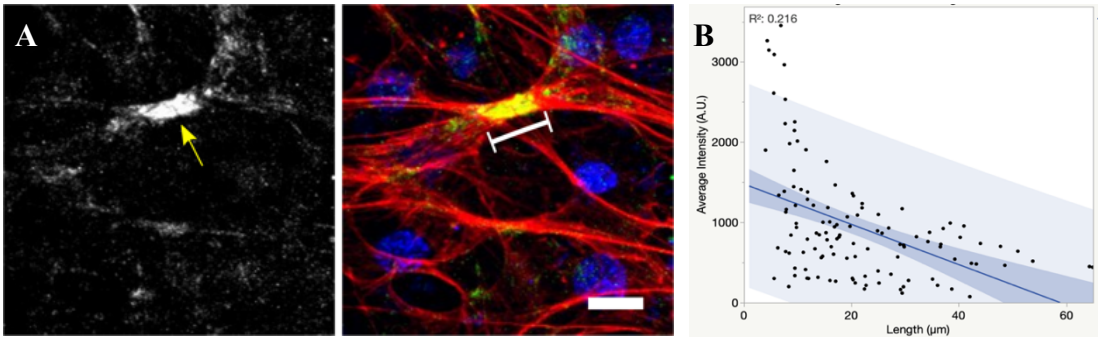

Figure 54. In contracted sponges, strong pRLC is found at short actin tracts. (a) Confocal image of a contracted sponge stained for pRLC (green), actin (red), and DNA (blue). Raw pRLC staining in grayscale. A highly contracted actin tract (white bar) shows very strong pRLC signal (yellow arrow). **(b)** Length of actin tract was measured on actin channel image and then average intensity in the pRLC channel was taken along length of measurement. Pearson coorelation coefficient for average intensity and length of actin tract was R=-0.4649 which is statistically significant ($p<<0.001$). n=118. Scale bar 5µm.

length of the actin tract and the intensity of the pRLC staining (Pearson correlation coefficient R=-0.4649, p<<0.001) (**Figure 54**).

MLCK inhibition with MLCK inhibitor peptide 18 did not show any difference in the sponge's ability to contract as well as any change in the pRLC staining pattern (**Figure S16**). Treatment with ML-7 on the other hand did appear to decrease the pRLC staining as well as reduce the sponge's ability to contract (**Figure 55**) and appeared to affect the staining levels in a contracted sponge (**Figure 56**). This did not appear to be complete, but in the ink/DiI trials it showed the greatest effect on ability to effectively clear the ink from the canals (**Figure 57**). The incomplete inhibitor is likely either a result of limited activity of the drug or the sponge's ability to clear some of it from the cytoplasm. Treatment with Y-27632 results in a decrease in the ability of the sponge to contract, both when treated during development of juvenile tissue and when treated after reaching juvenile stage (**Figure 58**). Both of these showed a less pronounced effect

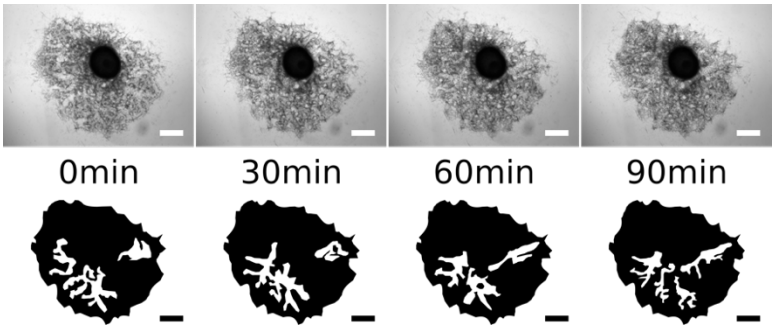

Figure 55. Treatment with MLCK inhibitor ML-7 reduces the Ca^{2+} dependent contractile response. Sponge treated with ML-7 was induced to contract with 500nM thapsigargin. Bottom panel shows outline of major excurrent canals. Some movement of canals is visible, with localized expansion and contraction, but there is no evidence of the coordinated inflation and contraction behavior. Scale bars 500μm.

compared with ML-7 treatment. Treatment during development had a greater effect on the sponge than treatment just prior to contraction.

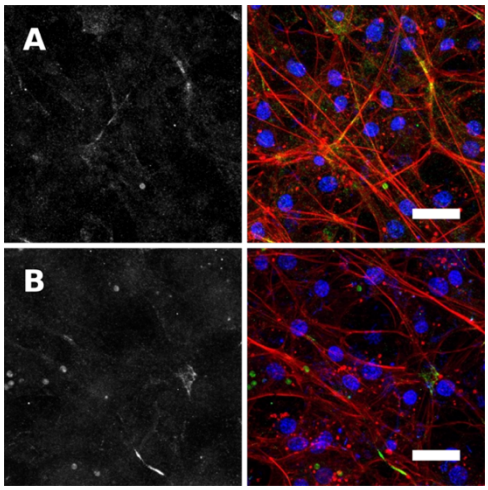

Figure 56. pRLC staining in ML-7 treated sponges resembles that of uninduced sponges. Sponges were treated with ML-7 and then induced to contract with 500nM thapsigarin prior to fixation and staining for pRLC (green), actin (red), and DNA (blue). Raw pRLC staining shown in grayscale on the **(a)** Control sponge, that was not induced to contract, shows limited staining for pRLC along the actin tracts. **(b)** ML-7 treated sponge induced to contract prior to staining show pRLC staining patterns similar to those seen in the relaxed sponge. Scale bars 20µm.

Discussion

Based on the staining pattern for phosphorylated RLC, it seems highly likely that active phosphorylation is involved in activation of stMyHC mediated contraction of the actin tracts. Since *E. muelleri* has a single gene for RLC, it is surprising that the staining is only really seen at the actin tracts. Even if the function of MLCK, for example, is restricted to the endopinacocytes, phosphorylation of the RLC is likely used in many cellular contexts (as other kinases can act on it). This can be explained by the high relative abundance of RLC along the actin tracts coupled with the localized coordination of phosphorylation events, leading to these being the only structures that stain beyond background with this antibody. The specificity of the antibody in *E. muelleri* is an assumption. Other commercial antibodies tested, such as a general RLC (MYL12B Antibody(N-Term), Abgent #AP19667a-ev), a nmMyHC (CMII 23-MyosinIIB, DSHB #CMII23), and a pan-MyHC (Anti-Myosin (Skeletal and Smooth), Sigma-Aldrich #M7648) (see appendix II) did not produce interpretable staining patterns. However,

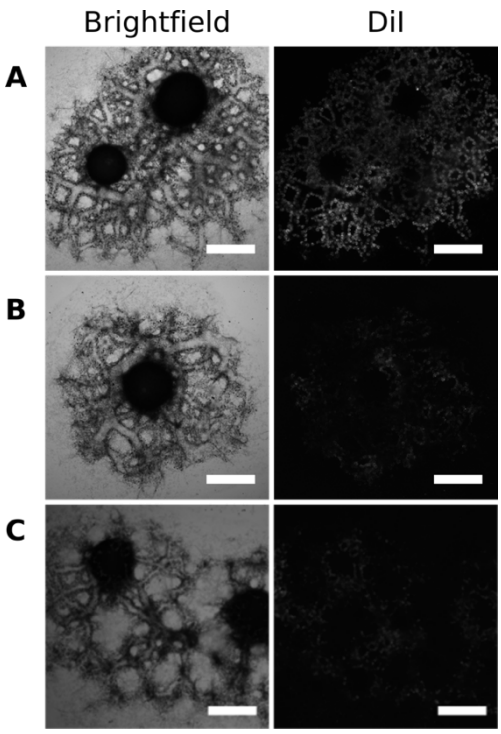

Figure 57. Treatment with ML-7 blocks ability to contract under physiological conditions. Sponge were either treated with DMSO **(a),** 1μM ML-7 **(b)** or 50μM blebbistatin **(c)** prior to treatment with 1:20 sumi ink. Strong ink staining in the choanocyte chambers shows internal flow. Sponges were then treated with DiI stain to see if flow is maintained following treatment with ink. Control sponges show DiI labeled choanocyte chamber while ML-7 and blebbistatin treated sponges do not. ML-7 treated sponges lacked DiI staining 71.6% of the time (n=21) while blebbistatin treated sponges lacked DiI staining 62.5% of the time (n=24). Scale bars 500μm.

studies showing this antibody even works outside of animals (Brunet et al., 2019) coupled with conserved phosphorylatable residues in EmRLC and the interpretable and predictable patterns seen in *E. muelleri* strongly suggests that it is recognizing pRLC.

The regulation of phosphorylation state of the RLC along the actin tracts appears to be primarily under the control of MLCK. Because of the huge amount of evolutionary time separating sponges from any of the biomedical model organisms, the effectiveness of well-established drugs is difficult to predict. For this reason, negative results cannot be considered biologically relevant as they could be a result of ineffectiveness in this organism. A positive result for one known inhibitor of MLCK (ML-7) but a negative result for another (Peptide 18) suggests that the negative result is because peptide 18 is ineffective in *E. muelleri.* This could be the result of an inability to directly act on EmMLCK (ex. lack of a conserved binding site) or due to increased effectiveness in clearing it from the cell. As a result of the sessile nature of sponges, they have well

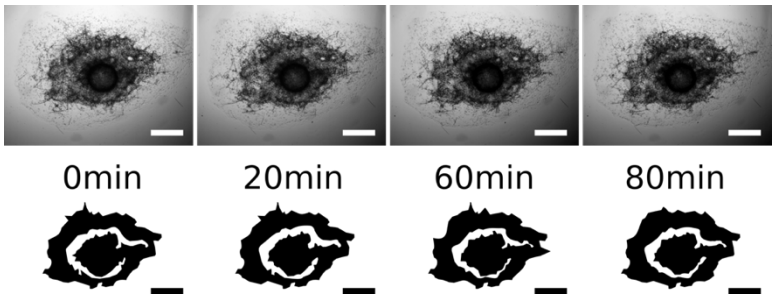

Figure 58. ROCK inhibition effects ability to contract. Sponges treated with the ROCK inhibitor Y-27632 were induced to contract with 1:1000 sumi ink. Limited contraction of the incurrent canals is seen over the first 20 minutes while excurrent canals can be seen contracting slightly over the next 40 minutes. Scale bars 500μm.

developed mechanisms for dealing with foreign substances in the water around them (Kenny et al., n.d.). Based on this, the seemingly contradictory results are interpreted as the positive inhibitory effect of ML-7 is sufficient to say MLCK is involved in contractions in *E. muelleri.* ROCK also appears to have an effect on the sponge's ability to contract. This appears to be less pronounced compared to the effect of treatment with ML-7. However, since neither of these are completely effective, it is difficult to compare size effect of inhibition for the reasons stated above. The results of the contraction assays are consistent with a role of active phosphorylation of RLC regulating contractions. Treatment with ML-7 has a similar effect as treatment with the myosin II inhibitor blebbistatin, suggesting that both MyHC ATPase activity is required for the contraction as well as MLCK activity. Combining the finding that increase in cytosolic Ca^{2+} concentration triggers a contraction with an increase in pRLC during contraction and inhibition of MLCK limits this, strongly suggests that this is the primary mechanism of activation of the contractile machinery as this would act upstream of ROCK. Rho-ROCK signaling likely plays a role in modulation of the contractions based on localized forces. It is interesting the earlier treatment has a stronger effect due to the pleiotropic nature of

ROCK. Rho-ROCK signaling plays a role in many cellular processes including myocardin related transcription factor (MRTF) activity, which is a regulator of expression of genes involved in building actomyosin contractile machinery and functions in a variety of muscles of different animals (Zhou et al., 2017; Esnault et al., 2014). Treatment with the ROCK inhibitor during development may actually reduce the amount of contractile tissue that develops by inhibiting MRTF (discussed in the Developmental Regulation chapter).

It should also be noted that with both ML-7 and blebbistatin treatment, the canals had a slightly inflated appearance (**Figure 57 b&c**). This occurred with a large degree of variability, sometimes apparent in the incurrent canals and sometimes in the excurrent canals. Given the plasticity of the sponge body it is difficult quantify this. However, conceptually, this taken with the basal levels of pRLC seen along the actin tracts seems consistent with actomyosin contraction serving an active role in maintaining tone through the canal system, analogous to vertebrate vascular smooth muscle. This is likely the primary purpose of the tissue, which offers a degree of regulation over water movement while maintaining consistent flagellar beating patterns in the choanocyte chambers. Under this, body contractions represent the extreme end of the behavior. Consistent with this, it was observed that long term treatment with blebbistatin in developing juveniles resulted in the occurrence of many oscula at different areas of the body (**Figure S17**). The location of an osculum is thought to be patterned by localized signaling in the canal system and flow sensitive cilia (Ludeman et al., 2014; Reid et al., 2018). Under consistent flow from the choanocyte chambers, loss of tone in aquiferous system would result in increased localized pooling and turbulence in the excurrent canals. The expected

result of this would be development of oscula at these sites. This is based on limited observations though, and further work needs to be done to understand the mechanism.

Conclusions

The finding that stMyHC is found exclusively at the contractile actin tracts strengthens the argument for their homology to muscles of other animals. Since nmMyHC is found in muscles of a variety of animals there was no initial expectation for the type of myosin that would be found at these structures in *E. muelleri.* The presence of stMyHC at these structures, which is restricted to muscles in other animals, could be due to convergence, or it could be the result of endopinacocytes and myocytes of other animals being derived from a common ancestor cell type, which was involved in body movement in the last common ancestor. The orientation of the contractile bundles in the tissues is similar to what is seen in the myoepithelial muscles of cnidarians, which may be a retained feature from their common ancestor.

From a regulatory standpoint, it appears that the actin tracts shorten as a result of increased phosphorylation of the RLC in a MLCK dependent manner. This is consistent with the finding that increased cytosolic Ca2+ levels trigger contractions and suggests that it is occuring in the cells that are actually contracting. The negative correlation between actin tract length and level or pRLC suggests that contractions are the result of active shortening as opposed to a reduction in counter pressure. The basal levels of myosin activity and pRLC also suggest that the endopinacoderm actively regulates canal tone under normal flow conditions, which likely represents the ancestral function of the tissue from which the coordinated contraction behavior evolved.

Taken together with the structure and composition of these structures, this is consistent with the endopinacoderm undergoing muscle-like contractions which may be due to a shared ancestral tissue type with muscles of other animals. However, this type of regulation is not specific to muscles, function is not a good judge of homology, and the split between stMyHC and nmMyHC occurred before animals but nothing is known about how they are used in unicellular organisms. For these reasons, it is important to understand the developmental processes that give rise to these tissues in order to build a fuller picture of their evolutionary relationship in distantly related lineages.

Chapter 5: Developmental Regulation of Contractile Tissue in *Ephydatia muelleri*

Introduction

The actomyosin contractile module likely dates back to the stem eukaryote (Brunet & Arendt, 2016) and has been shown to self-assemble in a highly organized fashion in non-muscle cells (Hu et al., 2017). There is also strong evidence that the striated muscles found in medusozoan cnidarians evolved their striations independently of bilaterian striated muscle (Steinmetz et al., 2012) and that there have been repeat occurrences of co-option of either the striated contractile module (as in vertebrate cardiomyocytes) or the smooth contractile module (as in planarian somatic myocytes) in specific myocyte lineages (Brunet et al., 2016). Based on this, structure and function of contractile cells alone is insufficient for judging homology across phyla. In bilaterians, all muscles are derived from the mesoderm, though their presence in non-bilaterians suggest an evolutionary history predating the occurrence of a mesoderm. Since the origin of these cell types is fundamentally different in bilaterians (triploblasts) and non-bilaterians (diploblasts), there is good reason to focus on the core regulatory complex (CoRC) of terminal selectors for cell fate determination in order to judge homology. Myogenic Regulatory Factors (MRFs), such as MyoD, are well studied for regulating expression of the core set of striated myocyte target genes (Shi & Garry, 2006), but have not been identified outside of bilaterians (Steinmetz et al., 2012). In smooth and cardiac myocytes,

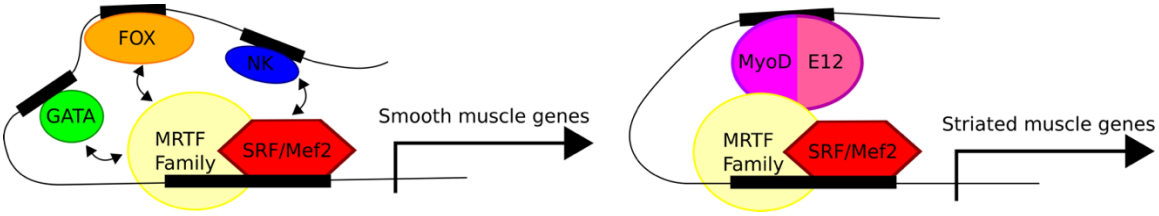

Figure 59. Core group of terminal myogenic regulatory factors present in the stem bilaterian. Based on (Brunet *et al.* 2016) the stem bilaterian had two primary muscle types; fast contracted striated and slow contracting smooth, which had unique sets of core transcription factors involved in terminal differentiation. Both complexes are built around the interaction of an MRTF family protein and a MADS-box transcription factor.

MRFs are replaced by NK, GATA, and Fox family proteins (Nishida et al., 2002; Hoggatt et al., 2013). In both cases, these interact with a myocardin related transcription factor (MRTF) family protein (MASTR in vertebrate striated, myocardin in vertebrate smooth and cardiac) and a MADS box transcription factor (serum response factor (SRF) or myocyte enhancer factor 2 (Mef2)) (Brunet et al., 2016) (**Figure 59**). *E. muelleri* has a single gene for a MRTF family member (hereafter referred to as EmMRTF) as well as SRF and Mef2 with highly conserved MADS box domains (**Figure 60**). The interaction of MRTF and a MADS box protein drives transcription of contractile genes in a variety of cells, with myocardin originally identified as a master switch for smooth muscle differentiation in vertebrates (Wang et al., 2003). However, the function of MRTF and its interactions with these other proteins has never been studied outside of bilaterians.

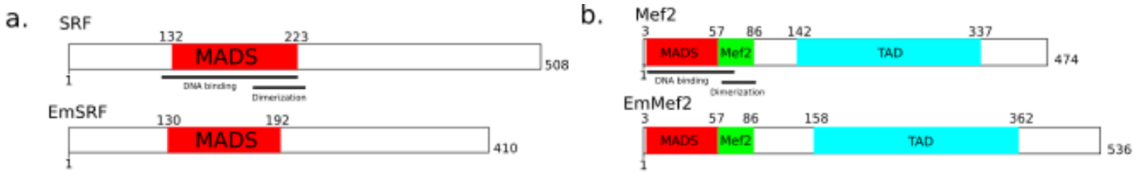

Figure 60. *E. muelleri* has well conserved SRF and Mef2 orthologs. Predicted domain structures of EmSRF and EmMef2, identified in the *E. muelleri* transcriptome, compared to mammalian orthologs. Functional domain predictions based on pfam predictions and alignment with functionally characterized proteins. Numbers represent amino acid position.

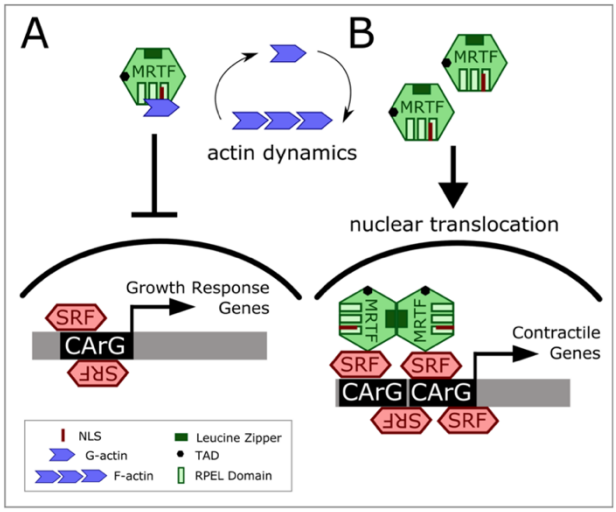

Figure 61. Actin dynamics modulates MRTF function. (a) Binding of the RPEL domains of MRTF to G-actin blocks the nuclear localization signal (NLS), resulting in cytoplasmic localization. Nuclear localized SRF drives expression of many growth responsive genes by binding to CArG sequences in promoters. **(b)** Increasing actin polymerization results in the freeing of MRTF from G-actin, exposing the NLS. MRTFs dimerize via the leucine zipper-like domain and each bind an SRF dimer in the nucleus. The strong transactional activation domain (TAD) on MRTF drives expression of contractile apparatus related genes.

Expression of target genes of the MRTF/MADS box interaction is driven by the strong transcriptional activation domain on the C-terminus of MRTF. The N-terminus of MRTF family members contains RPEL repeats which bind to G-actin imparting mechanosensitivity (lost in myocardin but present in EmMRTF). Increased actin polymerization, often driven by Rho signaling, decreases the amount of G-actin in the cell freeing MRTF which exposes a nuclear localization signal which leads to nuclear translocation and interaction with either SRF or Mef2 (Medjkane et al., 2009) (**Figure 61**). Sponges are unique to animals in the occurrence of asymmetry and the degree of plasticity in their body plan (Leys et al., 2011). As sessile aquatic animals, their body shape and patterning is influenced by the current and turbulence of the surrounding water (Leys et al., 2011; Dunn et al., 2015). Our hypothesis is that MRTF plays a large role in

this body plan plasticity by patterning contractile tissues, which both regulate water flow through the aquiferous system and resist deformative stress from external flow.

From a structural perspective, the MRTF consists of N-terminal RPEL repeats which mediate the interaction with G-actin, a basic region followed by a glutamine-rich regions which mediate the interaction with SRF, a SAP domain which mediates promoter binding, a leucine zipper which mediates dimerization, and a C-terminal transcriptional activation domain (TAD) (Mouilleron et al., 2011). These regions and domains appear to all be present in the same order in the *E. muelleri* orthologue (**Figure 62**). Searching non-animal holozoans, there are SAP domain proteins, but nothing with this exact domain architecture could be identified, suggesting that this may be an animal innovation.

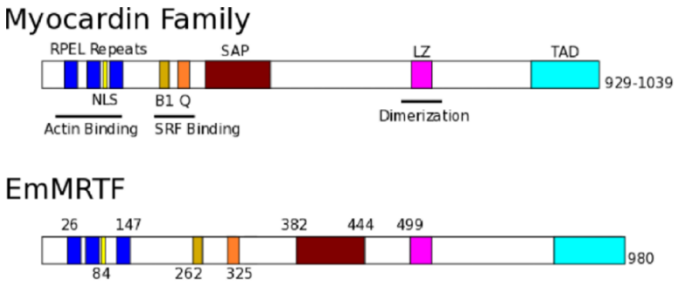

Figure 62. Domain structure of EmMRTF. The predicted domain structure of EmMRTF resembles that of mammalian MRTF family proteins. Functional domain predictions based on pfam predictions and alignment with functionally characterized proteins. Numbers represent amino acid position.

Myocardin was originally identified in vertebrates as the primary myogenic factor involved in smooth muscle differentiation (Wang et al., 2003). Similar to the ability of forced expression of MyoD to convert pluripotent cells and fibroblasts into skeletal muscles (Tapscott, 2005), myocardin can be sufficient to induce a smooth muscle cell fate (Long et al., 2008). Related proteins, termed myocardin related transcription factors (MRTFs), were then identified and found to serve functions in development of contractile

structures (Pipes et al., 2006) as well as direct roles in myogenesis (Cenik et al., 2016). Vertebrates have the broadly expressed MRTF-A and MRTF-B which is more restricted (Li et al., 2005; Wei et al., 2007). These three proteins, MRTF-A, MRTF-B, and myocardin are all closely related in their domain architecture except myocardin lacks the N-terminal RPEL repeats and is constitutively found in the nucleus (Pipes et al., 2006). Vertebrates also have a fourth related protein, MASTR, which functions in embryonic myogenesis and skeletal muscle development (Meadows et al., 2008). Outside of vertebrates, single MRTF family orthologs can be identified, though limited functional work has been done. In *Drosophila*, an MRTF ortholog has been identified and shown to have a conserved function with SRF (Han et al., 2004). There is also evidence that this serves an essential function in early myogenesis (DeAguero et al., 2019). Based on the distribution of MRTF family proteins, it appears that there were duplications and

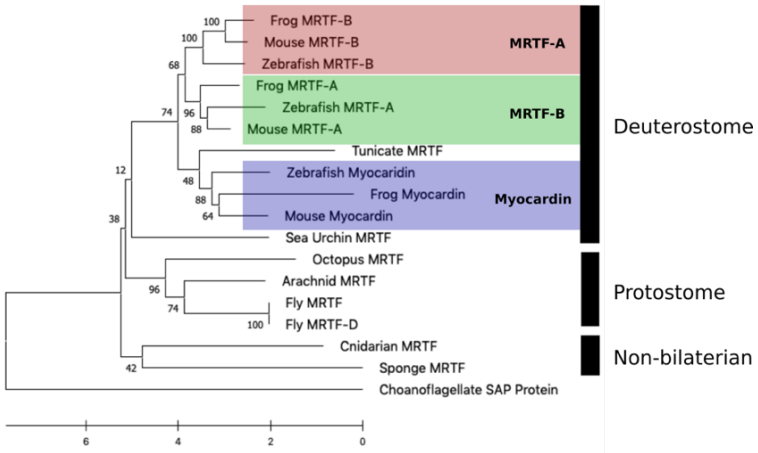

Figure 63. MRTF family underwent expansion in vertebrate lineage. Maximum likelihood phylogeny of MRTF family proteins from a variety of animals, which closely matches their phylogenetic positioning. Single orthologs are generally present for non-bilaterians, protostomes, echinoderms, and hemichordates while vertebrate proteins can be divided into MRTF-A, MRTF-B, and myocardin. Choanoflagellate SAP domain containing protein was used as an outgroup. Support values based on 100 bootstrap iterations.

radiation that occurred in the vertebrate stem lineage (**Figure 63)**. That all of the MRTF family proteins function in myogenesis in vertebrate and that this function is also seen in the limited invertebrate studies, lead to the hypothesis that the ancestral protein functioned in myogenesis.

Myocardin Related Transcription Factor Localization in Ephydatia muelleri

Background

Because of the mechanism of action for MRTF, expression data alone is likely insufficient for understanding its function in sponges. It is hypothesized that MRTF is widely expressed in *E. muelleri*, primarily in the archeocytes and pinacocytes, with limited or no expression in the choanocytes. Testing this is important to understanding the role of MRTF in *E. muelleri*, but it is also important to see the distribution of cytosolic and nuclear pools. For this reason, efforts were focused on producing a custom antibody targeting EmMRTF. MRTF has not been found to drive transcription alone, but rather through an interaction with SRF or Mef2 (Medjkane et al., 2009; Gau & Roy, 2018; Creemers et al., 2006). In developing myocytes this interaction also associates with other transcription factors forming a CoRC. Apart from monitoring spatiotemporal expression and subcellular localization of EmMRTF, a good antibody could allow for co-immunoprecipitation (CoIP) of interacting partners. This could provide a powerful means of *de novo* identification of other factors involved in development of contractile tissues in *E. muelleri.* Being a transcriptional regulator, it is also important to understand what genes are targeted by MRTF. If CoIP works with this antibody, then chromatin immunoprecipitation sequencing (ChIP seq) can also be utilized to identify the genomic

sequences to which MRTF is bound during different developmental stages. At the time of writing this, a well assembled genome for *E. muelleri* has just become available (Kenny et al., n.d.) which would allow very accurate mapping of EmMRTF activated genes.

Methods

Antibody production

The sequence for EmMRTF was amplified from cDNA using the following primer set;

Forward - TACTTCCAATCCAATGCATCTTGCGAGCCGCTGAGCTT

Reverse - TTATCCACTTCCAATGTTATTACTAGCATGCAACATGAGTTA

The amplified product was gel extracted and cloned into a pET His6 SUMO TEV LIC vector (Addgene#29659) and transformed into a Rosetta strain of *E. coli* for recombinant protein expression. Protein was expressed for 4 hours at 30^{o}C and was purified using HisPur™ cobalt resin (ThermoFisher Scientific #89966). Following purification, the recombinant protein was dialyzed into 1x PBS pH 7.4 with 5% glycerol and sent for rabbit injection. Anti-EmMRTF was affinity purified from rabbit serum using the same protocol followed for anti-stMyHC antibody. Affinity purified antibody was then transferred to 1x PBS and concentrated using Amicon® Ultra-4 Centrifugal Filter tubes (Millipore #UFC801008). Two fractions of antibody were saved consisting of more concentrated early elutions and more dilute later elutions. Since near full length EmMRTF did not express very well, the SAP domain was also cloned following the same procedure and using the following primer set;

EmMRTF-SAP

Forward - TACTTCCAATCCAATGCAGAGGCTGGAACTGCAGTAGG

Reverse - TTATCCACTTCCAATGTTATTACTAGTTCAAAGAGAGGCGTCTGG

This recombinant protein was used to build an affinity purification column which the anti-EmMRTF serum was passed through. This purified antibody was labeled EmMRTF-SAP and showed consistent staining patterns seen with anti-EmMRTF.

Immunostaining

Gemmules were plated and hatched as described earlier in either glass bottom dishes or on glass slides. For samples grown in glass bottom dishes, sponges were fixed and stained following the standard 3.7% formaldehyde in EtOH protocol. For samples grown on slides, some were fixed in 3.7% formaldehyde in LW for 10 minutes at room temperature. They were then transferred to 3.7% formaldehyde in 1x PBS for 45 minutes at room temperature. Samples were then washed into 1x PBST. Samples were then blocked in 3% BSA in PBST for 1 hour at room temperature. Regardless of fixation method, samples were treated with 1:200 primary antibody in blocking solution (a variety of concentrations were tested). Samples were treated with a secondary solution of anti-rabbit AF™488 (Life Technologies, 1:500), phalloidin AF™568 (Life Technologies, 1:120), and Hoechst (33,342 1µg/mL) dye in blocking solution. For mounting, samples on slides were treated with 50µL of mounting media and a coverslip was slowly placed over the sponge under a dissecting microscope until it made contact with the pinacoderm and was then sealed. For competition stainings, primary antibody was mixed with 10µg of recombinant protein prior adding it to the sample.

Western Blot

Approximately 50 gemmules were plated and hatched in LW+100µg/mL ampicillin in a petri dish. After hatching water was refreshed daily with LW (no antibiotics). At 3 days post hatching, the sponges were inspected for the presence of canals and choanocyte chambers. The majority of the water was then drained from the dish, leaving approximately 1mL in the edge. The sponges were then scraped with a clean razor blade into the remaining liquid and the tissue was transferred to a clean 1.5mL Eppendorf tube. This was spun on a benchtop centrifuge at the lowest setting for 2 minutes and all but ~280µL of water was removed. The sample was then mixed with 100µL of 4x SDS PAGE loading buffer and 20µL of 2-mercaptoethanol (BME), vortexed, and boiled for 8 minutes on a heat block. After spinning down, the sample was run on a 10% SDS PAGE gel and transferred in 5% MeOH buffer at 350mA for 28 minutes on ice. The membrane was then blocked in 5% Milk in PBST for 1 hour at room temperature and incubated with primary antibody diluted in blocking solution overnight at 4^{o}C. Primary antibody was visualized by adding anti-rabbit AF™488 (Life Technologies, 1:2000) in blocking solution and incubating at room temperature for 45 minutes.

Immunoprecipitation

Approximately 200 gemmules were plated between two petri dishes in LW+100µg/mL ampicillin. After hatching water was replaced with just LW (no antibiotics) and sponges were grown for 3 days with daily water changes. Whole cell lysates and immunoprecipitation (IP) were performed as described for the stMyHC IP

utilizing the Pierce Crosslink IP kit (ThermoFisher Scientific #26147). For the column, 100µg of affinity purified anti-EmMRTF was used and 100µg of anti-rabbit IgG was used for a control. 600µL of sponge whole cell lysates was added to each column and they were incubated overnight at 4ºC on a rotisserie. After elution, samples were separated using SDS PAGE and one gel was Coomassie stained and the other was transferred for blotting with anti-EmMRTF, following the western blot procedure above.

Results

Due to the predicted nature of this protein, it is not expected to specifically localize to any cellular structures. Rather, there should be a diffuse cytoplasmic as well as a nuclear pool, with the ratio of the two reflecting amounts of active (nuclear) to inactive (cytoplasmic) protein. Because of this, staining patterns are difficult to interpret directly, due to background autofluorescence in the sponge. There does appear to be a good amount of signal in a variety of cells with some showing predominantly nuclear staining and other showing strong cytoplasmic staining (**Figure S18**). Looking closer at specific tissues, it appears that cells in the pinacoderm contain primarily nuclear pools, while cells in the mesohyl show strong cytoplasmic staining (**Figure 64**).

There was very strong staining in the basopinacocytes, which showed a large nuclear pool as well as a cytoplasmic pool (**Figure 64a**). Choanocyte chambers showed limited staining, which appears to be predominantly in the cytoplasm, based on comparison to the blue channel, but it is difficult to resolve due to the small size of these cells (**Figure 64b**). Archeocytes (sponge stem cells), which are discernable by their large nucleolus (cyan arrow heads), showed strong cytoplasmic staining (**Figure 64b-d**). Cells

in the apical pinacoderm showed primarily nuclear staining, with very limited cytoplasmic signal (**Figure 64d**). When competed with EmMRTF recombinant protein, the general staining patterns went away, but were replaced by large puncta staining.

The western blot of *E. muelleri* whole cell lysates shows a banding pattern that correlates with the predicted size of EmMRTF (**Figure S19**). This pattern increases in

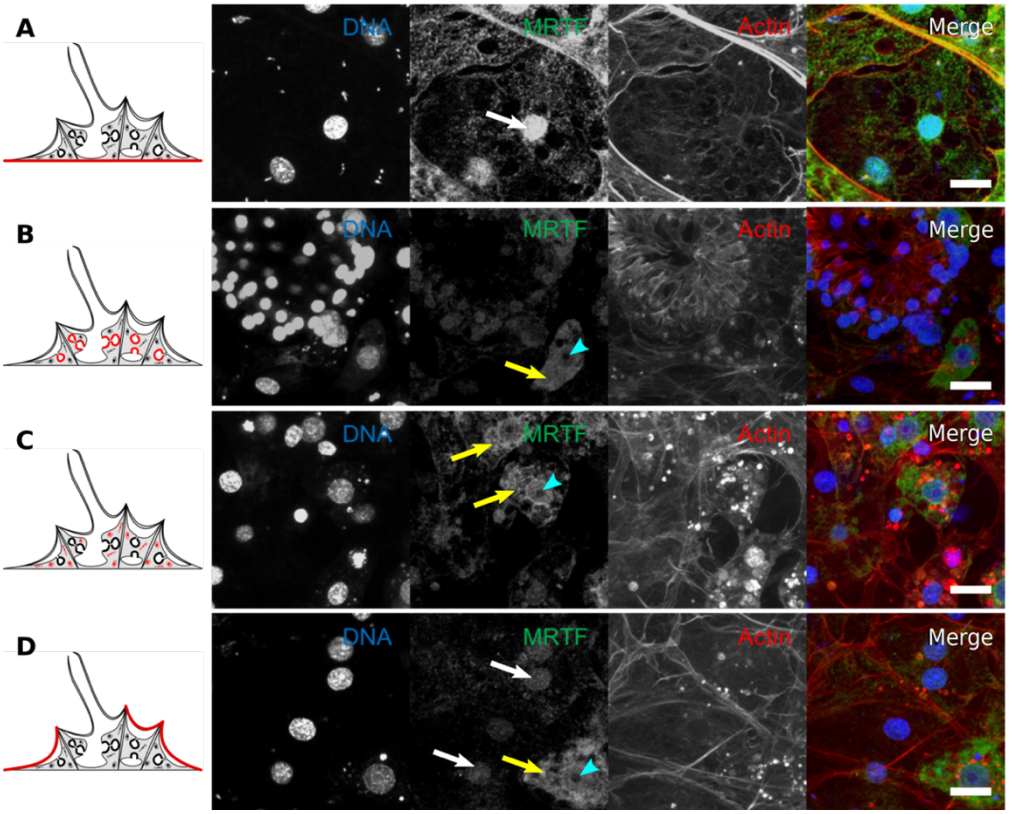

Figure 64. Subcellular localization of EmMRTF seems cell type specific. Confocal images of sponges stained with EmMRTF (green), actin (red), and DNA (blue). Grayscale images from each channels show overlapping MRTF signal in either the nucleus (DNA) or cytoplasms (actin). **(a)** Strong nuclear staining (white arrow) is seen in the basopinacocytes of the attachment epithelium, **(b)** Limited staining is visible in choanocytes thou it appears to be cytoplasmic. Strong staining is visible in cell near the choanocyte chamber (yellow arrow) which appears to be an archeocyte based on the prominent nucleolus (cyan arrow). **(c)** In the mesohyl, migratory cells show strong cytoplasmic staining (yellow arrows). This is most obvious in cells with a prominent nucleolus (cyan arrow) suggesting they are archeocytes. **(d)** Cells of the apical pinacoderm show primarily nuclear staining (white arrows) while cytoplasmic staining can be seen in adjacent cells which also contain a clear nucleolus (yellow and cyan arrows respectively). Scale bars 5μm.

intensity as antibody concentration increases. There is a second, slightly lower band that is faintly visible in the higher concentration strips.

Immunoprecipitations were performed several times with subtle changes to the protocol, such as number of sponges used, amount of antibody used, more thorough washing, and not crosslinking the antibody in the column. These all methods showed similar results, with very consistent staining patterns for the whole cell lyases (**Figure 65**). The flow through following precipitation showed a similar banding pattern as the raw lysates, without a strong decrease in intensity. Precipitates did not show strong signal at the predicted size for EmMRTF, though a faint band was visible in some trials, which was absent from the IgG control (**Figure 65b**). For coomassie stained gels, no protein other than IgG was visible in any of the precipitates.

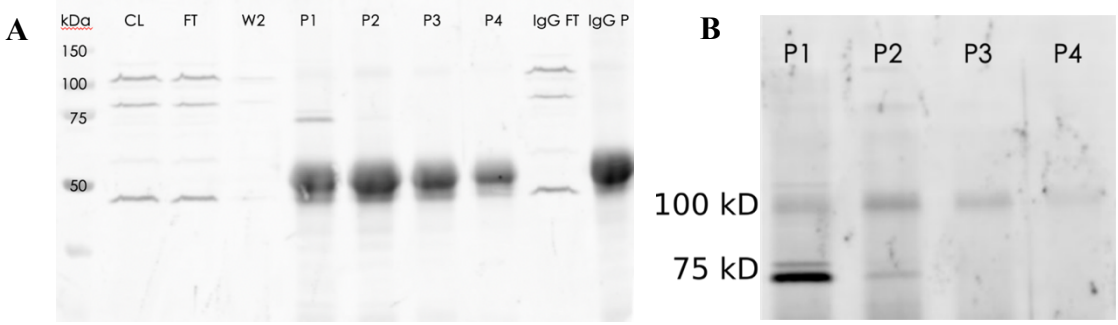

Figure 65. Immunoprecipitation with antibody produces inconsistent results. **(a)** Raw cell lysates (CL) show three strong bands, the largest of which corresponds to the predicted protein size. These do not significantly change in the flow through (FT) following precipitation. The final wash step (W2) contains traces of these proteins. Precipitates 1-4 (P1-4) show a band around 75kD in P1 which is faintly visible in P2. IgG control flow through (IgG FT) shows the same pattern as the raw lysates. There are no visible bands in the IgG precipitates (IgG P). **(b)** Zoom in and higher exposure of the precipitates above the antibody.

Discussion

The western blot and immunostaining results are consistent with the predictions for this protein. There does appear to be a cytoplasmic and nuclear pool of EmMRTF with an increased cytoplasmic pool in archeocytes and an increased nuclear pool in pinacocytes. Archeocytes are pluripotent cells which can differentiate into pinacocytes to help establish new tissue or replace damaged or old cells (Funayama, 2010). The large amount of cytoplasmic EmMRTF could be reflective of a waiting pool that can become activated during differentiation or these cells could be in a developmental stage in which MRTF expression is increased but activation is prevented. The staining in archeocytes is fairly inconsistent with respect to intensity, which could support the latter, but could also be explained by variation in the penetration of the antibody through the mesohyl. Pinacocytes appeared to have increased nuclear localization, with the most obvious staining in the basopinacocytes. These cells form the very large stress-fiber-like structures, which function in substrate attachment as well as a variety of other functions which have not been fully characterized (Mitchell & Nichols, 2019). If these structures are organized like stress fibers seen in fibroblasts and other cell types (Burridge & Guilluy, 2016), it would not be surprising that they are regulated by MRTF, in that they form stable contractile actomyosin structures that connect two adhesion sites. Staining in the apical pinacoderm is less pronounced, but there does appear to be a larger nuclear pool than cytoplasmic. Despite orienting the tissue against the coverslip, it is difficult to resolve between the endo and exopinacocytes which became more pronounced when scanning through the mesohyl. There was no strong staining in the choanocytes. Overall this staining pattern is consistent with expectations if there is a conserved function of

MRTF in *E. muelleri.* Having a resting pool of MRTF in archeocytes could allow for rapid activation and expression of contractile targets after integration into the tissue. In other animals, rho signaling, which can be induced by mechanical stress (Lessey et al., 2012), as well as the YAP/TAZ pathway, which responds to changes in substrate stiffness (Dobrokhotov et al., 2018), have been shown to be regulators of MRTF activity (Esnault et al., 2014; Fearing et al., 2019; Bialik et al., 2019). Archeocytes are migratory, so likely experience transient localized force as they move through the mesohyl. Pinacocytes comparably form stable adhesion structures, seen at the putative cell-cell adhesion plaques between endopinacocytes, the dense cortical actin structures in exopinacocytes, or the various adhesion structures seen in the basopinacocytes. One possibility is that as archeocytes integrate into these tissues, formation of stable adhesions leads to consistent mechanical stress along these points, which activates signaling pathways involved in increased actin polymerization, freeing the interaction of MRTF and G-actin leading to an accumulation of MRTF in the nucleus. There it can interact with either SRF or Mef2 leading to expression of target genes involved in building contractile machinery. If this is the case, the basic mechanism for development and maintenance of the endopinacoderm would be similar to satellite cell regeneration of myofibers (Mokalled et al., 2012).

The results for the western blot are also consistent with the known function of MRTF in other animals. The antibody appears to recognize a protein of the correct size for EmMRTF and produces two bands, with the lower one fainter than the upper. One interpretation of this is that the lower band represents a phosphorylated version of the protein. There are several phosphorylation sites that have been documented for MRTF, which play roles in both activity and inhibition of function. Rho and ERK dependent

phosphorylation have been shown to free the inhibitory interaction with nuclear actin and lower affinity for G-actin and increase nuclear translocation respectively (Panayiotou et al., 2016). Phosphorylation at a different site has been shown to expose a nuclear export signal, leading to increased cytoplasmic accumulation (Muehlich et al., 2008). These phosphorylation events affect the function of the protein, but are not required for activity, rather modulate function. Because of this, it is difficult to use relative amounts of pMRTF to MRTF as an indicator of function in *E. muelleri.*

The IP results are difficult to interpret. There is not a large decrease in protein between the raw cell lysates and the flow through, suggesting that these proteins are not being removed efficiently. The blotting pattern for the cell lysates shows additional bands that are not present when sponge lysates are prepared by transferring tissue directly into loading buffer and boiling. The additional bands are generally lower molecular weight compared to the predicted size of EmMRTF. These could represent degradation products that form during the time between initial harvesting and preparation to run the gel. The amount of protein in the precipitates was generally low and was not of a consistent size. This could be due to low specificity or it could be a result of precipitation of various fragments of degraded protein, which only a few were abundant enough to visualize. Because of the low amount of protein and inconsistency in size, mass spectrometry was not performed on any of the samples which means that the antibody could not be directly validated. For this reason, the finding from the immunostainings and western blots should be taken with some degree of skepticism. However, I do not believe they should be completely disregarded, as in both cases they produced predictable and repeatable patterns which were lost when competed with recombinant protein. The puncta that

appeared as a result of the immunostaining competition is interpreted as the formation of aggregates of EmMRTF with recombinant protein and other interacting partners, which is an expected result for this protein, due to the presence of the leucine zipper (Shen et al., 2005; Ciaccio & Laurence, 2009).

Pharmacological perturbation of MRTF pathway

Background

Apart from its role in myogenesis, MRTF-A has been shown to regulate neuronal growth cone development and factors involved in cell migration in vertebrates (Mokalled et al., 2010; Gau & Roy, 2018). This has become the focus of active research due to its role in epithelial mesenchymal transition (EMT) in cancerous cells as well as fibrosis related diseases (Xu et al., 2018; Shiwen et al., 2015). For this reason, drugs targeting MRTF activity have been designed for therapeutic purposes. CCG-203971 is a cell permeable, inhibitor of Rho/MRTF/SRF dependent transcription in mammals, which is used as an antifibrotic (Yu-Wai-Man et al., 2017). The mechanism of action for this drug appears to be by stabilizing the interaction between MRTF and G-actin and therefore preventing nuclear translocation (Hayashi et al., 2014). This drug is effective on both MRTF-A and MRTF-B in mammals (Haak et al., 2014), and looking at the *E. muelleri* ortholog of MRTF, the putative binding region is well conserved.

Because of its role in myogenesis as regeneration of myofibrils, activation of MRTF has also been targeted for treatment of disease states (Mokalled et al., 2012). Due to the general mechanism of action for MRTF, these tend to act by disrupting the association with G-actin. In a screen of small molecule activators, the cell permeable

drug ISX-9 was identified as a potent activator of MRTF dependent transcription without inhibiting general actin dynamics (Velasquez et al., 2013). This is thought to be through a non-competitive lowering of the affinity for G-actin (Finch-Edmondson & Sudol, 2016). Less is known about the actual binding of this molecule, so predictions could not be made for its activity on EmMRTF. However, since the drug does not appear to have an off-target effect on actin dynamics, it prevents a strong opportunity to interrogate EmMRTF role in development of the contractile actin tracts.

Another method of activating MRTF that is widely utilized is to treat a cell with cytochalasin D (Olson & Nordheim, 2010). In this case, cytochalasin D binds to G-actin with a higher affinity than MRTF, therefore depleting the G-actin pool and increasing nuclear translocation of MRTF. This can be seen as an increase in expression of MRTF target genes. However, since cytochalasin D is competitively inhibiting the MRTF G-actin association, it also blocks general polymerization of actin decreasing levels of F-actin (Schliwa, 1982). Since increased actin polymerization and development of large contractile actin structures is generally the result of MRTF activation, phenotypes associated with cytochalasin D mediated activation are difficult to interpret. However, this can be used to see if there is increased expression of MRTF effectors following treatment.

Methods

Physiological changes following treatment

Gemmules were plated and hatched as described before in 24-well format but in varying concentrations of CCG-203971 (Sigma-Aldrich SML1422) in LW. Initial

concentrations tested were 1μM, 10μM, and 100μM with an equal volume of DMSO as the 100μM serving as a control. Six replicates were made for each concentration. A similar test was then performed hatching the gemmules in LW+100μg/mL ampicillin and treating with CCG-203971 following hatching. For this assay, 1μM, 10μM, 20μM, 50μM, and 100μM were tested, with 4 replicates of each. For contraction assays, gemmules were plated and hatched in glass bottom dishes and were treated with 20μM CCG-203971 in LW following hatching, which was refreshed daily. At 3 days post hatching, sponges were examined to verify the presence of choanocyte chambers and canals and then contraction assays were performed with ink treatment as described earlier using high (1:100) and low (1:1000) concentrations of ink. Equally aged treated sponges were also fixed in 3.7% formaldehyde in EtOH and stained with phalloidin AF™488 (Life Technologies, 1:120) as described earlier. Confocal Images were acquired on an Olympus Fluoview FV3000 confocal laser scanning microscope using either a 60×/1.4 NA or 100×/1.4 NA objectives. Laser levels and acquisition setting were not adjusted for imaging controls. Images were processed in FIJI (Schindelin et al. 2012).

For ISX-9 (Tocris #4439) treated sponges, similar hatching and kill curves were performed in order to identify the optimal concentration for treating sponges. Concentrations tested ranged from 1μM to 500μM. Ability to contract was tested with treatment with 0.5nM thapsigargin and samples were fixed and stained for actin in the same manner as for CCG-203971 treated sponges.

qRT-PCR following treatment

Gemmules were plated and hatched in 6-well format on coverslips with between 10-12 sponges per well in LW+100μg/mL ampicillin. After hatching, samples were washed with LW, which was refreshed daily. For MRTF inhibition, sponges were treated with 20μM CCG-203971 in LW beginning at tent stage, with media refreshed daily. For activation, sponges were treated with 50μM ISX9 beginning at tent stage, with media refreshed daily. For alternative activation, Sponges were treated with 10μM cytochalasin D (ThermoFisher Scientific #PHZ1063) for 30 minutes prior to harvesting. RNA was extracted by washing sponges off of coverslips with Trizol (ThermoFisher Scientific #15596-018), followed by EtOH precipitation and rehydration in nuclease free H_2O. Purified RNA concentration was measured by spectrophotometry and an equal mass from each extraction was used to generate cDNA using Takara RNA to cDNA EcoDry mix (Takara #639549). qRT-PCR was performed using a BioRad iQ5 Real-Time PCR detection system (BioRad #170-9780), with an initial denaturing step at 95^{o}C for 30 seconds followed by a two-step cycle; 95^{o}C for 10 seconds, 60^{o}C for 55 seconds, repeated 45x. A melt curve was performed after the run to verify the signal was not due to primer dimers. Prior to performing the qRT-PCR reaction a dilution series of purified cDNA library template was used to calculate the amplification efficiency for each of the primer sets in order to verify that it was greater than 1.8 per cycle (2.0 equates to 100% efficiency or doubling each cycle). Primer sets used were;

EmEF1alpha

Forward - AAGCCTATGTGCGTGGAGTCATTT

Reverse - GACACCTACTGCTACGGTCTGCTTC

EmGAPDH

Forward - GGTGATGGGTGTGAACGAAGA

Reverse - CAAGCAGTTGGTAGTGCAAGAGG

EmHptr1

Forward - ACGAATTTGTGGTGGGCTAC

Reverse - CACCACACGTACAGCTCGAT

EmActin

Forward - GACAATGGTTCAGGCATGTG

Reverse - TGGGATACTTCAGGGTGAGG

EmTAGLN2

Forward - AACCAACAAGGGTGCATCTC

Reverse - GACCACAAGGCATGCACTAA

Activation of MRTF in archeocytes

Approximately 50 gemmules were plated and hatched in a petri dish in LW+100µg/mL ampicillin. After hatching water was changed daily to LW (no antibiotic). At 3 days post hatching, sponges were scraped with a sterile razor blade into a 1.5mL Eppendorf tube and tissue was spun at the lowest setting for 2 minutes. All liquid above the sponges was removed and samples were resuspended in LW+1mM EDTA. Sponges were then gently mixed and placed on a rotisserie for 15 minutes at room temperature with intermittent mixing. Dissociated cells were then passed through a 70µm filter, washing in an additional 2mL of LW+1mM EDTA over the filter. The cell suspension was then spun at 1000xG for 5 minutes at room temperature, to pellet the

heavier cell fraction which includes archeocytes. The supernatant was removed and then the pellet was resuspended in 150µL of treatment solution. Using a wide-bore pipette, the sample was gently pipetted up and down to evenly suspend the cells and then 25µL was transferred for plating. For 'hanging drop' experiments, the plating consisted of a petri dish lid which contained rings of VALAP that had been drawn using the wide end of a Pasteur pipette as a guide. Drops containing cell suspension were placed in the middle of this ring and the lid was inverted onto a petri dish filled with a small volume of water and left to incubate. After aggregates formed, solutions were refreshed daily by gently transferring the existing drop into 1mL of fresh solution and then washing and replating in 25µL. Aggregates were incubated in this adhesion free environment for 3 days (which was determined to have no effect on ability to attach once transferred to a plate). The effect of MRTF inhibition were tested with 20µM CCG-203791, the effect of MRTF activation was tested with 50µM ISX-9, the effect of inhibiting actin dynamics was tested with 10µM latrunculin B, and the effect of inhibiting myosin-based contractility was tested with 50µM Blebbistatin. Morphology of aggregates was documented and ability to re-attach following treatment was tested by transferring and allowing settlement in a 6-well plate.

For fixation of unattached aggregates, samples were carefully transferred to 1mL of 3.7% formaldehyde in EtOH in a 1.5mL Eppendorf tube and were incubated for 40 minutes at room temperature. Samples were then thoroughly washed with 1x PBST and incubated in 3% BSA in 1x PBST for 1 hour at room temperature. If stained with an antibody, samples were treated in blocking solution overnight at 4^{o}C (1:100 dilution for pRLC, 1:500 dilution for beta-tubulin). For secondary staining, samples were incubated

with anti-rabbit AF™488 (Life Technologies, 1:500), phalloidin AF™568 (Life Technologies, 1:120), and Hoechst (33,342 1µg/mL) dye in blocking solution for 45 minutes at room temperature. If an antibody was not used, secondary was omitted.

Contraction assays were performed as described for the floating sponges, by transferring aggregates to the small well of a glass bottom dish and carefully removing liquid until it was suspended in the middle of this well. In order to induce a contraction, a 25µL drop of 1mM thapsigargin was placed in the dish outside of the central well and a pipette tip was used to gently drag it to the edge so that it could mix. Time lapse imaging was set up at 30 second per frame for 60 minutes. Time lapse series were then analyzed in Fiji (Schindelin et al., 2012) to measure the area of the aggregates over time.

Aggregates were also removed from the hanging drop and allowed to reattach in glass bottom dishes and develop following treatment. Gross morphology of re-attached aggregates was examined and then sponges were fixed following standard 3.7% formaldehyde in EtOH protocol. Samples were treated with 1:100 anti-pRLC in blocking solution and incubated overnight at 4^{o}C. Secondary staining consisted of anti-rabbit AF™488 (Life Technologies, 1:500), phalloidin AF™568 (Life Technologies, 1:120), and Hoechst (33,342 1µg/mL) dye in blocking solution. Samples that were only stained for actin and DNA had the secondary antibody omitted. Confocal Images were acquired on an Olympus Fluoview FV3000 confocal laser scanning microscope using either a 60×/1.4 NA or 100×/1.4 NA objectives. Laser levels and acquisition setting were not adjusted for imaging controls. Images were processed in FIJI (Schindelin et al., 2012).

WB for anti-stMyHC following attachment

Sponges were dissociated as described above and suspended in either DMSO+LW or 50μM ISX9+LW. They were then transferred to 60mm petri dishes and placed on a benchtop orbital shaker at a low setting, to help position cells towards the center of the dish and limit early settlement. Media was carefully replaced twice a day and sponges were harvested after 2 days. Tissue was scrapped into 1.5mL Eppendorf tubes and excess liquid was gently removed. Tissue was then lysed in trypsin lysis buffer as described for IPs. Protein concentration was estimated by spectrophotometry and 30μg of each sample in SDS PAGE loading buffer was run on a 10% SDS PAGE gel. Transfer was performed as described in Myosin II chapter. One membrane was blotted with 1:200 (v/v) anti-GAPDH (Proteintech #10494-1AP) and 1:1000 (v/v) anti-EmVin1 in 5% milk (wt/v) in 1xPBST, and the other with 1:200 (v/v) anti-GAPDH and 1:500 (v/v) anti-EmstMyHC-N in 5% milk (wt/v) in 1xPBST. Visualization was performed with 1:2000 (v/v) anti-rabbit AF™488 and 1:1000 (v/v) anti-mouse IgG (Alexa Fluor™ 647) (abcam #ab150115).

Contractility assay

Adding ink to the water induces a contraction because the ink particles aggregate and block flow in the aquiferous system. It was observed that when using ink to induce contractions in sponges treated with L-NAME and CCG-203971 (both which inhibit contractions) the sponges did not clear the ink from their canals. In order to rapidly screen for the sponges ability to contract, this assay was designed. Sponges were treated with a very high concentration of ink (just below the determined threshold) and then left to contract. Following this, they were treated with DiI as a tracer. The basic idea is that as

sponges draw in the ink it strongly stains the choanocyte chambers, demonstrating that flow is maintained following treatment. If the sponge is able to effectively clear the ink from their canals, then the DiI will also label choanocyte chambers, show that flow has been maintained following ink treatment. If the sponge is not able to effectively clear the ink from the canal, the flow will be stopped. In this case, the DiI will not efficiently enter the sponge and choanocyte chambers will not be labeled. In order to identify the optimal concentration of ink to use for this assay, gemmules were plated in 24 well format under normal condition. A tight dilution series from pure ink to 1:50 dilution of ink in LW were tested. During this time, care was taken to minimize movement of the dish and sponges as the increased density and weight in the aquiferous system could cause large amounts of tissue damage. All water changes and washes were performed using very gentle suction. Viability following this treatment was first judged based on the pinacoderm remaining intact. Sponges in which the apical pinacoderm had maintained integrity were then treated with 2.5μg/mL DiI Stain (ThermoFisher Scientific D282) in order to confirm incurrent flow through the choanocyte chambers. Follow these trials, the optimal concentration of ink was determined to be a 1:30 dilution in LW, which was used for experimental trials. In these trials, either LW or LW+DMSO served as negative controls and treatment with 50μg/mL L-NAME was used as a positive control for inhibited contractions. For experimental treatments, working concentration and treatment timing depended on the chemical being used. For MRTF inhibition, sponges were treated with 20μM CCG-203791 or 50μM CCG-203791 beginning at tent stage, with media refreshed daily. For inhibition of myosin II, sponges were treated with 50μM blebbistatin 2 hours prior to initiation of the contraction assay. In order to inhibit ryanodine receptors,

sponges were treated with 50μM dantrolene or 20μM ryanodine for 2 hours or 6 hours prior to assays respectively.

Results

Due to the lack of a clearly defined body plan and the very high degree of plasticity, assessing sponge phenotypes can be very difficult. For gemmules treated with CCG-203791, none hatch at 100μM concentration, whereas all sponges hatched in 10μM and 1μM. Of the hatched gemmules treated, canals, choanocytes, and an osculum did not form in sponges treated with 100μM and 50μM concentrations. Overall morphology of sponges treated with the lower concentrations did not appear noticeably different from controls. Whole mount actin staining of samples treated with 20μM CCG-203791 was observed and appeared to be somewhat less organized than control samples (**Figure S20**). High magnification of similar structures in these sponges relative to control showed what appears to be a decrease in the amount and organization of the actin tracts in the pinacoderm, with no change in cell number based on DNA staining (**Figure 66**).

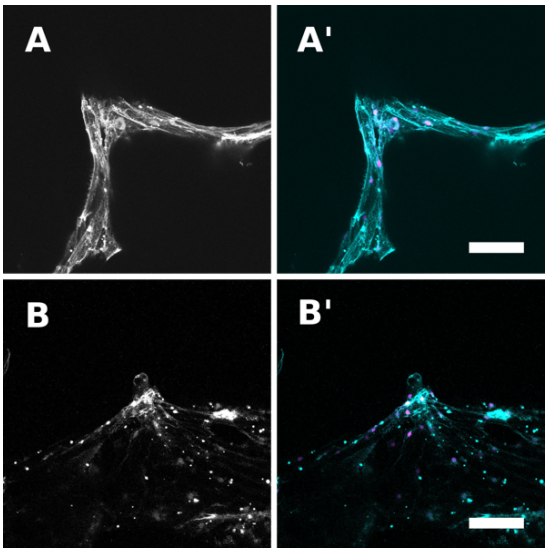

Figure 66. Actin staining in the pinacoderm is reduced in treated sponges. Confocal images of sponges stained for actin (cyan) and DNA (magenta). **(a)** Control sponges show large amounts in the apical pinacoderm. **(b)** Samples treated with CCG-203791 have reduced actin in comparative regions of the sponge. This does not appear to be a result of decreased cell number based on number of nuclei present. Scale bars 50μm.

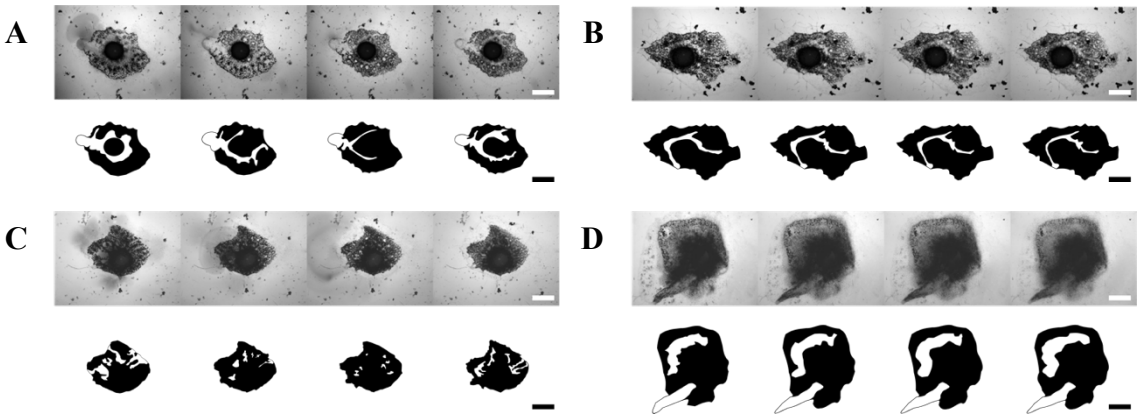

Figure 67. Inhibition of MRTF during development limits the sponge's ability to contract. Frames correspond to time points 0, 20, 40, and 60 minutes following start of imaging. **(a)** Control sponges treated with 1:1000 sumi ink show a normal contractile response. Bottom panels show major excurrent canals, which show an inflation and contraction cycle. **(b)** Sponge treated with CCG-203791 shows a reduced response. Major excurrent canals show limited inflation and contraction over the course of imaging. **(c)** Control sponge treated with 1:100 sumi ink shows a contractile response. Bottom panels show outlines of major excurrent canals and can be seen inflating and contracting over the course of imaging. A plume of ink can be seen exiting the osculum in panel three, in which the canals are fully contracted, suggesting a clearing event. **(d)** Sponge treated with CCG-203791 does not show a contractile response and ink is clearly visible in the osculum. The bottom panel, depicting major excurrent canals, shows a minor swelling of the canal over the course of imaging. Scale bars 500μm.

Sponges that were treated with CCG-203791 showed a reduced contractile response when treated with ink. Treatment with a low concentration of ink showed limited inflation and contraction of the major excurrent canals (**Figure 67a&b**). When treated with a high concentration of ink, the excurrent canals appeared to be completely blocked, which was apparent based on the dark staining in the osculum **(Figure 67c&d**). It was difficult to make out the canals of these sponges, but there did appear to be some swelling in excurrent canals system over the time of imaging. This could be reflective of the disruption of out-current flow and continued incurrent flow, as would be expected if the osculum were blocked.

For the ISX-9 treated sponges, concentrations of 100μM and above prevented hatching and appeared to be toxic to developing sponges. Sponges treated with 50μM appeared to be normal in that they had an osculum, choanocyte chambers, and a clear canal system. However, the canals appeared to be much larger with dense tissue around them (**Figure S21**). Phalloidin staining to visualize actin structures did not reveal anything strikingly different from the control sponges though.

qRT-PCR

Following treatment with 20μM CCG-203791 sponges showed a decrease in the relative expression of actin as well as EmTAGLN2. Treatment with 50μM ISX-9 showed an increase in the relative expression of these targets, which was also seen in the samples short term treated cytochalasin D (**Figure 68**). These results were consistent regardless of the reference gene that they were measured against and the reference genes did not show significant variation when analyzed relative to each other.

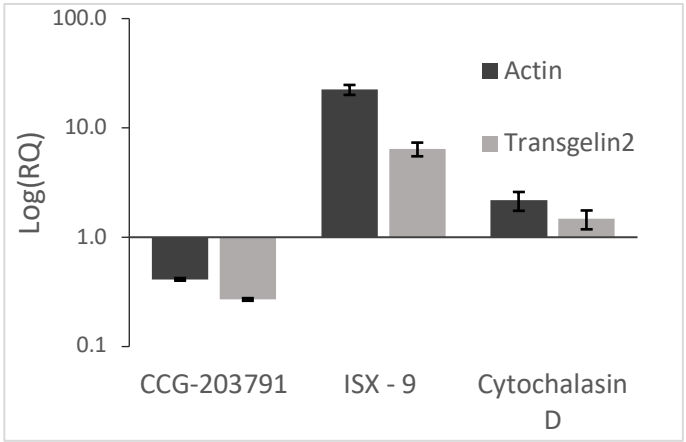

Figure 68. EmMRTF has conserved targets. qRT-PCR for putative targets, actin and transgelin 2 shows a decrease in expression following treatment with CCG-203791 and increase following treatment with ISX-9 and cytochalasin D. Expression relative to EmEF1alpha. Based on 3 biological and 6 technical replicates.

Activation of MRTF in archeocytes

Aggregation of control cells occurred within a few hours and if left to settle, reattachment occurred within 20 hours. Aggregates that were maintained in an attachment free environment continued to develop and form a semi-hollow mass (primmorph) containing rudimentary canals and choanocyte chambers (**Figure 69**). These primmorphs form a cohesive outer epithelial layer with no evidence of actin tracts (**Figure 69c**). Upon settlement, as the tissue spreads out, and choanocyte chambers and the actin tracts are clearly visible (**Figure S22**). Aggregates were maintained for up to 6 days in an attachment free environment and no evidence of actin tracts was found, and when treated with thapsigargin they did not significantly change shape or size.

Treatment of cells with either blebbistatin or latrunculin B resulted in formation of aggregates which persisted in the hanging drop. These aggregates appeared to be round and dense (**Figure S23**), and when transferred to a dish for settlement, they did not

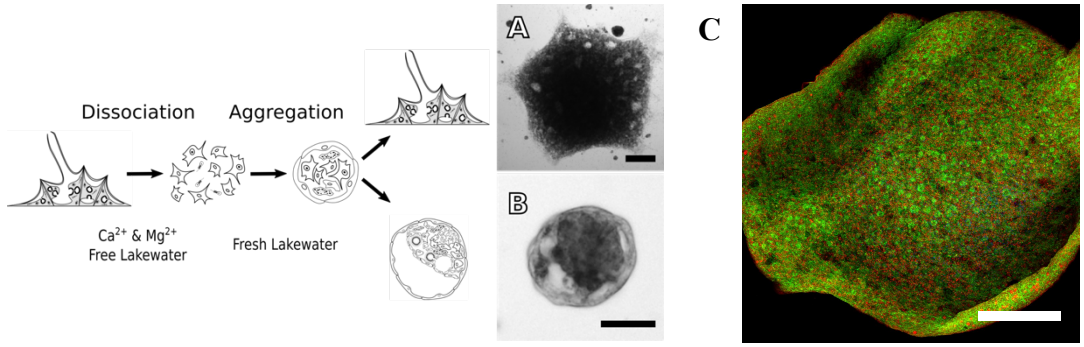

Figure 69. Workflow for aggregation assay. Juvenile sponges are dissociated in CMFM. Isolated cells are then incubated in lake water where they form aggregates. If left to settle, aggregates reattach to the substrate and develop tissues seen in juvenile sponges. If placed into an attachment free environment, aggregates continue to develop, forming rudimentary canals and choanocyte chambers. **(a)** Example of an aggregate that were allowed attach. **(b)** Example of a 3 day aggregate maintained in an attachment free environment. **(c)** A 3 day aggregate stained for actin (green) and tubulin (red). Scale bars 100µm**(a&b)**, 50µm**(c)**.

reattach (**Figure S24**). Aggregates of cells treated with CCG-203791 did not appear to differ from the control aggregates. However, when placed back in a dish for settlement, they reattached as a much lower rate than control aggregates (**Figure 70**).

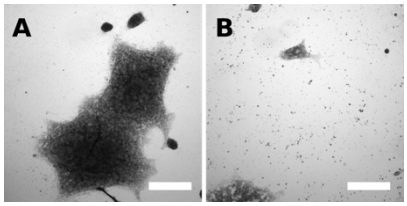

Figure 70. Inhibition of MRTF effects attachment and spreading. Dissociated cells were treated with CCG-203791 and allowed to settle. **(a)** DMSO control of aggregates. **b)** Treated aggregates showed limited attachment and spreading.. Scale bars. 200µm.

Aggregates treated with ISX-9 took on a very striking phenotype in that they appeared smaller and denser. When actin was visualized the aggregates are seen to contain dense actin structure towards the periphery of the mass (**Figure 71**). These structures appear to span across the tissue, running above developing choanocyte chambers seen in aggregates (**Figure S25**). Along these bundles there are areas of dense actin staining that resemble adhesion plaques, suggesting that these structures are aligned between adjacent cells (**Figure 72)**. When stained for pRLC these aggregates also showed staining, which was absent in normal aggregates suggesting that type-II myosin is present at these structures (**Figure 73**). This also resembled the staining pattern seen in

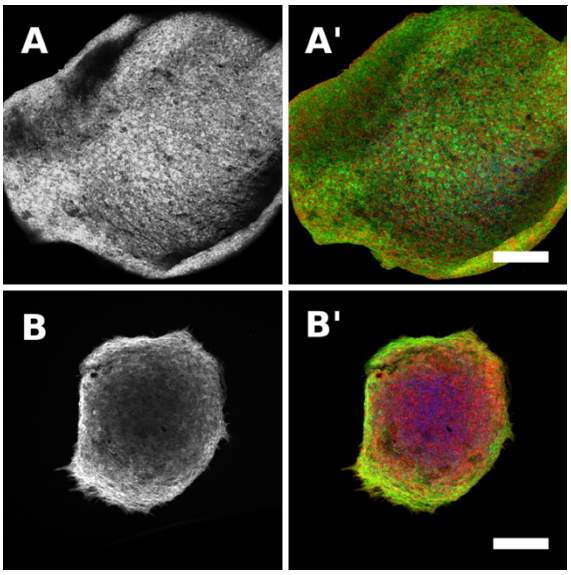

Figure 71. Activation of MRTF in aggregates induces development of dense actin network. Dissociated cells were either treated with ISX9 or DMSO and maintained in an attachment free environment for 3 days. They were then fixed and stained for actin (green), tubulin (red), and DNA (blue). Raw images for the actin channel shown on the left. **(a)** Confocal images of control sponges show a large semi-hollow mass. **(b)** Confocal images of ISX9 aggregates appeared dense with large amounts of actin surrounding the mass. Scale bars 50µm.

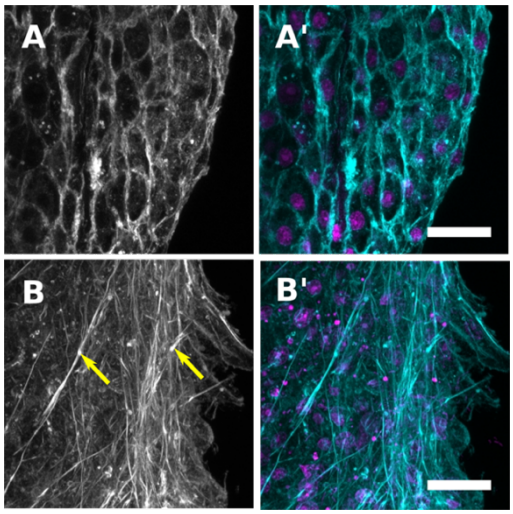

Figure 72. Actin structures along the edge of aggregates resemble actin tracts. (a) Actin staining of a control aggregate showing what appears to be cortical actin structures in the tissue surrounding the mass. **(a')** Merge of actin (cyan) and DNA (magenta) show a single nucleus surrounded by each actin ring. **(b)** Actin staining for ISX9 treated aggregates shows actin dense structures resembling adhesion plaques seen along the actin tracts (yellow arrows). **(b')** Merge of actin (cyan) and DNA (magenta) show these actin structures are aligned between adjacent cells. Scale bars 10μm.

juvenile sponges, suggesting that these structures further resemble the actin tracts that run through the endopinacoderm. Attempts to stain for stMyHC were unsuccessful due to the fragile nature of the aggregates and harsh fixation methods used with this antibody. Upon settlement, they also formed very large tent structures that gave the appearance of expanded canals (**Figure 74a&b**). Expression of stMyHC is increased following treatment with ISX-9, though there was no detectable increase in the levels of EmVin1 present (**Figure 74c**). As a marker of the adhesion plaques connecting actin tracts, it was expected that vinculin levels would increase. However, as this protein is found at

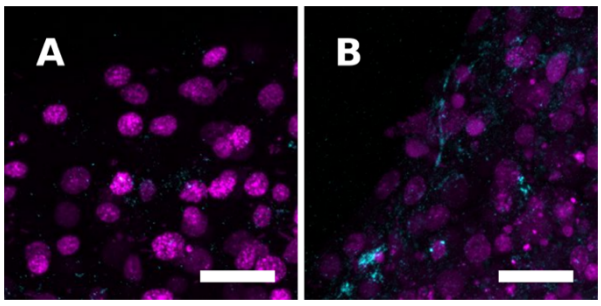

Figure 73. ISX9 treated aggregates contain pRLC in the area of the actin bundles. Dissociated cells were treated with ISX9 or DMSO and kept in an adhesion free environment for 3 days, then fixed and stained for pRLC (cyan) and DNA (magenta). **(a)** DMSO treated controls. **(b)** ISX9 treated sponges show pRLC staining along structures that resemble the actin bundles running through this tissue. Scale bars 5μm.

multiple structures in the sponge, this lack of change could be due to a relatively high proportion of the protein being localized to other structures. In order to collect enough tissue for the western blot, the aggregates were allowed to reattach prior to harvesting. This is likely why there are detectable levels of stMyHC in the control sponges, as the actin tracts, which this protein localizes to, begin to develop following attachment. Based on the developmental staining with stMyHC (see Myosin II chapter), the actin tracts appear to develop prior to the recruitment of stMyHC+ filaments. Presumably, this would include initial development of the adhesion plaques at the end of the actin tracts in the

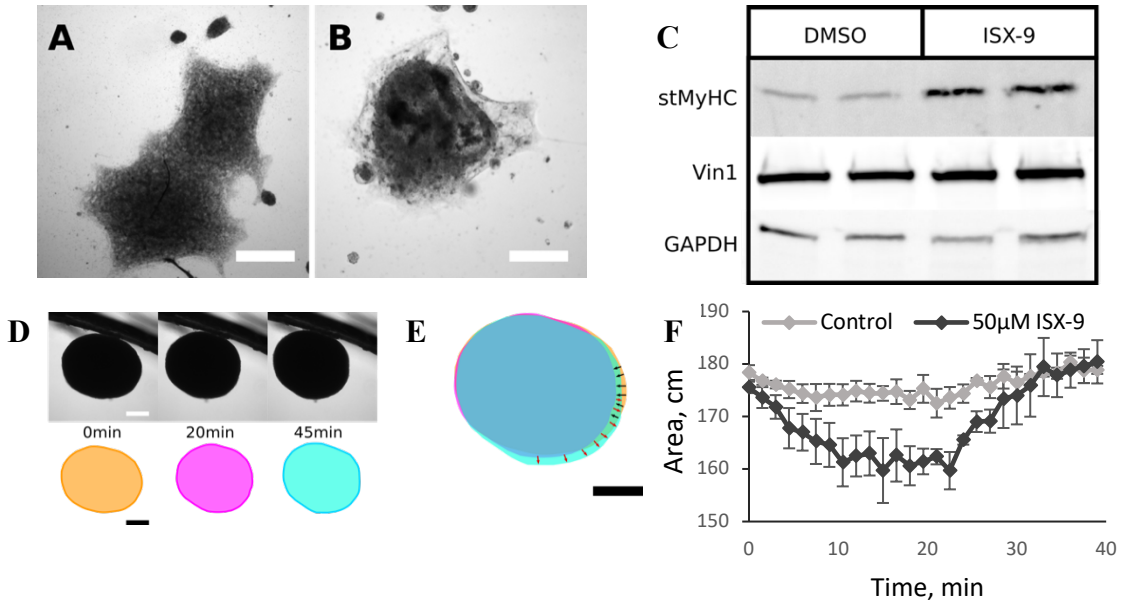

Figure 74. ISX9 treated aggregates have a contractile phenotype. Dissociated cells were treated with either ISX9 or DMSO and allowed attach to dishes. **(a)** DMSO treated aggregates. **(b)** ISX9 treated aggregates form an extended apical pinacoderm surrounding the reattached aggregate mass. **(c)** Western blot of DMSO treated or ISX9 treated aggregates following reattachment. Levels of stMyHC dramatically increase in ISX9 treated samples and EmVin1 levels show little difference. GAPDH used as a loading control. **(d)** Time series from a time lapse video of an ISX9 treated aggregate induced to contract by the addition of ~500nM thapsigargin. Bottom panel show outline of aggregate at each time point. **(e)** Overlay of the outline at each timepoint following color code in **(d)**. Contraction is seen as decrease from orange to magenta (black arrows) and relaxation is seen as expansion from magenta to cyan (red arrows). **(f)** Area following induction of contraction for DMSO or ISX9 treated aggregates. Scale bars **(a&b)** 200μm, **(d&e)** 50μm.

cells as well. When these aggregates were treated with thapsigarin they showed a decrease in size followed by a return to resting (**Figure 74**), which is interpreted as a contraction (**Figure 74f**).

Contractility assays

Control sponges, treated with DMSO (**Figure 75a**), stained positive for both ink and DiI 96.2% of the time. By opposition, L-NAME treated sponges (**Figure 75b**) showed dual staining 12% of the time. Treatment with 20μM CCG-203791 (**Figure 75c)** showed comparative staining 46.2% of the time, while treatment with 50μM CCG-203791 (**Figure 75d**) showed dual staining 28% of the time, though sponges looked unhealthy in general. Treatment with blebbistatin (**Figure 75e**) showed dual staining 37.5% of the time. Treatment with both ryanodine and dantrolene (**Figure 75f**) showed no inhibitory activity, with dual staining 100% and 95.8% respectively (**Figure 75g**).

Discussion

Treatment with less than 50μM CCG-203791 did not have strong phenotypes associated with it. Higher concentrations did prevent development of the aquiferous system and choanocyte chambers. This is difficult to interpret though, as it could be a result of specific activity of the drug or due to general toxicity. A previous study targeting Rho signaling by inhibiting ROCK with Y-27632 and GSK429286A found similar phenotypes associated with these treatments (Schenkelaars et al., 2016). This was interpreted to be a result of the interaction with Rho/ROCK signaling and the Wnt signaling pathway during early development. Seeing similar phenotypes associated with

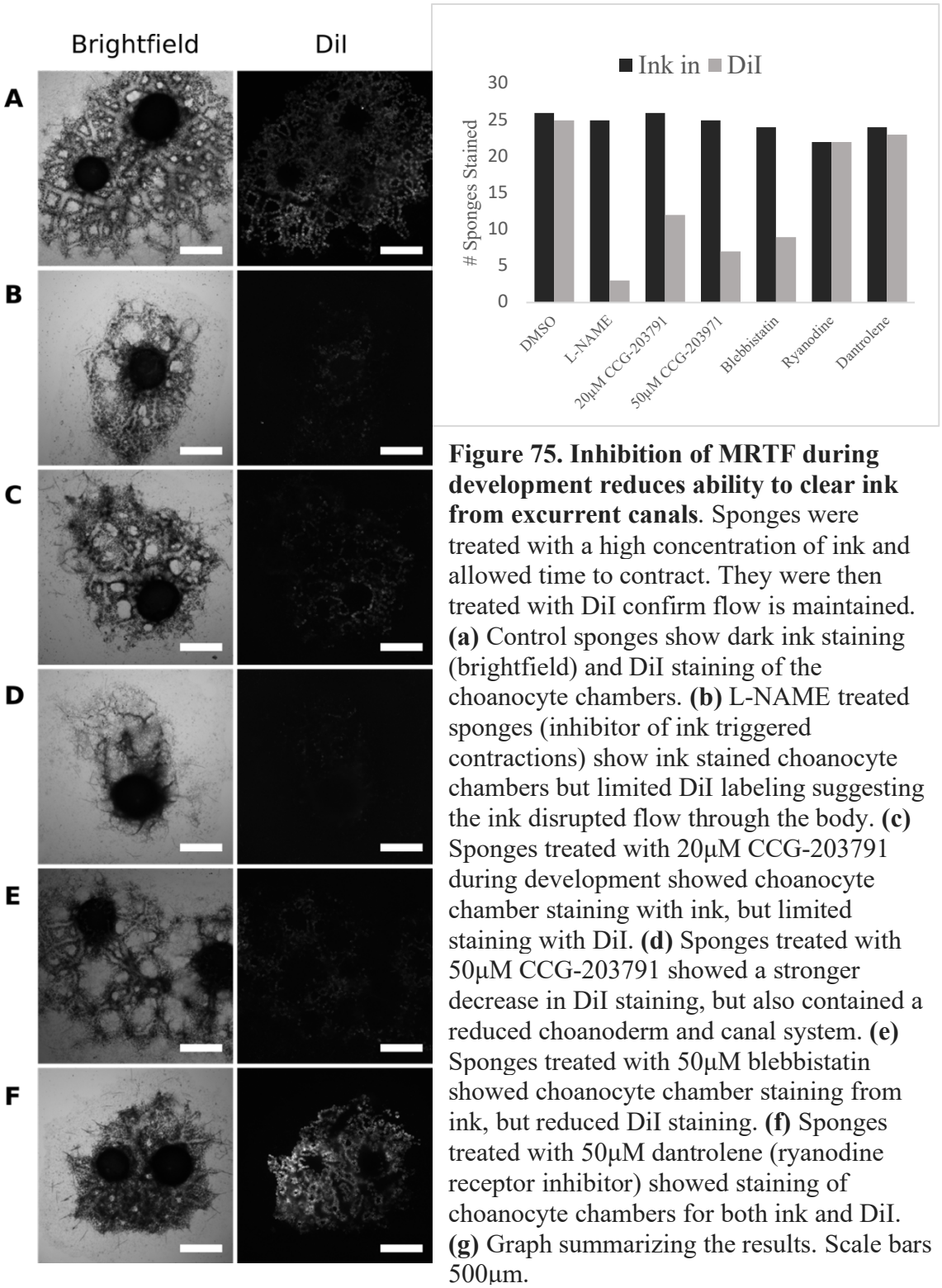

Figure 75. Inhibition of MRTF during development reduces ability to clear ink from excurrent canals. Sponges were treated with a high concentration of ink and allowed time to contract. They were then treated with DiI confirm flow is maintained. **(a)** Control sponges show dark ink staining (brightfield) and DiI staining of the choanocyte chambers. **(b)** L-NAME treated sponges (inhibitor of ink triggered contractions) show ink stained choanocyte chambers but limited DiI labeling suggesting the ink disrupted flow through the body. **(c)** Sponges treated with 20μM CCG-203791 during development showed choanocyte chamber staining with ink, but limited staining with DiI. **(d)** Sponges treated with 50μM CCG-203791 showed a stronger decrease in DiI staining, but also contained a reduced choanoderm and canal system. **(e)** Sponges treated with 50μM blebbistatin showed choanocyte chamber staining from ink, but reduced DiI staining. **(f)** Sponges treated with 50μM dantrolene (ryanodine receptor inhibitor) showed staining of choanocyte chambers for both ink and DiI. **(g)** Graph summarizing the results. Scale bars 500μm.

MRTF inhibition, a known downstream target of ROCK, suggests that the Rho/MRTF/SRF pathway could be responsible for this phenotype. Endopinacocytes form

the lining of the canal system, and my previous work has suggested that in a 'relaxed' state phosphorylation of the RLC is detectable along the actin tracts, suggesting basal activity which likely maintains proper tension across the tissue. This could be a mechanical feedback loop that helps to properly develop and inflate the canal system. The large nuclear pool of MRTF in the basopinacocytes is also consistent with their finding of impaired growth and formation of the basal pinacoderm in ROCK inhibited sponges (Schenkelaars et al., 2016). The large stress fiber-like structures associated with attachment to the substrate likely play a developmental role in this tissue by limiting cell movement and increasing traction force, in a MRTF dependent manner. Inhibition of MRTF signaling, either through ROCK or MRTF directly, could prevent proper development of these structures leading to increased cell movement through the tissue creating the spike-like extensions along the sponge body. However, these phenotypes could also be due to general toxicity. *E. muelleri* shows a similar response when treated with a variety of substances and could be due to the persistence of archeocytes, due to their relative protection in mesohyl relative to pinacocytes and choanocytes. Another possibility is that this is a common physiological response of the sponge upon detection of something in their water supply. Cell shedding has been documented in sponges (De Goeij et al., 2009; Alexander et al., 2014) and could be a method of tissue renewal. Since sponges are sessile, when in an inhospitable environment, they cannot readily move to a different one. Living in variable environments, this may be a method of closing off flow through their body, effectively limiting exposure, until conditions become more favorable. This general idea that the phenotype is not a direct result of the target of the drug is supported by the finding of a

similar phenotype following treatment with high concentrations of the MRTF activating drug (ISX-9). This could be a case of different feedback loops leading to the same end, in which inhibition of MRTF activity and overactivity lead to different physiological changes (underdevelopment of the endopinacoderm with insufficient tension to support the canal system and overdevelopment of the endopinacoderm which prevents inflow and proper inflation, respectively). Since this is difficult to tease out and predictions are not clear for each possibility (global expression changes for example), focus is moved to the maximum treatment concentrations in which gross morphology was not greatly changed. For treatment with CCG-203791 there did appear to be a decrease in the density of actin in the apical pinacoderm and a reduced ability to contract when stimulated with ink. When treated with ink, the sponge did not contract though and the following day its tissue had begun to lose integrity. This is likely a result of the inability to clear the blockage leading to a complete halting of flow through the aquiferous system. For sponges treated with ISX-9, the canal morphology seemed to be altered leading to the appearance of very large excurrent canals. These sponges were still able to contract as normal. Due to all the factors that could go into this morphology, it is difficult to interpret it without knowing the full role or function of MRTF in *E. muelleri.*

qRT-PCR

A major target of MRTF activity should be actin expression which is utilized in building contractile machinery in the cell (Pipes et al., 2006). This also serves as a feedback loop in that as polymerization slows, the increased G-actin pool sequesters MRTF to the cytoplasm reducing activity (Finch-Edmondson & Sudol, 2016). To aid in

this regulation, well established MRTF targets also consist of actin bundling and regulatory proteins. In a variety of animals, muscle specific proteins that are under control of MRTF dependent expression fall into the transgelin family of proteins. Muscle specific members of this family include, the vertebrate smooth muscle specific SM22alpha (Hinson et al., 2007), and fly muscle specific protein MP20 (DeAguero et al., 2019). There are three transgelin-like proteins in the *E. muelleri* transcriptome (discussed in more detail in Chapter 3). Of these, EmTAGLN2 looks most similar to the muscle specific proteins of other animals (based on alignments of functional domains as well as predicted protein properties such as pI values) and was seen to predominately localize to the actin tracts. Based on the qRT-PCR results, treatment with the inhibitor lead to a decrease in expression of these two putative EmMRTF targets while treatment with the activators lead to an increase. Treatment with cytochalasin D is not practical because of its disruption of global actin dynamics, but serves as a good control to demonstrate that the mechanism of action of EmMRTF is conserved. Overall these results suggest that disruption of the G-actin/MRTF interaction leads to increased expression of genes involved in building contractile structures. This can be taken as confirmation of the effectiveness of the drugs for other functional work as well as evidence that the general function of MRTF is conserved in *E. muelleri.*

Aggregation assays

The basic development of aggregates into primmorphs has been documented in a variety of sponges and is consistent in this assay (Lavrov & Kosevich, 2016). An important finding here was that prolonged development in an attachment free

environment leads to some differentiation (formation of choanocyte chambers) but does not lead to formation of actin tracts, which develop after settlement. Therefore, we have access to sponge stem cells (archeocytes) which under normal conditions do not differentiate into endopinacocytes (cells housing the actin tracts). Treatment with blebbistatin and latrunculin B did not inhibit aggregation formation, but aggregates did not expand and differentiate and did not settle. This suggests that aggregation occurs independent of actin dynamics and myosin activity, but formation of a mature primmorph and settlement is an actomyosin dependent process. Treating aggregates with CCG-203791 led to a decrease in the rate at which aggregates re-attached, suggesting the actomyosin dependent contractility needed for this process is MRTF dependent. This treatment was not completely effective though, which could be due to incomplete inhibition of MRTF or it could be a result of some redundancy in the pathways, where contractile elements are upregulated in the presence of MRTF activity but are not fully dependent on it. The most striking result from this assay is from the MRTF activator. In this case, it appears that archeocytes were pushed to differentiate into endopinacocytes, based on the presence of prominent actin tracts, under conditions in which they normally would not form. This suggests that MRTF activity alone is sufficient to drive differentiation into this contractile cell type. Not only do the structures form in these aggregates, they appear to be functionally contractile. Since very little tissue is available in these aggregates, archeocytes were treated in larger volumes and then left to settle. Just after settlement, there was an increase in the amount of stMyHC (which can serve as a marker for contractile actin tracts) as well. Overall, this finding suggests that activating MRTF in a stem cell is sufficient to force differentiation into a contractile cell type in *E.*

muelleri. This is consistent with the finding that archeocytes contain a large cytoplasmic pool of MRTF and is consistent with the mechanism of differentiation discussed in the immunostaining section above.

Contractility Assay

DMSO treated sponges showed a high rate of dual staining while L-NAME treated sponges showed a very low rate, which is consistent with the previous finding that L-NAME inhibits ink induced contractions. Following treatment with the MRTF activator CCG-20391, there was a reduction in the number of sponges showing dual staining suggesting the ability to effectively contract was lost in these individuals. A similar, but less pronounced effect was seen in samples treated with the myosin II inhibitor blebbistatin. Blebbistatin has very poor solubility in water and had begun to precipitate out of solution at these treatment concentrations. This could explain the incomplete inhibition of the sponges' ability to contract, while maintaining that it is a myosin dependent behavior. Treatment with ML-7 had a greater effect on the sponges' ability to effectively clear ink, further confirming that MLCK dependent phosphorylation of the RLC is necessary for contractions. The finding that peptide 18 did not have an effect is consistent with the results for the immunostaining with pRLC, in which the peptide appears to be an ineffective inhibitor of EmMLCK. Sponges were also treated with ryanodine receptor (RyR) inhibitors, ryanodine and dantrolene (Zhao et al., 2001; Meissner, 1986). Ryanodine receptors are transmembrane Ca^{2+}channels found in the ER or SR, predominately in muscles of other animals. These function as Ca^{2+}dependent quick release Ca^{2+} channels, so when cytoplasmic Ca^{2+}levels increase, binding to the

RyR opens it leading to a rapid release of Ca^{2+}sufficient to trigger a cellular response (Coronado et al. 1994). *E. muelleri* has a well conserved RyR in its transcriptome, and given the finding that contractions are Ca^{2+} dependent, it was hypothesized that these channels likely functioned in this context. The treatment with both ryanodine and Dantrolene showed no inhibition on the ability to contract. Shortly after this was performed, published single cell RNA sequencing data from a closely related sponge (Musser et al., 2019) showed that RyR expression is restricted to one cell type that is not associated with the pinacoderm.

Conclusions

MRTF family proteins serve a role in myogenesis in a variety of animals. It seems that there has been a radiation within the family in the vertebrate lineage, resulting in a variety of related proteins which serve specific roles in both muscle and non-muscle contexts. Limited studies have performed in invertebrate lineages making the ancestral function unclear, but structurally the ancestral protein likely resembled the vertebrate mechanosensitive MRTF-A or B. The mechanism of action for the sponge ortholog appears to be conserved and serves a role in endopinacoderm differentiation and actin tract development. The ability to force archeocyte differentiation into endopinacocytes with MRTF activation suggests that MRTF activity is sufficient to drive development of contractile tissue in *E. muelleri.* The mechanosensitive properties of this protein are intriguing with respect to the sponge body plan. As described in more depth in the first chapter, sponges have highly responsive body plans, which rearrange with changes in their environment. As the primary lining of the incurrent and excurrent canals, the

endopinacoderm must maintain sufficient tension to maintain flow through the canal system while resisting the force of turbulent flow that occurs around the sponge. A mechanosensitive transcriptional switch, like MRTF-MADS-box interaction, is a good mechanism for guiding development of this tissue in response to constantly changing signals and feedback. If the last common ancestor of sponges and other animals was sessile with a plastic body plan, then guiding the development of contractile tissue in response to environmental cues is likely the ancestral function of MRTF. To help resolve this further, looking at the function of MRTF in patterning muscles of other non-bilaterians like cnidarians would be highly informative. Understanding the function of MRTF in other non-bilaterian animal lineages, placozoans and ctenophores, would be informative and no doubt very interesting, but is not as pressing in understanding the evolutionary relationship with muscles. Placozoans are thought to have undergone a significant decrease in cell type complexity, losing things like muscles and neurons. This coupled with the small number of described species in the lineage make it very difficult to understand comparative structures in other animals. For ctenophores, it would be beneficial to understand if MRTF functions in development of their muscles, though their ambiguous phylogenetic placement would make this difficult to interpret. The relationship between cnidarian muscles and bilaterian muscles is rarely debated, while there have been suggestions that ctenophores neuromuscular systems are independently derived (Moroz, 2015). In order to better understand the transition between the contractile endopinacoderm of sponges and muscles of other animals, the role of MRTF in development of cnidarian muscles is a good starting point.

Chapter 6: Myogenesis in *Nematostella vectensis*

Introduction

The anthrozoan cnidarian *Nematostella vectensis* provides a strong comparative model for the work that I have done in sponges. *N. vectensis*, has muscles which develop in predictable location and number (Jahnel et al., 2014) (**Figure 75**). These muscles are all smooth in ultrastructure and form a myoepithelium, in-which the apical region of the cell forms a cohesive epithelial layer and the basal region contains large actomyosin bundles. The level of connectivity between these two regions varies from a continuous cytoplasm to long bridges which in some cases fully separate (Jahnel et al., 2014). *N. vectensis* also has a single copy of both nmMyHC and stMyHC, with evidence of separation of function (Steinmetz et al., 2012). stMyHC is restricted to two muscle types, the retractor muscles of the body and the longitudinal muscles of the tentacles. These muscles serve in rapid movement of the body during an escape response and the swinging and movement of the tentacles towards the pharynx during prey capture, respectively. Both of these are characterized as fast contractions and the muscle types contain the largest actomyosin bundles in the animal. On the other hand, nmMyHC serves a variety of non-muscle functions as well as being found in body muscles involved in slow peristaltic-like contractions (Steinmetz et al., 2012; Renfer et al., 2010). It is important to note that in comparing sponges, cnidarian myoepithelial tissue, and bilaterian muscles,

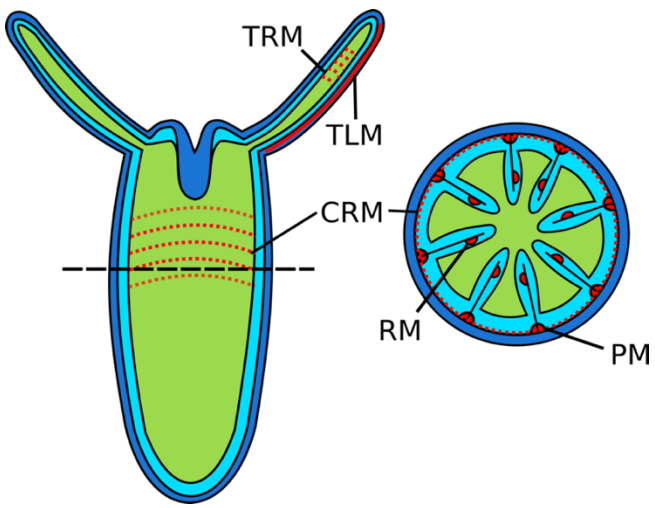

Figure 75. Schematic of *N. vectensis* muscles. Endoderm derived tissues shown in light blue and ectoderm derived tissues in dark blue. Muscle groups are outlined in red and include the circular body muscles (CRM), tentacle ring muscles (TRM), tentacle longitudinal muscles (TLM), retractor muscle (RM), and parietal muscle (PM). Right diagram is cross section along dashed line. TLM and RM contain stMyHC and TLM are the only ectodermally derived muscles.

one is not viewing a progression in which sponges represent the ancestral tissue type, cnidarians some intermediary, and mesodermal derived muscle the end point. Each of these has been shaped by unique evolutionary pressures over the course of hundreds of millions of years. However, if these structures are homologous in that they are derived from a common contractile cell type in the last common ancestors of these animals, then features shared amongst them can be informative of the ancestral state.

Cnidarian muscles predominantly have a smooth ultrastructure and form as an epithelium. In the medusa stage of some scyphozoan cnidarians muscles with a striated ultrastructure are present (Leclère & Röttinger, 2016; Seipel & Schmid, 2005). Evidence points to the striations being independently derived in the cnidarian lineage (Steinmetz et al., 2012). However, there is a division of function between stMyHC and nmMyHC in these animals and from a functional standpoint muscle cells can be separated into stMyHC+ fast contracting and nmMyHC+ slow contracting myocytes (Renfer et al., 2010; Brunet et al., 2016). The striated myoepithelium of adult moon jelly, *Aurelia* sp. runs along the sub-umbrella of the medusa and is large enough to dissect out. Proteomic

studies on this tissue have revealed that contractions are likely regulated by MLCK as opposed to some unique mechanism that was replaced by the troponin complex in bilaterian striated muscles (Tanaka et al., 2018). Like other non-bilaterian animals, cnidarians are diploblastic, though recent research has identified a population of cells that inhabit a type of endomesoderm, though not all muscles are derived from these (Wijesena et al., 2017; Salinas-Saavedra et al., 2018; Pukhlyakova et al., 2019). Muscles, therefore, predate the occurrence of a mesoderm meaning that homology cannot be judged based on germ layer of origin. In *N. vectensis,* all of the body muscles and the circular muscles in the tentacles are derived from the endoderm or endomesoderm, whereas the stMyHC+ longitudinal muscles of the tentacles are derived from the ectoderm.

Within the lab, *N. vectensis* can be maintained in standard glassware and spawning can be induced with changes in light and temperature (Stefanik et al., 2013). Initially our stock was maintained in a small tank within a dark cabinet. They were kept in 1/3 artificial sea water (ASW) which was prepared by dissolving 12g of Instant Ocean (Instant Ocean #927988) per 1L of dH_2O. Individuals were fed freshly hatched artemia every 1-2 days. Storage was eventually transferred to a small refrigerator which maintained a temperature of 18ºC, which is optimal for inducing spawning. Spawning is induced by exposure to bright light and raising the temperature to 25ºC. In order to achieve this, a 60W light was installed in an incubator which was set to maintain 25ºC. Male and female *N. vectensis* cannot easily be identified by morphological features (Stefanik et al., 2013), so initial spawnings were performed with individuals in isolated containers. Individuals that released eggs were then separated to establish a female only population from which eggs could be recovered prior to fertilization.

Myocardin Related Transcription Factor in Nematostella vectensis

Background

N. vectensis has a single ortholog for a MRTF-family protein (referred to as NvMRTF hereafter). This contains the same basic domain structure and spacing found in vertebrate MRTF-A and MRTF-B as well as EmMRTF (**Figure 76).** To my knowledge, expression patterns or the role of NvMRTF, or any cnidarian ortholog, in muscle development has not been previously studied. Because of their role in establishment of the mesoderm, proteins like Mef2 and GATA have been studied in *N. vectensis,* with primary focus on germ layer establishment (Martindale 2004; Wijesena et al., 2017). Mef2 has been shown to have various splice variants in *N. vectensis* which serve a diversity of functions including endomesoderm establishment, differentiation of neuronal cell types, and proliferation and differentiation of endodermal cells (Genikhovich & Technau, 2011). Because of this role in early establishment of the endomesoderm and endodermal layers, it is difficult to assess whether NvMef2 directly function in development of muscles (as a terminal transcription factor in myocytes) or in establishment of the tissue from which muscles are derived. In order to get at the role of MRTF in *N. vectensis* a fundamental first step is to look at the spatiotemporal expression

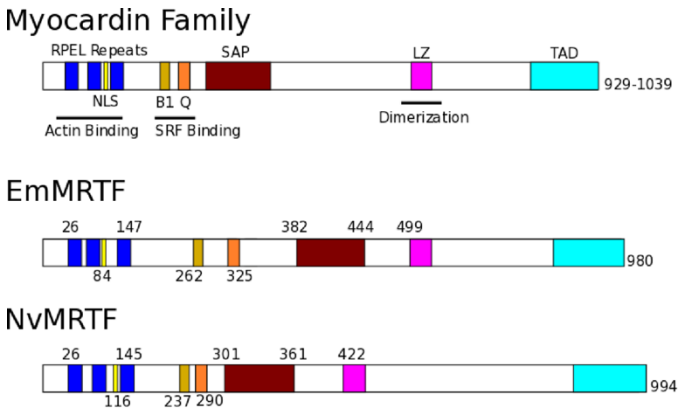

Figure 76. Domain structure of NvMRTF. Predicted domain structure of NvMRTF based on pfam predictions and alignment with functionally categorized proteins. Numbers represent amino acid positions.

pattern of the protein. Under the hypothesis that MRTF is required for myocyte differentiation, there are a few possible outcomes that are expected. These are built on the assumption that NvMRTF continues to serve a role in terminal differentiation and therefore is active as the cells are building the contractile machinery of the muscles. First, NvMRTF may show broad expression in a variety of cell types with two distinct populations, a cytoplasmic inactive pool and a nuclear active pool, as is seen in *E. muelleri.* Second, NvMRTF could show a restricted expression pattern, only being found in muscle precursor cells. This could also be seen as low ubiquitous expression with elevated expression levels in the muscle precursors. Lastly, there could be ubiquitous expression without a clear pattern of cytoplasmic and nuclear pools relative to developing muscles. In this case, the differential function in muscles and non-muscles could be regulated by some other nuclear factor, such as relative levels of SRF and Mef2 in those cell types. Looking at NvMRTF mRNA levels during development should allow for the distinction between the second possibility and the first and third. If expression patterns are broad and consistent, then it would be necessary to visualize the protein to understand subcellular localization, either with an antibody or expressing a labeled version of it. If expression shows some restriction to muscles and muscle precursors, then efforts will be focused on functional characterization of the protein.

Methods

Collection and fixation

Nematostella were spawned as described in (Stefanik et al., 2013) in two groups staggered by 6 hours. The following day egg sacs were collected at recorded times and

mixed with water from the male spawning dish to fertilize. These were then left to develop for a specific amount of time, ranging from 0 hours to 96 hours. At each staggered developmental timepoints, samples were collected, fixed and dehydrated in MeOH as described in (Wolenski et al., 2013). Samples were then stored in 100% MeOH at -20^{o}C until ready for hybridization.

Probe synthesis

Target sequence was identified from the available *N. vectensis* genome and transcriptome (Putnam et al., 2007). Whole organism's early polyp stage mRNA was prepared by collecting approximately 20 budding polyps. This was done with the expectation that NvMRTF would be most highly expressed during development of the major muscles, increasing the chance of getting good template. Polyps were homogenized in Trizol and RNA was purified as described in (Stefanik et al., 2013). Following preparation, 100ng was used to generate cDNA using Takara RNA to cDNA EcoDry Premix, which served as template for the PCR of the target. Core primers used to generate template where;

Forward - AATCAAATGTCGCCACACAA

Reverse – TGTCTGCGATTTCTCACCTG

Two sets were ordered, one with the T7 promoter sequence (taatacgactcactataggg) on the forward primer and one with it on the reverse primer, allowing for generation of sense and antisense probes respectively. PCR was performed with Phusion polymerase (New England BioLabs #M0530S) and 1µL of template cDNA. Cycling parameters used were; 98^{o}C for 2 minutes followed by 35 cycles of, 98^{o}C for 30 seconds, 55^{o}C for 30 seconds, and 72^{o}C for 1 minute, followed by 72^{o}C for 10 minutes and then holding at 4^{o}C. After

amplification, the amplicon was gel extracted using a NucleoSpin Gel and PCR clean-up kit (Macherey-Nagel #740609) and phenol chloroform extracted. 1mg of clean template was then used as template for DIG labeled RNA probe synthesis following the standard DIG RNA labeling kit (SP6/T7) (Roche #11175025910) protocol. Clean probe was then hydrolyzed for 10 minutes at 60^{o}C in 40mM sodium bicarbonate, 60mM sodium carbonate buffer.

Hybridization

Samples were rehydrated and prepared for hybridization following the standard protocol described in (Wolenski et al., 2013). Hybridization was performed for 72 hours at 55^{o}C using either 0.1ng/µL or 1.0 ng/µL of probe. Following hybridization, samples were treated with 1:1000 anti-DIG AP Fab-fragments (Roche #11093274910) and antibody was visualized by adding 3.3µL BCIP (Roche #11383221001) and 3.3µL NBT (Roche #11383213001) and incubating at room temperature in the dark. Samples were periodically checked for development level and reaction was stopped by the addition of 1x PBST. Following the visualization reaction, samples were incubated for 12 hours at 55^{o}C in hybridization buffer to clear background staining. Samples then equilibrated in 90% glycerol in 1xPBS and mounted on glass slides.

Results

With the antisense probe, staining first appeared at around 18hpf in the late blastula stage. During gastrulation, expression was most intense along the site of invagination, along the endomesoderm. Stain persisted in the endoderm which intensified

between 48-56hpf. There was no noticeable ectodermal staining until after tentacle buds had developed. During tentacle development, this staining became very prominent. The only other ectodermal staining was along the developing foot, after loss of the apical tuft (**Figure 77**). There was no staining visible at any stage using the sense strand probe.

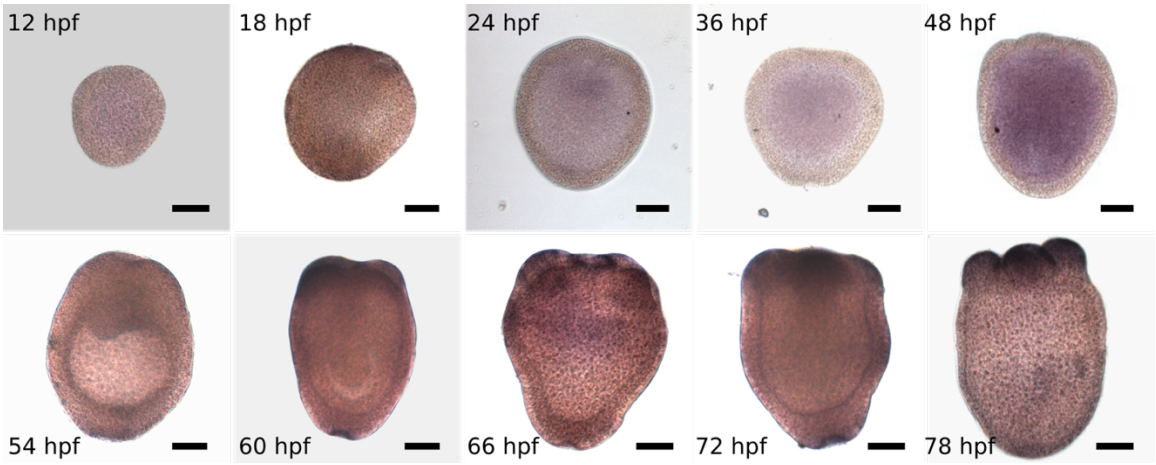

Figure 77. Development expression pattern for NvMRTF shows strong expression in tissues that give rise to muscles. Whole mount *In situ* hybridization using DIG labeled probes targeting NvMRTF. Expression strengthens in the developing endoderm are 24hpf and intensifies through larval development. During polyp formation and development of tentacles, expression remains strong in the endoderm and appears in the ectoderm at sites of developing tentacles. Scale bar 100μm.

Discussion

The early expression, prior to the development of muscles, could speak to a role in different cell processes not directly related to muscle development. However, this population may not be active, so further work will be needed to understand this. The later expression patterns suggest a role in establishment of the endomesoderm followed by high expression in the endoderm, which gives rise to all the muscles that develop during this time. During the budding polyp stage, expression is very high in the ectoderm of the

developing tentacles as well as the regions of the endoderm that give rise to the retractor muscles. These regions both give rise to the stMyHC+ muscles of *N. vectensis*. There does appear to be strong, local expression in the ectoderm of the developing foot, which does not give rise to any muscles, but is a site of rapid cell division during elongation of the body (Fritz et al., 2013). This suggests that NvMRTF may not function exclusively in myogenesis and may play a role in regulating cytokinesis in highly proliferative cells (Shaposhnikov et al., 2013). If this is the case, the early expression in the blastula may then serve an essential function which would pose an issue for knockdowns or knockouts, as myogenesis occurs later in development. The overall expression patterns do suggest a role in myogenesis that is consistent with the hypothesis in which expression levels are regulated and not just localized activity. It is intriguing that the strongest expression was in the two tissues that contain stMyHC+ fast contracting myocytes, which house the largest contractile bundles in the organism.

Functional evidence for MRTF activity

Background

Unlike *E. muelleri, N. vectensis* can be induced to spawn in a laboratory setting and produces injectable oocytes. A commonly utilized and effective method for knocking down a gene in this system is the injection of morpholinos (Layden et al., 2013). There are some limitations and caveats to consider when designing an experiment and interpreting the results. One of these is how far the morpholinos will persist during development. In most systems, effects are seen within the first 3 days, though phenotypes have been judged as late as five days post injection (Bill et al., 2009). For genes that

become active later, especially if in a small population of cells, injecting higher concentrations of morpholinos can help combat as concentration per cell decreases with each division. Another issue when using a global knockdown approach like morpholinos is if the gene target is pleiotropic. The *in situ* hybridization results for NvMRTF suggest that it is highly expressed in regions containing myogenic cells, but also appears in areas of highly proliferative cells. The greatest concern with this is the widespread, low expression during the late blastula stage. If this expression is important for proliferative cells at this stage, knockdown of the protein may be lethal at this stage prior to the onset of myogenesis. Since expression at this stage is much lower than seen in the endoderm and ectoderm in later stages, if knockdown is lethal at this stage, then lowering the concentration of morpholinos to prevent this would likely lead to an ineffective concentration to knockdown function during myogenesis.

Another recently published method for knockdown of a specific gene in *N. vectensis* is the electroporation of shRNAs. The same considerations are necessary when using this method, but because of the rapid process involved, it allows for greater testing of concentrations as well as experimental numbers. Morpholinos have also been shown to have a high rate of off-target effects and toxicity (Bedell et al., 2011). For this reason, utilizing multiple methods to look for consistency in phenotypes will help to strengthen the assumption that effects are target specific as opposed to the result of general morpholino toxicity.

The pharmacological agents, CCG-203791 and ISX-9, will also be tested on *N. vectensis*, as they have been shown to be effective in *E. muelleri*. The greatest benefit of this is, assuming that inhibition is not lethal, drugs can be washed out to look for signs of

rescue from a phenotype. This is particularly beneficial for the inhibitor CCG-203791, in that treatment can begin at a specific time in order to target myogenesis and avoid off target effects on proliferation or establishment of the endomesoderm, should this be an issue with knockdown techniques. If we are able to target and disrupt myogenesis, then rescue of the phenotype following washout of the drug would greatly strengthen the argument for specificity of action.

MRTF drives transcription of specific targets through an interaction with either SFR or Mef2. Mef2 has been investigated in *N. vectensis* as it is a mesodermal marker in a variety of animals. These studies have found that it plays a role in endodermal specification as well neuron development (Genikhovich & Technau, 2011) and cnidocyte development (Babonis & Martindale, 2017). The other animal MADS-box protein, SRF, has not been functionally studied in *N. vectensis.* In bilaterian models, SRF tends to be more broadly expressed whereas Mef2 serves a more restricted function in myogenesis. For this reason, it is generally assumed that Mef2 is a marker of myogenesis. However, the separation of function between the two could have arisen following establishment of a mesoderm. Signal cell sequencing data from sponges have found elevated expression of SRF in the cells that express markers for contractile cell types, whereas Mef2 is restricted to a single cell type that does not highly express those same markers (Musser et al., 2019). If the sponge contractile tissues are homologous to the muscles in *N. vectensis* then we may expect a more restricted expression and function of NvSRF, rather than a ubiquitous distribution.

N. vectensis is developing rapidly as a model system and powerful genetic techniques such as CRISPR mediated genome editing have been shown to work (Ikmi et

al., 2014; Layden et al., 2016). This could be a very powerful tool for getting at NvMRTF function, especially if it is pleiotropic, in that it could allow for the targeted knockdown or knockout in specific cells or at specific developmental stages. The greatest caveat of this is the long time in which it takes *N. vectensis* to reach reproductive age, which can be up to 6 months (Stefanik et al., 2013). This coupled with the relatively low efficiency of these methods made them impractical for our lab, having just brought in the organism, although attempts were made to utilize these.

Methods

Morpholino injections

The gene and pre-mRNA for NvMRTF were identified from the *N. vectensis* genome (Putnam et al., 2007). Slice blocking morpholinos were designed targeting the intron 3:exon 4 splice site. Morpholinos were synthesized by Gene Tools, LLC (www.gene-tools.com). The sequence of the morpholinos is;

5'-TCTCCAGTCTAGTAGGCAAAAACAAT-3'

Lyophilized product was dissolved in nuclease free H_2O to a concentration of 1mM and stored at -20°C. *N. vectensis* was spawned as previously described with females and males in separate containers. Egg packages were collected and de-jellied in 4% cysteine in 1/3 ASW for 15 minutes at room temperature with rocking. Eggs were then transferred to a petri dish, scored with linear lines to stabilize the cells. Morpholinos were diluted 1:1 (v/v) in 1% phenol red and then pulled glass capillaries (WPI #PB150F-4) were back loaded with 0.5µL in preparation for injection. Oocytes were injected with 5nL and then transferred to water from the male spawning container to fertilize. Eggs were monitored

twice daily for development. At 36hpf and 48hpf samples were removed and fixed in 4% paraformaldehyde (PFA) in 1/3 ASW. Samples were then washed in 1x PBS+0.1%Triton X-100 (PTx) and treated with ice cold acetone for 7 minutes on ice. Staining was performed with 3µL phalloidin AF™488 (Life Technologies #A12379) in 100µL PTx, overnight at 4°C with rocking. Samples were washed with PTx, then equilibrated with 90% glycerol in 1x PBS and mounted on slides.

In situ for NvSRF

Probes targeting NvSRF were designed and synthesized as described above and were hydrolyzed in carbonate buffer for 10 minutes at 60°C. Hybridization was performed with 0.1ng/µL of probe for 72 hours at 62°C. Samples were visualized and mounted as described above. Primers used to generate the probe where;
Forward – AGAGCGACGAAGACGATGAT
Reverse - GAAATTAATACGACTCACTATAGGCCTATGGAGGCCTCACTCAC

Electroporation of shRNA

Target sequence in the NvMRTF and NvSRF transcripts were chosen using open shWizard software (http://www.invivogen.com/sirnawizard/index.php). Putative sequences were then BLAST'd against the *N. vectensis* genome (Putnam et al., 2007) and were analyzed with mfold to confirm secondary structure (Zuker, 2003). The following oligo pair was then ordered with a T7 promoter placed 5' of the target sequence;

NvMRTF Forward;

TAATACGACTCACTATAGCCAATTTCCCCTGACTCTTTCAAGAGAAGAGTCAG

GGGAAATTGGCTT

NvMRTF Reverse;

AAGCCAATTTCCCCTGACTCTTCTCTTGAAAGAGTCAGGGGAAATTGGCTATA

GTGAGTCGTATTA

NvSRF Forward;

TAATACGACTCACTATAGGATTTCAGAGCAGAGTGATTCAAGAGATCACTCT

GCTCTGAAATCCTT

NvSRF Reverse;

AAGGATTTCAGAGCAGAGTGATCTCTTGAATCACTCTGCTCTGAAATCCTATA

GTGAGTCGTATTA

The oligo pair was hybridized and used as template for *in vitro* transcription. The AmpliScribe T7-Flash Transcription kit (Lucigen #ASF3257) was used following that standard protocol. Following reaction DNA template was digested and RNA was phenol chloroform extracted to purify. *N. vectensis* was spawned as described earlier and transferred to electroporation media (Stefanik, Friedman, and Finnerty 2013). Electroporation cuvettes were loaded with 100µL of oocyte solution and 200ng/µL shRNA. Electroporation was performed using a Gene Pulser Xcell electroporation system (BioRad #1652660) with a single pulse at 50V for 25ms. Following treatment, oocytes were mixed with water from the male spawning container to fertilize. Developing *N. vectensis* were monitored twice daily with samples collected at 48hpf and 72hpf for staining. Phalloidin staining was performed as described above.

CCG-203791 and ISX-9 Treatments

A container of male and of female *N. vectensis* were spawned as described above and egg packages were collected and de-jellied prior to fertilization in 4% cysteine in 1/3 ASW. Groups of fertilized eggs were treated either at fertilization, 1dpf, 3dpf (following gastrulation), and 5dpf (prior to formation of tentacle buds and settlement). Concentrations tested ranged from 1μM to 100μM,

After establishing a rough concentration and timing for treatment, *N. vectensis* was spawned in a mixed culture of males and females and fertilized egg packages were transferred to a 6-well plate to develop. At 3dpf water was replaced with 5μM CCG-203791 in 1/3 ASW or 10μL DMSO in 1/3 ASW and individuals were left to develop. At 6dpf, when individuals in DMSO control had visible tentacles, samples were collected for fixation and staining. Samples were fixed using 4% PFA in 1/3 ASW as described previously and were stained with phalloidin AF™488 (Life Technologies, 1:100) overnight at 4ºC.

Treatment with ISX-9 during early development appeared to be lethal. In order to try to avoid this effect while still assaying the effect of ISX-9 on myogenesis, we made use of the high *N. vectensis* regenerative capacity (Layden et al., 2016). Though early myogenic gene regulatory networks are likely not active in this context, it is assumed that terminal differentiation factors, such as MRTF do function in the formation of regenerated muscles. Juvenile polyps were bisected with a sterile razor blade to generate an oral and aboral section. Sections were transferred to a 12-well plate and incubated in either 50μM ISX-9 in 1/3 ASW or equal volume DMSO in 1/3 ASW for 36-72hpa.

Samples were then collected and fixed in 4% PFA in 1/3 ASW and stained for actin with phalloidin AF™488 as previously described.

Confocal Images were acquired on an Olympus Fluoview FV3000 confocal laser scanning microscope using either a 60×/1.4 NA or 100×/1.4 NA objectives. Laser levels and acquisition setting were not adjusted for imaging controls. Images were processed in FIJI (Schindelin et al., 2012).

Results

Morpholinos

Phenol red positive individuals were separated into wells based on concentration of injected morpholinos. At 2dpf, non-developing individuals were removed. There was no statistical difference in the number of individuals removed from control and 100nM Concentration wells, but all individuals injected with 500nM Concentration of morpholinos had stopped developing. At the time of collection for staining, all larvae were swimming, demonstrating that they were alive at the time. Actin organization in

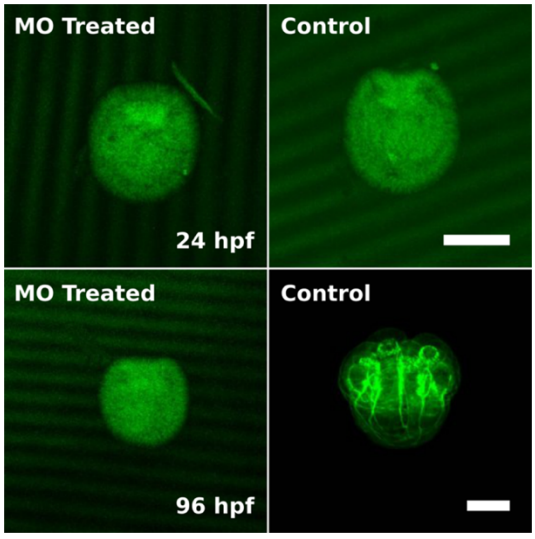

Figure 78. NvMRTF morphants do not develop body muscles or tentacles. Individuals injected with splice blocking morpholinos for NvMRTF were fixed at various stages and stained for actin (green). At 24 hpf morphants and controls do not show a strong difference, with both showing dark actin staining at the developing endomesoderm. By 96 hpf morphants show no additional development of tissues, while controls have well developed muscles, with the retractor muscles visible through the body and longitudinal tentacle muscles beginning to develop. Scale bars 200µm.

injected individuals appeared consistent between 36 and 48hpf and appeared as denser staining around the site of gastrulation with overall light staining relative to the controls (**Figure 78**). No individuals continued to develop past this stage, and tentacle budding was not observed.

Electroporation of shRNA

Knockdown of NvMRTF with shRNA mirrored the phenotypes observed in MRTF morphants. At 48hpf, individuals that were collected were swimming, though actin staining showed little organization to the larvae, without a clear endomesoderm or endoderm (**Figure 79**). Individuals collected at 72hpf showed little development of the endoderm as well as a lack of visible musculature (**Figure 80**). This occurred on a spectrum of severity, in which some individuals showed no clear actin organization in the endoderm, without any muscles, to individuals with partially stained endoderm, which contained some clear musculature. All of these individuals were observed to be moving at time of collection and had a clear blastopore/pharynx.

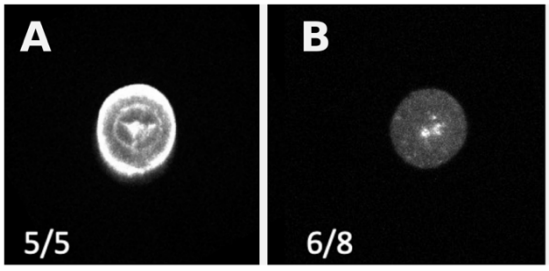

Figure 79. Knockdown of NvMRTF with shRNA shows similar phenotype to morpholinos. Individuals were collected 2 dpf and stained for actin. **(a)** Oral view of control larvae show regions of strong actin staining. **(b)** Oral view of MRTF knockdown larvae has much less pronounced staining. Scale bars 100μm.

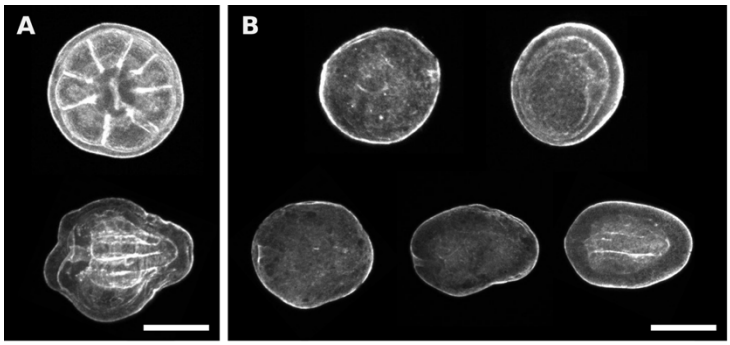

Figure 80. Knockdown of NvMRTF prevents proper endoderm formation and muscle development. **(a)** Actin stained 3dpf individuals show general actin organization from oral (top) and lateral (bottom) views. **(b)** Individuals treated with shRNA targeting NvMRTF show reduced development of major actin structures on a spectrum from complete loss (left) to partial loss (right). All of these individuals were actively swimming at time of fixation. Scale bars 100µm.

Expression Patterns and Knockdown of NvSRF

Focusing on expression patterns during developmental stages during which myogenesis is occuring, NvSRF shows strong expression in the endodermal tissue during late larval stage in which the mesenteries are developing, with clear expression in internal tissue separating these, from which the retractor and parietal muscles arise. Expression remains strong in the endoderm through polyp development, with little to no expression in the ectodermal tissue (**Figure 81)**. There is no detectable expression in the ectoderm of the developing tentacles though. Knockdown of NvSRF with shRNA Results in phenotypes that resembled those seen in NvMRTF knockdown which included reduced endoderm and limited muscled development (**Figure 82**). This appeared on a spectrum, appearnet loss of structure in the endoderm to reduced development of large actin structures without changes to

Figure 81. Expression of NvSRF. High expression is seen in the endoderm around the mesenteries in larval stage, which persists through budding and early polyp stage. Scale bars 100µm.

overall body organization. It was interesting that tentacle development was reduced, as seen by lack of tentacle buds, in most of these, despite the lack of strong expression in this tissue. This could be the result of global developmental disruption or it could be that levels of SRF in the ectoderm at tentacle buds are below detection level, due to high relative amounts in the endoderm.

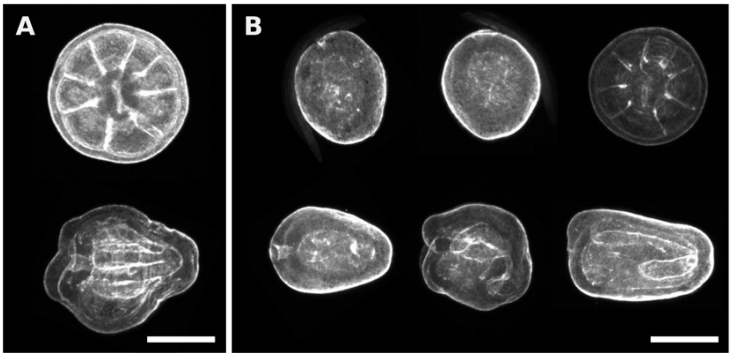

Figure 82. Knockdown of NvSRF prevents proper endoderm formation and muscle development. **(a)** Actin stained 3dpf individuals show general actin organization from oral (top) and lateral (bottom) views. **(b)** Individuals treated with shRNA targeting NvSRF show reduced development of major actin structures on a spectrum from complete loss (left) to partial loss (right). All of these individuals were actively swimming at time of fixation. Scale bars 100μm.

CCG-203791 treatment

Individuals treated with CCG-2013791 at fertilization and at 1dpf did not show a significant increase in developmental arrest. High concentrations of CCG-203791 showed a high rate of developmental arrest and lack of movement following 3dpf, while lower concentrations showed steady movement of the larvae at this time. For this reason, 5μM CCG-203791 were used and treatment began at 3dpf, after gastrulation begins but prior to myogenesis. At 6dpf, no individuals in the treatment group showed evidence of tentacle formation which could be seen in the control individuals. Of the treatment group, 90% were visibly moving around the well. The individuals that were collected and stained at

this time showed phenotypes similar to the morphants and shRNA knockdown individuals with respect to the actin organization (**Figure 83**). There were low levels of staining for actin in the endoderm, with no musculature visible. Of the individuals collected and washed into clean 1/3 ASW, 60% showed rescue of development, in which they formed clear tentacle buds. When these individuals were fixed and stained for actin, major muscle groups were now visible (**Figure 83c**).

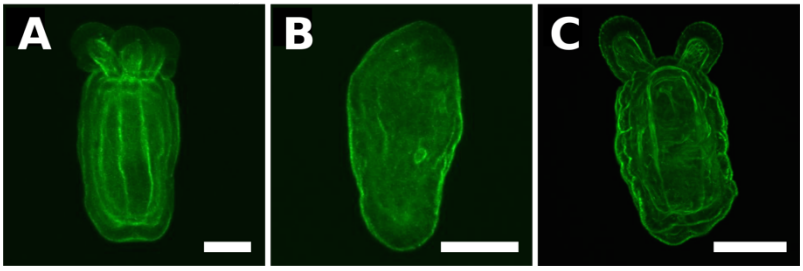

Figure 83. Pharmacological inhibition of MRTF activity shows a similar but reversable phenotype. Individuals were treated with either CCG-203791 or DMSO during larval development and then fixed and stained for actin. **(a)** DMSO control shows normal morphology, with large retractor muscles running through the body and strong staining of the tentacle muscles. **(b)** CCG-203791 treated individuals showed reduced actin structures, similar to what was seen in the morphants and shRNA knockdowns. **(c)** Follow washout, individuals were incubated for an additional three days and then fixed and stained for actin. These showed evidence of development of muscles, with retractor and longitudinal tentacle muscles visible. Scale bars 100µm.

ISX-9 treatment

Individuals treated with ISX-9 during early development did not develop past 3dpf with none being seen moving past this time in any treatment above 20µM. Of the individuals that continued movement following treatment with 20µM ISX-9, these all developed normally relative to the controls. Individuals treated with 50µM ISX-9 following bisection developed striking phenotypes during regeneration which were consistent for both the head and aboral regenerations. The clear features of these

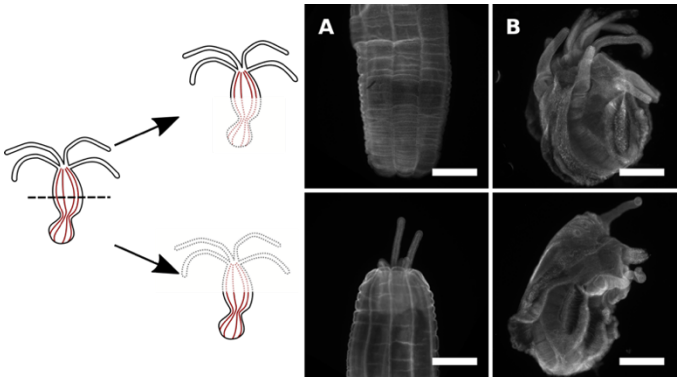

Figure 84. Activation of MRTF during regeneration gives strong phenotypes. Polyps were bisected and left to regenerated in the presence of ISX9 or DMSO. **(a)** DMSO treated polyps foot (top panel) and the head (bottom panel) regeneration. **(b)** ISX9 treated individuals show ectopic tentacle development and excessive tissue ruffling. Scale bars 100μm.

phenotypes were a large number of ectopic tentacles with body regions containing disorganized endodermal tissues containing cells filled with large amounts of f-actin with inconsistent morphology but consistent orientation (**Figure 84)**. In individuals regenerating aboral regions, the tentacles could be compared directly with those present prior to bisection. Ectopic tentacles contained no evidence of cell types other than muscles in the ectoderm, with dense actin bundles running in close proximity to the apical region of the cells (**Figure 85a&b**). The body of these individuals also included wide regions containing longitudinal actin bundles, as opposed to the normal circular muscles (**Figure 85c&d**). These bundles contained central regions composed of sickle shaped cells which appear to be completely filled with actin. Viewing these cells under higher magnification, the actin bundles that fill the cells appear to be oriented along the length of the cell (**Figure 86**). Within these regions the brightest and widest stained cells appear to lack visible adhesions to other cells (**Figure 86a**). This morphology could suggest a rapid shortening of the bundles following the loss of lateral points of adhesion, and therefore opposing force.

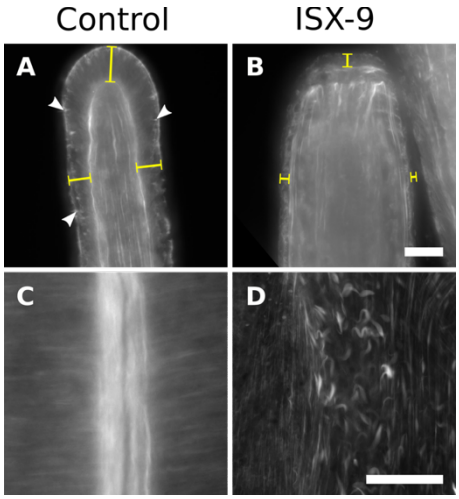

Figure 85. Ectopic tentacles contain primarily muscles and tissue ruffles contain actin dense cells. **(a)** Actin staining of control individual following regeneration shows relative size of ectodermal layer (yellow bars) with contractile bundles running along the base. Sensory hair cells are also visible (white arrows). **(b)** Actin staining of an ectopic tentacle of a treated individual following regeneration. Apical cell size is dramatically reduced (yellow bars) and there is no evidence of different cell types in the tissue. **(c)** Actin staining of retractor muscle in a control polyp with body muscles running perpendicular. **(d)** Actin staining of tissue ruffle in an ISX9 treated polyp. Actin bundles are running along the oral-aboral axis, as with the retractor muscle. In the middle of the structure are several sickle shaped actin dense cells which are disconnected from other cells. Scale bars 20μM.

Discussion

For the morpholino treatments, it did appear that knocking down MRTF either during or just after gastrulation resulted in developmental arrest. As no individuals made it past this general stage of development suggests that it did not stall development which could be rescued by time (as the morpholino effects wore off), but rather blocked an essential step. That all of the morphants examined at this stage were swimming, suggests that they were viable at the time so lack of development of specific tissues can be taken as a specific result of the knockdown as opposed to broad toxicity. This does not rule out non-specific activity in that tissue though. The largest outstanding question is similar to

what was encountered in previous studies of Mef2 in *N. vectensis*, which is whether developmental arrest is due to the lack of muscle differentiation or if it results from disruption of the endoderm prior to myogenesis. The clearest finding from this experiment is that morphants persisted past blastula stage in which NvMRTF expression begins. One interpretation of this is that the result of this early expression is not an active pool of protein. The shRNA mediated knockdowns showed a similar phenotype of that seen in the morpholinos, which strengthens this finding and supports the idea that NvMRTF is essential for proper development of the larvae and transition to polyp stage. The appearance of partial knockdowns or intermediate phenotypes is likely a result of incomplete and inconsistent penetrance of this knockdown using this technique. This could be a result of how far into development the shRNA must be carried forward. It does appear that unaffected cells/tissues populate localized areas of the body which suggests they originate from a common precursor. In this, there is more clear staining along the general endodermal tissue with few large muscles visible, which suggests that endoderm still formed but full myogenesis did not occur. Apart from the movement observed in these individuals suggesting they were still viable, the blastopore or pharynx were clearly visible, giving a good gage of developmental stage at which effects could be

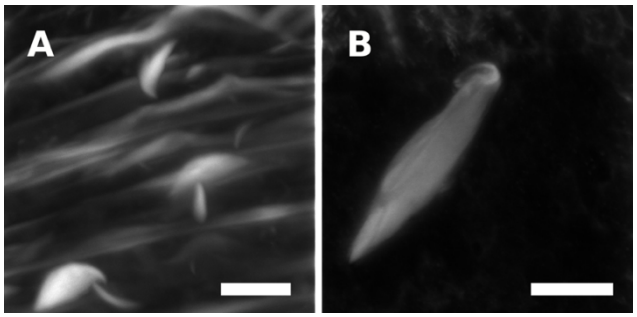

Figure 86. Disconnected cells are wider and shorter and contain oriented actin bundles. **(a)** Actin staining of ISX9 treated polyp shows tissue containing actin bundles with disconnected, actin dense cells. These cells are wider and shorter than those in the tissue below based on the actin bundles visible. **(b)** Isolated cell shows faint banding which suggests actin in the cell is oriented between the two narrow ends. Scale bars **(a)** 10μm and **(b)** 5μm.

seen (**Figures 79&80**). Like the NvMRTF morphants, none of the shRNA treated individuals that displayed the associated phenotype of lack of tentacle buds at 72dpf continued to develop into polyps. This suggests that expression of NvMRTF is likely developmentally regulated and necessary for proper development. This seems consistent with the findings for time series expression patterns, and differs from what is seen in *E. muelleri*, in which expression seems ubiquitous and regulation of subcellular protein localization regulates its activity.

Treatment with CCG-203791 was consistent with the phenotypes associated with both knockdown techniques. This alone is an interesting finding in that it suggests that the activity at the protein level is necessary for normal development and the mechanism of action for NvMRTF is conserved. Because of the broad nature of the phenotype, the specificity of the treatment is always an assumption though. The consistency seen in the three methods of knockdown does strengthen the argument that this is a specific effect of the blocking of the MRTF pathway in *N. vectensis.* Rescue of normal development following washout suggests specificity of action as well. There did appear to be some additional tissue ruffling in individuals following treatment and washout, but major muscle groups did develop (**Figure 83c**). Taken together, these findings strongly suggest that NvMRTF expression and activity are necessary for development of muscles in *N. vectensis* larvae and early polyps.

Results of ISX-9 treatment during early development were difficult to interpret. One possibility is unregulated activation of the early population of MRTF (seen in blastula) could prevent normal formation of the blastopore and endomesoderm, which halts development. However, similar results were seen in treatment after gastrulation had

occurred which suggests this could be a result of general toxicity. The findings from the regeneration trials are a lot clearer and match the expectations under the assumption that the NvMRTF mechanism of action is conserved and NvMRTF plays a primary role in myogenesis. During regeneration, populations of stem cells migrate to the area of the wound and then begin to proliferate and differentiate (DuBuc et al., 2014). It seems in this case, these cells follow the trajectory towards formation of tentacles, which are composed of the only ectodermally derived myocytes. During normal development there is a very strong expression of NvMRTF in elongating tentacles. By looking closely at the ectopic tentacles, the ectodermal tissues appear to only contain myocytes with no evidence of cnidocytes which normally populate this tissue (Fritz et al., 2013) (**Figure 85a)**. Both wnt and notch signaling have been implemented in tentacle development (Marlow et al., 2012) and are known to regulate in feedback loops with MRTF (He et al., 2018). Muscle development and actin dynamics are also requirements for tentacle elongation, in which cells at the tip are differentiated while proliferative cells persist at the base (Jahnel et al., 2014; Fritz et al., 2013). It is possible that the activation of MRTF leads to differentiation into a tentacle myocyte, which activates the signaling cascade for elongation of the tentacle. Constitutively active MRTF leads to all cells in the developing tentacle to differentiate into myocytes, which gives rise to the observed phenotype. The other unique cell type observed in these treatments are the endodermal cells which appear to be completely filled with f-actin. This appearance closely resembles phenotypes observed in the muscles of other organisms in which specific sarcomeric proteins are knocked out. In *Caenorhabditis elegans*, a very similar phenotype is observed when tropomodulin and ADF/cofilin are knocked out resulting in unregulated development of

contractile bundles in the body wall muscles (Yamashiro et al., 2008). These two proteins are not known to be targets of MRTF activity and aid in regulating actin stability. One interpretation for this phenotype in *N. vectensis* is that constitutively active MRTF leads to over-expression of core contractile bundle proteins. Overexpression of these proteins could lead to overdevelopment of contractile structures and increased force generation, which results in detachment of cell adhesions. Another possibility is that not all structural proteins are under the control of MRTF. Actomyosin has been shown to self-assemble when overexpressed in a variety of systems (Hu et al., 2017). This is primarily driven by the bundling properties of myosin II thick filaments, which can increase interactions when stabilized by F-actin (Ideses et al., 2014). Myosin II mediated bundling can be limited by association with stabilizing proteins such as tropomyosin and alpha-actinin, which regulate regular spacing of the thin filaments (Sanger et al., 1984). Overexpression of core actomyosin proteins, without increased expression of one or more of the stabilizing proteins could phenocopy the outcome of knocking out said protein, like what is seen in *C. elegans* (Yamashiro et al., 2008). Based on this, it is possible that MRTF activity alone is not sufficient to drive differentiation into a specific contractile cell type as seen in *E. muelleri*. However, striking nature of the phenotypes associated with this treatment, coupled with their consistency based on cell types, which seem to correlate with regions of myogenesis during regeneration, suggests that MRTF plays an important role in myocyte differentiation. Combining these findings with the knockout/inhibition findings further supports that NvMRTF has a conserved mechanism of action as well as is an essential myogenic factor.

Other Myogenic Factors, HAND, Dach, and FoxL-like

Background

The findings above suggest a role for MRTF in myogenesis in *N. vectensis*. However, unlike *E. muelleri* in which MRTF activity seems to be the primary regulator of contractile cell fate and EmMRTF is either widely or ubiquitously expressed, NvMRTF shows a restricted expression pattern and its activity does not seem sufficient in some context (though it does in other) to drive differentiation into a functional myocyte. This suggests that there are other regulatory factors involved in expression and activation of NvMRTF as well as general myogenesis in *N. vectensis*. Mef2 expression has an overlapping spatiotemporal expression pattern with NvMRTF (Martindale, 2004), GATA expression is restricted to the developing endomesoderm, prior to myogenesis (Wijesena et al., 2017; Martindale, 2004), and other myogenic factors such as MyoD, Myogenin, and Mrf4 are absent (Steinmetz et al., 2012). Developmental transcriptomes as well as signal cell RNA sequencing data (Sebé-Pedrós et al., 2018) provide a glimpse of general expression patterns during specific cellular trajectories. In order to identify candidates for a role in *N. vectensis* myogenesis, a short list of putative myogenic factors was chosen based on timing in global expression patterns during development. This list was then shortened by looking at correlation with specific myocyte markers (such as stMyHC expression) in scRNA-seq datasets by following expected differentiation pathways. The factors that were chosen to investigate based on this were; HAND1/2 (McFadden et al., 2005), FoxL-like (Golson & Kaestner, 2016), and dachshund (Heanue et al., 1999).

Heart and neuronal crest derivatives-expressed proteins (HAND1 and HAND2 in vertebrates) are basic Helix-loop-helix (bHLH) transcription factors that play an important role in cardiac morphogenesis and differentiation of cardiomyocytes (George & Firulli, 2019; McFadden et al., 2005). There are three HAND family-like proteins in the *N. vectensis* genome, though they do not clearly group with HAND1 or HAND2. To my knowledge, the function of these proteins has not yet been explored in *N. vectensis.*

Fox-L-like is a forkhead transcription factor that is found in developing tentacles of *N. vectnesis* (Sebé-Pedrós et al., 2018). It was identified here based on strong expression along the differentiation trajectory that gave rise to stMyHC+ longitudinal tentacle muscles. There are 15 Fox proteins that can be identified in the *N. vectensis* genome (Magie et al., 2005) based on the conservation of the forkhead domain. The Fox protein family predates animals and can be separated into two primary clades (Hannenhalli & Kaestner, 2009; Shimeld et al., 2010). Clade II contains proteins that predated animals and has undergone limited expansion, evident by comparisons between lineages of non-bilaterians and bilaterians. Clade I has undergone wide expansion during animal evolution with relatively few present in the genomes of modern sponges and many found in the genomes of modern bilaterians (Shimeld et al., 2010). Within this clade are the two members that have been found to function in differentiation of bilaterian muscles, FoxC (cardiomyocytes) (Lambers et al., 2016) and FoxF (vertebrate smooth) (Hoggatt et al., 2013). There is a FoxC-like protein found in *N. vectensis,* but it does not seem to function in myogenesis, rather it is solely expressed in developing mesentery (Magie et al., 2005). There are no FoxF like proteins in *N. vectensis*. In vertebrates FoxL2 is highly expressed in ovaries and plays a role in sex-determination

during development (Uhlenhaut & Treier, 2006). FoxL1 has been shown to function in differentiation of the gastrointestinal epithelium (Aoki et al., 2016). It has been shown to be a target of hedgehog signaling (Madison et al., 2009) and modulates wnt/β-catenin signaling in the gut (Perreault et al., 2001). FoxC, FoxF, and FoxL1 are molecularly similar proteins (Hannenhalli & Kaestner, 2009) and are thought to have made up an ancestral gene cluster in the animal stem lineage (Shimeld et al., 2010). This could have been the result of an early series of duplications in which they maintained redundancy in their function as early lineages diversified. As specialized muscle types arose in specific lineages, their function specialized as well.

Dachshund (dach) was originally identified in *Drosophila melanogaster,* in which it played an essential role in eye development (Mardon et al., 1994). In this, it functioned synergistically with eyes absent (eya) during compound eye development and overexpression leads to ectopic compound eyes (Chen et al., 1997). However, the vertebrate orthologs dach2 and eya2 have been shown to function in myogenesis, through a similar synergistic mechanism (Heanue et al., 1999). In this, it seems that the mechanism of action for the two proteins originated prior to the protostome/deuterostome split, but their downstream effects have specialized in different lineages. *N. vectensis* has well conserved orthologs of dach and eya, and prior studies have shown expression in the endoderm during development (Steinmetz et al., 2017).

Methods

In situ hybridization

Spatiotemporal expression patterns were analyzed by *in situ* hybridization with DIG labeled RNA probes as described earlier following the general protocol described in (cite). Probes were generated by amplifying cDNA generated from RNA extracted from a mixture of larvae and polyps, following the standard Trizol protocol described above. Primer sets used to amplify each target were;

NvHAND1

Forward - CAACTGAACGGATAGCGTGTT

Reverse - GAAATTAATACGACTCACTATAGGGCAGGCATGCTTGCACTATCA

NvHAND2

Forward – CGCTTCGACTAGCGATTAGC

Reverse - GAAATTAATACGACTCACTATAGGGCCCATGGTATATCTGACG

NvHAND3

Forward – ATCACCCAGCCGTATCTCAC

Reverse - GAAATTAATACGACTCACTATAGGGTTTTTCGACACCTCACCACA

NvFOXL-like

Forward – GCACAACCACGATACTGACG

Reverse - GAAATTAATACGACTCACTATAGGGCGACCTTGGAGGTACATCGT

NvDach

Forward – ACGACACACCTTCGTTACCC

Reverse - GAAATTAATACGACTCACTATAGGGGATGAATTCGTGGGGTTTTG

Gel extracted amplicons were cleaned by phenol chloroform extraction and EtOH precipitation, and then were used to generate DIG-labeled RNA via *in vitro* transcription following DIG labeling protocol used above. Probes were then hydrolyzed in 40mM sodium bicarbonate, 60mM sodium carbonate for 10 At 60ºC. Samples were hybridized for 52 hours in either 0.1ng/μL or 1.0ng/μL concentration probes at 62ºC. Probes were visualized with BCIP and NBT as described earlier.

shRNA knockdowns

shRNA was generated by *in vitro* transcription off the T7 promoter using AmpliScribe T7-Flash Transcription kit. Template oligos used for each were;

NvHAND1 Forward;

TAATACGACTCACTATAGTCCTGAAAGAGCTTACGATTCAAGAGATCGTAAG
CTCTTTCAGGACTT

NvHAND1 Reverse;

AAGTCCTGAAAGAGCTTACGATCTCTTGAATCGTAAGCTCTTTCAGGACTATA
GTGAGTCGTATTA

NvDach Forward;

TAATACGACTCACTATAGGTAGGAGTCTGGGTACAATTCAAGAGATTGTACC
CAGACTCCTACCTT

NvDach Reverse;

AAGGTAGGAGTCTGGGTACAATCTCTTGAATTGTACCCAGACTCCTACCTATA
GTGAGTCGTATTA

NvFoxL-like Forward;

TAATACGACTCACTATAGGCGAGAGAAAGGGTAACTTTCAAGAGAAGTTACC

CTTTCTCTCGCCTT

NvFoxL-Like Reverse;

AAGGCGAGAGAAAGGGTAACTTCTCTTGAAAGTTACCCTTTCTCTCGCCTATA

GTGAGTCGTATTA

Generated shRNA was cleaned with phenol chloroform extraction and EtOH precipitation. Spawning and preparation was performed as previously described using 200ng/µL of shRNA per treatment. Samples were then collected at 5dpf and 7dpf and fixed in 4% PFA in 1/3 ASW and stained with phalloidin to assess muscle development as previously described.

Confocal Images were acquired on an Olympus Fluoview FV3000 confocal laser scanning microscope using either a 60×/1.4 NA or 100×/1.4 NA objectives. Laser levels and acquisition setting were not adjusted for imaging controls. Images were processed in FIJI (Schindelin et al., 2012).

Results

Expression of HAND1/2/3 and dach did not show strong patterning during larval stages but did show strong expression in specific regions during the polyp stage. HAND1 showed expression along the mesentery in a line pattern that appears consistent with the parietal muscles (**Figure 87a)**. There also appears to be some broad expression in the endoderm of the polyp. There is strong expression of the HAND2 and HAND3 in the endoderm through the body of the polyp (**Figure 87b&c**). Dach shows broad expression

along the endoderm, slightly intensified near the retractor muscles, as well as in the endoderm of the tentacles (**Figure 88**). FoxL-like showed the most restricted developmental pattern, showing localized staining in ectodermal cells at developing tentacles (**Figure 89a**). This persisted into polyp stage at the tips of the growing tentacles (**Figure 89b**).

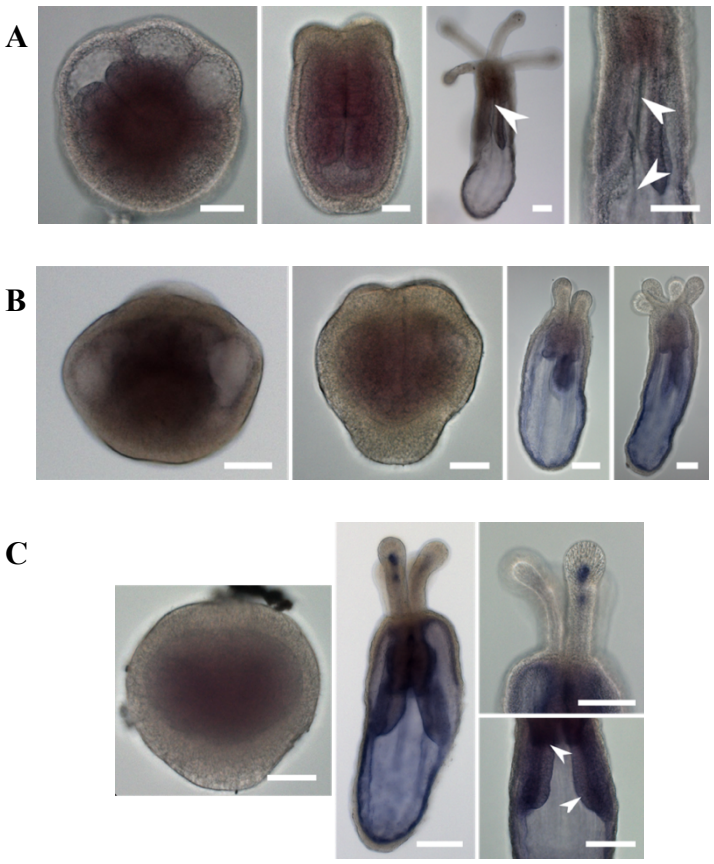

Figure 87. Developmental expression of NvHAND proteins. Colorimetric *in situ* hybridization for **(a)** HAND1, **(b)** HAND 2, and **(c)** HAND3 in larval, early polyp, and polyp stage. For all three, expression begins to show in the endodermal tissue of the mesenteries, which persists as strong endodermal expression in early polyp stage. HAND1 shows polyp stage expression is seen in the endoderm as well as what appears to be the parietal muscles, which is also visible for HAND3 (white arrows). HAND 3 is the only one to show expression in the tentacles, which is in the endoderm. Scale bars **(a-c)** 50µm, **(c)** 100µm for polyp.

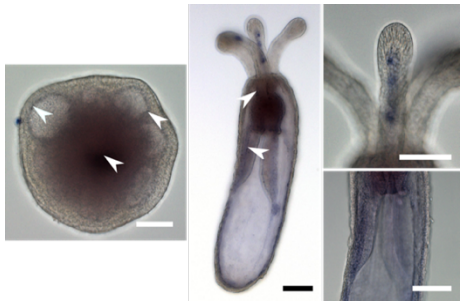

Figure 88. Developmental expression of NvDach. Colorimetric *in situ* hybridization for Dach in larval and polyp stages. Larval expression can be faintly seen in the endoderm around the mesenteries, with stronger staining in the pharynx. Polyp expression in the endoderm of the body is more intense in bands running along the mesenteries (white arrowheads). Expression can also be seen in endodermal cells of the tentacles. Scale bars 50µm for larvae and 100µm for polyp.

Knockdown of HAND resulted in no clear effect during early development of the larvae with 18 of 23 individuals showing continued development and swimming behavior at 7dpf. At 7dpf, phenotypes ranged from full loss of the endodermal actin organization to reduced organization of the mesentery which appears to be coupled with loss of the retractor muscles. This phenotype also showed disfunction in tentacle development (**Figure 90b**). Knockdown of dach appeared to have a strong effect on development of the larvae as well as transition to polyp stage, with only 8 of 15 individuals surviving past

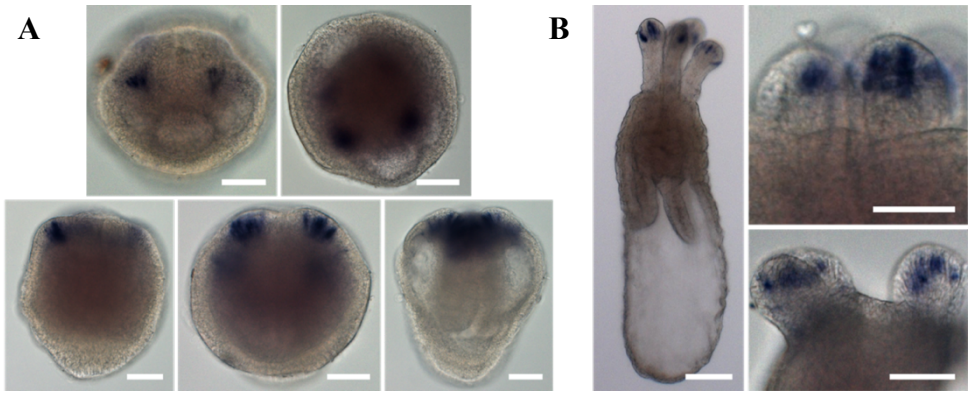

Figure 89. Expression of NvFoxL-like is highly restricted to the ectoderm of developing tentacles. Colorimetric *in situ* hybridization for FoxL-like during development. **(a)** Larval developmental series shows expression in a small number of cells as the larvae elongates prior to developing tentacles. Expression increases in cells in this region as tentacle development begins. **(b)** As tentacles grow during polyp stage, expression is seen in the ectodermal cells at the end of the tentacle. Scale bars **(a)** 50µm and **(b)** 100µm for left panel 50µm right panel.

5dpf. Of the ones that survived to 7dpf, the majority showed highly reduced actin organization in the endoderm with no development of muscles or tentacle buds (**Figure 90c**). Some patterning could be seen in the mesenteries, but this was highly irregular. For FoxL-like knockdowns, 12 of 12 individuals survived between 5dpf and 7dpf with phenotypes ranging from reduced tentacles to, lack of tentacle buds and loss of retractor muscles (**Figure 91**). In cases where tentacle buds were present, actin bundles became irregular and did not extend down through the mesoglea towards the body (**Figure 92**).

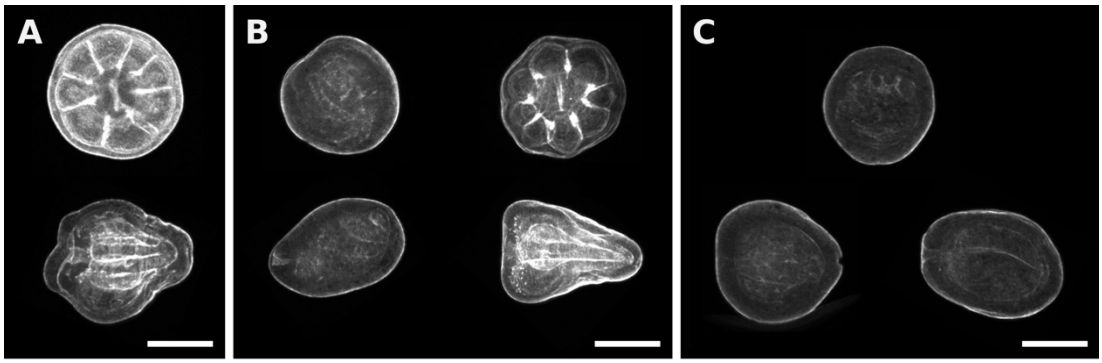

Figure 90. Knockdown of HAND1 and Dach result in actin disruption and a reduced endoderm. Proteins were knocked down with electroporation of shRNA in gametes and individuals were fixed and stained for actin at 3dpf. **(a)** Control larvae show general actin organization from oral (top) and lateral (bottom) views. **(b)** Knockdown of HAND showed phenotypes that ranged from full loss of large actin structures in the endoderm to altered morphology through the mesenteries and elongation of the body. **(c)** Knockdown of Dach showed severe disruption of endodermal structures. Scale bars 50μm.

Discussion

Expression patterns of these proteins, with the exception of NvFoxL-like, tended to show broad expression across the endoderm into polyp stage. This is consistent with previous findings and suggests function may not be restricted to myogenesis. HAND2 and HAND3 showed a lot of overlap in their patterns and may serve redundant functions, based on the close relationship of the two proteins. NvFoxL-like showed the most

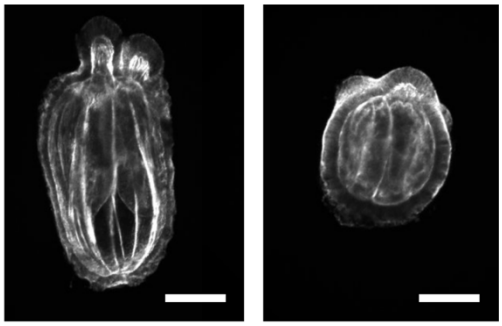

Figure 91. Knockdown of NvFoxL-like inhibits tentacle formation. Individuals were stained for actin at 7dpf. Control polyp (left) has large retractor muscles and elongating tentacles contain longitudinal muscles. Knockdown of NvFoxL-like (right) results in reduced tentacles, without longitudinally oriented actin bundles. There also appears to be a reduction in the sized of the retractor muscles and a shortening of the body. Scale bars 100µm.

restricted expression pattern in which there was low levels of endodermal expression in the larvae, but very strong expression in the ectodermal cells that formed the tentacle buds which persisted in a small number of cells at the tips of extending tentacles. During tentacle formation, the cells at the tip differentiate first with proliferative cells closer to the body (Fritz et al., 2013). As the tentacles elongate, the proliferative cells migrate towards the tip moving differentiated cells (including the myocytes) towards the body (Jahnel, Walzl, & Technau, 2014). This leads to the longitudinal muscles forming at the tip but extending from the body. The expression pattern for NvFoxL-like, coupled with correlation with expression of stMyHC, suggests a role in myogenesis. However, this

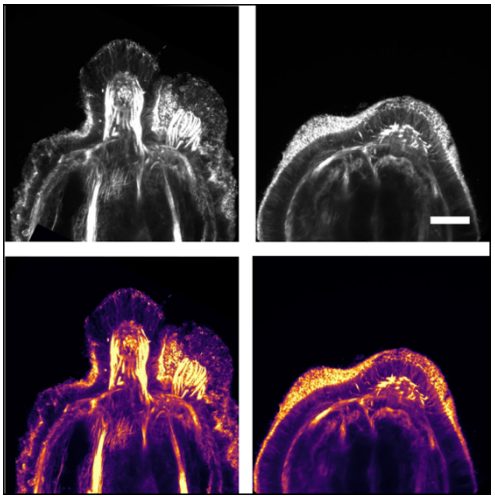

Figure 92. Reduction in longitudinal tentacle muscles and retractor muscles is seen following knockdown of NvFoxL-like. The control polyp (left) shows large actin bundles of the longitudinal tentacle muscles expending down into the body towards retractor muscles. Knockdown of NvFoxL-like (right) leads to disordered actin structures at the base of ectodermal cells at the tentacle buds. There is also a reduction in the relative intensity of actin staining along the retractor muscles. Bottom panels show intensity colored images, in which warmer colors indicate stronger signal, to help visualize actin dense structure in each sample. Scale bar 20µm.

may not be a direct role, in that NvFoxL-like could pattern tentacle formation, which happens to overlap with cells that differentiate into myocytes in the tentacles.

The high mortality rate and phenotypes associated with the knockdown of NvDach suggests an essential role in endoderm formation, which is important prior to the formation of muscles. The knockdown of NvHAND1 showed a wide spectrum of phenotypes, from those resembling the knockdown of dach to ones that appear to have normal body patterning but with elongated bodies, rounded mesenteries, and no tentacle buds. The latter could be a result of the disruption of stMyHC+ muscles (longitudinal tentacle and retractor) during development. The retractor muscles run the length of the body and are used in rapid contractions during the escape response (Jahnel et al., 2014). These are the largest muscles which form from the endoderm in the mesentery (Jahnel et al., 2014). Disruption of development of these muscles could lead to the loss of basal tension through the mesenteries, which could lead to the rounding and folding seen in the knockdowns. This could also be a result of a loss in the parietal muscles which form along the interface of the ectoderm and endoderm at the edge of the mesenteries. Loss of these muscles could lead to the folding in and rounding along the mesenteries as is seen in the knockdowns. Based on the more severe phenotypes, it is likely that NvHAND1 function is not restricted to regulating myogenesis. However, the less severe phenotypes do support that a major role of this transcription factor is in patterning muscle development. Knockdown of FoxL-like results in a reduction in tentacle formation and also a reduction in the size of the retractor muscles. In the reduced tentacle buds, there are some visible actin bundles, but these are not aligned with the direction of the extending tentacle, as is normally seen, and are reduced in size. One interpretation of this is that

FoxL-like patterns the integration of the ectodermal derived longitudinal tentacle muscles with the endoderm derived body muscles. When this function is lost, there is no anchoring of the muscles at the base of the tentacles (as seen in the disordered bundles in the knockdown). This would result in a reduced force from tension on the developing tissues, which could disrupt MRTF signaling, stopping muscle development. This could explain the apparent decrease in retractor muscle size despite no evidence for expression in the region. The two stMyHC+ muscle groups could utilize a developmental feedback loop, in which mechanical force generated by the development of one tissue could help regulate the development of the other. This type of development is seen in a variety of tissues in different animals in which contractile forces generated by developing muscles help guide patterning (Lemke & Schnorrer, 2017; Vining & Mooney, 2017). Future work could be done to better understand the mechanism by which this phenotype arises, which may be informative in how the myonemes guild attachment with neighboring cells as well as with connective tissue. This has been studied in striated muscle development in both invertebrates and vertebrates (Felsenthal & Zelzer, 2017; Grzelkowska-Kowalczyk, 2016; Maartens & Brown, 2015; Pérez-Moreno et al., 2017), but is not understood in myoepithelial tissue, in which apical cell-cell adhesions are present.

Conclusions

MRTF appears to function in development of muscles in the cnidarian *N. vectensis.* Expression patterns show increased levels during development in tissues which gives rise to muscles. Knockdown of the protein or blocking its function results in an absence of musculature while activation of it results in ectopic growth of structures which

contain muscle like fibers. These findings highlight the developmental as well as structural similarities between these muscles and the endopinacoderm of *E. muelleri,* suggesting a shared evolutionary history.

Unlike contractile tissue of sponges, cnidarian muscles develop in predictable numbers and locations. For this, other putative myogenic factors were investigated as well. The epithelial nature of the *N. vectensis* muscles can make phenotypes difficult to interpret because lack of contractile bundle development is generally accompanied with developmental arrest. The two exceptions to this were NvHAND1, which in some cases appeared to selectively reduce development of the parietal muscles, and NvFoxL-like, which resulted in lack of tentacles as well as retractor muscles. The phenotypes associated with NvFoxL-like are interesting mainly because of the lack of expression outside of the tentacle buds. When NvFoxL-like is knocked down, some cells in the tentacle still develop actin dense structures, which are similar to those seen in the membrane ruffles following MRTF activation. One interpretation of this is that MRTF activity acts upstream of NvFoxL-like in the developing tentacles, while NvFoxL-like activity functions in establishing multicellular organization of the contractile structures. If this is the case, this would also result in limited integration between the tentacle muscles and the retractor muscles around the pharynx. These muscle types are involved in the rapid retraction of the body or tentacles, and likely exert opposing force on the pharynx region during development. This could serve a signal for heightened MRTF activity in these tissues.

Overall, it seems that the dependence on MRTF activity for the development of contractile tissues in *E. muelleri* is also seen in the development of muscles in *N.*

vectensis. Combining this with the highly similar structures and arrangement of the contractile bundles, it is likely that they are evolutionarily related tissues. Although the striated muscles found in cnidarians are likely independently derived, the ancestor of cnidarians and bilaterians likely had muscles, with a smooth ultrastructure, which have given rise to the variety of different forms seen in extant animals. Based on these findings, the common ancestor of sponges and cnidarians likely had a contractile tissue, involved in maintenance of body tension and movement, that was primarily patterned by MRTF activity and gave rise to the endopinacoderm in the demosponge lineage and muscles in the lineage that gave rise to cnidarians.

References

Achim, K., & Arendt, D. (2014). Structural evolution of cell types by step-wise assembly of cellular modules. *Current Opinion in Genetics & Development*, *27*, 102–108.

Adams, E. D. M., Goss, G. G., & Leys, S. P. (2010). Freshwater sponges have functional, sealing epithelia with high transepithelial resistance and negative transepithelial potential. *PloS One*, *5*(11), e15040.

Adamska, M. (2016). Sponges as the rosetta stone of colonial-to-multicellular transition. *Multicellularity. Origins and Evolution. Cambridge, Massachusetts*.

Adamska, M., Degnan, S. M., Green, K. M., Adamski, M., Craigie, A., Larroux, C., & Degnan, B. M. (2007). Wnt and TGF-beta expression in the sponge Amphimedon queenslandica and the origin of metazoan embryonic patterning. *PloS One*, *2*(10), e1031.

Adamska, M., Larroux, C., Adamski, M., Green, K., Lovas, E., Koop, D., Richards, G. S., Zwafink, C., & Degnan, B. M. (2010). Structure and expression of conserved Wnt pathway components in the demosponge Amphimedon queenslandica. *Evolution & Development*, *12*(5), 494–518.

Adrian, R. H. (1956). The effect of internal and external potassium concentration on the membrane potential of frog muscle. *The Journal of Physiology*, *133*(3), 631–658.

Agarwal, P., & Zaidel-Bar, R. (2019). Diverse roles of non-muscle myosin II contractility in 3D cell migration. *Essays in Biochemistry*, *63*(5), 497–508.

Alamo, L., Li, X. E., Espinoza-Fonseca, L. M., Pinto, A., Thomas, D. D., Lehman, W., & Padrón, R. (2015). Tarantula myosin free head regulatory light chain phosphorylation stiffens N-terminal extension, releasing it and blocking its docking back. *Molecular bioSystems*, *11*(8), 2180–2189.

Alegado, R. A., & King, N. (2014). Bacterial influences on animal origins. *Cold Spring Harbor Perspectives in Biology*, *6*(11), a016162.

Alexander, B. E., Liebrand, K., Osinga, R., van der Geest, H. G., Admiraal, W., Cleutjens, J. P. M., Schutte, B., Verheyen, F., Ribes, M., van Loon, E., & de Goeij, J. M. (2014). Cell turnover and detritus production in marine sponges from tropical and temperate benthic ecosystems. *PloS One*, *9*(10), e109486.

Alié, A., Hayashi, T., Sugimura, I., Manuel, M., Sugano, W., Mano, A., Satoh, N., Agata, K., & Funayama, N. (2015). The ancestral gene repertoire of animal stem cells. In *Proceedings of the National Academy of Sciences* (Vol. 112, Issue 51, pp. E7093–E7100). https://doi.org/10.1073/pnas.1514789112

Altshuler, I., Vaillant, J. J., Xu, S., & Cristescu, M. E. (2012). The Evolutionary History of Sarco(endo)plasmic Calcium ATPase (SERCA). In *PLoS ONE* (Vol. 7, Issue 12, p. e52617). https://doi.org/10.1371/journal.pone.0052617

Amano, M., Nakayama, M., & Kaibuchi, K. (2010). Rho-kinase/ROCK: A key regulator of the cytoskeleton and cell polarity. *Cytoskeleton*, *67*(9), 545–554.

Anvarian, Z., Mykytyn, K., Mukhopadhyay, S., Pedersen, L. B., & Christensen, S. T. (2019). Cellular signalling by primary cilia in development, organ function and disease. *Nature Reviews. Nephrology*, *15*(4), 199–219.

Aoki, R., Shoshkes-Carmel, M., Gao, N., Shin, S., May, C. L., Golson, M. L., Zahm, A. M., Ray, M., Wiser, C. L., Wright, C. V. E., & Kaestner, K. H. (2016). Foxl1-expressing mesenchymal cells constitute the intestinal stem cell niche. *Cellular and Molecular Gastroenterology and Hepatology*, *2*(2), 175–188.

Arendt, D., Musser, J. M., Baker, C. V. H., Bergman, A., Cepko, C., Erwin, D. H., Pavlicev, M., Schlosser, G., Widder, S., Laubichler, M. D., & Wagner, G. P. (2016). The origin and evolution of cell types. In *Nature Reviews Genetics* (Vol. 17, Issue 12, pp. 744–757). https://doi.org/10.1038/nrg.2016.127

Armon, S., & Prakash, M. (2018). Ultra Fast Contractions and Emergent Dynamics in a Living Active Solid-The Epithelium of the Primitive Animal Trichoplax adhaerens. *Biophysical Journal*, *114*(3), 649a.

Asadzadeh, S. S., Larsen, P. S., Riisgård, H. U., & Walther, J. H. (2019). Hydrodynamics of the leucon sponge pump. *Journal of the Royal Society, Interface / the Royal Society*, *16*(150), 20180630.

Assinder, S. J., Stanton, J.-A. L., & Prasad, P. D. (2009). Transgelin: an actin-binding protein and tumour suppressor. *The International Journal of Biochemistry & Cell Biology*, *41*(3), 482–486.

Ayme-Southgate, A., Lasko, P., French, C., & Pardue, M. L. (1989). Characterization of the gene for mp20: a Drosophila muscle protein that is not found in asynchronous oscillatory flight muscle. *The Journal of Cell Biology*, *108*(2), 521–531.

Babonis, L. S., & Martindale, M. Q. (2017). PaxA, but not PaxC, is required for cnidocyte development in the sea anemone Nematostella vectensis. *EvoDevo*, *8*, 14.

Baeyens, N., & Schwartz, M. A. (2016). Biomechanics of vascular mechanosensation and remodeling. *Molecular Biology of the Cell*, *27*(1), 7–11.

Bagby, R. M. (1966). The fine structure of myocytes in the sponges microciona prolifera (Ellis and Solander) and tedania ignis (Duchassaing and Michelotti). *Journal of Morphology*, *118*(2), 167–181.

Barbeau, M. A., Reiswig, H. M., & Rath, L. C. (1989). Hatching of freshwater sponge gemmules after low temperature exposure: Ephydatia mülleri (Porifera: Spongillidae). *Journal of Thermal Biology*, *14*(4), 225–231.

Barton, S. H., & Addis, J. S. (1997). FRESHWATER SPONGES (PORIFERA: SPONGILLIDAE) OF WESTERN MONTANA. *The Great Basin Naturalist*, *57*(2), 93–103.

Basten, S. G., & Giles, R. H. (2013). Functional aspects of primary cilia in signaling, cell cycle and tumorigenesis. *Cilia*, *2*(1), 6.

Bays, J. L., & DeMali, K. A. (2017). Vinculin in cell–cell and cell–matrix adhesions. *Cellular and Molecular Life Sciences: CMLS*, *74*(16), 2999–3009.

Becerro, M. A. (2012). *Advances in sponge science: physiology, chemical and microbial diversity, biotechnology*. Elsevier/Academic Press.

Bedell, V. M., Westcot, S. E., & Ekker, S. C. (2011). Lessons from morpholino-based screening in zebrafish. *Briefings in Functional Genomics*, *10*(4), 181–188.

Bement, W. M., Mandato, C. A., & Kirsch, M. N. (1999). Wound-induced assembly and closure of an actomyosin purse string in Xenopus oocytes. In *Current Biology* (Vol. 9, Issue 11, pp. 579–587). https://doi.org/10.1016/s0960-9822(99)80261-9

Bhakdi, S., Tranum-Jensen, J., & Sziegoleit, A. (1985). Mechanism of membrane damage by streptolysin-O. *Infection and Immunity*, *47*(1), 52–60.

Bi, S., Yue, S., & Zhang, S. (2017). Hybridization chain reaction: a versatile molecular tool for biosensing, bioimaging, and biomedicine. *Chemical Society Reviews*, *46*(14), 4281–4298.

Bialik, J. F., Ding, M., Speight, P., Dan, Q., Miranda, M. Z., Di Ciano-Oliveira, C., Kofler, M. M., Rotstein, O. D., Pedersen, S. F., Szászi, K., & Kapus, A. (2019). Profibrotic epithelial phenotype: a central role for MRTF and TAZ. In *Scientific Reports* (Vol. 9, Issue 1). https://doi.org/10.1038/s41598-019-40764-7

Bill, B. R., Petzold, A. M., Clark, K. J., Schimmenti, L. A., & Ekker, S. C. (2009). A Primer for Morpholino Use in Zebrafish. *Zebrafish*, *6*(1), 69–77.

Bond, C. (2013). Locomotion and contraction in an asconoid calcareous sponge. *Invertebrate Biology: A Quarterly Journal of the American Microscopical Society and the Division of Invertebrate Zoology/ASZ*, *132*(4), 283–290.

Boute, N., Exposito, J. Y., Boury-Esnault, N., Vacelet, J., Noro, N., Miyazaki, K., Yoshizato, K., & Garrone, R. (1996). Type IV collagen in sponges, the missing link in basement membrane ubiquity. *Biology of the Cell / under the Auspices of the European Cell Biology Organization*, *88*(1-2), 37–44.

Brunet, T., & Arendt, D. (2016). From damage response to action potentials: early evolution of neural and contractile modules in stem eukaryotes. *Philosophical Transactions of the Royal Society of London. Series B, Biological Sciences*, *371*(1685), 20150043.

Brunet, T., Fischer, A. H. L., Steinmetz, P. R. H., Lauri, A., Bertucci, P., & Arendt, D. (2016). The evolutionary origin of bilaterian smooth and striated myocytes. In *eLife* (Vol. 5). https://doi.org/10.7554/elife.19607

Brunet, T., & King, N. (2017). The Origin of Animal Multicellularity and Cell Differentiation. *Developmental Cell*, *43*(2), 124–140.

Brunet, T., Larson, B. T., Linden, T. A., Vermeij, M. J. A., McDonald, K., & King, N. (2019). Light-regulated collective contractility in a multicellular choanoflagellate. *Science*, *366*(6463), 326–334.

Burger, G., Forget, L., Zhu, Y., Gray, M. W., & Lang, B. F. (2003). Unique mitochondrial genome architecture in unicellular relatives of animals. *Proceedings of the National Academy of Sciences of the United States of America*, *100*(3), 892–897.

Burridge, K., & Guilluy, C. (2016). Focal adhesions, stress fibers and mechanical tension. *Experimental Cell Research*, *343*(1), 14–20.

Butler, M. B., Short, N. E., Maniou, E., Alexandre, P., Greene, N. D. E., Copp, A. J., & Galea, G. L. (2019). Rho kinase-dependent apical constriction counteracts M-phase apical expansion to enable mouse neural tube closure. *Journal of Cell Science*, *132*(13). https://doi.org/10.1242/jcs.230300

Butler, T. M., Mooers, S. U., Li, C., Narayan, S., & Siegman, M. J. (1998). Regulation of catch muscle by twitchin phosphorylation: effects on force, ATPase, and shortening. *Biophysical Journal*, *75*(4), 1904–1914.

Camoretti-Mercado, B., Forsythe, S. M., LeBeau, M. M., Espinosa, R., 3rd, Vieira, J. E., Halayko, A. J., Willadsen, S., Kurtz, B., Ober, C., Evans, G. A., Thweatt, R., Shapiro, S., Niu, Q., Qin, Y., Padrid, P. A., & Solway, J. (1998). Expression and cytogenetic localization of the human SM22 gene (TAGLN). *Genomics*, *49*(3), 452–457.

Carroll, S. B. (2008). Evo-devo and an expanding evolutionary synthesis: a genetic theory of morphological evolution. *Cell*, *134*(1), 25–36.

Casola, C. (2018). From de novo to “de nono”: The majority of novel protein coding genes identified with phylostratigraphy are old genes or recent duplicates. In *Genome Biology and Evolution*. https://doi.org/10.1093/gbe/evy231

Cenik, B. K., Liu, N., Chen, B., Bezprozvannaya, S., Olson, E. N., & Bassel-Duby, R. (2016). Myocardin-related transcription factors are required for skeletal muscle development. *Development*, *143*(15), 2853–2861.

Chandrasekaran, A., Upadhyaya, A., & Papoian, G. A. (2019). Remarkable structural transformations of actin bundles are driven by their initial polarity, motor activity, crosslinking, and filament treadmilling. *PLoS Computational Biology*, *15*(7), e1007156.

Chen, C., Tao, T., Wen, C., He, W.-Q., Qiao, Y.-N., Gao, Y.-Q., Chen, X., Wang, P., Chen, C.-P., Zhao, W., Chen, H.-Q., Ye, A.-P., Peng, Y.-J., & Zhu, M.-S. (2014). Myosin light chain kinase (MLCK) regulates cell migration in a myosin regulatory light chain phosphorylation-independent mechanism. *The Journal of Biological Chemistry*, *289*(41), 28478–28488.

Chen, R., Amoui, M., Zhang, Z., & Mardon, G. (1997). Dachshund and eyes absent proteins form a complex and function synergistically to induce ectopic eye development in Drosophila. *Cell*, *91*(7), 893–903.

Chen, X., Gays, D., Milia, C., & Santoro, M. M. (2017). Cilia Control Vascular Mural Cell Recruitment in Vertebrates. *Cell Reports*, *18*(4), 1033–1047.

Cheng, X., Wang, X., Wan, Y., Zhou, Q., Zhu, H., & Wang, Y. (2015). Myosin light chain kinase inhibitor ML7 improves vascular endothelial dysfunction via tight junction regulation in a rabbit model of atherosclerosis. *Molecular Medicine Reports*, *12*(3), 4109–4116.

Chi, Q., Yin, T., Gregersen, H., Deng, X., Fan, Y., Zhao, J., Liao, D., & Wang, G. (2014). Rear actomyosin contractility-driven directional cell migration in three-dimensional matrices: a mechano-chemical coupling mechanism. *Journal of the Royal Society, Interface / the Royal Society*, *11*(95), 20131072.

Choi, H. M. T., Schwarzkopf, M., Fornace, M. E., Acharya, A., Artavanis, G., Stegmaier, J., Cunha, A., & Pierce, N. A. (2018). Third-generation in situ hybridization chain reaction: multiplexed, quantitative, sensitive, versatile, robust. *Development*, *145*(12). https://doi.org/10.1242/dev.165753

Chu, J., Pham, N. T., Olate, N., Kislitsyna, K., Day, M.-C., LeTourneau, P. A., Kots, A., Stewart, R. H., Laine, G. A., Cox, C. S., Jr, & Uray, K. (2013). Biphasic regulation of myosin light chain phosphorylation by p21-activated kinase modulates intestinal smooth muscle contractility. *The Journal of Biological Chemistry*, *288*(2), 1200–1213.

Ciaccio, N. A., & Laurence, J. S. (2009). Effects of Disulfide Bond Formation and Protein Helicity on the Aggregation of Activating Transcription Factor 5. In *Molecular Pharmaceutics* (Vol. 6, Issue 4, pp. 1205–1215). https://doi.org/10.1021/mp900058t

Clark, H. J. (1866). Conclusive proofs of the animality of the ciliate sponges, and of their affinities with the Infusoria flagellata. In *American Journal of Science* (Vols. s2–s42, Issue 126, pp. 320–324). https://doi.org/10.2475/ajs.s2-42.126.320

Clevers, H., & Nusse, R. (2012). Wnt/β-catenin signaling and disease. *Cell*, *149*(6), 1192–1205.

Closs, E. I., Simon, A., Vékony, N., & Rotmann, A. (2004). Plasma membrane transporters for arginine. *The Journal of Nutrition*, *134*(10 Suppl), 2752S – 2759S; discussion 2765S – 2767S.

Conkling, M., Hesp, K., Munroe, S., Sandoval, K., Martens, D. E., Sipkema, D., Wijffels, R. H., & Pomponi, S. A. (2019). Breakthrough in Marine Invertebrate Cell Culture: Sponge Cells Divide Rapidly in Improved Nutrient Medium. *Scientific Reports*, *9*(1), 17321.

Coronado, R., Morrissette, J., Sukhareva, M., & Vaughan, D. M. (1994). Structure and function of ryanodine receptors. *The American Journal of Physiology*, *266*(6 Pt 1), C1485–C1504.

Colgren J., & Nichols, SA. (2019). The significance of sponges for comparative studies of developmental evolution. *WIREs Dev Bio. 2020*(9), e359.

Creemers, E. E., Sutherland, L. B., Oh, J., Barbosa, A. C., & Olson, E. N. (2006). Coactivation of MEF2 by the SAP domain proteins myocardin and MASTR. *Molecular Cell*, *23*(1), 83–96.

d'Albis, A., Anger, M., & Lompré, A. M. (1993). Rabbit masseter expresses the cardiac alpha myosin heavy chain gene. Evidence from mRNA sequence analysis. *FEBS Letters*, *324*(2), 178–180.

Dasgupta, A., & Amack, J. D. (2016). Cilia in vertebrate left–right patterning. *Philosophical Transactions of the Royal Society of London. Series B, Biological Sciences*, *371*(1710), 20150410.

Dayraud, C., Alié, A., Jager, M., Chang, P., Le Guyader, H., Manuel, M., & Quéinnec, E. (2012). Independent specialisation of myosin II paralogues in muscle vs. non-muscle functions during early animal evolution: a ctenophore perspective. *BMC Evolutionary Biology*, *12*, 107.

de Ceccatty, M. P. (1974). Coordination in Sponges. The Foundations of Integration. *Integrative and Comparative Biology*, *14*(3), 895–903.

De Goeij, J. M., De Kluijver, A., Van Duyl, F. C., Vacelet, J., Wijffels, R. H., De Goeij, A. F. P. M., Cleutjens, J. P. M., & Schutte, B. (2009). Cell kinetics of the marine sponge Halisarca caerulea reveal rapid cell turnover and shedding. *The Journal of Experimental Biology*, *212*(Pt 23), 3892–3900.

De Sutter, D., & Van de Vyver, G. (1977). Aggregative properties of different cell types of the fresh-water spongeEphydatia fluviatilis isolated on ficoll gradients. *Wilhelm Roux's Archives of Developmental Biology*, *181*(2), 151–161.

DeAguero, A. A., Castillo, L., Oas, S. T., Kiani, K., Bryantsev, A. L., & Cripps, R. M. (2019). Regulation of fiber-specific actin expression by the Drosophila SRF ortholog Blistered. *Development*, *146*(7). https://doi.org/10.1242/dev.164129

Dobrokhotov, O., Samsonov, M., Sokabe, M., & Hirata, H. (2018). Mechanoregulation and pathology of YAP/TAZ via Hippo and non-Hippo mechanisms. In *Clinical and Translational Medicine* (Vol. 7, Issue 1). https://doi.org/10.1186/s40169-018-0202-9

DuBuc, T. Q., Bobkov, Y., Ryan, J., & Martindale, M. Q. (2018). The radial expression of dorsal-ventral patterning genes in placozoans, Trichoplax adhaerens, argues for an oral-aboral axis. In *bioRxiv* (p. 345777). https://doi.org/10.1101/345777

DuBuc, T. Q., Dattoli, A. A., Babonis, L. S., Salinas-Saavedra, M., Röttinger, E., Martindale, M. Q., & Postma, M. (2014). In vivo imaging of Nematostella vectensis embryogenesis and late development using fluorescent probes. *BMC Cell Biology*, *15*, 44.

DuBuc, T. Q., Traylor-Knowles, N., & Martindale, M. Q. (2014). Initiating a regenerative response; cellular and molecular features of wound healing in the cnidarian Nematostella vectensis. *BMC Biology*, *12*, 24.

Dunham, P., Anderson, C., Rich, A. M., & Weissmann, G. (1983). Stimulus-response coupling in sponge cell aggregation: Evidence for calcium as an intracellular messenger. *Proceedings of the National Academy of Sciences of the United States of America*, *80*(15), 4756–4760.

Dunn, C. W., Leys, S. P., & Haddock, S. H. D. (2015). The hidden biology of sponges and ctenophores. *Trends in Ecology & Evolution*, *30*(5), 282–291.

Dvorakova, M., Nenutil, R., & Bouchal, P. (2014). Transgelins, cytoskeletal proteins implicated in different aspects of cancer development. *Expert Review of Proteomics*, *11*(2), 149–165.

Edgar, R. C. (2004). MUSCLE: a multiple sequence alignment method with reduced time and space complexity. *BMC Bioinformatics*, *5*, 113.

Elhaik, E., Sabath, N., & Graur, D. (2006). The "Inverse Relationship Between Evolutionary Rate and Age of Mammalian Genes" Is an Artifact of Increased Genetic Distance with Rate of Evolution and Time of Divergence. In *Molecular Biology and Evolution* (Vol. 23, Issue 1, pp. 1–3). https://doi.org/10.1093/molbev/msj006

Elliott, G. R. D., & Leys, S. P. (2007). Coordinated contractions effectively expel water from the aquiferous system of a freshwater sponge. *The Journal of Experimental Biology*, *210*(Pt 21), 3736–3748.

Elliott, G. R. D., & Leys, S. P. (2010). Evidence for glutamate, GABA and NO in coordinating behaviour in the sponge, Ephydatia muelleri (Demospongiae, Spongillidae). *The Journal of Experimental Biology*, *213*(Pt 13), 2310–2321.

Ellwanger, K., Eich, A., & Nickel, M. (2007). GABA and glutamate specifically induce contractions in the sponge Tethya wilhelma. *Journal of Comparative Physiology. A, Neuroethology, Sensory, Neural, and Behavioral Physiology*, *193*(1), 1–11.

Eric, M., & Olson, E. N. (2018). Modulation of MRTF-A activity in pathologic fibrosis and wound healing. In *US Patent 9,937,156*. https://patents.google.com/patent/US9937156B2/en

Esnault, C., Stewart, A., Gualdrini, F., East, P., Horswell, S., Matthews, N., & Treisman, R. (2014). Rho-actin signaling to the MRTF coactivators dominates the immediate transcriptional response to serum in fibroblasts. *Genes & Development*, *28*(9), 943–958.

Ezratty, E. J., Stokes, N., Chai, S., Shah, A. S., Williams, S. E., & Fuchs, E. (2011). A role for the primary cilium in Notch signaling and epidermal differentiation during skin development. *Cell*, *145*(7), 1129–1141.

Fahey, B., & Degnan, B. M. (2010). Origin of animal epithelia: insights from the sponge genome. *Evolution & Development*, *12*(6), 601–617.

Farah, C. S., & Reinach, F. C. (1995). The troponin complex and regulation of muscle contraction. *FASEB Journal: Official Publication of the Federation of American Societies for Experimental Biology*, *9*(9), 755–767.

Farman, G. P., Tachampa, K., Mateja, R., Cazorla, O., Lacampagne, A., & de Tombe, P. P. (2008). Blebbistatin: use as inhibitor of muscle contraction. *Pflugers Archiv: European Journal of Physiology*, *455*(6), 995–1005.

Fearing, B. V., Jing, L., Barcellona, M. N., Witte, S. E., Buchowski, J. M., Zebala, L. P., Kelly, M. P., Luhmann, S., Gupta, M. C., Pathak, A., & Setton, L. A. (2019). Mechanosensitive transcriptional coactivators MRTF-A and YAP/TAZ regulate nucleus pulposus cell phenotype through cell shape. *FASEB Journal: Official Publication of the Federation of American Societies for Experimental Biology*, *33*(12), 14022–14035.

Felsenthal, N., & Zelzer, E. (2017). Mechanical regulation of musculoskeletal system development. *Development*, *144*(23), 4271–4283.

Feuda, R., Dohrmann, M., Pett, W., Philippe, H., Rota-Stabelli, O., Lartillot, N., Wörheide, G., & Pisani, D. (2017). Improved Modeling of Compositional Heterogeneity Supports Sponges as Sister to All Other Animals. In *Current Biology* (Vol. 27, Issue 24, pp. 3864–3870.e4). https://doi.org/10.1016/j.cub.2017.11.008

Fidler, A. L., Darris, C. E., Chetyrkin, S. V., Pedchenko, V. K., Boudko, S. P., Brown, K. L., Gray Jerome, W., Hudson, J. K., Rokas, A., & Hudson, B. G. (2017). Collagen IV and basement membrane at the evolutionary dawn of metazoan tissues. *eLife*, *6*. https://doi.org/10.7554/eLife.24176

Finch-Edmondson, M., & Sudol, M. (2016). Framework to function: mechanosensitive regulators of gene transcription. *Cellular & Molecular Biology Letters*, *21*, 28.

Fortunato, A., & Aktipis, A. (2019). Social feeding behavior of Trichoplax adhaerens. *Frontiers in Ecology and Evolution*, *7*. https://doi.org/10.3389/fevo.2019.00019

Foster, C. J., Johnston, S. A., Sunday, B., & Gaeta, F. C. (1990). Potent peptide inhibitors of smooth muscle myosin light chain kinase: mapping of the pseudosubstrate and calmodulin binding domains. *Archives of Biochemistry and Biophysics*, *280*(2), 397–404.

Fritz, A. E., Ikmi, A., Seidel, C., Paulson, A., & Gibson, M. C. (2013). Mechanisms of tentacle morphogenesis in the sea anemone Nematostella vectensis. *Development*, *140*(10), 2212–2223.

Fromont, J. (1999). Reproduction of some demosponges in a temperate Australian shallow water habitat. *MEMOIRS-QUEENSLAND MUSEUM*, *44*, 185–192.

Funayama, N. (2010). The stem cell system in demosponges: insights into the origin of somatic stem cells. *Development, Growth & Differentiation*, *52*(1), 1–14.

Funayama, N., Nakatsukasa, M., Hayashi, T., & Agata, K. (2005). Isolation of the choanocyte in the fresh water sponge, Ephydatia fluviatilis and its lineage marker, Ef annexin. *Development, Growth & Differentiation*, *47*(4), 243–253.

Funayama, N., Nakatsukasa, M., Kuraku, S., Takechi, K., Dohi, M., Iwabe, N., Miyata, T., & Agata, K. (2005). Isolation of Ef silicatein and Ef lectin as molecular markers for sclerocytes and cells involved in innate immunity in the freshwater sponge Ephydatia fluviatilis. *Zoological Science*, *22*(10), 1113–1122.

Funayama, N., Nakatsukasa, M., Mohri, K., Masuda, Y., & Agata, K. (2010). Piwi expression in archeocytes and choanocytes in demosponges: insights into the stem cell system in demosponges. *Evolution & Development*, *12*(3), 275–287.

Gaino, E., & Burlando, B. (1990). Sponge cell motility: A model system for the study of morphogenetic processes. *Bollettino Di Zoologia*, *57*(2), 109–118.

Gaino, E., Burlando, B., Zunino, L., Pansini, M., & Buffa, P. (1984). Origin of male gametes from choanocytes in Spongia officinalis (Porifera, Demospongiae). *International Journal of Invertebrate Reproduction and Development*, *7*(2), 83–93.

Gaino, E., Magnino, G. (1999) Dissociated cells of the calcareous sponge *Clathrina*: a model for investigating cell adhesion and cell motility in vitro. *Microscopy Research & Technique. 44*(4), 279-292.

Gau, D., & Roy, P. (2018). SRF'ing and SAP'ing--the role of MRTF proteins in cell migration. *Journal of Cell Science*, *131*(19), jcs218222.

Gautel, M., & Djinović-Carugo, K. (2016). The sarcomeric cytoskeleton: from molecules to motion. *The Journal of Experimental Biology*, *219*(Pt 2), 135–145.

Genikhovich, G., & Technau, U. (2011). Complex functions of Mef2 splice variants in the differentiation of endoderm and of a neuronal cell type in a sea anemone. *Development*, *138*(22), 4911–4919.

George, R. M., & Firulli, A. B. (2019). Hand Factors in Cardiac Development. *Anatomical Record*, *302*(1), 101–107.

Gerthoffer, W. T., & Pohl, J. (1994). Caldesmon and calponin phosphorylation in regulation of smooth muscle contraction. *Canadian Journal of Physiology and Pharmacology*, *72*(11), 1410–1414.

Godefroy, N., Le Goff, E., Martinand-Mari, C., Belkhir, K., Vacelet, J., & Baghdiguian, S. (2019). Sponge digestive system diversity and evolution: filter feeding to carnivory. *Cell and Tissue Research*, *377*(3), 341–351.

Goetinck, S., & Waterston, R. H. (1994). The Caenorhabditis elegans muscle-affecting gene unc-87 encodes a novel thin filament-associated protein. *The Journal of Cell Biology*, *127*(1), 79–93.

Goetz, S. C., & Anderson, K. V. (2010). The primary cilium: a signalling centre during vertebrate development. *Nature Reviews. Genetics*, *11*(5), 331–344.

Gokhin, D. S., & Fowler, V. M. (2011). Tropomodulin capping of actin filaments in striated muscle development and physiology. *Journal of Biomedicine & Biotechnology*, *2011*, 103069.

Gold, D. A., Grabenstatter, J., de Mendoza, A., Riesgo, A., Ruiz-Trillo, I., & Summons, R. E. (2016). Sterol and genomic analyses validate the sponge biomarker hypothesis. *Proceedings of the National Academy of Sciences of the United States of America*, *113*(10), 2684–2689.

Golson, M. L., & Kaestner, K. H. (2016). Fox transcription factors: from development to disease. *Development*, *143*(24), 4558–4570.

Gordon, A. M. (1992). Regulation of muscle contraction: dual role of calcium and cross-bridges. In *Muscular Contraction* (pp. 163–180). https://doi.org/10.1017/cbo9780511574672.013

Gordon, A. M., Homsher, E., & Regnier, M. (2000). Regulation of contraction in striated muscle. *Physiological Reviews*, *80*(2), 853–924.

Grzelkowska-Kowalczyk, K. (2016). The importance of extracellular matrix in skeletal muscle development and function. *Composition and Function of the Extracellular Matrix in the Human Body*, 3–24.

Haak, A. J., Tsou, P.-S., Amin, M. A., Ruth, J. H., Campbell, P., Fox, D. A., Khanna, D., Larsen, S. D., & Neubig, R. R. (2014). Targeting the Myofibroblast Genetic Switch: Inhibitors of Myocardin-Related Transcription Factor/Serum Response Factor–Regulated Gene Transcription Prevent Fibrosis in a Murine Model of Skin Injury. In *Journal of Pharmacology and Experimental Therapeutics* (Vol. 349, Issue 3, pp. 480–486). https://doi.org/10.1124/jpet.114.213520

Hall, C., Rodriguez, M., Garcia, J., Posfai, D., DuMez, R., Wictor, E., Quintero, O. A., Hill, M. S., Rivera, A. S., & Hill, A. L. (2019). Secreted frizzled related protein is a target of PaxB and plays a role in aquiferous system development in the freshwater sponge, Ephydatia muelleri. *PloS One*, *14*(2), e0212005.

Hammel, J. U., & Nickel, M. (2014). A new flow-regulating cell type in the demosponge Tethya wilhelma--functional cellular anatomy of a leuconoid canal system. *PloS One*, *9*(11), e113153.

Han, Z., Li, X., Wu, J., & Olson, E. N. (2004). A myocardin-related transcription factor regulates activity of serum response factor in Drosophila. *Proceedings of the National Academy of Sciences of the United States of America*, *101*(34), 12567–12572.

Hannenhalli, S., & Kaestner, K. H. (2009). The evolution of Fox genes and their role in development and disease. *Nature Reviews. Genetics*, *10*(4), 233–240.

Harrison, J. F., Waters, J. S., Biddulph, T. A., Kovacevic, A., Jaco Klok, C., & Socha, J. J. (2018). Developmental plasticity and stability in the tracheal networks supplying Drosophila flight muscle in response to rearing oxygen level. In *Journal of Insect Physiology* (Vol. 106, pp. 189–198). https://doi.org/10.1016/j.jinsphys.2017.09.006

Hayashi, K. 'ichiro, Watanabe, B., Nakagawa, Y., Minami, S., & Morita, T. (2014). RPEL proteins are the molecular targets for CCG-1423, an inhibitor of Rho signaling. *PloS One*, *9*(2), e89016.

He, H., Du, F., He, Y., Wei, Z., Meng, C., Xu, Y., Zhou, H., Wang, N., Luo, X.-G., Ma, W., & Zhang, T.-C. (2018). The Wnt-β-catenin signaling regulated MRTF-A transcription to activate migration-related genes in human breast cancer cells. *Oncotarget*, *9*(20), 15239–15251.

Heanue, T. A., Reshef, R., Davis, R. J., Mardon, G., Oliver, G., Tomarev, S., Lassar, A. B., & Tabin, C. J. (1999). Synergistic regulation of vertebrate muscle development by Dach2, Eya2, and Six1, homologs of genes required for Drosophila eye formation. *Genes & Development*, *13*(24), 3231–3243.

Hilfer, S. R., & Searls, R. L. (1986). Cytoskeletal dynamics in animal morphogenesis. *Developmental Biology* , *2*, 3–29.

Hill, M. S., & Hill, A. L. (2002). Morphological plasticity in the tropical sponge Anthosigmella varians: responses to predators and wave energy. *The Biological Bulletin*, *202*(1), 86–95.

Himmel, D. M., Mui, S., O'Neall-Hennessey, E., Szent-Györgyi, A. G., & Cohen, C. (2009). The On–Off Switch in Regulated Myosins: Different Triggers but Related Mechanisms. *Journal of Molecular Biology*, *394*(3), 496–505.

Hinson, J. S., Medlin, M. D., Lockman, K., Taylor, J. M., & Mack, C. P. (2007). Smooth muscle cell-specific transcription is regulated by nuclear localization of the myocardin-related transcription factors. *American Journal of Physiology. Heart and Circulatory Physiology*, *292*(2), H1170–H1180.

Hoggatt, A. M., Kim, J.-R., Ustiyan, V., Ren, X., Kalin, T. V., Kalinichenko, V. V., & Herring, B. P. (2013). The transcription factor Foxf1 binds to serum response factor and myocardin to regulate gene transcription in visceral smooth muscle cells. *The Journal of Biological Chemistry*, *288*(40), 28477–28487.

Holzer, P., & Izzo, A. A. (2014). The pharmacology of TRP channels. *British Journal of Pharmacology*, *171*(10), 2469–2473.

Hong, F., Haldeman, B. D., Jackson, D., Carter, M., Baker, J. E., & Cremo, C. R. (2011). Biochemistry of smooth muscle myosin light chain kinase. *Archives of Biochemistry and Biophysics*, *510*(2), 135–146.

Hooper, S. L., Hobbs, K. H., & Thuma, J. B. (2008). Invertebrate muscles: thin and thick filament structure; molecular basis of contraction and its regulation, catch and asynchronous muscle. *Progress in Neurobiology*, *86*(2), 72–127.

Hooper, S. L., & Thuma, J. B. (2005). Invertebrate muscles: muscle specific genes and proteins. *Physiological Reviews*, *85*(3), 1001–1060.

Hu, S., Dasbiswas, K., Guo, Z., Tee, Y.-H., Thiagarajan, V., Hersen, P., Chew, T.-L., Safran, S. A., Zaidel-Bar, R., & Bershadsky, A. D. (2017). Long-range self-organization of cytoskeletal myosin II filament stacks. In *Nature Cell Biology* (Vol. 19, Issue 2, pp. 133–141). https://doi.org/10.1038/ncb3466

Ideses, Y., Bernheim, A., Sonn, A., & Roichman, Y. (2014). Myosin II Does it All: Assembly, Remodeling, and Disassembly of Actin Networks are Governed by Myosin II Activity. In *Biophysical Journal* (Vol. 106, Issue 2, p. 568a). https://doi.org/10.1016/j.bpj.2013.11.3150

Ikmi, A., McKinney, S. A., Delventhal, K. M., & Gibson, M. C. (2014). TALEN and CRISPR/Cas9-mediated genome editing in the early-branching metazoan Nematostella vectensis. *Nature Communications*, *5*, 5486.

Imsiecke, G. (1993). Ingestion, digestion, and egestion in Spongilla lacustris (Porifera, Spongillidae) after pulse feeding with Chlamydomonas reinhardtii (Volvocales). *Zoomorphology*, *113*(4), 233–244.

Jahnel, S. M., Walzl, M., & Technau, U. (2014). Development and epithelial organisation of muscle cells in the sea anemone Nematostella vectensis. *Frontiers in Zoology*, *11*, 44.

Jeffery, N. W., Jardine, C. B., & Gregory, T. R. (2013). A first exploration of genome size diversity in sponges. *Genome / National Research Council Canada = Genome / Conseil National de Recherches Canada*, *56*(8), 451–456.

Johnson, J. D., Holroyde, M. J., Crouch, T. H., Solaro, R. J., & Potter, J. D. (1981). Fluorescence studies of the interaction of calmodulin with myosin light chain kinase. *The Journal of Biological Chemistry*, *256*(23), 12194–12198.

Jordan, E. T., Collins, M., Terefe, J., Ugozzoli, L., & Rubio, T. (2008). Optimizing electroporation conditions in primary and other difficult-to-transfect cells. *Journal of Biomolecular Techniques: JBT*, *19*(5), 328–334.

Jung, H. S., Komatsu, S., Ikebe, M., & Craig, R. (2008a). Head–Head and Head–Tail Interaction: A General Mechanism for Switching Off Myosin II Activity in Cells. *Molecular Biology of the Cell*, *19*(8), 3234–3242.

Jung, H. S., Komatsu, S., Ikebe, M., & Craig, R. (2008b). Head–Head and Head–Tail Interaction: A General Mechanism for Switching Off Myosin II Activity in Cells. *Molecular Biology of the Cell*, *19*(8), 3234–3242.

Kaandorp, J. A. (1991). Modelling growth forms of the spongeHaliclona oculata (Porifera, Demospongiae) using fractal techniques. *Marine Biology*, *110*(2), 203–215.

Kaneko-Kawano, T., Takasu, F., Naoki, H., Sakumura, Y., Ishii, S., Ueba, T., Eiyama, A., Okada, A., Kawano, Y., & Suzuki, K. (2012). Dynamic regulation of myosin light chain phosphorylation by Rho-kinase. *PloS One*, *7*(6), e39269.

Karabulut, A., He, S., Chen, C.-Y., McKinney, S. A., & Gibson, M. C. (2019). Electroporation of short hairpin RNAs for rapid and efficient gene knockdown in the starlet sea anemone, Nematostella vectensis. *Developmental Biology*, *448*(1), 7–15.

Kayal, E., Bentlage, B., Sabrina Pankey, M., Ohdera, A. H., Medina, M., Plachetzki, D. C., Collins, A. G., & Ryan, J. F. (2018). Phylogenomics provides a robust topology of the major cnidarian lineages and insights on the origins of key organismal traits. *BMC Evolutionary Biology*, *18*(1), 68.

Kelley, L. A., Mezulis, S., Yates, C. M., Wass, M. N., & Sternberg, M. J. E. (2015). The Phyre2 web portal for protein modeling, prediction and analysis. *Nature Protocols*, *10*(6), 845–858.

Kenny, N. J., Francis, W. R., Rivera-Vicéns, R. E., Juravel, K., de Mendoza, A., Díez-Vives, C., Lister, R., Bezares-Calderon, L., Grombacher, L., Roller, M., Barlow, L. D., Camilli, S., Ryan, J. F., Wörheide, G., Hill, A. L., Riesgo, A., & Leys, S. P. (n.d.). *The genomic basis of animal origins: a chromosomal perspective from the sponge Ephydatia muelleri*. https://doi.org/10.1101/2020.02.18.954784

Keyel, P. A., Loultcheva, L., Roth, R., Salter, R. D., Watkins, S. C., Yokoyama, W. M., & Heuser, J. E. (2011). Streptolysin O clearance through sequestration into blebs that bud passively from the plasma membrane. *Journal of Cell Science*, *124*(Pt 14), 2414–2423.

Kiernan, J. A., & Wessendorf, M. (2001). Autofluorescence: Causes and cures. *Toronto Western Research Institute,[DirectLink]*.

King, N., Jody Westbrook, M., Young, S. L., Kuo, A., Abedin, M., Chapman, J., Fairclough, S., Hellsten, U., Isogai, Y., Letunic, I., Marr, M., Pincus, D., Putnam, N., Rokas, A., Wright, K. J., Zuzow, R., Dirks, W., Good, M., Goodstein, D., … Rokhsar, D. (2008). The genome of the choanoflagellate Monosiga brevicollis and the origin of metazoans. In *Nature* (Vol. 451, Issue 7180, pp. 783–788). https://doi.org/10.1038/nature06617

King, N., & Rokas, A. (2017). Embracing Uncertainty in Reconstructing Early Animal Evolution. *Current Biology: CB*, *27*(19), R1081–R1088.

Kiosses, W. B., Daniels, R. H., Otey, C., Bokoch, G. M., & Schwartz, M. A. (1999). A role for p21-activated kinase in endothelial cell migration. *The Journal of Cell Biology*, *147*(4), 831–844.

Kirfel, G., & Stockem, W. (1997). Detection and cytoplasmic localization of two different microtubule motor proteins in basal epithelial cells of freshwater sponges. *Protoplasma*, *196*(3), 167–180.

Ko, H. W. (2012). The primary cilium as a multiple cellular signaling scaffold in development and disease. *BMB Reports*, *45*(8), 427–432.

Kobayashi, T., Jin, L., & de Tombe, P. P. (2008). Cardiac thin filament regulation. *Pflugers Archiv: European Journal of Physiology*, *457*(1), 37–46.

Kollmar, M., & Mühlhausen, S. (2017). Myosin repertoire expansion coincides with eukaryotic diversification in the Mesoproterozoic era. *BMC Evolutionary Biology*, *17*(1), 211.

Kotsis, F., Boehlke, C., & Kuehn, E. W. (2013). The ciliary flow sensor and polycystic kidney disease. *Nephrology, Dialysis, Transplantation: Official Publication of the European Dialysis and Transplant Association - European Renal Association*, *28*(3), 518–526.

Kumar, S., Stecher, G., & Tamura, K. (2016). MEGA7: Molecular Evolutionary Genetics Analysis Version 7.0 for Bigger Datasets. *Molecular Biology and Evolution*, *33*(7), 1870–1874.

Kuo, I. Y., & Ehrlich, B. E. (2015). Signaling in muscle contraction. *Cold Spring Harbor Perspectives in Biology*, *7*(2), a006023.

Kusserow, A., Pang, K., Sturm, C., Hrouda, M., Lentfer, J., Schmidt, H. A., Technau, U., von Haeseler, A., Hobmayer, B., Martindale, M. Q., & Holstein, T. W. (2005). Unexpected complexity of the Wnt gene family in a sea anemone. *Nature*, *433*(7022), 156–160.

Lambers, E., Arnone, B., Fatima, A., Qin, G., Wasserstrom, J. A., & Kume, T. (2016). Foxc1 Regulates Early Cardiomyogenesis and Functional Properties of Embryonic Stem Cell Derived Cardiomyocytes. *Stem Cells*, *34*(6), 1487–1500.

Larsen, M., Wei, C., & Yamada, K. M. (2006). Cell and fibronectin dynamics during branching morphogenesis. *Journal of Cell Science*, *119*(Pt 16), 3376–3384.

Laundon, D., Larson, B. T., McDonald, K., King, N., & Burkhardt, P. (2019). The architecture of cell differentiation in choanoflagellates and sponge choanocytes. *PLoS Biology*, *17*(4), e3000226.

Lavrov, A. I., & Kosevich, I. A. (2014). Sponge cell reaggregation: Mechanisms and dynamics of the process. *Russian Journal of Developmental Biology*, *45*(4), 205–223.

Lavrov, A. I., & Kosevich, I. A. (2016). Sponge cell reaggregation: Cellular structure and morphogenetic potencies of multicellular aggregates. *Journal of Experimental Zoology. Part A, Ecological Genetics and Physiology*, *325*(2), 158–177.

Layden, M. J., Rentzsch, F., & Röttinger, E. (2016). The rise of the starlet sea anemone Nematostella vectensis as a model system to investigate development and regeneration. *Wiley Interdisciplinary Reviews. Developmental Biology*, *5*(4), 408–428.

Layden, M. J., Röttinger, E., Wolenski, F. S., Gilmore, T. D., & Martindale, M. Q. (2013). Microinjection of mRNA or morpholinos for reverse genetic analysis in the starlet sea anemone, Nematostella vectensis. *Nature Protocols*, *8*(5), 924–934.

Leclère, L., Horin, C., Chevalier, S., Lapébie, P., Dru, P., Peron, S., Jager, M., Condamine, T., Pottin, K., Romano, S., Steger, J., Sinigaglia, C., Barreau, C., Quiroga Artigas, G., Ruggiero, A., Fourrage, C., Kraus, J. E. M., Poulain, J., Aury, J.-M., … Copley, R. R. (2019). The genome of the jellyfish Clytia hemisphaerica and the evolution of the cnidarian life-cycle. *Nature Ecology & Evolution*, *3*(5), 801–810.

Leclère, L., & Röttinger, E. (2016). Diversity of Cnidarian Muscles: Function, Anatomy, Development and Regeneration. *Frontiers in Cell and Developmental Biology*, *4*, 157.

Lee, K. H., Sulbarán, G., Yang, S., Mun, J. Y., Alamo, L., Pinto, A., Sato, O., Ikebe, M., Liu, X., Korn, E. D., Sarsoza, F., Bernstein, S. I., Padrón, R., & Craig, R. (2018). Interacting-heads motif has been conserved as a mechanism of myosin II inhibition since before the origin of animals. *Proceedings of the National Academy of Sciences of the United States of America*, *115*(9), E1991–E2000.

Lee, K., Yang, S., Liu, X., Korn, E. D., Sarsoza, F., Bernstein, S. I., Pollard, L., Lord, M. J., Trybus, K. M., & Craig, R. (2016). Myosin II head interaction in primitive species. *Biophysical Journal*, *110*(3), 615a.

Lees-Miller, J. P., Heeley, D. H., & Smillie, L. B. (1987). An abundant and novel protein of 22 kDa (SM22) is widely distributed in smooth muscles. Purification from bovine aorta. *Biochemical Journal*, *244*(3), 705–709.

Leininger, S., Adamski, M., Bergum, B., Guder, C., Liu, J., Laplante, M., Bråte, J., Hoffmann, F., Fortunato, S., Jordal, S., Rapp, H. T., & Adamska, M. (2014). Developmental gene expression provides clues to relationships between sponge and eumetazoan body plans. *Nature Communications*, *5*, 3905.

Lemke, S. B., & Schnorrer, F. (2017). Mechanical forces during muscle development. *Mechanisms of Development*, *144*(Pt A), 92–101.

Lessey, E. C., Guilluy, C., & Burridge, K. (2012). From mechanical force to RhoA activation. *Biochemistry*, *51*(38), 7420–7432.

Leys, S. P. (2015). Elements of a “nervous system” in sponges. *The Journal of Experimental Biology*, *218*(Pt 4), 581–591.

Leys, S. P., & Ereskovsky, A. V. (2006). Embryogenesis and larval differentiation in sponges. *Canadian Journal of Zoology*, *84*(2), 262–287.

Leys, S. P., & Hill, A. (2012). The physiology and molecular biology of sponge tissues. *Advances in Marine Biology*, *62*, 1–56.

Leys, S. P. & Mackie, G. O. (1997). Electrical recording from a glass sponge. *Nature*, *387*(6628), 29–30.

Leys, S. P., Mackie, G. O., & Meech, R. W. (1999). Impulse conduction in a sponge. *The Journal of Experimental Biology*, *202 (Pt 9)*, 1139–1150.

Leys, S. P., Mackie, G. O., & Reiswig, H. M. (2007). The biology of glass sponges. *Advances in Marine Biology*, *52*, 1–145.

Leys, S. P., & Meech, R. W. (2006). Physiology of coordination in sponges. *Canadian Journal of Zoology*, *84*(2), 288–306.

Leys, S. P., Nichols, S. A., & Adams, E. D. M. (2009). Epithelia and integration in sponges. *Integrative and Comparative Biology*, *49*(2), 167–177.

Leys, S. P., Yahel, G., Reidenbach, M. A., Tunnicliffe, V., Shavit, U., & Reiswig, H. M. (2011a). The Sponge Pump: The Role of Current Induced Flow in the Design of the Sponge Body Plan. In *PLoS ONE* (Vol. 6, Issue 12, p. e27787). https://doi.org/10.1371/journal.pone.0027787

Leys, S. P., Yahel, G., Reidenbach, M. A., Tunnicliffe, V., Shavit, U., & Reiswig, H. M. (2011b). The sponge pump: the role of current induced flow in the design of the sponge body plan. *PloS One*, *6*(12), e27787.

Li, J., Zhu, X., Chen, M., Cheng, L., Zhou, D., Lu, M. M., Du, K., Epstein, J. A., & Parmacek, M. S. (2005). Myocardin-related transcription factor B is required in cardiac neural crest for smooth muscle differentiation and cardiovascular development. *Proceedings of the National Academy of Sciences of the United States of America*, *102*(25), 8916–8921.

Li, L., Miano, J. M., Mercer, B., & Olson, E. N. (1996). Expression of the SM22alpha promoter in transgenic mice provides evidence for distinct transcriptional regulatory programs in vascular and visceral smooth muscle cells. *The Journal of Cell Biology*, *132*(5), 849–859.

Li, Li, L., Miano, J. M., Cserjesi, P., & Olson, E. N. (1996). SM22α, a Marker of Adult Smooth Muscle, Is Expressed in Multiple Myogenic Lineages During Embryogenesis. In *Circulation Research* (Vol. 78, Issue 2, pp. 188–195). https://doi.org/10.1161/01.res.78.2.188

Liang, C., Musser, J. M., Cloutier, A., Prum, R. O., & Wagner, G. P. (2018). Pervasive Correlated Evolution in Gene Expression Shapes Cell and Tissue Type Transcriptomes. In *Genome Biology and Evolution* (Vol. 10, Issue 2, pp. 538–552). https://doi.org/10.1093/gbe/evy016

Liu, X., Shu, S., Yamashita, R. A., Xu, Y., & Korn, E. D. (2000). Chimeras of Dictyostelium myosin II head and neck domains with Acanthamoeba or chicken smooth muscle myosin II tail domain have greatly increased and unregulated actin-dependent MgATPase activity. In *Proceedings of the National Academy of Sciences* (Vol. 97, Issue 23, pp. 12553–12558). https://doi.org/10.1073/pnas.230441497

Long, X., Bell, R. D., Gerthoffer, W. T., Zlokovic, B. V., & Miano, J. M. (2008). Myocardin is sufficient for a smooth muscle-like contractile phenotype. *Arteriosclerosis, Thrombosis, and Vascular Biology*, *28*(8), 1505–1510.

Long, X., Creemers, E. E., Wang, D.-Z., Olson, E. N., & Miano, J. M. (2007). Myocardin is a bifunctional switch for smooth versus skeletal muscle differentiation. *Proceedings of the National Academy of Sciences of the United States of America*, *104*(42), 16570–16575.

Lorenz, B., Bohnensack, R., Gamulin, V., Steffen, R., & Müller, W. E. (1996). Regulation of motility of cells from marine sponges by calcium ions. *Cellular Signalling*, *8*(7), 517–524.

Ludeman, D. A., Farrar, N., Riesgo, A., Paps, J., & Leys, S. P. (2014). Evolutionary origins of sensation in metazoans: functional evidence for a new sensory organ in sponges. In *BMC Evolutionary Biology* (Vol. 14, Issue 1, p. 3). https://doi.org/10.1186/1471-2148-14-3

Lupas, A., Van Dyke, M., & Stock, J. (1991). Predicting coiled coils from protein sequences. *Science*, *252*(5009), 1162–1164.

Maartens, A. P., & Brown, N. H. (2015). The many faces of cell adhesion during Drosophila muscle development. *Developmental Biology*, *401*(1), 62–74.

Madison, B. B., McKenna, L. B., Dolson, D., Epstein, D. J., & Kaestner, K. H. (2009). FoxF1 and FoxL1 link hedgehog signaling and the control of epithelial proliferation in the developing stomach and intestine. *The Journal of Biological Chemistry*, *284*(9), 5936–5944.

Magie, C. R., Pang, K., & Martindale, M. Q. (2005). Genomic inventory and expression of Sox and Fox genes in the cnidarian Nematostella vectensis. *Development Genes and Evolution*, *215*(12), 618–630.

Mah, J. L., Christensen-Dalsgaard, K. K., & Leys, S. P. (2014). Choanoflagellate and choanocyte collar-flagellar systems and the assumption of homology. In *Evolution & Development* (Vol. 16, Issue 1, pp. 25–37). https://doi.org/10.1111/ede.12060

Mahaut-Smith, M. P., Hussain, J. F., & Mason, M. J. (1999). Depolarization-evoked Ca2+ release in a non-excitable cell, the rat megakaryocyte. *The Journal of Physiology*, *515*(2), 385–390.

Maldonado, M. (2005). Choanoflagellates, choanocytes, and animal multicellularity. *Invertebrate Biology: A Quarterly Journal of the American Microscopical Society and the Division of Invertebrate Zoology/ASZ*, *123*(1), 1–22.

Mardon, G., Solomon, N. M., & Rubin, G. M. (1994). dachshund encodes a nuclear protein required for normal eye and leg development in Drosophila. *Development* , *120*(12), 3473–3486.

Mariani, L. E., & Caspary, T. (2013). Primary Cilia, Sonic Hedgehog Signaling, and Spinal Cord Development. In K. L. Tucker & T. Caspary (Eds.), *Cilia and Nervous System Development and Function* (pp. 55–82). Springer Netherlands.

Marlow, H., Roettinger, E., Boekhout, M., & Martindale, M. Q. (2012). Functional roles of Notch signaling in the cnidarian Nematostella vectensis. *Developmental Biology*, *362*(2), 295–308.

Martin, R. M., Gasser, R. B., Jones, M. K., & Lightowlers, M. W. (1995). Identification and characterization of myophilin, a muscle-specific antigen of Echinococcus granulosus. *Molecular and Biochemical Parasitology*, *70*(1-2), 139–148.

Martindale, M. Q. (2004). Investigating the origins of triploblasty: `mesodermal' gene expression in a diploblastic animal, the sea anemone Nematostella vectensis (phylum, Cnidaria; class, Anthozoa). In *Development* (Vol. 131, Issue 10, pp. 2463–2474). https://doi.org/10.1242/dev.01119

Matsuno, A., Ishida, H., Kuroda, M., & Masuda, Y. (1988). Ultrastructures of contractile bundles in epithelial cells of the sponge. *Zoological Science*, *5*, 1212.

McFadden, D. G., Barbosa, A. C., Richardson, J. A., Schneider, M. D., Srivastava, D., & Olson, E. N. (2005). The Hand1 and Hand2 transcription factors regulate expansion of the embryonic cardiac ventricles in a gene dosage-dependent manner. *Development*, *132*(1), 189–201.

McNAIR, G. T. (1923). MOTOR REACTIONS OF THE FRESH-WATER SPONGE, EPHYDATIA FLUVIATILIS. *The Biological Bulletin*, *44*(4), 153–166.

Meadows, S. M., Warkman, A. S., Salanga, M. C., Small, E. M., & Krieg, P. A. (2008). The myocardin-related transcription factor, MASTR, cooperates with MyoD to activate skeletal muscle gene expression. *Proceedings of the National Academy of Sciences of the United States of America*, *105*(5), 1545–1550.

Medjkane, S., Perez-Sanchez, C., Gaggioli, C., Sahai, E., & Treisman, R. (2009). Myocardin-related transcription factors and SRF are required for cytoskeletal dynamics and experimental metastasis. *Nature Cell Biology*, *11*(3), 257–268.

Meissner, G. (1986). Ryanodine activation and inhibition of the Ca2+ release channel of sarcoplasmic reticulum. *The Journal of Biological Chemistry*, *261*(14), 6300–6306.

Mercurio, M., Corriero, G., & Gaino, E. (2007). A 3-year investigation of sexual reproduction in Geodia cydonium (Jameson 1811) (Porifera, Demospongiae) from a semi-enclosed Mediterranean bay. *Marine Biology*, *151*(4), 1491–1500.

Miano, J. M., Long, X., & Fujiwara, K. (2007). Serum response factor: master regulator of the actin cytoskeleton and contractile apparatus. *American Journal of Physiology. Cell Physiology*, *292*(1), C70–C81.

Miilsch, A., & Busse, R. (1990). NG-nitro-L-arginine (N5-[imino(nitroamino)methyl]-L-ornithine) impairs endothelium-dependent dilations by inhibiting cytosolic nitric oxide synthesis from l-arginine. *Naunyn-Schmiedeberg's Archives of Pharmacology*, *341*(1), 143–147.

Mikami, T., Yoshida, K., Sawada, H., Esaki, M., Yasumura, K., & Ono, M. (2015). Inhibition of Rho-associated kinases disturbs the collective cell migration of stratified TE-10 cells. *Biological Research*, *48*, 48.

Miller, P. W., Pokutta, S., Mitchell, J. M., Chodaparambil, J. V., Clarke, D. N., Nelson, W. J., Weis, W. I., & Nichols, S. A. (2018). Analysis of a vinculin homolog in a sponge (phylum Porifera) reveals that vertebrate-like cell adhesions emerged early in animal evolution. *The Journal of Biological Chemistry*, *293*(30), 11674–11686.

Miralles, F., Posern, G., Zaromytidou, A.-I., & Treisman, R. (2003). Actin dynamics control SRF activity by regulation of its coactivator MAL. *Cell*, *113*(3), 329–342.

Mitchell, J. M., & Nichols, S. A. (2019). Diverse cell junctions with unique molecular composition in tissues of a sponge (Porifera). *EvoDevo*, *10*, 26.

Mohieldin, A. M., Zubayer, H. S. M., Al Omran, A. J., Saternos, H. C., Zarban, A. A., Nauli, S. M., & AbouAlaiwi, W. A. (2016). Vascular Endothelial Primary Cilia: Mechanosensation and Hypertension. *Current Hypertension Reviews*, *12*(1), 57–67.

Mokalled, M. H., Johnson, A., Kim, Y., Oh, J., & Olson, E. N. (2010). Myocardin-related transcription factors regulate the Cdk5/Pctaire1 kinase cascade to control neurite outgrowth, neuronal migration and brain development. *Development*, *137*(14), 2365–2374.

Mokalled, M. H., Johnson, A. N., Creemers, E. E., & Olson, E. N. (2012). MASTR directs MyoD-dependent satellite cell differentiation during skeletal muscle regeneration. In *Genes & Development* (Vol. 26, Issue 2, pp. 190–202). https://doi.org/10.1101/gad.179663.111

Moroz, L. L. (2015). Convergent evolution of neural systems in ctenophores. *The Journal of Experimental Biology*, *218*(Pt 4), 598–611.

Mouilleron, S., Langer, C. A., Guettler, S., McDonald, N. Q., & Treisman, R. (2011). Structure of a pentavalent G-actin• MRTF-A complex reveals how G-actin controls nucleocytoplasmic shuttling of a transcriptional coactivator. *Science Signaling*, *4*(177), ra40–ra40.

Moyers, B. A., & Zhang, J. (2017). Further Simulations and Analyses Demonstrate Open Problems of Phylostratigraphy. *Genome Biology and Evolution*, *9*(6), 1519–1527.

Muehlich, S., Wang, R., Lee, S.-M., Lewis, T. C., Dai, C., & Prywes, R. (2008). Serum-Induced Phosphorylation of the Serum Response Factor Coactivator MKL1 by the Extracellular Signal-Regulated Kinase 1/2 Pathway Inhibits Its Nuclear Localization. In *Molecular and Cellular Biology* (Vol. 28, Issue 20, pp. 6302–6313). https://doi.org/10.1128/mcb.00427-08

Müller, W. E. G. (1998). Origin of Metazoa: Sponges as Living Fossils. In *Naturwissenschaften* (Vol. 85, Issue 1, pp. 11–25). https://doi.org/10.1007/s001140050444

Murrell, M., Oakes, P. W., Lenz, M., & Gardel, M. L. (2015). Forcing cells into shape: the mechanics of actomyosin contractility. *Nature Reviews. Molecular Cell Biology*, *16*(8), 486–498.

Musser, J. M., Schippers, K. J., Nickel, M., & Mizzon, G. (2019). Profiling cellular diversity in sponges informs animal cell type and nervous system evolution. *BioRxiv*. https://www.biorxiv.org/content/10.1101/758276v1.abstract

Nakanishi, N., Sogabe, S., & Degnan, B. M. (2014). Evolutionary origin of gastrulation: insights from sponge development. *BMC Biology*, *12*, 26.

Nakayama, S., & Kretsinger, R. H. (1994). Evolution of the EF-hand family of proteins. *Annual Review of Biophysics and Biomolecular Structure*, *23*, 473–507.

Nichols, S. A., Dayel, M. J., & King, N. (2009). Genomic, phylogenetic, and cell biological insights into metazoan origins. *Animal Evolution: Genes, Genomes, Fossils and Trees*, 24–32.

Nichols, S. A., Dirks, W., Pearse, J. S., & King, N. (2006). Early evolution of animal cell signaling and adhesion genes. *Proceedings of the National Academy of Sciences of the United States of America*, *103*(33), 12451–12456.

Nickel, M. (2004). Kinetics and rhythm of body contractions in the sponge Tethya wilhelma (Porifera: Demospongiae). *The Journal of Experimental Biology*, *207*(Pt 26), 4515–4524.

Nickel, M. (2010). Evolutionary emergence of synaptic nervous systems: what can we learn from the non-synaptic, nerveless Porifera? In *Invertebrate Biology* (Vol. 129, Issue 1, pp. 1–16). https://doi.org/10.1111/j.1744-7410.2010.00193.x

Nickel, M., Scheer, C., Hammel, J. U., Herzen, J., & Beckmann, F. (2011). The contractile sponge epithelium sensu lato--body contraction of the demosponge Tethya wilhelma is mediated by the pinacoderm. *The Journal of Experimental Biology*, *214*(Pt 10), 1692–1698.

Nielsen, C. (2008). Six major steps in animal evolution: are we derived sponge larvae? *Evolution & Development*, *10*(2), 241–257.

Nishida, W., Nakamura, M., Mori, S., Takahashi, M., Ohkawa, Y., Tadokoro, S., Yoshida, K., Hiwada, K., Hayashi, K. 'ichiro, & Sobue, K. (2002). A triad of serum response factor and the GATA and NK families governs the transcription of smooth and cardiac muscle genes. *The Journal of Biological Chemistry*, *277*(9), 7308–7317.

Nogara, L., Naber, N., Pate, E., Canton, M., Reggiani, C., & Cooke, R. (2016). Spectroscopic Studies of the Super Relaxed State of Skeletal Muscle. *PloS One*, *11*(8), e0160100.

O'Keefe, E. P. (2013). siRNAs and shRNAs: Tools for protein knockdown by gene silencing. *Word Lab*.

Olson, E. N., & Nordheim, A. (2010). Linking actin dynamics and gene transcription to drive cellular motile functions. *Nature Reviews. Molecular Cell Biology*, *11*(5), 353–365.

Ono, S. (2010). Dynamic regulation of sarcomeric actin filaments in striated muscle. *Cytoskeleton* , *67*(11), 677–692.

Orjalo, A., Johansson, H. E., & Ruth, J. L. (2011). Stellaris™ fluorescence in situ hybridization (FISH) probes: a powerful tool for mRNA detection. *Nature Methods*, *8*(10), i – ii.

Palumbi, S. R. (1986). How Body Plans Limit Acclimation: Responses of a Demosponge to Wave Force. *Ecology*, *67*(1), 208–214.

Panayiotou, R., Miralles, F., Pawlowski, R., Diring, J., Flynn, H. R., Skehel, M., & Treisman, R. (2016). Phosphorylation acts positively and negatively to regulate MRTF-A subcellular localisation and activity. *eLife*, *5*. https://doi.org/10.7554/eLife.15460

Parker, G. H. (1919). *The Elementary Nervous System*. J.B. Lippincott Company.

Paulus, W., & Weissenfels, N. (1986). The spermatogenesis of Ephydatia fluviatilis (Porifera). *Zoomorphology*, *106*(3), 155–162.

Peh, G. S. L., Adnan, K., George, B. L., Ang, H.-P., Seah, X.-Y., Tan, D. T., & Mehta, J. S. (2015). The effects of Rho-associated kinase inhibitor Y-27632 on primary human corneal endothelial cells propagated using a dual media approach. In *Scientific Reports* (Vol. 5, Issue 1). https://doi.org/10.1038/srep09167

Peña, J. F., Alié, A., Richter, D. J., Wang, L., Funayama, N., & Nichols, S. A. (2016). Conserved expression of vertebrate microvillar gene homologs in choanocytes of freshwater sponges. *EvoDevo*, *7*, 13.

Pérez-Moreno, J. J., Espina-Zambrano, A. G., García-Calderón, C. B., & Estrada, B. (2017). Kon-tiki enhances PS2 integrin adhesion and localizes its ligand, Thrombospondin, in the myotendinous junction. *Journal of Cell Science*, *130*(5), 950–962.

Perreault, N., Katz, J. P., & Sackett, S. D. (2001). Foxl1 controls the Wnt/β-catenin pathway by modulating the expression of proteoglycans in the gut. *Journal of Biological*. http://www.jbc.org/content/276/46/43328.short

Pfannkuchen, M., & Brmmer, F. (2009). Heterologous expression of DsRed2 in young sponges (Porifera). In *The International Journal of Developmental Biology* (Vol. 53, Issue 7, pp. 1113–1117). https://doi.org/10.1387/ijdb.072526mp

Pipes, G. C. T., Creemers, E. E., & Olson, E. N. (2006). The myocardin family of transcriptional coactivators: versatile regulators of cell growth, migration, and myogenesis. *Genes & Development*, *20*(12), 1545–1556.

Prinjha, R. K., Shapland, C. E., Hsuan, J. J., Totty, N. F., Mason, I. J., & Lawson, D. (1994). Cloning and sequencing of cDNAs encoding the actin cross-linking protein transgelin defines a new family of actin-associated proteins. *Cell Motility and the Cytoskeleton*, *28*(3), 243–255.

Prosser, C. L. (1967). Ionic analyses and effects of ions on contractions of sponge tissues. *Zeitschrift Fur Vergleichende Physiologie*, *54*(2), 109–120.

Prosser, C. L., Nagai, T., & Nystrom, R. A. (1962). Oscular contractions in sponges. *Comparative Biochemistry and Physiology*, *6*, 69–74.

Pukhlyakova, E. A., Kirillova, A. O., Kraus, Y. A., Zimmermann, B., & Technau, U. (2019). A cadherin switch marks germ layer formation in the diploblastic sea anemone Nematostella vectensis. *Development*, *146*(20). https://doi.org/10.1242/dev.174623

Putnam, N. H., Srivastava, M., Hellsten, U., Dirks, B., Chapman, J., Salamov, A., Terry, A., Shapiro, H., Lindquist, E., Kapitonov, V. V., Jurka, J., Genikhovich, G., Grigoriev, I. V., Lucas, S. M., Steele, R. E., Finnerty, J. R., Technau, U., Martindale, M. Q., & Rokhsar, D. S. (2007). Sea anemone genome reveals ancestral eumetazoan gene repertoire and genomic organization. *Science*, *317*(5834), 86–94.

Ramoino, P., Gallus, L., Paluzzi, S., Raiteri, L., Diaspro, A., Fato, M., Bonanno, G., Tagliafierro, G., Ferretti, C., & Manconi, R. (2007). The GABAergic-like system in the marine demosponge Chondrilla nucula. *Microscopy Research and Technique*, *70*(11), 944–951.

Reiswig, H. M. (1971). In situ pumping activities of tropical Demospongiae. *Marine Biology*, *9*(1), 38–50.

Renard, E., Leys, S. P., Wörheide, G., & Borchiellini, C. (2018). Understanding Animal Evolution: The Added Value of Sponge Transcriptomics and Genomics. In *BioEssays* (Vol. 40, Issue 9, p. 1700237). https://doi.org/10.1002/bies.201700237

Renfer, E., Amon-Hassenzahl, A., Steinmetz, P. R. H., & Technau, U. (2010). A muscle-specific transgenic reporter line of the sea anemone, Nematostella vectensis. *Proceedings of the National Academy of Sciences of the United States of America*, *107*(1), 104–108.

Renfer, E., & Technau, U. (2017). Meganuclease-assisted generation of stable transgenics in the sea anemone Nematostella vectensis. *Nature Protocols*, *12*(9), 1844–1854.

Retailleau, K., & Duprat, F. (2014). Polycystins and partners: proposed role in mechanosensitivity. *The Journal of Physiology*, *592*(12), 2453–2471.

Revilla-I-Domingo, R., Schmidt, C., Zifko, C., & Raible, F. (2018). Establishment of Transgenesis in the Demosponge Suberites domuncula. *Genetics*, *210*(2), 435–443.

Ridley, A. J. (2001). Rho GTPases and cell migration. *Journal of Cell Science*, *114*(Pt 15), 2713–2722.

Rieppel, O. (2015). Wagner, G. P. 2014. Homology, Genes, and Evolutionary Novelties. Princeton University Press, Princeton, NJ. 498 pp. ISBN 978-0-691-15646-0. In *Journal of Zoological Systematics and Evolutionary Research* (Vol. 53, Issue 1, pp. 95–95). https://doi.org/10.1111/jzs.12089

Riesgo, A., Farrar, N., Windsor, P. J., Giribet, G., & Leys, S. P. (2014). The analysis of eight transcriptomes from all poriferan classes reveals surprising genetic complexity in sponges. *Molecular Biology and Evolution*, *31*(5), 1102–1120.

Riesgo, A., Maldonado, M., & Durfort, M. (2007). Dynamics of gametogenesis, embryogenesis, and larval release in a Mediterranean homosclerophorid demosponge. *Marine and Freshwater Research*, *58*(4), 398–417.

Rivera, A. S., Hammel, J. U., Haen, K. M., Danka, E. S., Cieniewicz, B., Winters, I. P., Posfai, D., Wörheide, G., Lavrov, D. V., Knight, S. W., Hill, M. S., Hill, A. L., & Nickel, M. (2011). RNA interference in marine and freshwater sponges: actin knockdown in Tethya wilhelma and Ephydatia muelleri by ingested dsRNA expressing bacteria. *BMC Biotechnology*, *11*, 67.

Rozenfeld, F., & Rasmont, R. (1977). Hydroxyurea: an inhibitor of the differentiation of choanocytes in fresh-water sponges and a possible agent for the isolation of embryonic cells. *Differentiation; Research in Biological Diversity*, *7*(1-3), 53–60.

Ryan, J. F., Pang, K., Schnitzler, C. E., Nguyen, A.-D., Moreland, R. T., Simmons, D. K., Koch, B. J., Francis, W. R., Havlak, P., NISC Comparative Sequencing Program, Smith, S. A., Putnam, N. H., Haddock, S. H. D., Dunn, C. W., Wolfsberg, T. G., Mullikin, J. C., Martindale, M. Q., & Baxevanis, A. D. (2013). The genome of the ctenophore Mnemiopsis leidyi and its implications for cell type evolution. *Science*, *342*(6164), 1242592.

Ryder, J. W., Lau, K. S., Kamm, K. E., & Stull, J. T. (2007). Enhanced skeletal muscle contraction with myosin light chain phosphorylation by a calmodulin-sensing kinase. *The Journal of Biological Chemistry*, *282*(28), 20447–20454.

Salinas-Saavedra, M., Rock, A. Q., & Martindale, M. Q. (2018). Germ layer-specific regulation of cell polarity and adhesion gives insight into the evolution of mesoderm. In *eLife* (Vol. 7). https://doi.org/10.7554/elife.36740

Saller, U. (1988). Oogenesis and larval development of Ephydatia fluviatilis (Porifera, Spongillidae). *Zoomorphology*, *108*(1), 23–28.

Sanger, J. W., Kang, S., Siebrands, C. C., Freeman, N., Du, A., Wang, J., Stout, A. L., & Sanger, J. M. (2005). How to build a myofibril. *Journal of Muscle Research and Cell Motility*, *26*(6-8), 343–354.

Sanger, J. W., Mittal, B., & Sanger, J. M. (1984). Analysis of myofibrillar structure and assembly using fluorescently labeled contractile proteins. *The Journal of Cell Biology*, *98*(3), 825–833.

Sawyer, J. M., Harrell, J. R., Shemer, G., Sullivan-Brown, J., Roh-Johnson, M., & Goldstein, B. (2010). Apical constriction: a cell shape change that can drive morphogenesis. *Developmental Biology*, *341*(1), 5–19.

Schaks, M., Giannone, G., & Rottner, K. (2019). Actin dynamics in cell migration. *Essays in Biochemistry*, *63*(5), 483–495.

Schenkelaars, Q., Pratlong, M., Kodjabachian, L., Fierro-Constain, L., Vacelet, J., Le Bivic, A., Renard, E., & Borchiellini, C. (2017). Animal multicellularity and polarity without Wnt signaling. *Scientific Reports*, *7*(1), 15383.

Schenkelaars, Q., Quintero, O., Hall, C., Fierro-Constain, L., Renard, E., Borchiellini, C., & Hill, A. L. (2016). ROCK inhibition abolishes the establishment of the aquiferous system in Ephydatia muelleri (Porifera, Demospongiae). *Developmental Biology*, *412*(2), 298–310.

Schiaffino, S., & Reggiani, C. (1994). Myosin isoforms in mammalian skeletal muscle. In *Journal of Applied Physiology* (Vol. 77, Issue 2, pp. 493–501). https://doi.org/10.1152/jappl.1994.77.2.493

Schindelin, J., Arganda-Carreras, I., Frise, E., Kaynig, V., Longair, M., Pietzsch, T., Preibisch, S., Rueden, C., Saalfeld, S., Schmid, B., Tinevez, J.-Y., White, D. J., Hartenstein, V., Eliceiri, K., Tomancak, P., & Cardona, A. (2012). Fiji: an open-source platform for biological-image analysis. *Nature Methods*, *9*(7), 676–682.

Schippers, K. J., & Nichols, S. A. (2018). Evidence of Signaling and Adhesion Roles for β-Catenin in the Sponge Ephydatia muelleri. *Molecular Biology and Evolution*, *35*(6), 1407–1421.

Schliwa, M. (1982). Action of cytochalasin D on cytoskeletal networks. *The Journal of Cell Biology*, *92*(1), 79–91.

Schoots, A. F. M., Afm, S., Jj, S., & Jm, D. (1977). *SOME CHARACTERISTICS OF ESTERASES IN EXTRACTS OF THE FRESH-WATER SPONGE, SPONGILLA SP*. https://pascal-francis.inist.fr/vibad/index.php?action=getRecordDetail&idt=PASCAL7750234142

Schulz, R., & Triggle, C. R. (1994). Role of NO in vascular smooth muscle and cardiac muscle function. *Trends in Pharmacological Sciences*, *15*(7), 255–259.

Schuster, A., Vargas, S., Knapp, I. S., Pomponi, S. A., Toonen, R. J., Erpenbeck, D., & Wörheide, G. (2018). Divergence times in demosponges (Porifera): first insights from new mitogenomes and the inclusion of fossils in a birth-death clock model. In *BMC Evolutionary Biology* (Vol. 18, Issue 1). https://doi.org/10.1186/s12862-018-1230-1

Sebé-Pedrós, A., Burkhardt, P., Sánchez-Pons, N., Fairclough, S. R., Lang, B. F., King, N., & Ruiz-Trillo, I. (2013). Insights into the origin of metazoan filopodia and microvilli. *Molecular Biology and Evolution*, *30*(9), 2013–2023.

Sebé-Pedrós, A., Chomsky, E., Pang, K., Lara-Astiaso, D., Gaiti, F., Mukamel, Z., Amit, I., Hejnol, A., Degnan, B. M., & Tanay, A. (2018). Early metazoan cell type diversity and the evolution of multicellular gene regulation. *Nature Ecology & Evolution*, *2*(7), 1176–1188.

Sebé-Pedrós, A., Grau-Bové, X., Richards, T. A., & Ruiz-Trillo, I. (2014). Evolution and classification of myosins, a paneukaryotic whole-genome approach. *Genome Biology and Evolution*, *6*(2), 290–305.

Sebé-Pedrós, A., Saudemont, B., Chomsky, E., Plessier, F., Mailhé, M.-P., Renno, J., Loe-Mie, Y., Lifshitz, A., Mukamel, Z., Schmutz, S., Novault, S., Steinmetz, P. R. H., Spitz, F., Tanay, A., & Marlow, H. (2018). Cnidarian Cell Type Diversity and Regulation Revealed by Whole-Organism Single-Cell RNA-Seq. *Cell*, *173*(6), 1520–1534.e20.

Seipel, K., & Schmid, V. (2005). Evolution of striated muscle: jellyfish and the origin of triploblasty. *Developmental Biology*, *282*(1), 14–26.

Sellers, J. R. (1985). Mechanism of the phosphorylation-dependent regulation of smooth muscle heavy meromyosin. *The Journal of Biological Chemistry*, *260*(29), 15815–15819.

Sellers, J. R. (1991). Regulation of cytoplasmic and smooth muscle myosin. *Current Opinion in Cell Biology*, *3*(1), 98–104.

Shapland, C., Lowings, P., & Lawson, D. (1988a). Identification of new actin-associated polypeptides that are modified by viral transformation and changes in cell shape. *The Journal of Cell Biology*, *107*(1), 153–161.

Shapland, C., Lowings, P., & Lawson, D. (1988b). Identification of new actin-associated polypeptides that are modified by viral transformation and changes in cell shape. *The Journal of Cell Biology*, *107*(1), 153–161.

Shaposhnikov, D., Kuffer, C., Storchova, Z., & Posern, G. (2013). Myocardin related transcription factors are required for coordinated cell cycle progression. *Cell Cycle* , *12*(11), 1762–1772.

Shen, W., Lammertink, R. G. H., Sakata, J. K., Kornfield, J. A., & Tirrell, D. A. (2005). Assembly of an Artificial Protein Hydrogel through Leucine Zipper Aggregation and Disulfide Bond Formation. *Macromolecules*, *38*(9), 3909–3916.

Shi, X., & Garry, D. J. (2006). Muscle stem cells in development, regeneration, and disease. *Genes & Development*, *20*(13), 1692–1708.

Shimeld, S. M., Degnan, B., & Luke, G. N. (2010). Evolutionary genomics of the Fox genes: origin of gene families and the ancestry of gene clusters. *Genomics*, *95*(5), 256–260.

Shiwen, X., Stratton, R., Nikitorowicz-Buniak, J., Ahmed-Abdi, B., Ponticos, M., Denton, C., Abraham, D., Takahashi, A., Suki, B., Layne, M. D., Lafyatis, R., & Smith, B. D. (2015). A Role of Myocardin Related Transcription Factor-A (MRTF-A) in Scleroderma Related Fibrosis. *PloS One*, *10*(5), e0126015.

Siebert, S., Farrell, J. A., Cazet, J. F., Abeykoon, Y., Primack, A. S., Schnitzler, C. E., & Juliano, C. E. (2019). Stem cell differentiation trajectories in Hydra resolved at single-cell resolution. *Science*, *365*(6451). https://doi.org/10.1126/science.aav9314

Simion, P., Philippe, H., Baurain, D., Jager, M., Richter, D. J., Di Franco, A., Roure, B., Satoh, N., Quéinnec, É., Ereskovsky, A., Lapébie, P., Corre, E., Delsuc, F., King, N., Wörheide, G., & Manuel, M. (2017). A Large and Consistent Phylogenomic Dataset Supports Sponges as the Sister Group to All Other Animals. *Current Biology: CB*, *27*(7), 958–967.

Simpson, T. L. (1984). *The cell biology of sponges.* Springer, Berlin Heidelberg, New York.

Sipkema, D., Holmes, B., Nichols, S. A., & Blanch, H. W. (2009). Biological Characterisation of Haliclona (?gellius) sp.: Sponge and Associated Microorganisms. In *Microbial Ecology* (Vol. 58, Issue 4, pp. 903–920). https://doi.org/10.1007/s00248-009-9534-8

Sjöblom, B., Salmazo, A., & Djinović-Carugo, K. (2008). α-Actinin structure and regulation. *Cellular and Molecular Life Sciences: CMLS*, *65*(17), 2688.

Smith, P. A., Sakura, H., Coles, B., Gummerson, N., Proks, P., & Ashcroft, F. M. (1997). Electrogenic arginine transport mediates stimulus-secretion coupling in mouse pancreatic beta-cells. *The Journal of Physiology*, *499*(3), 625–635.

Smith, S. A., & Pease, J. B. (2017). Heterogeneous molecular processes among the causes of how sequence similarity scores can fail to recapitulate phylogeny. *Briefings in Bioinformatics*, *18*(3), 451–457.

Sogabe, S., Hatleberg, W. L., Kocot, K. M., Say, T. E., Stoupin, D., Roper, K. E., Fernandez-Valverde, S. L., Degnan, S. M., & Degnan, B. M. (2019). Pluripotency and the origin of animal multicellularity. *Nature*, *570*(7762), 519–522.

Sotiropoulos, A., Gineitis, D., Copeland, J., & Treisman, R. (1999). Signal-regulated activation of serum response factor is mediated by changes in actin dynamics. *Cell*, *98*(2), 159–169.

Spudich, J. A., Huxley, H. E., & Finch, J. T. (1972). Regulation of skeletal muscle contraction. II. Structural studies of the interaction of the tropomyosin-troponin complex with actin. *Journal of Molecular Biology*, *72*(3), 619–632.

Spudich, J. A., & Watt, S. (1971). The Regulation of Rabbit Skeletal Muscle Contraction: I. Biochemical studies of the interaction of the tropomyosin-troponin complex with actin and the proteolytic fragments of myosin. *The Journal of Biological Chemistry*, *246*(15), 4866–4871.

Srivastava, M., Simakov, O., Chapman, J., Fahey, B., Gauthier, M. E. A., Mitros, T., Richards, G. S., Conaco, C., Dacre, M., Hellsten, U., Larroux, C., Putnam, N. H., Stanke, M., Adamska, M., Darling, A., Degnan, S. M., Oakley, T. H., Plachetzki, D. C., Zhai, Y., … Rokhsar, D. S. (2010). The Amphimedon queenslandica genome and the evolution of animal complexity. *Nature*, *466*(7307), 720–726.

Steenkamp, E. T., Wright, J., & Baldauf, S. L. (2006). The protistan origins of animals and fungi. *Molecular Biology and Evolution*, *23*(1), 93–106.

Stefanik, D. J., Friedman, L. E., & Finnerty, J. R. (2013). Collecting, rearing, spawning and inducing regeneration of the starlet sea anemone, Nematostella vectensis. *Nature Protocols*, *8*(5), 916–923.

Stefanik, D. J., Wolenski, F. S., Friedman, L. E., Gilmore, T. D., & Finnerty, J. R. (2013). Isolation of DNA, RNA and protein from the starlet sea anemone Nematostella vectensis. *Nature Protocols*, *8*(5), 892–899.

Steinmetz, P. R. H., Aman, A., Kraus, J. E. M., & Technau, U. (2017). Gut-like ectodermal tissue in a sea anemone challenges germ layer homology. *Nature Ecology & Evolution*, *1*(10), 1535–1542.

Steinmetz, P. R. H., Kraus, J. E. M., Larroux, C., Hammel, J. U., Amon-Hassenzahl, A., Houliston, E., Wörheide, G., Nickel, M., Degnan, B. M., & Technau, U. (2012). Independent evolution of striated muscles in cnidarians and bilaterians. *Nature*, *487*(7406), 231–234.

Sulbarán, G., Alamo, L., Pinto, A., Márquez, G., Méndez, F., Padrón, R., & Craig, R. (2015). An invertebrate smooth muscle with striated muscle myosin filaments. *Proceedings of the National Academy of Sciences of the United States of America*, *112*(42), E5660–E5668.

Sun, J. J., Wu, Z. H., & Zhong, T. (2016). Cilia function in cell signaling and organ development. *Scientia Sinica Vitae*. http://engine.scichina.com/publisher/scp/journal/SSV/46/4/10.1360/N052016-00134

Svitkina, T. (2018). The Actin Cytoskeleton and Actin-Based Motility. *Cold Spring Harbor Perspectives in Biology*, *10*(1). https://doi.org/10.1101/cshperspect.a018267

Szent-Györgyi, A. G. (1996). Regulation of contraction by calcium binding myosins. *Biophysical Chemistry*, *59*(3), 357–363.

Tamm, S. L. (2019). Defecation by the ctenophore Mnemiopsis leidyi occurs with an ultradian rhythm through a single transient anal pore. In *Invertebrate Biology* (Vol. 138, Issue 1, pp. 3–16). https://doi.org/10.1111/ivb.12236

Tamm, S. L., & Tamm, S. (1993). Dynamic control of cell-cell adhesion and membrane-associated actin during food-induced mouth opening in Beroe. *Journal of Cell Science*, *106*(1), 355–364.

Tamm, S. L. (1999). Dynamic control of reversible cell adhesion and actin cytoskeleton in the mouth of Bero. Microscopy Research and Technique, 44(4), 293–303.

Tanaka, H., Ishimaru, S., Nagatsuka, Y., & Ohashi, K. (2018). Smooth muscle-like Ca2+-regulation of actin-myosin interaction in adult jellyfish striated muscle. *Scientific Reports*, *8*(1), 7776.

Tapscott, S. J. (2005). The circuitry of a master switch: Myod and the regulation of skeletal muscle gene transcription. *Development*, *132*(12), 2685–2695.

Tasouri, E., Willaredt, M. A., & Tucker, K. L. (2013). Primary Cilia and Brain Development. In *Cilia and Nervous System Development and Function* (pp. 83–104). https://doi.org/10.1007/978-94-007-5808-7_3

Taylor, K. A., Feig, M., Brooks, C. L., 3rd, Fagnant, P. M., Lowey, S., & Trybus, K. M. (2014). Role of the essential light chain in the activation of smooth muscle myosin by regulatory light chain phosphorylation. *Journal of Structural Biology*, *185*(3), 375–382.

Teng, K. W., Ren, P., & Selvin, P. R. (2018). Delivery of Fluorescent Probes Using Streptolysin O for Fluorescence Microscopy of Living Cells. *Current Protocols in Protein Science / Editorial Board, John E. Coligan... [et Al.]*, *93*(1), e60.

Thacker, R. W., Díaz, M. C., Kerner, A., Vignes-Lebbe, R., Segerdell, E., Haendel, M. A., & Mungall, C. J. (2014). The Porifera Ontology (PORO): enhancing sponge systematics with an anatomy ontology. *Journal of Biomedical Semantics*, *5*(1), 39.

Thomas, T., Moitinho-Silva, L., Lurgi, M., Björk, J. R., Easson, C., Astudillo-García, C., Olson, J. B., Erwin, P. M., López-Legentil, S., Luter, H., Chaves-Fonnegra, A., Costa, R., Schupp, P. J., Steindler, L., Erpenbeck, D., Gilbert, J., Knight, R., Ackermann, G., Victor Lopez, J., … Webster, N. S. (2016). Diversity, structure and convergent evolution of the global sponge microbiome. *Nature Communications*, *7*, 11870.

Tompkins-MacDonald, G. J., Gallin, W. J., Sakarya, O., Degnan, B., Leys, S. P., & Boland, L. M. (2009). Expression of a poriferan potassium channel: insights into the evolution of ion channels in metazoans. *The Journal of Experimental Biology*, *212*(6), 761–767.

Uhlenhaut, N. H., & Treier, M. (2006). Foxl2 function in ovarian development. *Molecular Genetics and Metabolism*, *88*(3), 225–234.

Usaj, M., & Kanduser, M. (2012). The systematic study of the electroporation and electrofusion of B16-F1 and CHO cells in isotonic and hypotonic buffer. *The Journal of Membrane Biology*, *245*(9), 583–590.

Van Der Ven, P. F. M., Ehler, E., Perriard, J.-C., & Fürst, D. O. (1999). Thick filament assembly occurs after the formation of a cytoskeletal scaffold. *Journal of Muscle Research and Cell Motility*, *20*(5), 569–579.

Vartiainen, M. K., Guettler, S., Larijani, B., & Treisman, R. (2007). Nuclear Actin Regulates Dynamic Subcellular Localization and Activity of the SRF Cofactor MAL. In *Science* (Vol. 316, Issue 5832, pp. 1749–1752). https://doi.org/10.1126/science.1141084

Velasquez, L. S., Sutherland, L. B., Liu, Z., Grinnell, F., Kamm, K. E., Schneider, J. W., Olson, E. N., & Small, E. M. (2013). Activation of MRTF-A–dependent gene expression with a small molecule promotes myofibroblast differentiation and wound healing. *Proceedings of the National Academy of Sciences of the United States of America*, *110*(42), 16850–16855.

Vining, K. H., & Mooney, D. J. (2017). Mechanical forces direct stem cell behaviour in development and regeneration. *Nature Reviews. Molecular Cell Biology*, *18*(12), 728–742.

Víteček, J., Lojek, A., Valacchi, G., & Kubala, L. (2012). Arginine-based inhibitors of nitric oxide synthase: therapeutic potential and challenges. *Mediators of Inflammation*, *2012*, 318087.

Vyver, G., & Willenz, P. (1975). An experimental study of the life-cycle of the fresh-water spongeEphydatia fluvitilis in its natural surroundings. *Development Genes and Evolution*, *177*(1), 41–52.

Wagner, G. P. (2014). Homology, genes, and evolutionary innovation. Princeton, NJ: Princeton University Press.

Waheed, A., Ludtmann, M. H. R., Pakes, N., Robery, S., Kuspa, A., Dinh, C., Baines, D., Williams, R. S. B., & Carew, M. A. (2014). Naringenin inhibits the growth of D ictyostelium and MDCK-derived cysts in a TRPP2 (polycystin-2)-dependent manner. *British Journal of Pharmacology*, *171*(10), 2659–2670.

Wainright, P., Hinkle, G., Sogin, M., & Stickel, S. (1993). Monophyletic origins of the metazoa: an evolutionary link with fungi. In *Science* (Vol. 260, Issue 5106, pp. 340–342). https://doi.org/10.1126/science.8469985

Wakatsuki, T., Schwab, B., Thompson, N. C., & Elson, E. L. (2001). Effects of cytochalasin D and latrunculin B on mechanical properties of cells. *Journal of Cell Science*, *114*(Pt 5), 1025–1036.

Wake, D. B. (2007). Homoplasy, Homology and the Problem of "Sameness" in Biology. In *Novartis Foundation Symposia* (pp. 24–46). https://doi.org/10.1002/9780470515655.ch3

Wallman J, Staak C, Luge E. (1990). Einfache methode zur isolierung von immunoglobulin (Y) aus eiern immunisierter Hühner, *J. Vet. Med.* **B37**, 317–320.

Wang, C. L. A. (2008). Caldesmon and the regulation of cytoskeletal functions. *Advances in Experimental Medicine and Biology*, *644*, 250–272.

Wang, Z., Wang, D.-Z., Pipes, G. C. T., & Olson, E. N. (2003). Myocardin is a master regulator of smooth muscle gene expression. *Proceedings of the National Academy of Sciences of the United States of America*, *100*(12), 7129–7134.

Webb, R. C. (2003). Smooth muscle contraction and relaxation. *Advances in Physiology Education*, *27*(1-4), 201–206.

Wei, K., Che, N., & Chen, F. (2007). Myocardin-related transcription factor B is required for normal mouse vascular development and smooth muscle gene expression. *Developmental Dynamics: An Official Publication of the American Association of Anatomists*, *236*(2), 416–425.

Weiss, A., & Leinwand, L. A. (1996). THE MAMMALIAN MYOSIN HEAVY CHAIN GENE FAMILY. In *Annual Review of Cell and Developmental Biology* (Vol. 12, Issue 1, pp. 417–439). https://doi.org/10.1146/annurev.cellbio.12.1.417

Weissenfels, N. (1992). The filtration apparatus for food collection in freshwater sponges (Porifera, Spongillidae). *Zoomorphology*, *112*(1), 51–55.

Wictome, M., Henderson, I., Lee, A. G., & East, J. M. (1992). Mechanism of inhibition of the calcium pump of sarcoplasmic reticulum by thapsigargin. *Biochemical Journal*, *283 (Pt 2)*, 525–529.

Wiens, M., Krasko, A., Müller, C. I., & Müller, W. E. G. (2000). Molecular Evolution of Apoptotic Pathways: Cloning of Key Domains from Sponges (Bcl-2 Homology Domains and Death Domains) and Their Phylogenetic Relationships. In *Journal of Molecular Evolution* (Vol. 50, Issue 6, pp. 520–531). https://doi.org/10.1007/s002390010055

Wiens, M., Krasko, A., Perovic, S., & Müller, W. E. G. (2003). Caspase-mediated apoptosis in sponges: cloning and function of the phylogenetic oldest apoptotic proteases from Metazoa. In *Biochimica et Biophysica Acta (BBA) - Molecular Cell Research* (Vol. 1593, Issues 2-3, pp. 179–189). https://doi.org/10.1016/s0167-4889(02)00388-9

Wiesinger, H. (2001). Arginine metabolism and the synthesis of nitric oxide in the nervous system. *Progress in Neurobiology*, *64*(4), 365–391.

Wijesena, N., Simmons, D. K., & Martindale, M. Q. (2017). Antagonistic BMP–cWNT signaling in the cnidarian Nematostella vectensis reveals insight into the evolution of mesoderm. *Proceedings of the National Academy of Sciences of the United States of America*, *114*(28), E5608–E5615.

Wilkinson, C. R., & Vacelet, J. (1979). Transplantation of marine sponges to different conditions of light and current. In *Journal of Experimental Marine Biology and Ecology* (Vol. 37, Issue 1, pp. 91–104). https://doi.org/10.1016/0022-0981(79)90028-5

Wilson, H. V. (1907). On some phenomena of coalescence and regeneration in sponges. In *Journal of Experimental Zoology* (Vol. 5, Issue 2, pp. 245–258). https://doi.org/10.1002/jez.1400050204

Winder, S. J., & Walsh, M. P. (1993). Calponin: thin filament-linked regulation of smooth muscle contraction. *Cellular Signalling*, *5*(6), 677–686.

Windsor, P. J., & Leys, S. P. (2010). Wnt signaling and induction in the sponge aquiferous system: evidence for an ancient origin of the organizer. In *Evolution & Development* (Vol. 12, Issue 5, pp. 484–493). https://doi.org/10.1111/j.1525-142x.2010.00434.x

Wolenski, F. S., Layden, M. J., Martindale, M. Q., Gilmore, T. D., & Finnerty, J. R. (2013). Characterizing the spatiotemporal expression of RNAs and proteins in the starlet sea anemone, Nematostella vectensis. *Nature Protocols*, *8*(5), 900–915.

Woodhead, J. L., -Q. Zhao, F., & Craig, R. (2013). Structural basis of the relaxed state of a Ca2 -regulated myosin filament and its evolutionary implications. In *Proceedings of the National Academy of Sciences* (Vol. 110, Issue 21, pp. 8561–8566). https://doi.org/10.1073/pnas.1218462110

Wu, X., Clack, B. A., Zhi, G., Stull, J. T., & Cremo, C. R. (1999). Phosphorylation-dependent structural changes in the regulatory light chain domain of smooth muscle heavy meromyosin. *The Journal of Biological Chemistry*, *274*(29), 20328–20335.

Xu, Y., Luo, Y., Liang, C., Xing, W., & Zhang, T. (2018). A regulation loop between Nrf1α and MRTF-A controls migration and invasion in MDA-MB-231 breast cancer cells. *International Journal of Molecular Medicine*, *42*(5), 2459–2468.

Yamashiro, S., Cox, E. A., Baillie, D. L., Hardin, J. D., & Ono, S. (2008). Sarcomeric actin organization is synergistically promoted by tropomodulin, ADF/cofilin, AIP1 and profilin in C. elegans. *Journal of Cell Science*, *121*(Pt 23), 3867–3877.

Yu, H., Chakravorty, S., Song, W., & Ferenczi, M. A. (2016). Phosphorylation of the regulatory light chain of myosin in striated muscle: methodological perspectives. *European Biophysics Journal: EBJ*, *45*(8), 779–805.

Yu, R., & Ono, S. (2006). Dual roles of tropomyosin as an F-actin stabilizer and a regulator of muscle contraction in Caenorhabditis elegans body wall muscle. *Cell Motility and the Cytoskeleton*, *63*(11), 659–672.

Yu, Y. T. (1996). Distinct domains of myocyte enhancer binding factor-2A determining nuclear localization and cell type-specific transcriptional activity. *The Journal of Biological Chemistry*, *271*(40), 24675–24683.

Yu-Wai-Man, C., Spencer-Dene, B., Lee, R. M. H., Hutchings, K., Lisabeth, E. M., Treisman, R., Bailly, M., Larsen, S. D., Neubig, R. R., & Khaw, P. T. (2017). Local delivery of novel MRTF/SRF inhibitors prevents scar tissue formation in a preclinical model of fibrosis. *Scientific Reports*, *7*(1), 518.

Zapata, F., Goetz, F. E., Smith, S. A., Howison, M., Siebert, S., Church, S. H., Sanders, S. M., Ames, C. L., McFadden, C. S., France, S. C., Daly, M., Collins, A. G., Haddock, S. H. D., Dunn, C. W., & Cartwright, P. (2015). Phylogenomic Analyses Support Traditional Relationships within Cnidaria. *PloS One*, *10*(10), e0139068.

Zhang, W., Bhetwal, B. P., & Gunst, S. J. (2018). Rho kinase collaborates with p21-activated kinase to regulate actin polymerization and contraction in airway smooth muscle. *The Journal of Physiology*, *596*(16), 3617–3635.

Zhao, F., Li, P., Chen, S. R., Louis, C. F., & Fruen, B. R. (2001). Dantrolene inhibition of ryanodine receptor Ca2+ release channels. Molecular mechanism and isoform selectivity. *The Journal of Biological Chemistry*, *276*(17), 13810–13816.

Zhao, X.-H., -H. Zhao, X., Laschinger, C., Arora, P., Szaszi, K., Kapus, A., & McCulloch, C. A. (2007). Force activates smooth muscle -actin promoter activity through the Rho signaling pathway. In *Journal of Cell Science* (Vol. 120, Issue 10, pp. 1801–1809). https://doi.org/10.1242/jcs.001586

Zhao, Y., Zheng, Z., Cohen, C. J., Gattinoni, L., Palmer, D. C., Restifo, N. P., Rosenberg, S. A., & Morgan, R. A. (2006). High-efficiency transfection of primary human and mouse T lymphocytes using RNA electroporation. *Molecular Therapy: The Journal of the American Society of Gene Therapy*, *13*(1), 151–159.

Zhou, N., Lee, J.-J., Stoll, S., Ma, B., Costa, K. D., & Qiu, H. (2017). Rho Kinase Regulates Aortic Vascular Smooth Muscle Cell Stiffness Via Actin/SRF/Myocardin in Hypertension. *Cellular Physiology and Biochemistry: International Journal of Experimental Cellular Physiology, Biochemistry, and Pharmacology*, *44*(2), 701–715.

Zuker, M. (2003). Mfold web server for nucleic acid folding and hybridization prediction. *Nucleic Acids Research*, *31*(13), 3406–3415.

Appendix I: Supplemental Figures

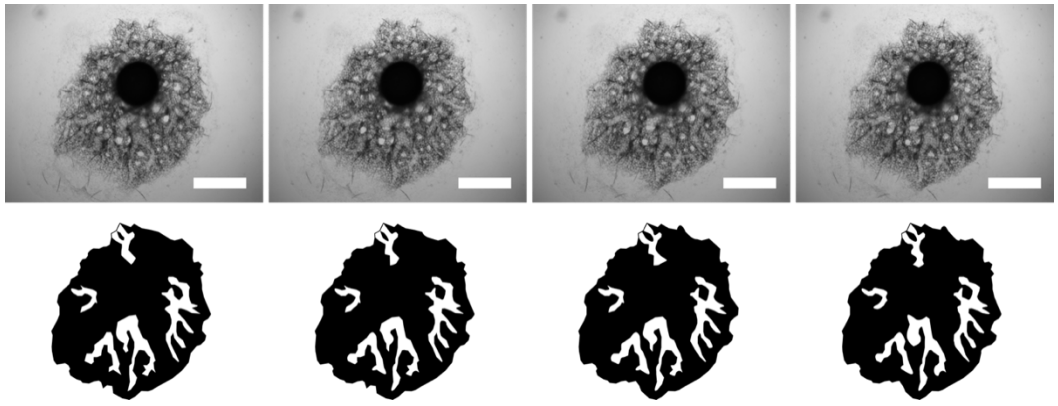

Figure S1. Time lapse series of *E. muelleri* without inducing a contraction. Sample was prepared for imaging in the same manner as induced sponges but only treated with lake water. Panels represent time points 0, 30, 60, and 90 minutes. Bottom panels show outlines of major excurrent canals over the time course. Some random movement and localized constrictions can be seen in this tissue, but coordinated contractions are not evident. Scale bars 500μm.

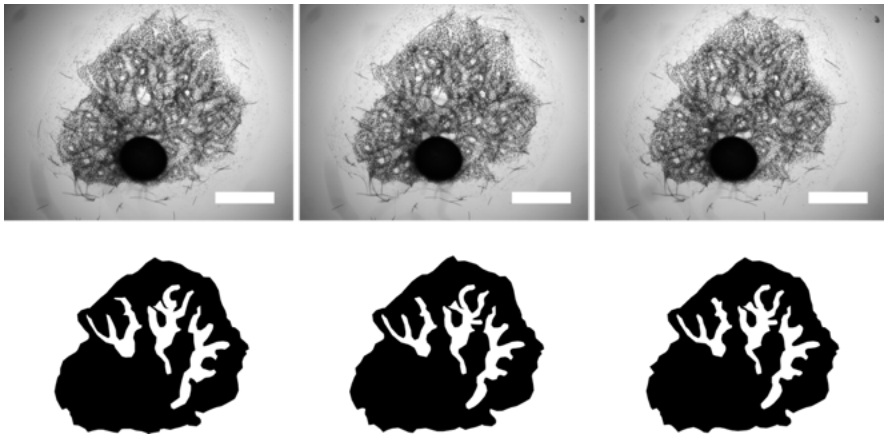

Figure S2. Time series of sponge treated with 30mM NaCl. Sponge was staged as before and treated with 30mM NaCl in lake water. Frames represent time points 0, 30, and 60 minutes. Bottom panel shows outlines of major excurrent canals. Little change is seen in the size of the canals, though they do reduce in diameter in the first 30 minutes. There is no evidence of major tissue rupture over the course of the 60 minutes of imaging. Scale bars 500μm.

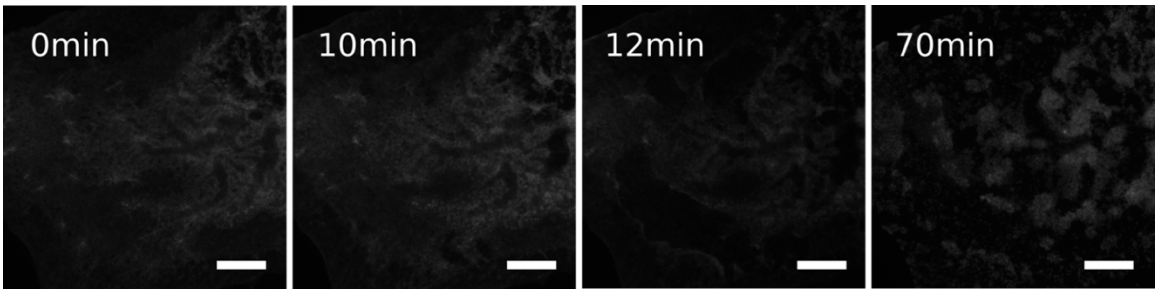

Figure S3. First trial live imaging with FluoVolt™ dye. Samples were stained and prepared for imaging and contractions were triggered with 1:1000 sumi ink in lake water. Over the first 10 minutes there is what appears to be a slight increase in fluorescent signal. Between 10 and 12 minutes, signal dramatically decreases as the tissue appears to lose integrity. Over the next 58 minutes, some signal returns, but there is excessive tissue damage through the body. Scale bars 200μm.

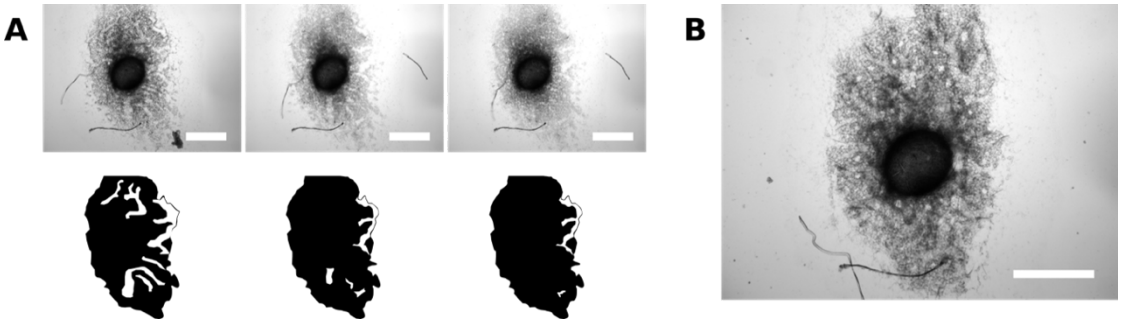

Figure S4. Strength of contraction is concentration dependent. **(a)** Time lapse series of a sponge treated with 3μM ionomycin. Frames represent time points 0, 20, and 40 minutes and bottom panel depicts outline of major excurrent canals. There is a strong contraction of both the incurrent and excurrent canals during the first 20 minutes, which persisted over the next 20 minutes. **(b)** The same sponge 18 hours after treatment, following washing with lake water, showing a return to a normal relaxed state. Scale bars 500μm.

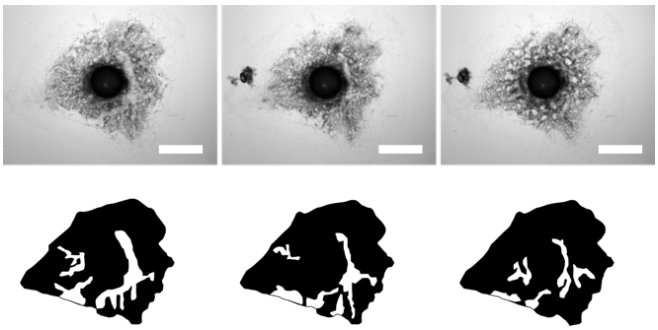

Figure S5. Contractions do not require external Ca^{2+}. Time lapse series of sponge maintained in CFM that was treated with 300nM ionomycin. Frames represent time points 0, 20, and 40 minutes. Bottom panel shows outline of major excurrent canals. Scale bars 500μm.

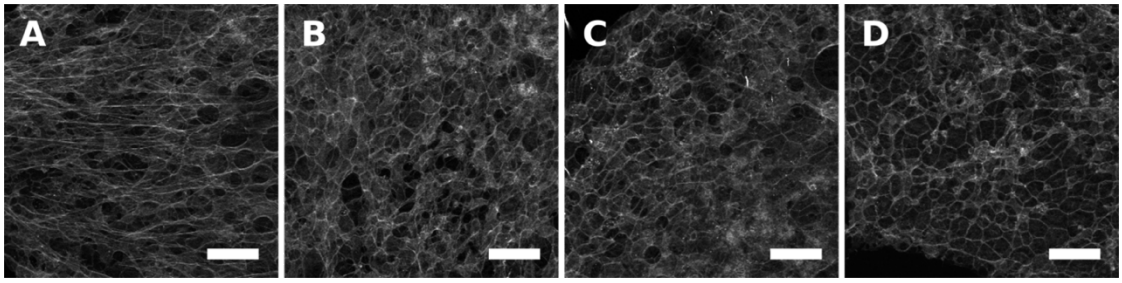

Figure S6. Concentration series of latrunculin B treatment. General actin staining reveals major tissues that are affected by different concentrations of latrunculin B following 20 minute treatment. **(a)** 2nM, **(b)** 5nM, **(c)** 10nM, and **(d)** 25nM. Scale bars 50μm.

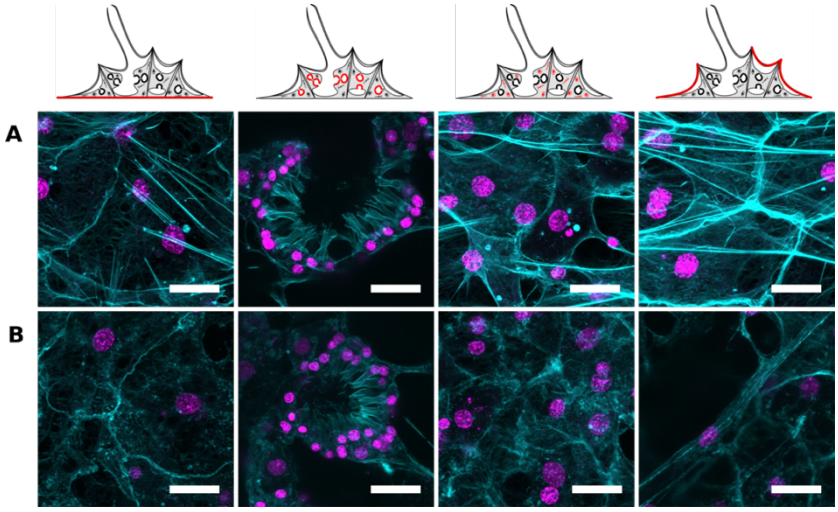

Figure S7. Cellular structures have different stability following treatment. Confocal images of phalloidin labeled sponges (cyan) following 20 minute treatment with either 2nM **(a)** or 25nM **(b)** latrunculin B. DNA in magenta. Scale bars 10μm.

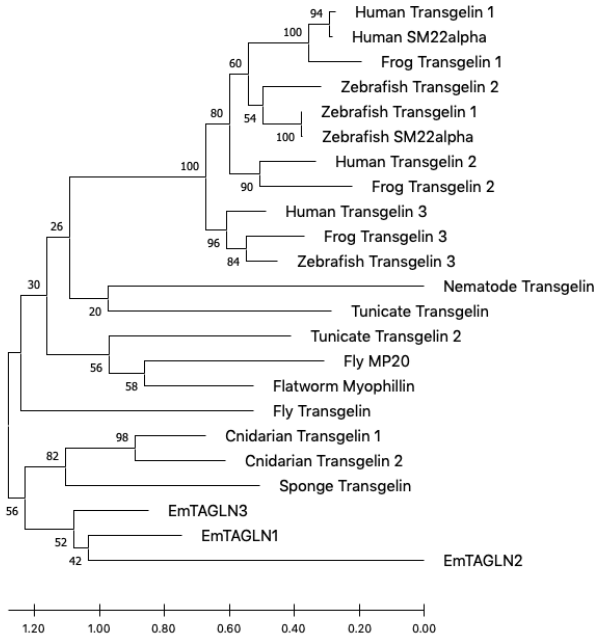

Figure S8. *E. muelleri* transgelins represent a lineage specific expansion. Maximum likelihood phylogeny of transgelin family proteins from a variety of animals. Proteins grouping fit nicely with the phylogenetic positions of the animal source, which suggests an expansion prior to the vertebrate radiation as well as in non-bilaterian lineages. Support values are based on 100 bootstrap iterations.

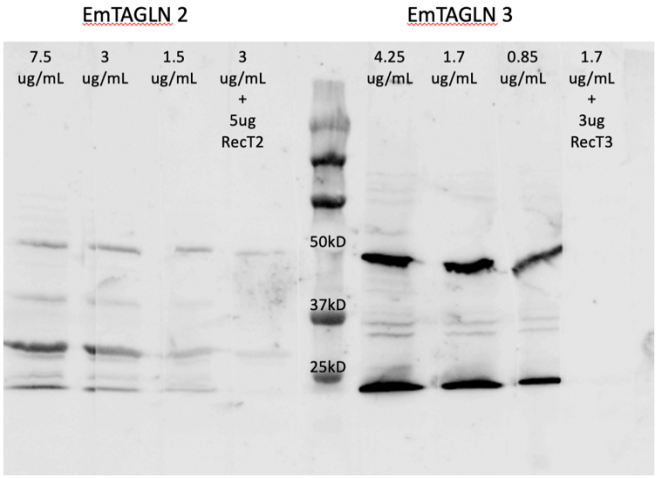

Figure S9. Western blot of sponge whole cell lysates with anti-EmTAGLN2 and anti-EmTAGLN3. Low molecular weight bands correspond with the predicted size of the proteins. Concetnration of antibody use on each strip is shown at the top. The middle concentration was competed with excess recombinant protein and appeared to abolish banding pattern in both cases.

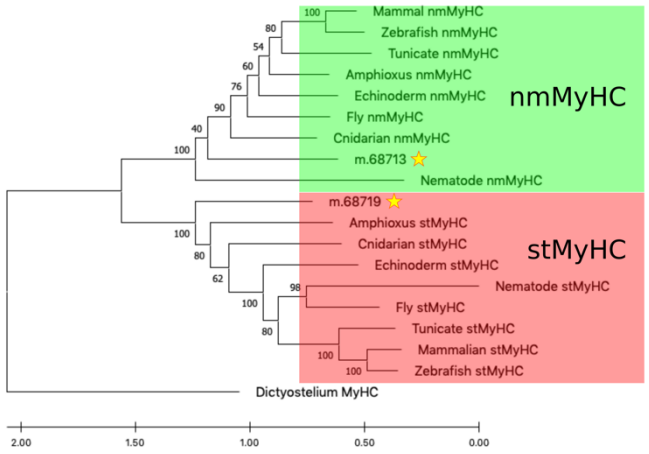

Figure S10. *E. muelleri* has a nmMyHC and stMyHC. The type II MyHC proteins found in *E. muelleri* (labeled with stars) fall into either stMyHC clade or nmMyHC clade. Phylogeny determined by maximum likelihood method. Tree rooted with MyHC from *Dictyostelium.* Support values represent 1000 bootstrap iterations.

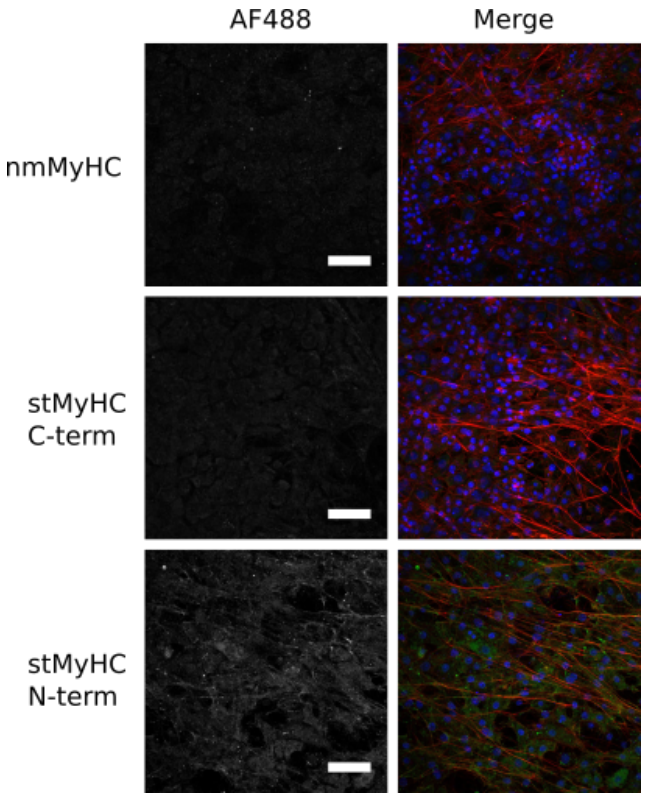

Figure S11. Initial staining do not provide intrepatble patterns. Immunostaining with anti-nmMyHC, anti-stMyHC C-term, and anti-stMyHC N-term using standard 3.7% formaldehyde in EtOH fixation. Counter stained for actin (Red) and DNA (blue). Scale bars 20µm.

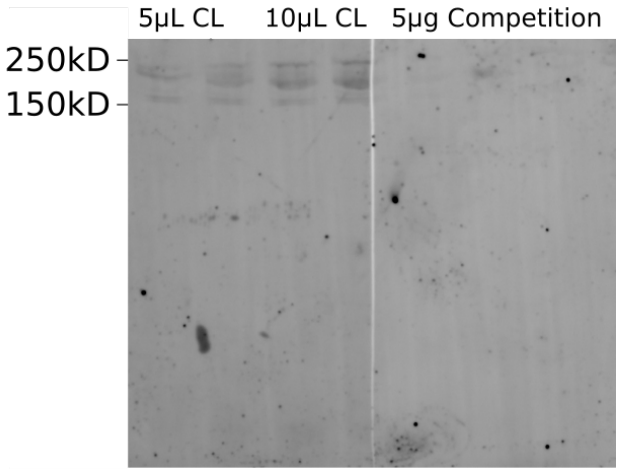

Figure S12. Western blot with anti-stMyHC N-term. Western blot showed a bands between 250kD and 150kD which seem to correlated with the predicted size of the protein (~230kD). The additional bands could correlate with degradation products or levels of phosphorylation on the MyHC as there are many documented sites. Bands intensify with increased concentration of cell lysates (CL). Pre-incubation of the antibody with 5µg of recombinant proteins abolishes signal.

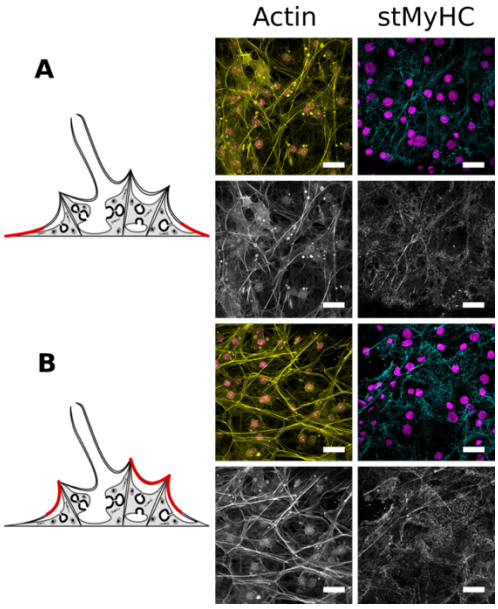

Figure S13. EmstMyHC staining resembles structures seen in the endopinacoderm. Comparative images of sponges stained for actin (yellow) and stMyHC (cyan) both counterstained for DNA (magenta). **(a)** Near the edge of the apical pinacoderm, staining for stMyHC resembles the actin-based structures in the endopinacoderm that extend down towards the attachment epithelium. **(b)** Over the body of the sponge, linear bundles of stMyHC strongly resemble the actin bundles running through the endopinacoderm and not the cortical actin structures of the exopinacoderm. Scale bars 10µm.

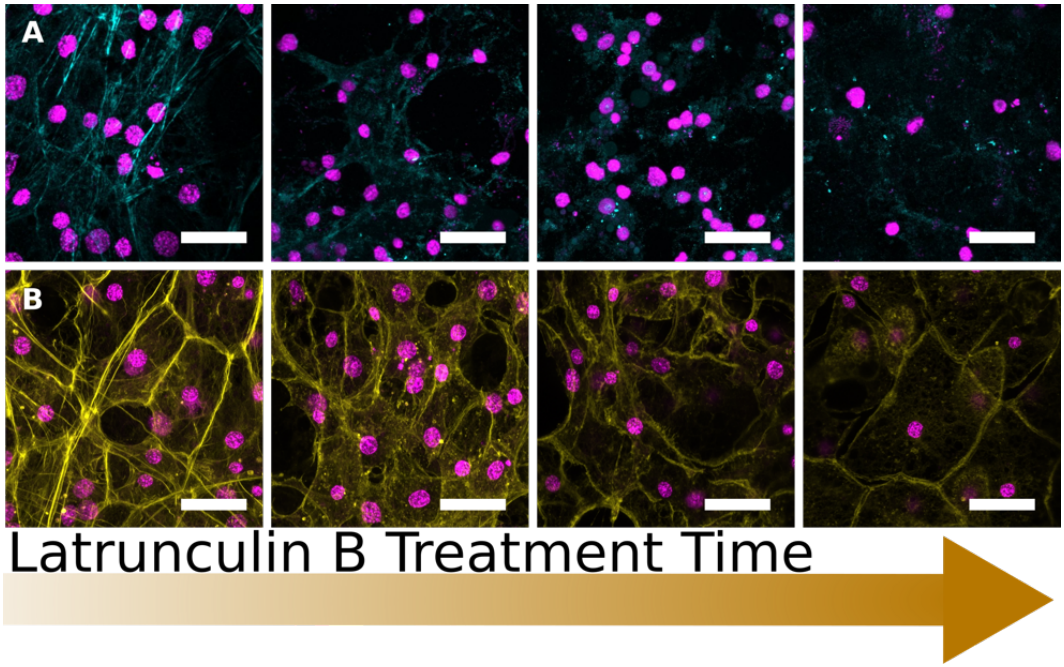

Figure S14. Treatment with latrunculin B leads to a loss of stMyHC structures with similar dynamics to loss of actin tracts. Sponges were treated with 25µM latrunculin B for either 1, 5, 10, or 30 minutes prior to fixation. **(a)** stMyHC (cyan) structures begin to decrease over the first 5 minutes and are completely absent by 30 minutes. **(b)** Comparatively timed actin staining (yellow) shows the loss of actin tracts over a similar timespan, followed by the apparent disruption of endopinacoderm by 30 minutes. DNA in magenta. Scale bars 20µm.

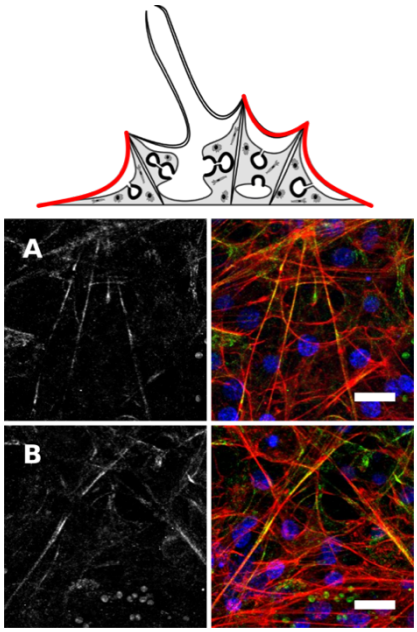

Figure S15. pRLC staining occurs at some but not all actin tracts. Confocal images of sponges stained for pRLC (green), actin (red), and DNA (blue), with pRLC channels shown in gray scale. **(a)** Branching actin tracts show differences in amount of pRLC staining. **(b)** In regions with many actin tracts running through, only some pRLC show signal which is not ubiquitous across them. Scale bars 10μm.

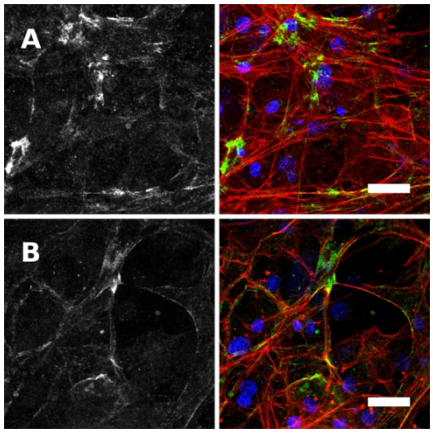

Figure S16. Treatment with MLCK inhibitor peptide 18 did not affect pRLC staining or sponge's ability to contract. Sponges were induced to contract with 500nM thapsigargin prior to fixation and staining for pRLC (green), actin (red), and DNA (blue). Raw pRLC staining in gray scale on left. **(a)** Control sponges show strong punctate pRLC in a fully contracted state. **(b)** Sponges treated with peptide-18 show a similar staining pattern following an induced contraction. Scale bars 20μm.

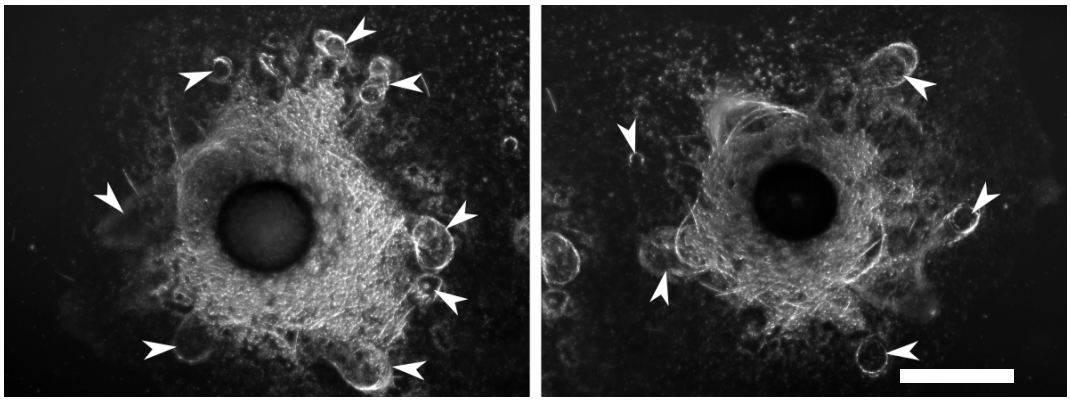

Figure S17. Blebbistatin treatment results in extra oscula. Examples of juvenile sponges treated for 24 hours with 50µM blebbistatin. Images were taken using phase contrast microscopy to help visualize the location of oscula. White arrows indicate location of developing or developed oscula. Scale bar 500µm.

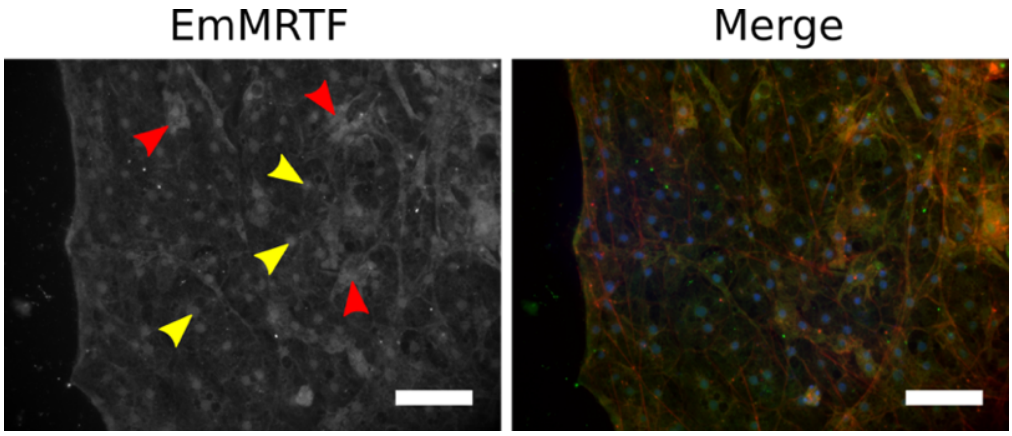

Figure S18. Immunostaining for EmMRTF show cytoplasmic and nuclear pools. Epifluorescent images of sponge stained for EmMRTF (green), actin (red), and DNA (blue), with raw green channel on left. Signal in green channel appears primarily nuclear in some cells (yellow arrowheads) and broadly cytoplasmic in others (red arrowheads). Scale bars 50µm

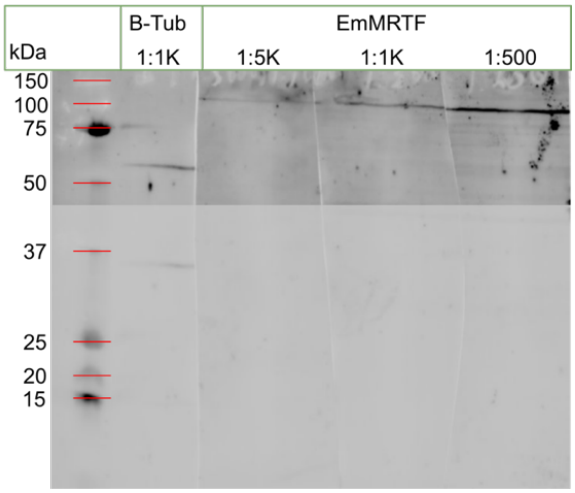

Figure S19. Western blot of sponge cell lysates shows a band at the predicted size of EmMRTF. Increasing concentrations of anti-EmMRTF from left to right, shows increased signal at the band. In the 1:500 dilution there is a faint band slightly below the band. Exposure increased on upper portion of blot to help visualize the band patterns.

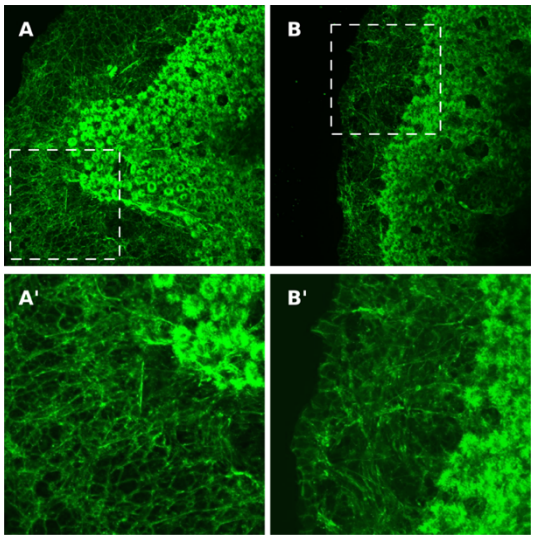

Figure S20. Sponges treated with MRTF inhibitor have disordered actin in pinacoderm. Treated sponges stained for actin. **(a)** Control sponges, actin bundles that radiate from the choanoderm towards the edge of the sponge, with bundles running perpendicular towards the edge. **(b)** Following treatment with CCG-203791, these bundles are reduced and run in random directions of through the tissue. **(a'&b')** are zooms of the regions indicated by the white box.

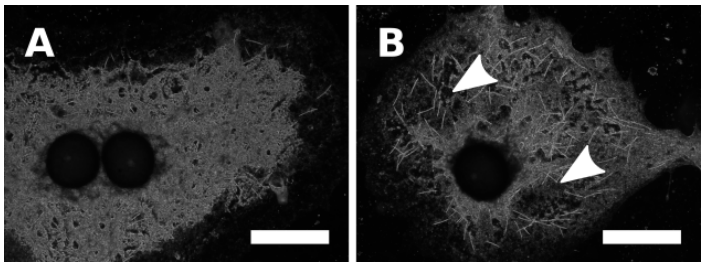

Figure S21. Treatment of developing sponges with ISX9 results in enlarged canals. Sponges were treated with ISX9 beginning at tent stage. Imaging was done using phase contrast to aid in visualizing major canal structure. **(a)** DMSO treated control sponges. **(b)** ISX9 treated sponges show a constricted choanoderm with what appears to be expanded canals. Scale bars 500μm.

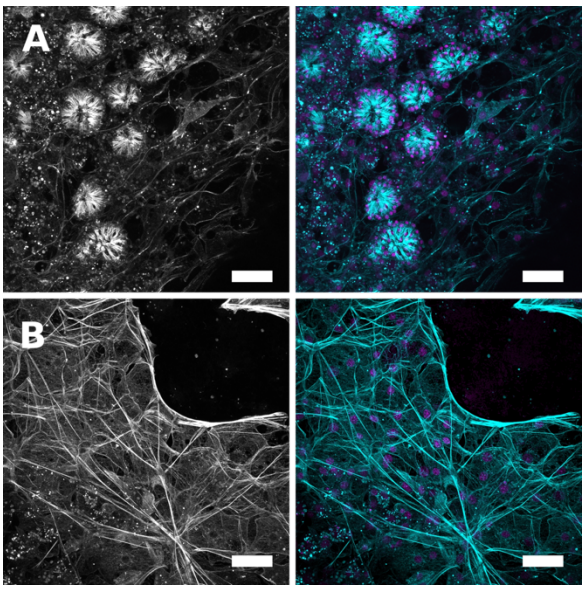

Figure S22. Actin tracts develop following reattachment. Sponges were maintained for 3 days in attachment free environment and then allowed to settle. These were then fixed and stained for actin (cyan) and DNA (magenta), with raw actin channel shown in grayscale. **(a)** Confocal image of newly attached sponge shows actin tracts organizing above the choanocyte chambers. **(b)** Confocal image of the edge of the sponge following re-attachment shows actin tracts extending through the apical pinacoderm from basopinacocytes. Scale bars 20μm.

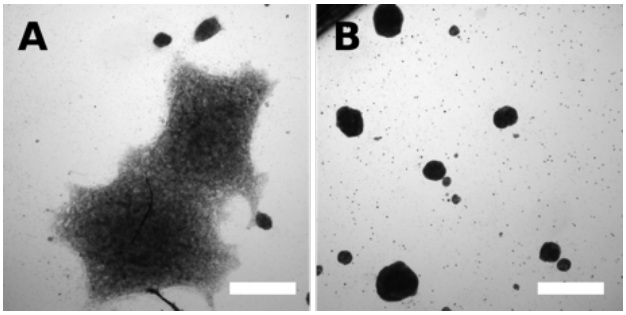

Figure S24. Blebbistatin does not prevent aggregation but does prevent reattachment. Dissociated cells were treated with blebbistatin and allowed to settle. **(a)** DMSO treated aggregates. **(b)** Blebbistatin treated aggregates maintained their structure, but did not reattach to the substrate. Scale bars 200µm.

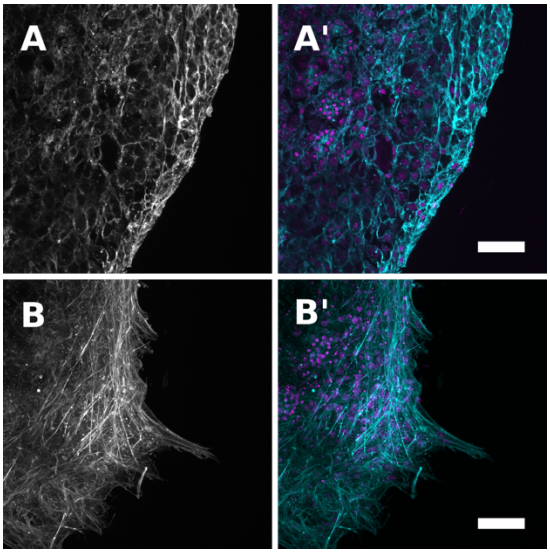

Figure S25. Actin bundles in ISX9 treated aggregates are absent in controls. **(a)** Actin staining of control aggregate. **(a')** Merge of actin (cyan) and DNA (magenta) show that actin towards the edge appears to be cortical actin of individual cells, while structures towards the body are developing choanocyte chambers. **(b)** Actin staining of ISX9 treated aggregate shows linear actin bundles running through the tissue near the edge of the aggregate. **(b')** Merge of actin (cyan) and DNA (magenta) shows a fairly consistent number of cells with the control, suggesting these are tissue spanning structures. Developing choanocyte chambers are still visible towards the body. Scale bars 20µm.

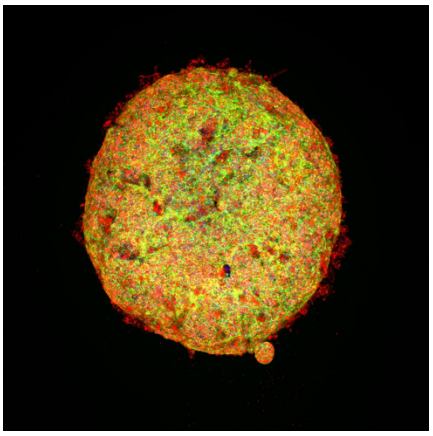

Figure S23. Latrunculin B does not disrupt aggregation but prevents development. Dissociated cells were treated with latrunculin B. Aggregates formed and were fixed and stained for actin (green) and tubulin (red). These aggregates appear as a dense mass of cells, which were adherent to each other. Scale bars 50μm**.**

Appendix II: Technique Development

Introduction

A good amount of my work has been toward further developing *Ephydatia muelleri* as a functional model system. Some techniques I have worked on or developed have shown promise but yielded results that do not directly add to the questions I have been addressing with work. In this section I will focus on these techniques as well as some future directions for them. I would also like to include some negative results, which I feel should be recorded, both for what can be learned of the techniques but also about the underlying biology. *E. muelleri* is adaptable to the laboratory environment in that they form overwintering structures, termed gemmules, which are filled with pluripotent stem cells (Simpson, n.d.; Barbeau, Reiswig, & Rath, 1989). This occurs seasonally in the Rocky Mountains, as the high alpine lakes that they occupy freeze over. As the weather warms, the cells migrate out of the gemmules to rebuild the tissues of the adult sponge. Since individuals produce thousands of gemmules each season. Adult tissue containing gemmules can be collected and transferred to the laboratory where they are stored at 4^{o}C, which maintains their dormant state. A single gemmule can then be plated in LW at room temperature and it will develop into a juvenile sponge, which contains all the tissues seen in the adult, within 4-6 days. Gemmules produced by an individual sponge are genetically clonal, and since a section of adult tissue contains thousands of gemmules, we can consistently work in the same genetic background. This type of asexual reproduction makes them well suited for growing under laboratory conditions. Sponges do reproduce sexually as well. Gametogenesis has been studied in a variety of sponges and usually

originates in archeocytes (which generally form oocytes) (Saller, 1988). Choanocytes have also been shown to undergo gametogenesis and generally give rise to sperm (Saller, 1988; Paulus & Weissenfels, 1986; Gaino et al., 1984). The sperm can be released into the water column where they are drawn in by other sponges to fertilize eggs (Paulus & Weissenfels, 1986). After fertilization, sponges often brood them embryos prior to release (Leys & Ereskovsky, 2006). Specific cues regulating gametogenesis have not been identified though things such as water temperature and the lunar cycle have been observed to correlate (Fromont, 1999; Mercurio et al., 2007; Riesgo et al., 2007). The lack of a distinct germline as well as no known methods of inducing gametogenesis and limited access to brooding embryos means that we do not have access to oocytes or zygotes for injection and we do not have means of establishing a transgenic line. This is a major limitation for doing functional work that we have been focused on addressing and trying to overcome.

Apart from the limited functional techniques available, established protocols for many traditional molecular biology techniques have not yet been adapted.

In situ Hybridization in Ephydatia muelleri

Background

In order to try and understand the function of a protein, one of the first questions is when and where is it expressed in the animal. This is a particularly effective tool when looking at developmental patterning genes. However, there are currently no published protocols for this technique in freshwater sponges. There have been published studies utilizing this technique in *E. muelleri* or closely related species (Funayama et al., 2005;

Funayama et al., 2005; Steinmetz et al., 2012; Alié et al., 2015; Hall et al., 2019), but these seem to only work consistently for very highly expressed targets. I initially worked on refining colorimetric *in situ* hybridization (CISH) methods and then switched focus to fluorescent *in situ* hybridization (FISH). Our basic protocol for CISH was to use digoxigenin (DIG) labeled RNA probes and anti-DIG AP antibodies to detect signal. This is a cost effective and practical method for *E. muelleri* in that it gives control over the level of development and allows for viewing of the expression pattern in brightfield. This is beneficial in sponges because of the irregular and plastic nature of their body plan which makes it difficult to orient oneself when viewing the tissues. *E. muelleri* also shows a high amount of auto-fluorescent background as a result of both aldehyde-based fixations and photosynthetic symbionts which means fluorescent probe signal needs to be high to overcome this. One of the major drawbacks of CISH is the high heat needed during the hybridization. In order to increase penetration of the probe through tissue, this step is generally performed with gentle rocking in the protocols for other organisms. However, in *E. muelleri* this tends to lead to loss of most of the tissue, which can occur during washing steps as well. In order to overcome this, either lower temperatures are used, or samples need to be kept still. To limit these effects, hydrolyzed or shorter probes can be used which can increase penetration and limit the formation of secondary structures that require high temperature to disrupt. However, this also increases non-specific binding and limits the amount of signal at each binding event. Most of my initial effort was placed on increasing the amount of tissue preservation while maintaining the temperatures used.

FISH is an effective method with the benefit of allowing for multiplexed experiments. RNA transcript painting can be performed using a mixture of small labeled probes that target different fragments of the transcript (Orjalo et al., 2011). This can allow visualization of very lowly expressed targets while providing the benefits of using small probes which include lower hybridization temperature. One of the largest initial challenges for this technique is finding an effective counterstain to visualize the call and tissue type in which staining is present. During hybridization, the organic solvent formamide is used to lower the melting temperature of DNA and RNA to limit secondary structure of single strand units and limit non-specific probe binding. Formamide also destroys F-actin structures, which prevents the use of phalloidin AF™568 as a counter stain to visualize cell boundaries. Cell membranes are also destroyed during the process due to the combination of solvents and heat, in-order to permeabilize the cells for hybridization, which means membrane dyes cannot be used to visualize cell boundaries.

Another challenge for FISH is overcoming background fluorescence in the sponge tissue. As stated earlier, aldehyde fixatives, which are commonly used in *in situ* hybridization, can create fluorescent byproducts (Kiernan & Wessendorf, 2001), which could compete with probe signal during detection. *E. muelleri* also contain endosymbiotic algae which can show very brightly in the green, red, and far red channels. Because of this, specific signal from the probes must be strong enough to detect above this background and unbound/non-specific probes. A recently developed method for amplifying FISH signal is termed hybridization chain reaction (HCR) (Choi et al., 2018; Bi et al., 2017). This basic mechanism of this technique is to add an adapter sequence to the oligo probe. Signal is then detected and amplified using a set of labeled metastable

hairpin loop sequences. The hairpins are metastable in that the sequences on their two arms don't perfectly complement each other. In contrast, the sequences of the arms of the two sets have better complementation with each other. Therefore, when the two hairpins are mixed, they open up and bind with each other forming a long, discontinuously double strand which contains the summation of signal from each hairpin. The adapter sequence on the probe perfectly complements with the arm of one of the hairpins, which sets off the reaction in the tissue. In order to combat background signal from non-specifically bound probe, the adapter sequence can be split between two probes that bind closely on the target transcript. By doing this, only probes that are in close proximity (and therefore likely bound specifically) can cause the amplification cascade to initiate (Choi et al., 2018). This is a promising method for overcoming the limitations of FISH in *E. muelleri.*

Methods

CISH fixation

Gemmules were plated and hatched in LW+100µg/mL ampicillin on coverslips in a 6-well plate. Following hatching water was changed daily. At 4dph samples were viewed to confirm presence of choanocyte chambers and canals and then the coverslip was gently transferred to FluoroDish™ (WPI #FD35-100) filled with LW, and placed inverted on the edge of the internal well (**Figure A1a**). A small weight (weighted washer wrapped in parafilm) was placed on top of the coverslip to keep it from moving. Washes could then be added directly over the coverslip (which is the opposite the sponge side) and be allowed to mix by diffusion, or could be gently drawn under the coverslip by capillary action by placing a kimwipe on the opposite side of the well, both of which

should limited turbulent flow across the sponge. Once setup, sponges were washed in LW and then fixed in a two-step process of, 15 minutes in ice cold 4% (v/v) paraformaldehyde, 0.3 (v/v) glutaraldehyde in ¼ Holtfreter's solution (14.75mM NaCl, 0.17mM KCl, 0.19mM $CaCl_2$, 0.6mM $NaHCO_3$) at room temperature followed by 2 hours in ice cold 4% (v/v) paraformaldehyde in ¼ Holtfreter's solution at 4°C. Samples were then dehydrated by walking from 1:1 (v/v) MeOH:¼ Holtfreter's solution to 100% MeOH. Samples were then transferred to 100% EtOH and then clarified in 50% (v/v) xylene in EtOH for 30 minutes at room temperature. Samples were washed with 100% EtOH and then rehydrated by walking into 1x PBS. Samples were then washed with 1x PBS+0.1% Tween20 (PBST) and post fixed with 4% (v/v) paraformaldehyde in 1x PBST for 30 minutes at 4°C. Samples were washed in 1x PBST and pre-hybridized for 1 hour at 65°C in hybridization buffer (50% formamide, 5x SSC, 100mg/mL salmon sperm DNA, 100U/mL heparin, 10% (wt/v) dextran sulfate, 0.02% (wt/v) BSA, 0.1% (v/v) Tween20, and 1mM DTT). Samples were then incubated overnight with 1µg/mL of DIG-labeled probes in hybridization buffer at 65°C. Samples were then thoroughly washed in wash solution (50% formamide, 5x SSC, 0.1% (v/v) Tween20) at hybridization temperature. This was followed by washes at 50°C and then room temperature. Samples were then thoroughly washed with malic acid wash buffer (0.1M malic acid, 0.15M NaCl, 0.1% Triton X-100). Sample were blocked in 1% (wt/v) blocking reagent (Roche #11096176001) in malic acid wash buffer for 1 hour at room temperature. Samples were then incubated overnight at 4°C with 1:2000 (v/v) anti-DIG AP fab fragment in blocking solution. Samples were then washed thoroughly with malic acid wash buffer and transferred to NTMT buffer (100mM Tris (pH9.5), 100mM NaCl, 50mM $MgCl_2$, 0.1%

(v/v) Tween20). Visualization was performed with 175µg/mL BCIP and 225µg/mL NBT and incubating in the dark. Development was monitored closely and stopped by washing in 1x PBST. RNase control samples were, then treated with 10µg/mL of RNase A in 1x PBS for 1 hour at 37°C, washed thoroughly with 1x PBST and mounted on slides. For the RNase controls, hybridization should protect the probe from degradation by forming double stranded RNA, so loss of signal would mean that the probe is not bound specifically. Images for developed sponges were not taken as a color camera was not available.

FISH with Stellaris probes

Custom Stellaris FISH probes targeting *E. muelleri* stMyHC (Compagen m.68719) were ordered and designed by BioSearch Technologies (biosearchtech.com), which were resuspended in TE buffer to 20µM stock. Gemmules were plated and hatched in LW+100µg/mL ampicillin on coverslips in 6-well format and sponges were prepared as described above. Sponges were fixed in 4% (v/v) paraformaldehyde in ¼ Holtfreter's solution for 1 hour at 4°C. Samples were then washed with ¼ Holtfreter's solution followed by permeabilizing with 70% EtOH for 1 hour at 4°C. Samples were then washed with 1x PBS followed by wash buffer (50% formamide, 5x SSC, 0.1% (v/v) Tween20) for 5 minutes at room temperature. Probes were diluted 1:100 (v/v) in hybridization buffer and 100µL was added to sample and incubated for 4 hours at 37°C in the dark. Samples were then washed with 1x PBS and counter stained with 1:100 Hoechst dye in 1x PBS and mounted. For actin preservation, formamide concentration in the hybridization buffer was lowered to 20% and samples were counterstained with

phalloidin AF 568 (Life Technologies, 1:120). For RNase controls, samples were treated with 10µg/mL RNase A prior to the hybridization step, with the goal of removing mRNA targets prior to addition of the probe to identify possible non-specific binding.

FISH was also performed on isolated oscula. Isolation and immobilization of oscula is described in detail in the osculum isolation section below. Briefly, an osculum was removed and then fixed in 4% (v/v) paraformaldehyde in ¼ Holtfreter's solution to a poly-L-lysine coated Fluorodish™. Hybridization was performed as above, but with 30% formamide wash and hybridization buffer. Samples were also treated with phalloidin AF™ 568 (Life Technologies, 1:120) in 1x PBS for 40 minutes at room temperature just prior to the hybridization steps, with the hope that the phalloidin would stabilize the F-actin structures.

Confocal Images were acquired on an Olympus Fluoview FV3000 confocal laser scanning microscope using either a 60×/1.4 NA or 100×/1.4 NA objectives. Laser levels and acquisition setting were not adjusted for imaging controls. Images were processed in FIJI (Schindelin et al., 2012).

FISH using HCR probes

Probes were ordered from and designed by Molecular Technologies (moleculartechnologies.org) with 20 split probes targeting EmVin1 (Compagen m.284417). EmVin1 was chosen because we have a very good antibody against it and good understanding of protein localization, so clear expectations for expression patterns. Overall the protocol used followed the developer's from (Choi et al., 2018).

Sponges were prepared for FISH as described above. RNase inhibitor SUPERase.in (ThermoFisher Scientific #AM2694) was added to all buffers and washes. Samples were fixed in 4% (v/v) paraformaldehyde in ¼ Holtfreter's solution for 2 hours at 4ºC and then washed with ¼ Holtfreter's solution. A dehydration series was performed to transfer the samples to 100% MeOH, then 100% EtOH followed by a rehydration series into 1x PBST. Samples were digested with 5µg/mL proteinase K in 1x PBST for 2 minutes at room temperature. Digestion was halted with 2mg/mL glycine. Samples were then post-fixed in 4% (v/v) paraformaldehyde in 1x PBST for 1 hour at room temperature and washed into 2x SSC.

Hybridization and amplification steps were performed with supplied buffers (molecular technologies.org). Samples were washed with hybridization buffer at room temperature and then pre-hybridized for 1 hour in hybridization buffer at 37ºC. Samples were then hybridized with 10pmol of Odd/Even probes for 16 hours at 37ºC in humidified chambers. Just Odd, just Even, and no probe controls were all performed. Samples were then washed with wash buffer at hybridization temperature, transferred to 2x SSC, and brought to room temperature. Samples were pre-amplified in amplification buffer for 30 minutes at room temperature and amplification hairpins were prepared by heating and snap cooling of 24pmol of each labeled hairpin in amplification buffer. These were combined and added to sampled for 16 hours at room temperature in the dark. Samples were then washed with 1x PBST and stained with 1:100 Hoechst dye and 5µg/mL EtBr prior to mounting.

Confocal Images were acquired on an Olympus Fluoview FV3000 confocal laser scanning microscope using either a 60×/1.4 NA or 100×/1.4 NA objectives. Laser levels

and acquisition setting were not adjusted for imaging controls. Images were processed in FIJI (Schindelin et al., 2012).

Results

The altered fixation method was able to preserve a good amount of the tissue that had been damaged in previous methods (**Figure A1b&c**). However, this still did not show evidence of specific signal which persisted following RNase treatment. For the Stellaris probes, there was some signal across the whole body, but no detectable regions of increased intensity (**Figure 93**). Viewing the tissue using confocal microscopy showed some cells with what appeared to be increased signal (**Figure 94**). However, it was difficult to interpret this pattern due to the lack of counter stain to show the tissue/cell type location. Actin preservation methods did not change the staining pattern, but also did not allow for clear interpretations of the patterns (**Figure A2**). Choanocyte chambers were clearly visible but the remaining tissue was difficult to resolve. This is not surprising given the high degree of stability found in the microvilli collars of the choanocytes based on latrunculin B staining. Counter staining with ethidium bromide showed ubiquitous cytoplasmic (and nuclear) staining in all cells, which aided in identifying the tissue location of regions of interest (**Figure A3**). For these stainings,

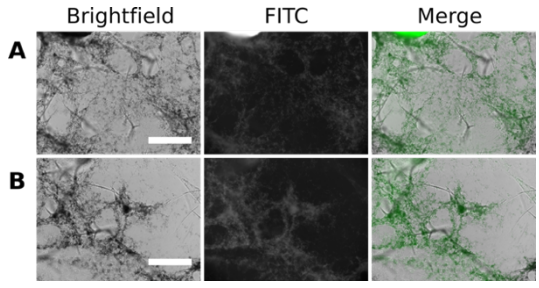

Figure 93. Stellaris probes targeting stMyHC show broad signal that is likely non-specific. (a) Sample treated with probes targeting stMyHC shown in brightfield and FITC channel. **(b)** Sample that was treated with RNase prior to hybridization to remove endogenous RNA targets. Staining pattern remains very similar as in **(a)**. Scale bars 100μm.

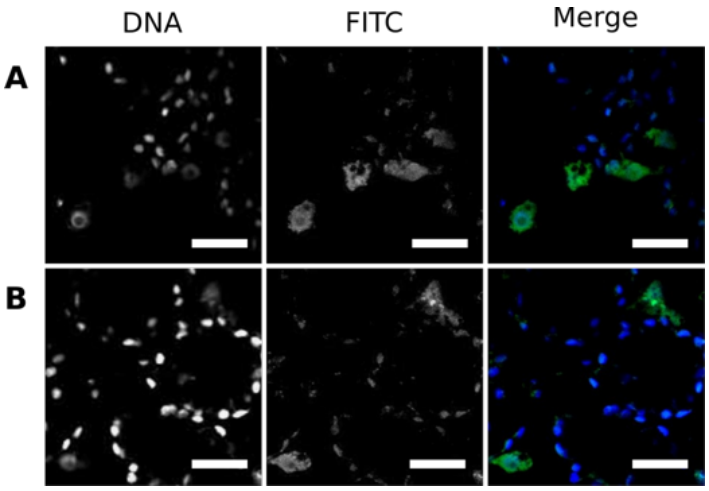

Figure 94. Cell level staining is difficult to interpret. Confocal images of region of **(a)** the area near the edge of the sponge and **(b)** the area around a choanocyte chamber. Both show a population of cells that show strong signal and some staining of nuclei. Without counter staining these patterns are difficult to interpret. Scale bars 10μm.

there was faint ubiquitous signal in the green channel, without noticeable differences between cell types. There were a few areas of bright, punctate signal, which were also present in non-probe controls. These are likely associated algae or auto-fluorescent products, which commonly occur in this sponge. Staining of the osculum gave signal, but this appeared ubiquitous through the tissue without a clear difference between cells (**Figure 95**). Within individual cells, there were no clear puncta of signal but rather a fairly even distribution.

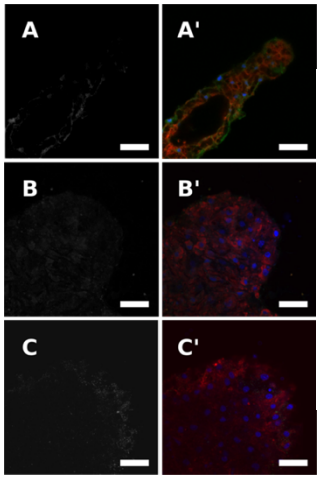

Figure 95. Isolated oscula show some signal. Grayscale of green channel (left) and merge (right) of stMyHC (green), actin (red), and DNA (blue). **(a)** Samples hybridized with stMyHC probes. **(b)** Osculum treated as in **(a)** without the addition of stMyHC. **(c)** Osculum treated as in **(a)** but treated with RNase prior to hybridization. Scale bars 5μm.

FISH using HCR probes shows strong signals in specific regions, which are mostly associated with the attachment epithelium and apical pinacoderm (**Figure A4**). Counterstaining with ethidium bromide helps to resolve cell boundaries and revealed areas of punctate staining throughout the cytoplasm of the attachment epithelium (**Figure 96**). Looking through the body of the sponge, there is some signal in the cells of the mesohyl but little to no signal in choanocytes (**Figure 97**). The strongest signal in these images is found in cells that are located higher in the tissue and appeared to form a loose epithelial sheet that resembles the endopinacoderm, with elongated cells and cellular protrusions that appear to form connections with other cells. These cells are known to contain large amounts of EmVin1 at the adhesion plaques seen at the ends of actin tracts. Staining appears as small localized puncta within cells as opposed to diffuse cytoplasmic staining seen with the Stellaris probes. Treatment of the sponge with RNase prior to hybridization abolishes all signal seen in untreated sample.

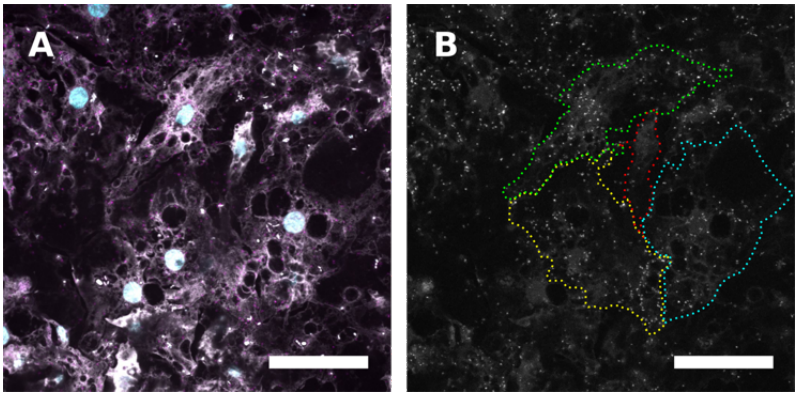

Figure 96. Signal in the attachment epithelium. (a) Confocal image showing EmVin1 (magenta), EtBr (white), and DNA (cyan). **(b)** Grayscale of green channel with outlines of four cells based on EtBr staining overlaid. Signal can be seen as small puncta within the cytoplasm, which is consistent with expectations for this method. Scale bars 20μm.

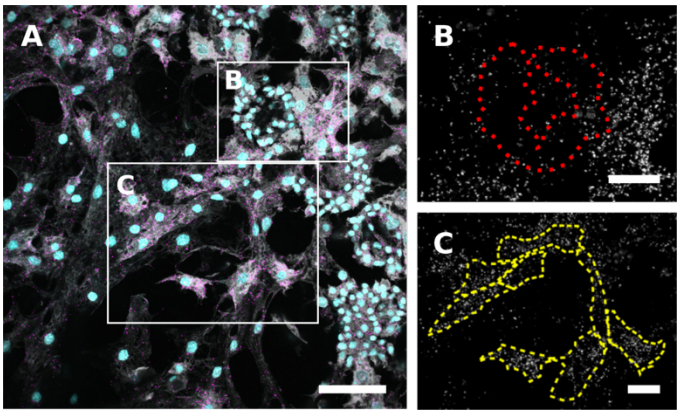

Figure 97. Signal is strong in pinacocytes and not choanocytes. (a) Confocal image of body region of the sponge showing EmVin1 (magenta), EtBr (white), and DNA (cyan). **(b)** EmVin1 signal in zoom of choanocyte chamber with outline of chamber in red, based on EtBr and DNA staining. **(c)** EmVin1 signal in zoom of region along a canal with outline of epithelial cells (based on proximity and apparent adhesions) overlaid in yellow. Cells that morphologically resemble endopinacocytes show strong signal. Scale bars 10μm.

Discussion

The fixation method appears to provide a good option for maintaining tissue integrity during harsh treatments such as the high temperatures during *in situ* hybridization. However, the colorimetric technique still does not appear to be sufficient to detect expression in *E. muelleri*. FISH using the Stellaris probes did not appear to produce specific signal either. The consistent staining pattern was one of diffuse signal through the tissue that did not become more resolved when individual cells were visualized with either phalloidin (in low formamide treatments) or EtBr counterstaining. The broad diffuse staining pattern could reflect the target (stMyHC) as the endopinacocytes are found all over the sponge body, but is more likely the result of auto-fluorescence mixed with non-specific probe binding. Based on the previous findings, the high levels of expression of stMyHC in the endopinacoderm allows it to be resolved as a

thin layer of tissue. This was not seen using FISH and the majority of signal came from what appeared to be migratory cells that morphologically resembled archeocytes. The staining pattern is also expected to be less diffuse through the cell as is seen in the samples. By using short oligo probes across the transcripts, it is expected that signal would be tightly localized to mRNA molecules, which should appear as more punctate staining than is seen. It is possible that transcripts are so abundant throughout the cell that it leads to the diffuse staining, but this is unlikely for the summation of the tissue. It is more likely that this pattern is the result of a mixture of autofluorescence (as some is seen in the no-probe controls) and non-specific probe binding (scrabbled control probes were not available). The staining pattern using the HCR probes is more consistent with the predicted signal pattern for this type of probe. Apart from this, the tissue staining patterns are consistent with the target, which is EmVin1 (vinculin). Based on immunostaining patterns this protein is found in abundance in the attachment epithelium and the apical pinacoderm, but is not seen in the migratory cells of the mesohyl or the choanocytes (Mitchell & Nichols, 2019). The strongest staining in for the HCR samples appeared to be in the attachment epithelia as well as in an optical plane which suggests that it is in the apical pinacoderm. There is some signal in the area between these two planes, which suggests that it is in cells of the mesohyl. This is inconsistent with immunostaining results, but could mean that the protein is expressed in these cells but the protein is either not maintained or is too diffuse through the cytoplasm to be visualized with immunostaining. This makes sense from a biological standpoint in that EmVin1 is found at large adhesion plaques, either at putative cell-ECM contacts or cell-cell contacts (Mitchell & Nichols, 2019). The protein is probably greatly enriched at these structures.

The lack of staining in the migratory cells in the mesohyl could be due to the transient nature of their adhesion structures. It is conceivable that expression of EmVin1 is positively regulated by the formation of stable adhesion structures. The low expression levels in the migratory cells could account for an unstable pool of protein that does not accumulate until the formation of stable adhesions is initiated. EtBr appears to be a good counterstain for visualizing individual cells when using higher magnifications and confocal imaging, but stains too brightly to discern between tissues under lower magnification. If using this method, it is probably best to look at general patterning in the probe channel when viewing the whole organism or large tissue regions and then using both channels to confirm cell type with a high-powered objective. Overall this seems like a good method for either confirming expectations for expression patterns (such as scRNA seq data) or for monitoring changes in expression levels in a given tissue type. However, without a consistent method of identifying cell boundaries or differentiating between tissues, it is difficult to interpret the data based if you don't have prior expectations of where expression is occurring. Because of the ability to use multiplexed probes, a catalog of different cell type markers could be developed to allow better understanding of the expression patterns of new targets. Major limiting factors for this technique right now are time and cost. The probes have to be designed and synthesized and the cost is about $500.00 for 10 reactions.

Unsuccessful Antibodies for Ephydatia muelleri

Background

We currently have good methods for immunostaining and immunoprecipitation working in *E. muelleri,* making an antibody approach a good method for understanding protein function in this system. With this approach it is impossible to predict the affinity and specificity of any antibody for its target. In this section I will describe some custom antibodies that were raised but do not appear to recognize their targets *in vivo* as well as a variety of commercial antibodies that were tested under a variety of conditions which did give interpretable results. As described in the MRTF section, during myogenesis an MRTF-family protein interacts with either SRF or Mef2 to drive expression of genes involved in building the contractile apparatus. Attempts were made to express recombinant EmSRF and EmMef2, neither of which were soluble. The N-terminus of EmMef2, which contains both the Mef2 domain and the MADS-box was able to be expressed and purified and was used to generate a custom polyclonal antibody. α-actinin is an integral part of contractile bundles, where it serves as a structural anchor point for F-actin and provides ideal spacing for thick filament integration (Sjöblom et al., 2008). Attempts were made to express Emα-actinin, but it was also found to be insoluble.

A variety of commercially available antibodies were also tested to see if they worked in *E. muelleri.* Santa Cruz Biotechnology (www.scbt.com) provides 10µg samples of various monoclonal antibodies they sell. Samples tested were SRF (Santa Cruz Biotechnology #sc-25290) and Mef2-C (F-10) (Santa Cruz Biotechnology #sc-365862). A recent paper on a newly described choanoflagellate species, *Choanoeca flexa*, utilized several commercially available antibodies to characterize the actomyosin

network in colonies (Brunet et al., 2019). These included two targeting, type II myosin heavy chain; CMII 23-MyosinIIB (DSHB #CMII23), a monoclonal antibody raised in mouse that targets non-muscle myosin heavy chain, and Anti-Myosin (Skeletal and Smooth) (Sigma-Aldrich #M7648) a polyclonal panMyHC serum. There was also an antibody targeting the RLC; MYL12B Antibody(N-term) (Abgent #AP19667a-ev). These were chosen by the authors because of their specificity in a broad range of animals and conservation at the epitope sites.

Methods

SRF and Mef2 custom attempts

Full length EmSRF and EmMef2 sequences were identified in the *E. muelleri* transcriptome (Peña et al. 2016) and were cloned into the pET His6 SUMO LIC vector using the following primer sets;

EmSRF

Forward – TACTTCCAATCCAATGCAGAAAAGCCAAAGCCTGCTC

Reverse - TTATCCACTTCCAATGTTATTAGGCTTCTGACGTAATCAT

EmMef2

Forward - TACTTCCAATCCAATGCAGGGCGTAAAAGATAGCAA

Reverse - TTATCCACTTCCAATGTTATTAGCTTTCGTCAGGATCTTTG

Plasmids were sequenced to verify insertion and used to transform Rosetta cells for expression. Protein expression was performed using our standard protocol, expression was induced with 250µM IPTG and each was expressed for 3 hours at 30^{o}C. Recombinant protein was purified by affinity chromatography using Ni-NTA resin

(ThermoFisher Scientific #88221). Purified EmMef2-N-Term was sent for rabbit injection and antibody was affinity purified from serum with ~6mg of recombinant protein as described earlier. Purified antibody was then concentrated and transferred to 1x PBS using Amicon® Ultra-4 centrifugal filter units (Millipore #UFC803024).

Immunostainings

Gemmules were plated and hatched as described earlier in glass bottom dishes and grown to tent stage (tent) or when canals and choanocyte chambers were visible (juvenile). Samples were fixed using the standard 3.7% formaldehyde in EtOH protocol. Immunostainings were performed with either 1:100, 1:250, or 1:500 dilution of primary anti-EmMef2 in 3% BSA 1x PBST overnight at 4^{o}C. Samples were then incubated for 45 minutes at room temperature in anti-rabbit AF™488 (Life Technologies, 1:500), phalloidin AF™568 (Life Technologies, 1:120), and Hoechst (33,342 1µg/mL) dye. After washing samples were mounted in anti-fade medium (0.1M propyl gallate, 1x PBS pH 7.6, and 90% glycerol).

Western Blot

Approximately 50 gemmules were plated and hatched in a petri dish containing LW+100µg/mL ampicillin. After hatching the water was replaced each day with just LW. At 3 days post hatching sponges were collected by scraping with a sterile razor blade into a 1.5mL Eppendorf tube. Excess water was pipetted off and 200µL of 1x SDS loading buffer was added. Samples were boiled for 10 minutes and run on a 10% acrylamide gel. Proteins were transferred to a PVFD membrane (Millipore #IPFL85R) at 350mA for 28

minutes on ice. Blotting was performed as described earlier using 1:500 dilution of primary antibody in blocking solution and was visualized with anti-rabbit AF™488 (Life Technologies, 1:2000) in blocking solution.

Santa Cruz Biotech Samples – Immunostaining

Gemmules were plated and hatched in glass bottom dishes as described earlier. After hatching sponges were monitored for development of choanocyte chambers and canals and just as canals began to form sponges were fixed using standard 3.7% formaldehyde in EtOH. Primary was applied in a 1:100 dilution in blocking solution and samples were incubated for 1 hour at room temperature. Secondary staining was performed by applying anti-rabbit AF™488 (Life Technologies, 1:500), phalloidin AF™568 (Life Technologies, 1:120), and Hoechst (33,342 1µg/mL) dye in blocking solution.

MyHC and RLC antibodies – Immunostainings

Gemmules were plated and hatched in glass bottom dishes as described before. Initial stainings were performed using the standard 3.7% formaldehyde in EtOH fixation. Primary was applied at using the highest and lowest suggested concentration from the manufacturer;

Anti-nmMyHC - CMII 23-MyosinIIB – 2µg/mL high and 5µg/mL low

Anti-panMyHC - Anti-Myosin (Skeletal and Smooth) – 1:10 (v/v) high and 1:100 (v/v) low

Anti-RLC - MYL12B Antibody(N-Term) – 1:100 (v/v) high and 1:250 (v/v) low

Secondary was applied in blocking solution with 1:100 Hoechst dye, and 1:120 phalloidin AF™568. For anti-panMyHC and anti-RLC anti-rabbit AF™488 was used and for anti-nmMyHC Goat anti-Mouse IgG H&L (Alexa Fluor™ 488) (abcam #ab150113) was used.

For anti-nmMyHC, samples were also fixed with Carnoy's solution (60% EtOH, 30% chloroform, 10% acetic acid). Samples were washed twice with fresh LW and then Carnoy's solution was added and incubated at room temperature for 3 minutes. Samples were then transferred to EtOH for 10 minutes at room temperature. Samples were washed several times with 1x PBS and then blocked in 3% BSA in 1xPBST for 1 hour at room temperature. Immunostaining was performed as described above, with primary antibody incubated overnight at 4^{o}C.

Confocal Images were acquired on an Olympus Fluoview FV3000 confocal laser scanning microscope using either a 60×/1.4 NA or 100×/1.4 NA objectives. Laser levels and acquisition setting were not adjusted for imaging controls. Images were processed in FIJI (Schindelin et al., 2012).

Western blot

Approximately 50 gemmules were plated and hatched in a petri dish as described earlier and were harvested at 3 days post hatching. Samples were boiled in 1x SDS loading buffer for 8 minutes before loading on a 10% acrylamide gel. Transfer was performed at 250mA for 60 minutes at 4^{o}C with 2% MeOH transfer buffer. The goal with this transfer was to balance the movement of large proteins, like MyHC, with that of small ones, like RLC. RLC was blotted with 1:500 and 1:1000 dilutions of anti-RLC in

blocking solution and MyHC was blotted with 1:250 anti-MyHC in blocking solution and all were incubated overnight at 4ºC. Secondary, either anti-rabbit AF™488 (Life Technologies) or anti-mouse AF™647 (Invitrogen #A-21235), was diluted 1:2000 in blocking solution and membranes were incubated for 45 minutes at room temperature.

Results

Full length protein for SRF and Mef2 were insoluble when expressed. The N-terminus region of Mef2 was soluble and was used to raise custom antibodies. Immunostainings with this antibody did not produce a clear pattern and appeared diffuse through cells (**Figure 98**). The western blot using affinity purified antibody produced one band around 30kD and two fainter bands around 25kD and a band around 15kD (**Figure 99**). Stainings performed with the antibody samples from Santa Cruz Biotech primarily showed diffuse staining, which is likely non-specific (**Figure 100**). There was some possible nuclear staining in some of the Mef2 samples but this was not consistent and laser levels and exposures had to be set very high (**Figure 100b**). There was no clear signal in the using the anti-SRF antibody (**Figure 101**) Similar results were seen with the two MyHC antibodies and the RLC antibody (**Figure 102 & 103**). There was some

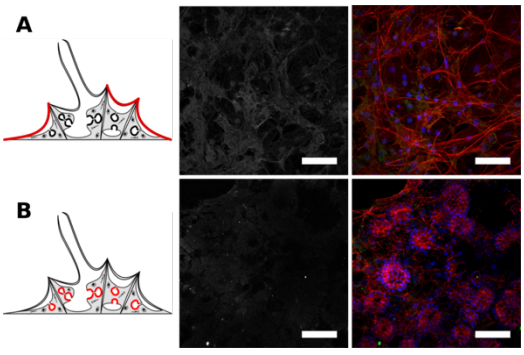

Figure 98. Immunostaining with anti-EmMef2. Confocal images, showing raw green channel (left) and merge (right) of EmMef2 (green), actin (red), and DNA (blue). **(a)** Staining through the apical pinacoderm. **(b)** Staining in the choanoderm gives limited signal. Both of these patterns are inconsistent with the expectation of constitutively nuclear localization. Scale bars 20µm.

staining with panMyHC antibody in the cortical actin networks in the exopinacocytes, but this was not seen consistently and did not stain much stronger than the surrounding area in the cell (**Figure 104**). The western blot for nmMyHC antibody showed a faint signal band at around 220kD, though resolution for this size was not ideal (**Figure 105a**). The RLC antibody produced a single band at around 37kD which was more intense in the higher concentration (**Figure 105b**).

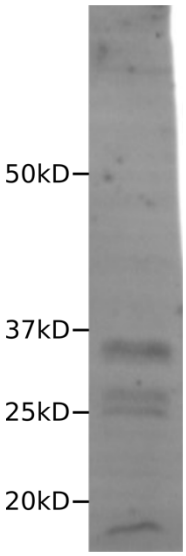

Figure 99. Western blot with anti-EmMef2. Blot of sponge whole cell lysates show 4 bands, one at around 30kD, one at around 27kD, one at around 25kD, and one at around 15kD.

Discussion

The N-terminus of Mef2 was chosen because it contained both the Mef2 domain, which is unique to this protein, and the MADS box which shows high conservation with the MADS box of SRF. With this it was assumed that IgG that recognized the MADS box would be cross reactive with SRF while IgG that recognized the Mef2 domain would be specific to Mef2, so serum could be purified with the full antigen serve as pan-MADS box antibody while serum purified with just the Mef2 domain could be used to recognize

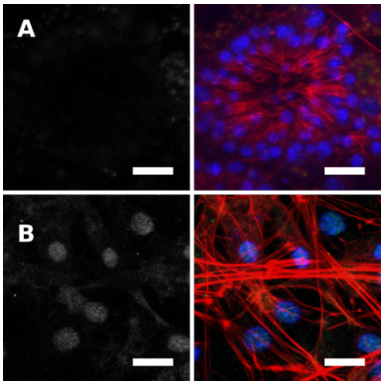

Figure 100. Immunostaining with commercial anti-Mef2 antibody. Raw green channel image (left) and merge (right) of Mef2 (green), actin (red), and DNA (blue). **(a)** Staining in the choanocyte gives little signal. **(b)** Nuclear staining is evident in cells of the pinacoderm and mesohyl. This was not always seen and did not follow a clear pattern though. Scale bars 5μm.

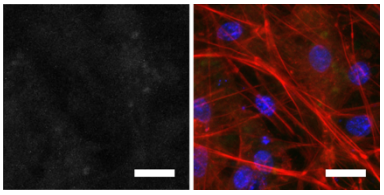

Figure 101. Immunostaining with commercial anti-SRF antibody. Raw green channel image (left) and merge (right) of SRF (green), actin (red), and DNA (blue). No clear pattern is seen for SRF staining, which is expected to be constitutively nuclear. Scale bars 5µm.

just this protein. Based on this, antigen purified antibody would be expected to produce broad nuclear staining, as both are transcription factors that are constitutively in the nucleus of other animals (Yu 1996). The lack of nuclear staining suggests that the antibody does not recognize either SRF or Mef2 *in vivo*. The western blot produces bands which do not directly correlate with the predicted size of either of the proteins (EmSRF ~50kD, EmMef2 ~55kD). It is intriguing that the sum of the bands correlated to roughly the correct size of the proteins, but since the antibody was raised against the N-terminus of the protein, it would only recognize one fragment if these were the result of protein cleavage. The lack of interpretable immunostaining patterns greatly limits the utility of this antibody though, and an unsuccessful IP was performed. At this same time, single cell RNA-seq data became available for a closely related species (*Spongilla lacustris* (Musser et al., 2019)) which showed low and restricted expression of Mef2 in cells which

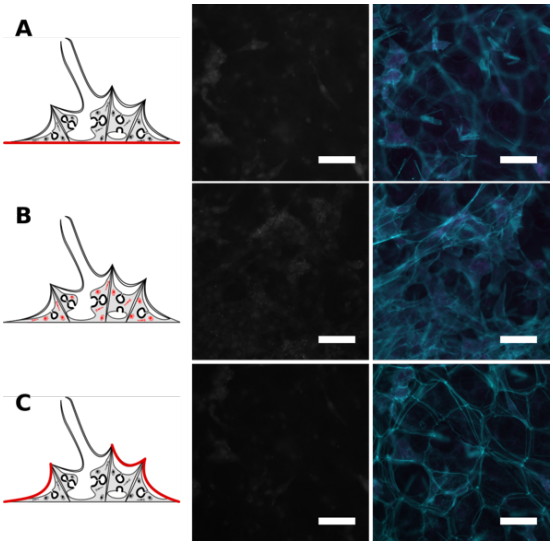

Figure 102. Immunostaining with commercial panMyHC antibody. Raw green channel (left) and merge (right) of actin (cyan) and MyHC (magenta). Limited signal and colocalization with actin is seen in **(a)** the attachment epithelium, **(b)** the mesohyl, and **(c)** apical pinacoderm. Scale bars 20µm.

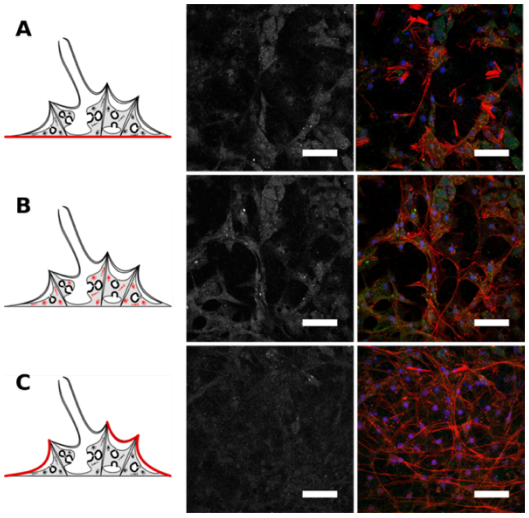

Figure 103. Immunostaining with commercial RLC antibody. Confocal images with raw green channel (left) and merge (right) of RLC (green), actin red, and DNA (blue). Limited signal and colocalization with actin is seen in **(a)** the attachment epithelium, **(b)** the mesohyl, and **(c)** apical pinacoderm. Scale bars 20µm.

were not associated with contractile markers, while SRF was highly expressed in pinacocytes which also expressed proteins associated with large contractile actomyosin bundles (Musser et al., 2019). Based on this, trouble shooting for the Mef2 antibody was abandoned and focus was switched to other experiments.

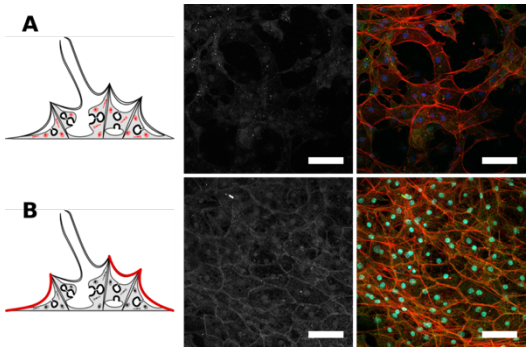

Figure 104. Immunostaining with nmMyHC antibody. Confocal images with raw green channel (left) and merge (right) of RLC (green), actin red, and DNA (blue). **(a)** Mesohyl and endopinacoderm has diffuse signal. **(b)** In the apical pinacoderm, signal can be seen along the boundaries of exopinacocytes, but also in the nucleus. Scale bars 20µm.

For the RLC antibody, immunostainings showed very diffuse staining through the cytoplasm, primarily in the migratory cells of the mesohyl, with very little staining in the pinacocytes. *E. muelleri* has a single gene for RLC, so the same protein is likely localizing to all type-II MyHC containing filaments. There, it is expected that RLC would be present in all cell types, but enriched in those that contain large contractile bundles, with clear localization to these structures. The apical pinacoderm contains

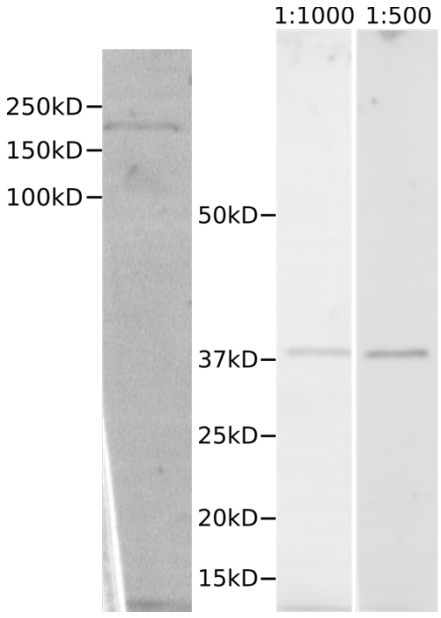

Figure 105. Western blot of sponge cell lysates with nmMyHC and RLC antibodies. (a) For nmMyHC, a single band is visible between 250 and 150kD which is consistent with the predicted protein size of ~220kD. No lower molecular weight bands are visible. **(b)** For RLC, a single band, a littler larger than 37kD is visible, which intensifies with increased antibody concentration. This is approximately twice the predicted size of the target (~19kD).

exopinacocytes, which have a dynamic size and shape and contain large amounts of cortical actin, suggesting these are contractile structures which likely contain type-II myosin filaments. This also contains the endopinacocytes, which house the large stMyHC+ contractile actin tracts. The basopinacoderm contains very large stress fiber like structures. There is faint pRLC staining at some of these structures, which suggests they contain myosin filament or are contractile. The lack of signal at any of these structures and limited signal in any of these cell types, suggests that this antibody does not work in *E. muelleri* for visualizing RLC *in vivo*. The diffuse staining in the migratory cells is likely non-specific binding to a target in these cells or autofluorescence, which is a common artifact in this cell type. It is possible that the diffuse staining is the result of a large pool of type-II myosin in the cells, which are highly dynamic and do not contain large actin structures but have elevated actin turnover relative to other cell types (based on Latrunculin B experiments). A common mechanism for cell migration, which is seen in a variety of animal cell types, is to extend the leading edge through actin ratcheting, while utilizing actomyosin contractility to constrict the trailing end, forcing the cytoplasm towards the leading edge

(Chi et al., 2014; Agarwal & Zaidel-Bar, 2019). The cells in the mesohyl follow what appears to be a random walk method of pathfinding, which involves many directional changes. As a result of this, the leading edge and trailing end are constantly changing, which would require a large pool of type-II myosin throughout the cytoplasm to rapidly build contractile structures opposite of the leading edge. The western blot shows a very specific band, in that there is nothing else visible and it intensifies with increased antibody. However, it is located at around 37kDa which is about twice the size of the predicted protein. This is around the size of the combination of RLC and essential light chain (ELC) which are expected to be in close proximity in the cell and to interact with each other or it could be a RLC-dimer. The manufacturer's documentation for the antibody showed a strong band at 19kDa and a weak one around 37kDa, so it is possible this is the case for the upper band. However, it would be very unlikely that the combination of SDS, boiling, and reducing agent wouldn't disrupt this interaction to the extent that monomers could be visualized. Another possibility is the antibody is identifying a related protein in *E. muelleri*. The RLC and ELC are members of the EF-hand family of proteins, which is a very large family of proteins derived from a common calcium binding ancestor (Nakayama & Kretsinger, 1994). There different degrees of conservation between the various subfamilies, but the *E. muelleri* transcriptome contains 12 other EF-hand proteins that vary in predicted size, for which EmRLC and EmELC closely group with. Based on this, the antibody was not pursued further.

The MyHC antibodies also did not produce interpretable or reproducible staining patterns. As we have a validated stMyHC, the main goal for these antibodies was to visualize the nmMyHC population in *E. muelleri*. That the nmMyHC antibody was raised

in a mouse host, would have allowed for co-staining with EmstMyHC, which was raised in rabbit. However, both aldehyde fixation and Carnoy's fixation did not produce clear results. The western blot showed what looked like a specific band of the correct size, so the antibody may recognize sponge MyHC when it is denatured on a membrane, but the lack of clear immunostaining results limits the utility of these antibodies.

Injectroporation in Ephydatia muelleri

Background

There are many challenges in working with non-traditional animal models, such as *E. muelleri.* The development of functional techniques could greatly expand our understanding of sponge cell and developmental biology. As discussed above, we do not have access to germ cells or zygotes in *E. muelleri* and cannot induce spawning, so therefore must rely on transient transfection. This puts particular importance on efficiency of any given technique. Targeting specific cell types is also an important consideration. The mesohyl is filled with stem cells (archeocytes) which are good targets for understanding factors involved in differentiation into different cell types. An effective method for specifically knocking down proteins in a variety of organisms is the electroporation of shRNA (O'Keefe, 2013; Karabulut et al., 2019). Electroporation can also be used to introduce *in vitro* synthesized mRNA to overexpress a given protein (Zhao et al., 2006). There are many factors to consider when performing electroporation of a cell culture or organism, one being the buffer to use. Traditionally low resistance (high ionic strength) buffers have been used to minimize arcing (Jordan et al., 2008). On the other hand, hypoosmotic buffers are sometimes utilized in order to increase flow rate

into the cell so that the pulsing time and strength can be decreased (Usaj & Kanduser, 2012). *E. muelleri* lives in freshwater lakes which contain very few solutes and therefore is extremely sensitive to ion concentrations meaning a high resistance, but a near isosmotic buffer must be used. They are not as sensitive to Ca^{2+} levels as they are to Na^{+} so $CaCl_2$ can be used to increase ionic strength of the buffer. Initial tests with this technique suggested the sponges can survive the treatment. However, attempts to dissociate sponges and then electroporate suspended cells (likely enriched with archeocytes) were unsuccessful. Based on the use of membrane dyes, bath application to juvenile sponges leads primarily to interactions with choanocytes and pinacocytes with limited penetration into the mesohyl, which contains archeocytes. This would likely be the same for molecules like shRNA added to the sponge medium. Phenotypes in these tissues are very difficult to interpret because of the high rate of cellular turnover and plasticity in their structure. In order to circumvent this, delivery of the molecules to be electroporated into the cells into the mesohyl could be used to increase the exposure to archeocytes. During development from a gemmule, the cells migrate out and differentiate into epithelial cells, forming the basiopinacoderm which attaches to the substrate and the apical pinacoderm which established the barrier with the surrounding water (reviewed in Simpson, 1984). During this stage (termed tent stage) the sponge is essentially an attached epithelial bag around the gemmule which contains thousands of stem cells. The idea for this technique is to inject the agent to be electroporated into the mesohyl of the tent and then electroporate to affect as many archeocytes as possible.

Methods

Electroporation apparatus setup

The electroporation setup was designed to work in a Fluorodish (WPI #FD35-100) glass bottom dish in which the sponges can be plated. A 4mm electroporation cuvette (BioRad #1652088) was cut along the top of the electrode, through the aluminum plates creating a smooth base. Positive and negative leads were then soldered to the outside of each plate at the base of the cuvette and one of the plastic sides between the plates was carefully cut away. The flat edge was then fed down through a Fluorodish lid until it made stable contact with the base of the dish and it was sealed in place with silicone rubber on all sides except for the one in which the plastic was removed from the cuvette. The lid then had a small region removed to fit a microinjection needle through.

Injection and electroporation

For initial experiments, *E. coli* expressed and purified supercharged GFP +36 (scGFP) was used so that the injected material could be tracked. Gemmules were plated in LW + 10mM CaCl in the middle grid of a Flourodish, between where the electroporation plate contacts. Water was changed each day after attachment to the glass. At 2 days post attachment, as when the tissue was expanded but no choanocyte chambers or canals were visible, samples were prepared for injection. A pulled glass needle was backloaded with scGFP solution and the nanoinjector was set to its largest volume (73.6nL). A control needle was loaded with PBS (what the scGFP was stored in). Three treatments were used, 1- injection with scGFP followed by pulsing with 300V exponential decay pulse, 2- injection with PBS followed by pulsing with 300V

exponential decay pulse, and 3- Injection with scGFP without pulsing. Injections were performed on an inverted epifluorescence microscope with an extra illumination source at the base. The needle was roughly placed under low magnification and then puncturing of the pinacoderm and setting in the mesohyl was performed using a 40x objective. Care was taken to locate the needle in the intercellular space of the mesohyl. Following injection, the tissue was viewed through the GFP filter set to monitor diffusion through the mesohyl prior to pulsing. After about 60 seconds, movement was not evident, so pulsing was performed. Sponges were then washed with fresh medium and samples injected with scGFP, both pulsed and not pulsed, were fixed in 4% paraformaldehyde (PFA) in 1x PBS for 40 minutes at room temperature.

Results

The rate of diffusion through the mesohyl was much slower than expected and the injected material stayed in a region of approximately 30μm surrounding the needle tip. Following electroporation, the PBS injected controls continued to develop normally and formed choanocyte chambers and canals after 2 days additional incubation. The sponges that were injected with scGFP but not electroporated showed some punctate staining around cells, which is likely along the plasma membrane (**Figure 106**). This was also present in the samples that were injected with scGFP and electroporated, but there were

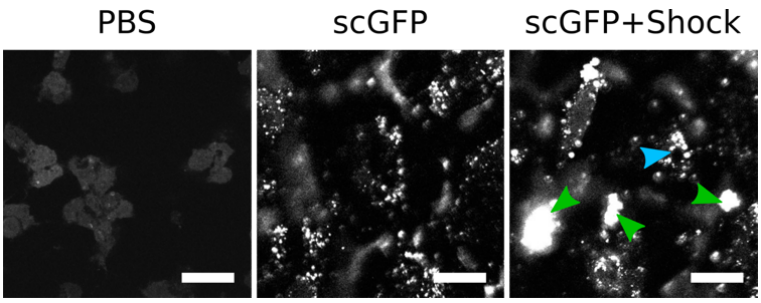

Figure 106. Injectroporation shows evidence of entry into cells. Comparative images of cells in the tent of sponges injected with PBS and shock, injected with scGFP and not shocked, and injected with scGFP and then shocked. Injected scGFP can be seen interacted with cells forming discrete puncta around the outline of cells. This is also present in shocked individuals (cyan arrowhead), but there are also very bright areas of staining (green arrowheads) suggesting concentration within the cells. Scale bars 10μm.

also cells that showed uniform staining through the cytoplasm, which was not seen in the samples that were not shocked. This only occurred in a few cells per sample.

Discussion

The presence of intracellular signal in the shocked samples, which was absent from the non-shocked samples suggests that the procedure was effective in moving that scGFP into the cell. The staining seen in the non-shock control is likely due to binding of the scGFP to negatively charged regions along the cell membrane. The lack of diffusion through the mesohyl presents a problem for this method though. It was hypothesized that there would be rapid movement through the intercellular space which would allow for an even distribution prior to electroporation. However, the extracellular matrix in this region appears to be denser and expected and limits movement of the solution. This could also result from the large size and charge on the molecule being tracked, but as it stands, this greatly reduces the number of cells that can be affected. Without being able to target a large proportion of archeocytes, the utility of this method is greatly reduced. This may

serve as a good method for cell tracking experiments, but is likely limited for functionally manipulating the cells, as phenotypic expectations are unclear with sponges. For this reason, focus was changed to identifying methods that could offer higher efficiency in sponges.

Streptolysin O Treatment

Background

Streptolysin O (SLO) is a bacterial toxin that creates pores in animal cells through an interaction with cholesterol in the plasma membrane. Upon binding to cholesterol, it oligomerizes into a ring-shaped complex forming transient pores of around 30nm in diameter (Bhakdi et al., 1985). The transient nature of these complexes allows for membrane repair following washout and can be used to introduce large molecules into cells with high efficiency and low toxicity (Teng et al., 2018). In a previous study, SLO was used to introduce large molecules to isolated sponge cells in the closely related sponge *Spongilla lacustris* (Kirfel & Stockem, 1997). Based on this, this seemed like a good option for introducing foreign molecules into *E. muelleri*, as well as a possible alternative for injection into *N. vectensis* embryos.

In order to assess the utility of this method in sponges, both sponges developing from gemmule and isolated cells will be treated. If efficiency is high enough molecules, such as lifeact, could be introduced to visualize *in vivo* actin dynamics in the pinacoderm during contractions. Adult sponge tissue can be mechanically or chemically dissociated into individual cells, which will then reaggregate and form an individual with all normal tissue types. Hypothetically, if performing functional work, dissociated cells could be

treated with SLO and those that took up the molecule intended to be introduced (based on the presence of a dye or other marker) could be selected for, using cell sorting techniques, and then used to form aggregates and then individuals derived solely from affected cells.

This method could also serve as an efficient method for introducing molecules to *N. vectnesis* embryos. Injection is a well-established technique but can be limiting in the number of individuals injected at any one time. Oocytes are viable for about two hours after release and the time between fertilization and first cleavage can be as short as 30 minutes (DuBuc et al., 2014), creating a window in which injections can take place. Since treatments with SLO can take place simultaneously, several molecules can be used on a very large spawning sample without a physical restriction on the number of individuals treated.

Methods

E. muelleri juvenile individuals

Gemmules were plated and hatched in 24-well format as described previously and were allowed to develop until choanocyte chambers and canals were visible. SLO stocks of 25-50U/µL were prepared in dH_2O from lyophilized powder (Sigma-Aldrich #S5265). Dilutions tested were 1:1000, 1:500, 1:250, 1:100, 1:50, and 1:10 in LW, and sponges were treated for either 10 minutes or 30 minutes at room temperature with gentle rocking. Sponges were then treated with either 1:100 phalloidin AF™488 (Life Technologies #A12379) in LW or 1:100 Cascade blue dye (ThermoFisher Scientific #C2284) in LW for 30 minutes at room temperature with gentle rocking. Following treatment, sponges were washed thoroughly with LW and then fixed in 4% PFA and 0.3% glutaraldehyde in

0.1M phosphate buffer (pH 7.2) (PB) for 10 minutes at room temperature with gentle rocking. This was replaced with 4% PFA in 0.1M PB for 1 hour at room temperature. Samples were then washed with 0.1M PB and mounted for imaging.

E. muelleri isolated cells

Approximately 50 gemmules were plated and hatched in petri dish and grown until 3 days post hatching. Sponges were then scraped into a 1.5mL Eppendorf tube and gently spun so that excess water could be removed. Tissue was then resuspended in 1mM EDTA in dH_2O an incubated for 15 minutes at room temperature with constant mixing. The contents were then passed through a 0.44µm filter and the cell suspension was divided evenly into treatment tubes. These tubes were then spun at 300xg for 5 minutes to pellet the cells. The supernatant was removed and then the cells were resuspended in 100µL of 1:250 SLO solution in dH_2O. The tubes were then incubated at 37^{o}C for 7 minutes with gentle mixing throughout. Samples were then spun at 300xg for 2 minutes and supernatant was removed, and cells were resuspended in 100µL of 0.2% Trypan blue and were incubated for 10 minutes at room temperature with constant mixing. Cells were then washed 3 times with 1mL of LW. Cells were then pelleted and resuspended in 50µL of LW and transferred to a glass bottom dish for viewing.

N. vectensis embryos

Spawning was induced using the standard protocol of placing individuals in bright light at 28^{o}C. Egg sacks from females were collected and incubated in water from the male dish for 15 minutes to fertilize. Fertilized eggs were then de-jellied in 3% cysteine

in 1/3 ASW for 15 minutes with constant agitation. Cleaned eggs were then transferred to a 24 well plate for treatment. SLO stock solution was diluted 1:100, 1:250, and 1:500 in 1/3 ASW with 1/3 ASW treatment serving as a control. Samples were treated with respective solutions for 10 minutes at room temperature and were then washed with 1/3 ASW. Samples were then incubated in 0.2% Trypan Blue in 1/3 ASW for 5 minutes at room temperature with gentle rocking. Samples were then washed thoroughly with 1/3 ASW and left to settle for viewing. In order to assess the practicality of this method, 1:250 SLO was used to deliver morpholinos targeting NvMRTF (see Chapter 6). These were applied in concentrations of 1mM, 800μM, and 400μM.

Results

E. muelleri

Juvenile sponges appeared to continue to develop normally following treatment with SLO of all concentrations. There was no evidence that phalloidin entered the cells and bound to any structures though (**Figure 107**). After washing there is no clear signal from the phalloidin in samples that are fixed but not permeabilized. The same result was seen in the samples that were treated with Cascade Blue dye and when using trypan blue to treat whole sponges. Dissociated cells also did not show evidence of permeabilizing following SLO treatment. Some cell could be seen with what looked like blue staining, but based on their morphology it is likely that these had lysed, or begun to lyse, during the procedure and were no longer viable (**Figure 108**).

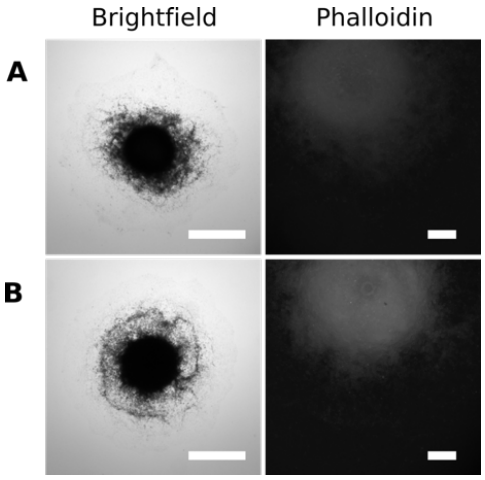

Figure 107. Treatment with SLO doesn't allow entry of phalloidin. **(a)** Control sponge, not treated with SLO but treated with phalloidin shows no evidence of staining. **(b)** Sponge treated with SLO and phalloidin also does not show staining of any cellular structures. Scale bars 500µm for brightfield, 100µm for phalloidin.

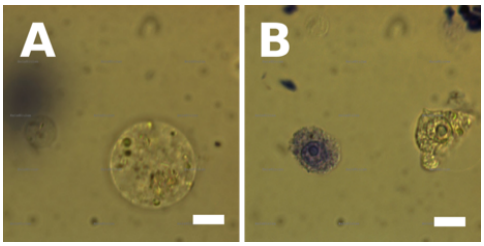

Figure 108. SLO shows some evidence of dye entry in isolated cells. Dissociated cells were treated with SLO and trypan blue. The vast majority of cells showed no evidence of staining, but a few cells did show cytoplasmic staining for trypan blue (right panel). Scale bars 5µm.

N. vectensis

Treatment of *N. vectensis* embryos with SLO did appear to have an effect. Embryos treated with the highest concentration (1:100) did not develop past the single cell stage. Samples treated with both 1:250 and 1:500 both continued to develop following treatment suggesting that this is below the toxic level. These samples also showed strong staining for Trypan Blue dye inside the cell, which is absent from the control (**Figure 109**). SLO treatment was used as a method of delivery for morpholinos targeting NvMRTF. Individuals treated with the morpholinos showed normal early development, but similar phenotypes as were seen with injection. These included reduced elongation of the body during larval stage and a lack of tentacle development. Treated individuals did not progress past larval stage and develop into polyps (**Figure 110**).

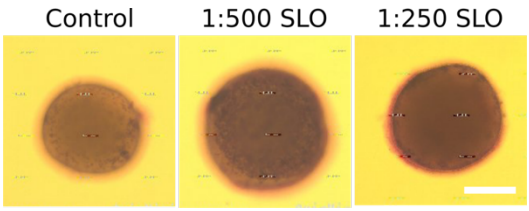

Figure 109. SLO appears to be effective in permeabilizing *N. vectensis* embryos. Embryos treated with just trypan blue do not show evidence of intracellular staining. Embryos treated with SLO show trypan blue staining, which appears stronger with a higher concentration of SLO. Scale bar 50µm.

Discussion

SLO treatment did not seem to be effective at permeabilizing cells in *E. muelleri* for delivery of large molecules. Phalloidin is small relative to the expected size of pores that form from SLO treatment. Differences in the abundance of cholesterol in the membrane as well as differences in the phospholipid composition of the plasma membrane, may lead to a different interaction of SLO, resulting in smaller, less stable, or malformed pores. Sponges have also been shown to produce a variety of modified types of cholesterol which may alter the interaction with SLO (Gold et al., 2016). The use of phalloidin AF™488 was chosen because it is normally not membrane permeable but should be small enough to pass through a pore, and becomes immobilized (through binding to F-actin) once inside the cell. Cascade Blue was used as it is also a membrane impermeable dye and is a small molecule. This was changed to Trypan Blue for the isolated cells as it is also membrane impermeable but is visible by eye to allow for rapid screening of cells. Overall, this does not seem like a technique that will work for either treatment of whole sponges or isolated cells.

This technique does appear to be effective with *N. vectensis* though. Treatment with high concentrations appears to be toxic, which is likely due to excess membrane damage, rapid influx of extracellular solution, or the merging of SLO pores leading to

leaking of the cytoplasm. The lower concentrations appear to show the presence of dye in the cytoplasm which is absent in the SLO- controls. The individuals treated with lower concentrations of SLO also appeared to develop normally following treatment suggesting that the effect is reversible as seen in other organisms (Keyel et al., 2011). This technique does appear to be an effective method for delivery of large molecules into *N. vectensis* cells. However, as this was being developed, a protocols for stable transfection (Renfer & Technau, 2017) and the electroporation of shRNA (Karabulut et al., 2019) became available for *N. vectensis.* Since the transfection method requires co-injection of insert and meganuclease and electroporation increases efficiency due to the movement of negatively charged molecules with the applied current, this technique was put aside. However, it does seem like it could serve a valuable function under certain circumstances. For example, the reversible nature of the treatment could make it useful in experiments being performed at later stages of development, where affecting a

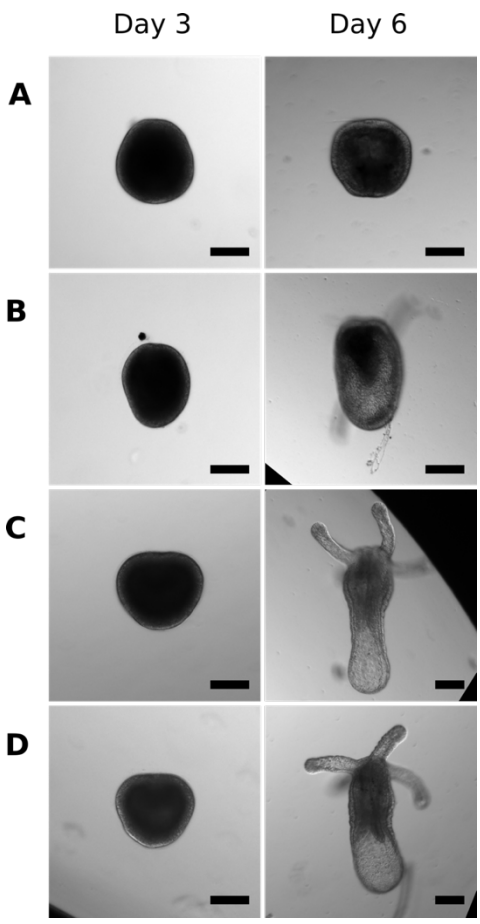

Figure 110. SLO treatment facilitates morpholino delivery. Individuals were treated with a 1:250 dilution of SLO and **(a)** 1mM morpholinos targeting NvMRTF, **(b)** 800µM morpholinos targeting NvMRTF, **(c)** 400µM morpholinos targeting NvMRTF, **(d)** No morpholinos. At day 3, individuals were developing at similar rate while development was reduced or halted in higher concentration morphants at day 6. Scale bars 100µm.

proportion of cells is sufficient. This could also be coupled with introduction of large molecules such as recombinant proteins or antibodies, which could be used to functional perturb the system.

Osculum Isolation

Background

The osculum is the primary excretory structure from the excurrent canal system. In *E. muelleri,* this tissue appears to be a bilayer composed of ciliated cells lining the internal region and exopinacocytes extending from the apical pinacoderm (Leys et al., 2009; Elliott & Leys, 2007). As this acts as the exit from the aquiferous system of the sponge, changes in diameter can greatly influence the rate of flow through the body. A variety of sponges have been shown to regulate the size of this opening, which is thought to be accomplished by actin dense cells erroneously referred to as myocytes (Prosser et al., 1962). The osculum in *E. muelleri* extends far from the body and appears to have contraction dynamics independent from the rest of the body. The rate of contraction in the osculum is also much higher than what is seen throughout the rest of the body (Ludeman et al., 2014; Elliott & Leys, 2007). This could be due to an enrichment of contractile cells or it could be a result of decreased resistance from the fine tissue and opening at the exit, or a combination of the two. Because of the fine nature of this tissue and that it appears to be partially or completely supported by internal flow, it is difficult to maintain during fixation following our normal protocol. This normally results in the tissue being damaged or collapsing and folding onto the apical pinacoderm, making the structure difficult if not impossible to understand. Where the structure forms on the

sponge is also difficult to predict which means sponges cannot consistently be grown in an orientation that makes the osculum clearly visible. In order to better understand this tissue, the following method was designed for isolating intact osculum from individual sponges and fixing them so that they can be used for immunostaining or *in situ* hybridization.

Method

Gemmules were plated and grown in a petri dish as described earlier. After hatching, water was refreshed daily with autoclaved LW. Sponge were examined using a dissecting microscope for the presence of an osculum. Prior to harvesting, poly-L-lysine (PLL) coated coverslips and glass bottom dishes were prepared by applying 50µL of 1% PLL to a labeled region and allowing evaporation in a laminar flow hood. In order to remove the osculum, a wide pipet was placed over the tissues and negative pressure was applied to maintain inflation and immobilize it. Concurrently, sterile fine tipped tweezers were placed at the base of the osculum and pinched the tissue off. A small razor blade was then used to excise the structure, which either remained in the pipet tip or floated towards the surface of the dish. The osculum was then pipetted onto the PLL coated slide or dish and allowed to settle. If settlement did not occur, it was positioned above the coating area and the LW around it was slowly removed until it contacted the slide/dish. Once the tissue made contact with the surface, it was briefly fixed with 3.7% formaldehyde (FA) or 4% paraformaldehyde (PFA) (depending on subsequent fixation) in LW for 10 minutes at room temperature in order to crosslink the osculum to the glass. For general actin staining and immunostainings, samples were further fixed in 3.7% FA

in EtOH for 35 minutes at room temperature and stainings were performed as described earlier. For *In situ* hybridization, samples were further fixed in 4% PFA in 1x PBST and then dehydrated with increasing concentrations of MeOH. Samples were rehydrated and hybridized with Stellaris probes following the protocol described above. All washes were performed under the dissecting scope and samples were equilibrated in 90% glycerol in PBS for 24 hours at 4ºC with very gentle rocking.

Results

The overall structure of the osculum did appear to be maintained with this protocol, including the ability to somewhat differentiate between the two layers by taking optical sections through the internal cavity (**Figure 111**). The staining patterns for actin did not reveal any clear structures that were organized at the tissue level as seen in the endopinacocytes, but there did appear to be some ring-like actin bundles **(Figure 111b**). The outside cell layer is composed of cells with a similar morphology to exopinacocytes and is likely composed of a continuous epithelial sheet with the body of the sponge (**Figure 111c**). However, the very small size of the cells being imaged may have made

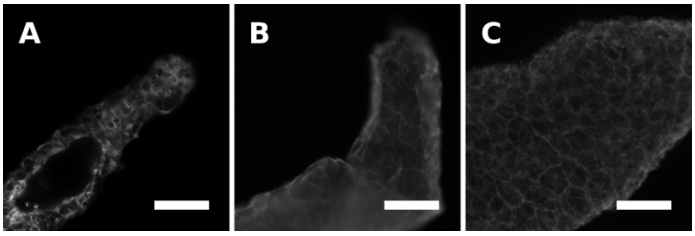

Figure 111. Actin organization in isolated oscula. Oscula were removed and stained for actin. **(a)** Small osculum has internal cavity visible and shows what appeared to be a bilayered tissue. **(b)** Osculum shows what appears to be actin rings running through the tissue near the tip. **(c)** Cell boundary staining is visible in the outer tissue layer of the osculum. These cells resemble the shape and structure of exopinacocytes of the apical pinacoderm, suggesting this is a continuous tissue. Scale bars 10μm.

this difficult to resolve. For the *in situ* hybridizations, with probes targeting the stMyHC, there was evidence of signal in this tissue (**Figure 95**). This suggests that the tissue does contain measurable amounts of myosin, though again the staining appeared ubiquitous and diffuse through the cells.

Discussion

Overall this method appears to be effective for preserving the overall structure of the osculum and allowing for downstream immunostaining or hybridizations. The extremely small size of the cells makes it difficult to understand the intracellular localization or organization of specific structures though. Because of this, it may serve best as a means of looking at expression patterns or simply presence or absence from specific cells in immunostainings. This could be informative for differences in the two cell layers, especially with respect to cells involved in non-motile cilia development and flow sensation, as this should be restricted to the internal lining (Ludeman et al., 2014). This could also be applied to understanding the cells that surround the excurrent pore at the tip of the osculum. In a variety of adult sponges, these cells serve to regulate the size of the opening and are contractile and actin dense (Prosser et al., 1962; Bagby, 1966). Understanding these structures during development of the osculum in *E. muelleri* could offer insight into the nature of these cells. They could resemble endopinacocytes, seen lining the excurrent canals, which form linear actin bundles that align with neighboring cells, or they could resemble exopinacocytes, with dense cortical actin which appear to rely on collective contraction to induce tissue movement. They could also represent an entirely independent lineage of contractile cells, which have unique development

regulators and contractile machinery. Based on the staining performed, it does seem that the majority of cells in the osculum, especially on the external tissue, resemble exopinacocytes. However, the actin rings observed in adult tissue of other sponges suggests that as this tissue matures it could take on a regional endopinacocyte-like structure.

Additional Figures for Appendix II

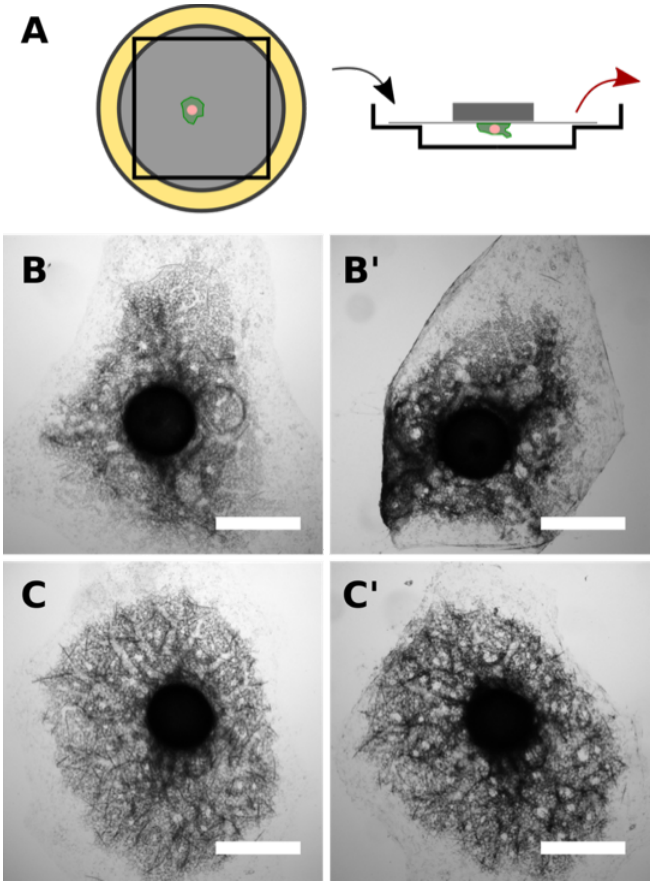

Figure A1. Increased tissue preservation. (a) Sponges are grown on coverslips which are then transferred to a glass bottom dish, held in place by a weight opposite the sponge. Liquid can then be added to the top of the coverslip with minimal agitation to the sponge tissue. Volumes down to 25µL can be directly applied under the coverslip. **(b)** Sample sponge prior to fixation. **(b')** Same sponge following hybridization protocol using traditional wash methods. **(c)** Sample sponge prior to fixation. **(c')** Same sponge using 'gentle' wash method described in **(a)**. Scale bars 500µm.

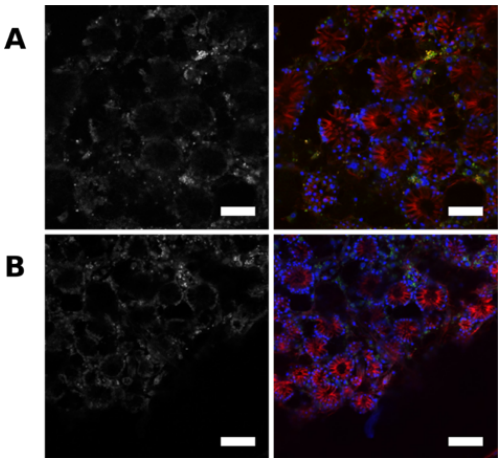

Figure A2. Actin preservation methods only maintain choanocyte collars. (a) Grayscale image of green channel and merge image showing stMyHC (green), actin (red) and DNA (blue). General pattern is consistent with previous trials. **(b)** RNase treated sponge showing similar region seen in **(a)**. Little difference is seen between the two, though brightly stained cells between chambers are less obvious. Scale bars 20µm.

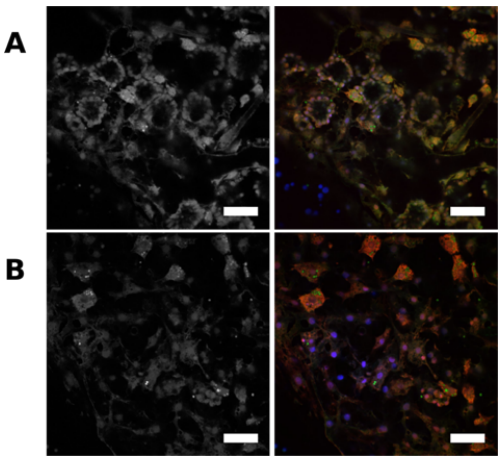

Figure A3. EtBr counterstaining helps to visualize individual cells. Grayscale images of green channel (left) and merge images of stMyHC (green), EtBr (red), and DNA (blue) for regions of the **(a)** choanoderm and **(b)** edge of the sponge. Bright punctate staining is only seen in the green channel, suggesting that it is from autofluorescent products or associate algae. Scale bars 20µm.

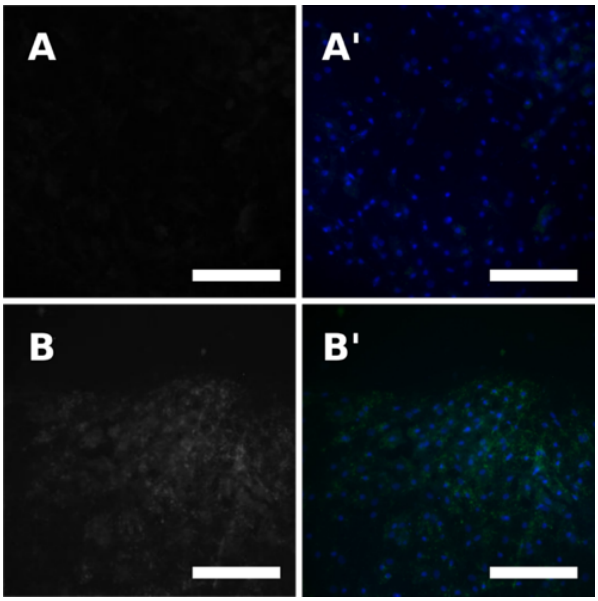

Figure A4. HCR for EmVin1 gives staining pattern along the pinacoderm. **(a)** Raw image of green channel for a sponge that went through full process (HCR amplifier were added) but EmVin1 probes were omitted. **(a')** Merge of green channel and DNA (blue). **(b)** Sample treated with EmVin1 probes shows signal along the tissue at the edge of the sponge, which is likely the pinacoderm. Scale bar 100μm.

Appendix III: Additional Information

Sequence information for sponge chapters;

List of UniProt entries used to generate Transgelin tree;

Human Transgelin 1, sp|Q01995; Human Transgelin 2, sp|P37802; Human Transgelin 3, sp|Q9UI15; Human SM22alpha, sp|Q5U0D2; Zebrafish Transgelin 1, tr|Q6P697; Zebrafish Transgelin 2, tr|Q6TGT5; Zebrafish Transgelin 3, tr|A2BEV4; Zebrafish SM22alpha, tr|Q29VH8; Frog Transgelin 1, tr|Q5U536; Frog Transgelin 2, tr|A0A1L8FCQ5; Frog Transgelin 3, tr|Q6P7J3; Fly Transgelin, tr|Q9VZI1; Nematode Transgelin, O44788; Fly MP20, sp|P14318; Tunicate Transgelin 2, tr|F7A7T2; Flatworm Myophillin, sp|Q24799; Tunicate Transgelin, tr|E4XQV3; Cnidarian Transgelin 1, tr|A7T059; Cnidarian Transgelin 2, tr|A7RPC0; Sponge Transgelin, tr|A0A1X7U007

E. muelleri transgelins sequences from transcriptome (Pena et al., 2016); EmTAGLN1, comp25280_c0_seq1; EmTAGLN2, comp47136_c0_seq2, EmTAGLN3, comp68850_c0_seq1

Sequences retrieved for MyHC Tree;

Mammal nmMyHC, sp|Q9UKX2, Mammal stMyHC, sp|P35579;Zebrafish nmMyHC tr|F8W3L6; Zebrafish stMyHC, tr|A0A0G2L6C1;Fly nmMyHC, sp|Q99323; Fly stMyHC sp|P05661; Nematode stMyHC, sp|P02567; Nematode nmMyHC, tr|Q22869; Tunicate stMyHC tr|A0A1W2W0I8; Tunicate nmMyHC, tr|A0A1W2W6Q6; Cnidarian stMyHC, tr|I2G9D5; Amphioxus nmMyHC, XP_003727482.1; Amphioxus stMyHC,

XP_019613454.1;Echinoderm stMyHC, XP_030839831; Echinoderm nmMyHC,

XP_003727482.1.

Type II-Myosin heavy chain sequences from *E. muelleri*. Fragments that antibodies were raised against are highlighted in gray;

>m.68719 (stMyHC)
MTDSDPSVYLRPGRTTDITEQMRMFDAKKWLWLNDEEECFKAAFVKSQKGDK
MVVELSNGSEVTVDINATQQMNPPKFEKIEDMASLTYLNEASVLHNLRQRYYSS
LIYTYSGLFCVAINPYRMLPVYTKTVIDMYRGKRKTEMPPHIFAVADNAYHDML
QDQENQSILITGESGAGKTENTKKVIQYFAVVAPSTQKQQTNLEDQVIQANPVLE
AFGNAKTIRNDNSSRFGKFIRVHFGNQGKISGADIEFYLLEKSRVIHQQAGERSYH
IFYQIMAGASQDLLNKLLLKRQPKSYSFLANSELTVDNVDDSQMFKLTQEAMET
LSFTEDEQMFLFKVIAGVLHFGNIEVKQRPREEWATIPTAEECDKVSHILGISSAD
LMKALIKPRIRVGNEYVQQGRNMDQVKYSIGALSKSLYERMFRWLVSRVNKTL
DTKTRKNFFIGVLDIAGFEIFKLNSFEQLCINYTNERLQQFFNHHMFVLEQEEYRK
EGINWEFIDFGLDLQPCIDLIEKPLGIFSILDEECLFPKASDQSFINKLNANHADKSP
NYIKAQFKTGGNTIDFEVAHYAGTVGYTAAGWLDKNKDPLNDNVVELLKKSTD
PGIASLWNDYLPEGERKGKGSQFVTMAHLHKQSLNNLMTTLGNTTPHFVRCIIP
NEMKRPGVIDAHLVLHQLRCNGVLEGIRICRKGFPNRLLYQEFRQRYIILAPKSIP
AGFMDGRKATEALIEALQLENTEYRLGHSKVFFRAGVLGRLEDMRDERLSIVLT
QFQSFCRGYSTRKTYRKLLDQRLAIAVIQRNVRKHLFLRDWKWWKLYTKVKPL
LNVARTEDELRQKEEELNKMREKLSKEEQGRKALEDIKTQLMEEKNQLFVQLQR
EHDACAEAEENLQRLLGKKTDLEAHLQELVDRLDEEVENNANISAARRKVEAEL
EHHKESLTELKITLEQTVQEKAQKEKDCATLDAELEKVNESLSRTNKEKTSLEER
LQELTNSLQNEEDKANRLSKLKIKLESTIQETHDELQKEKVARGELEKAKRKVEA
DLKSGQDALEQINRSKAELEKSLTGKDKEIADLVQKVEEDQSQVAALQRRIRELE
ARIEELEEDLENERSQRQKAEKQKADLTKELETLQDQLEEEGGAKTAQLELNKK
REVELVQLRKDQERVSEDHEKVVADLRKKHAQSVGELEEKVDSLQKAKAKLEK
EKASLSTEGSDLVAQVQQMEKTKVATEKRLKQLEEQNGEISARLREYESTIATLQ
AAQAKAQSENAELLQQATDAESKIGVITKAKNALEAQLDEAKAELESESNSKAD
IMVKLKAMESELNHAHESIEEEQEGKTELQKQLTATKNDAAQLRARLDNEATPR
IEELEDTKRKLQNKLKEAEEALTLSDSKYAALDKTKTRIATELEDLHLDLEKERS
NSAALENKQKKIDQQITEWRSKYESKQAELENAQKEARNYSTEVLKLKGQYDEL
HDQLEAANKENKHLQGEISDLEKQLSEGGSSVHDLEKAKRKLEQEKEELTQSLE
DAEGQLEGEQQRVLRIQLELTQLKQETERKLAEKDGEMESLRKNHGRQQESLQQ
SLEEESKAKNEQIRLKKVVEGQIDELQATIDAGEKAASDNQKKIKALQQQVKEIT
SSFEEEQRLRSEDRDLTTKAEKRANDLQREIEELRVNMEQLQKSLRNIEAENADA
QERLTEANNSKTSLVASKRKVDQQLATLQGEYEELESEGKENSEKLRKATELVV
RYQSEVMAEKEAANALEKARAALDQQVKDLTARLGEEVANATKSAKKEAQKL
QARITELEGELETETKGKGDAQRNLKRLDRRVKEVQAQMEEEKAASQRLQEQIN

SLNAKAKTLRREKEDTEGELEAMRTKNRQLRSALDESEEEKAGLQAQLSKARTT
TTTSARKGKPAPVDADDDK

>m.68713 (nmMyHC)
MAEEPLKYLSVHREKVSDALAQTEWAQKKLVWVPHPEAGFLSGSIKTEKGDEL
TVELQDGSKRTVHKDEVQKMNPPKFEKVEDMAELSFLNEASVLYNLQARYFSG
LIYTYSGLFCVVVNPYRMLPIYTETVVDLYRGKKRHELPPHIYAVTEQAFRNMLL
DHENQSILCTGESGAGKTENTKKVIQYLTSVAAAHHPHTKTLQRRGSSSLMVKT
GLTGSQGELEAQLLQANPILEAFGNAKTVKNDNSSRFGKFIRINFDQNGFIAGAN
VETYLLEKSRAVQQAPDERTFHIFYQILNGMTPQTKTEYLFEKPEAYAYLSNGNL
AVAGINDANDYEDTLEAMNIMGISEEERAAVFRVISAVLHFGNLKFKQERSSDQ
ALLVDDTIAQKISKLLGMPVTEFTKALLKPKIKTGREFTVRSQNMAQVEFSSQAL
TKALYERLFKWLVARINRSLDRSVKQGSSFIGILDIAGFEIFKINSFEQLCINYTNE
KLQQLFNHTMFVLEQEEYKTEGIEWTFIDFGLDLQPTIDLIEKPMGILSLLDEECW
FPKATDKSYTEKINREHGQSGKFSKPDFRSKADFTLVHYAGSVDYCCDNWLMK
NMDPLNDNVVQLLASSTDAFVAALWRDTANIVSLTARGDDTTPAAPSTVFGAQ
QRSTTRKGMFRTVGQLYKEQLANLMGVLTQTQPHFVRCIIPNHEKKANKIVAHL
VLDQLRCNGVLEGIRICRLGFPNRVLFQELRQRYEILCPGIIPKGFMDGKKAAQM
MLQALDLDSASYRIGHSKVFFRAGVLAQLEEERDIKLSEVIIQFQSWCRGFLGRK
AYQKRTEQTRAIRIVQRNVQSYLKLRNWGWWRLFTKVKPLLQVTAAEDQKRE
MEEELKRLSDQIDKFKFEYADLTKKNEQTVSENQRLEEQVREEKFLNQEAEELK
NMLTQKRAELEALLQEAESKLEEEAERAKALAEEKKKLQAGMQTLEEQLEEESN
ALHKITSEKAAAESKIKTLEEQITSNDDNISKLTRDRNTLEERLAETQKALATEEN
NSKQEHRQRLKLESSVQELEEKLDRESVRRQDLEKEKRKLQSDASDLLDQLTKA
KQRIADLEAVVARMEKDLAAANTKLEEEMAGRAKLDKEKRDLLVQLQELQDD
LESEREAKTKTEKQRKQLADELEKLRDSLEATVSSSAAQQEIRTQRENELAALKK
TLEDEANNHEAILTAMKQKQAKAAQETNDQIEALKRAKVNLDKSKLSLETENES
LASELKDLTYNYNESDKRRKQAESQLSEAQSRIAEDNAKLQELAKENERLKNEQ
SALSAQFETVDHKCSTLDKAVKSLKEQLKETEEHLTDETRQKIASSNKQKQLEDE
VQRLNQQLEDEEEIKAGIHSKMVQATQQLTESKKKCDELQAEVEEAALARRKQ
DKELEGAREKIDELTTENQKLSQSKKRVQEELDDLTVSTESLRGQIAQLDKKQKK
FDTQLAEEHALAERYASERDMAETRARQVETRSLSLTHELEEVREKLEEAEKFK
KQLQGERDALVESKDDVGKNVHELEKAKKSVEAELAEVKQMLEEAEDQIQLTE
DAKLRIEVNFQALKTNYERDLAAKEEQTEEARRKLTLQLRDLEGQMEEERKQRT
AAQNGRKKLESDIHDLQVQLDAEGKGKEELQRQLKKVQTQLKESQMSADEVLK
VKEDATSKLKELEKKVKTLETDLAQAQEEVAAAERVRRSAEAEKDELHDEVSTS
GSKLNTLAEEKRQLLNRITTLEEDLEEEQLNNDAAQEKAKKALQQVDVLTSEIA
ALQTSIQGSEATKAQLEKQIKDLRERLEEAESVGVRKMKGQLQSMEEKIRGLEEQ
LDTANKDRAQLTRTQRRQEKKLKEVQASIDDERRAAEQFKAEAEKAGGRMRTM
KRSMDEMEEENARLNATKRRLQRELEELTEQNEQLTRDLHSRKGGSTSSASGAG
AGGAGSRRSTFTGGSKGSTAGVGRKTSTRHDRQTGHGTDDSLPDDDED

List of hits from mass spec performed on stMyHC IP precipitates. Values report total spectrum number in each sample;

	IgG	stMyHC	Description
m.68719	0	23	stMyHC
m.4221	17	17	Thioredoxin Domain containing protein
m.284335	12	9	Neuroglobin-like
m.104798	0	8	cAMP-regulated phosphoprotein
m.234174	7	6	WASH complex subunit SWIP-like
m.180560	0	4	Hs71kDa Protein
m.7673	3	4	hippocalin-like
m.284156	0	3	endoplasmin
m.214461	0	3	multidrug resistance protein 1
m.123867	3	3	actin, cytoplasmic
m.23308	0	3	TNF receptor-associated factor 5-like
m.187327	0	2	cystatin-A-like
m.69839	0	2	pre-mRNA-processing-splicing factor 8

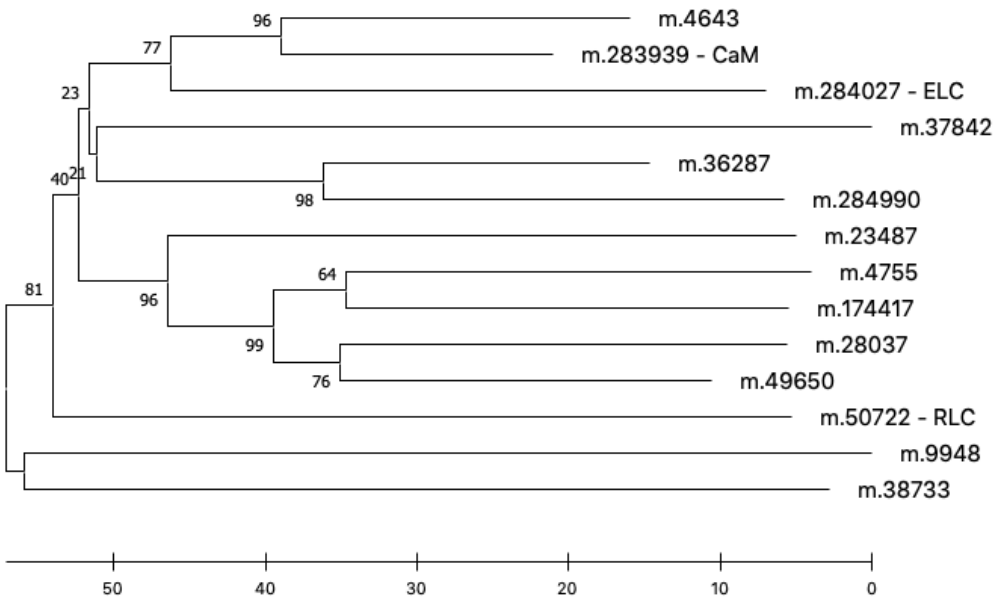

Maximum likelihood phylogeny of EF-hand proteins in *E. muelleri*, based on predicted protein sequences from the transcriptome (Pena et al., 2016). Predicted orthologs for calmodulin (CaM), myosin regulatory light chain (RLC), and myosin essential light chain (ELC) are labeled. Support based on 100 bootstrap iterations.

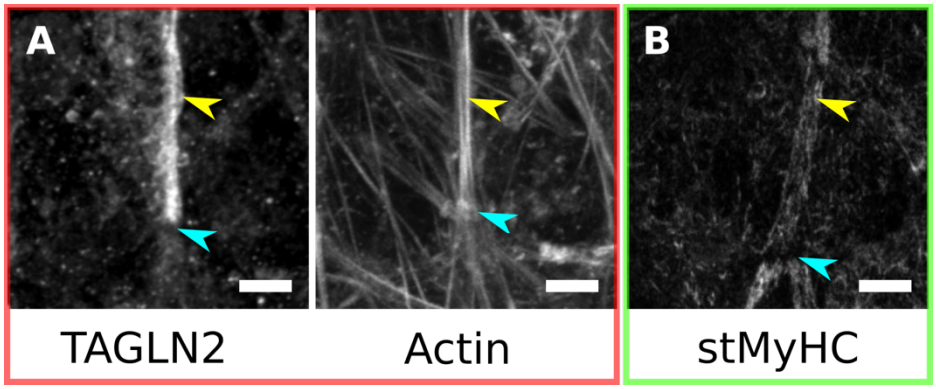

EmTAGLN2 and EmstMyHC stain similar structures. **(a)** Immunostaining of EmTAGLN2 shows strong signal along an actin tract (yellow arrows) with no staining at the adhesion plaque (cyan arrow). **(b)** Immunostaining of EmstMyHC at a similar structure shows a consistent pattern, with organized signal along a putative actin tract (yellow arrow) and no signal at a branch point which likely represents an adhesion plaque (cyan arrow). Scale bars 5μm.

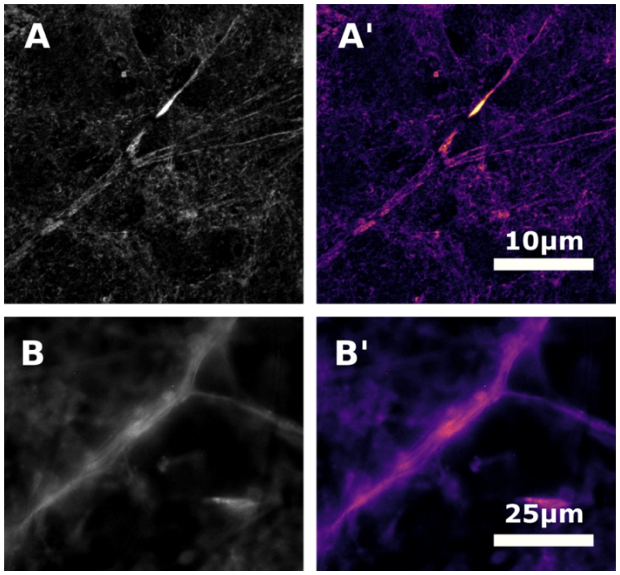

EmstMyHC+ structures are larger in aged sponges. (a) Immunostaining for stMyHC in a 5dph grown under standard conditions. **(a')** Intensity colored image from **(a)** with warmer colors representing higher intensity staining. **(b)** Immunostaining for stMyHC in *E. muelleri* which was maintained for 6 weeks in an aquarium seeded with fresh lakewater. **(b')** Intensity colored image of **(b)** shows high level of localization to the central structure with limited background compared to **(a')**. Sponges were only successfully maintained in the lab for this length of time once, so it has not been possible to replicate this.

Sequences retrieved for MRTF tree:

Mouse MRTF-A, tr|E7F9J6; Zebrafish MRTF-A, sp|Q8K4J6; Frog MRTF-A, sp|Q8AYC2; Mouse MRTF-B, sp|P59759; Zebrafish MRTF-B, tr|U3JAU7; Frog MRTF-B, sp|Q8AYC1; Mouse myocardin, sp|Q8VIM5; Zebrafish myocardin, XP_005169482.1; Frog myocardin, tr|B0ZE99; Fly MRTF-D, tr|Q9VZY2; Fly MRTF, tr|Q6B4I4; Octopus MRTF, tr|A0A0L8H4W5; Arachnid MRTF, XP_015906589; Sea Urchin MRTF, SPU_005255.3a; Tunicate MRTF, jgi|Cioin2|287879; Choanoflagellate SAP protein, XP_001745005.1

Sequence for *E. muelleri* MRTF ortholog from the transcriptome (Pena et al., 2016).

Region cloned for recombinant expression is highlighted in gray. Primer sites are

underlined;

>EmMRTF (comp66601_c2_seq2)
CGGTATGTTTTTTTTTTAATGTAAGTGGTGCTTCTCTTGTATAGCTCAGCGGAC
CTTCACTCATAAAACTTGTTACCACCACCGACACCTCCTCCCTCAACCCCAGC
GCCTCTCATGCTCTAGTCGAACCTTGGTGTTTTGGTGGGGCGACTTGTCCCTC
TCGCGTAGCTTCGCCCTCATCTGTGCCTCCAAATCCACTAGCGCCTCGTATTC
GGCGTCCCTGGGGTGGCATATCGTTACAGCACCAGTGAGGAGTGTCAATTAC
TTACCACGAGTTTTGGCTGTGGTAGTCCATTCTCTTGGGATTGCAAACCGAAG
GCAAACAAAACAAGCCTGCTGAATACTGGATGACGTCATTGGGAGGAGTCCA
AATTAGGCCCGAGTGCTGTGTATCCAAAACTGTGGAGGTTTGAGTTCATAGA
ATTGATTGCCCTTACCTTGGAAAGGCGAATTGATATTGACATTGGGAATCGTC
TTGGAACCAACAGTTAGACTGGTGACATTCCCACGCCAAGAGTTGTGGAGGA
GACGCTGTGGTACGGCGACACACCTTGGGCCCAGAATGCTCGTACTGTCCTA
TGGACTGCATGTACACCGTTCGTAGCTGTGCACAGACCTATTGCTTTTGGCTG
TTACGAGTAGAAGTAAGAGTGAATCACCGAAACACAGGTGTGTACCAAAGTG
TCCGTCAAACGGCGGTCGAGTTATTAGCATATTATGAGCTCTTGCGAGCCGCT
GAGCTTGGACTGGCTGGACGAAGAACTATCTGCCAGCCATTCTGTGGACCAA
CGCTCCATGAATCGAGCTACTGTGCAAGGCGAACTTGAGAAGAGGCTTCGCT
GTCGCGCTGATCGCGATGATCTCGTGAAGAAGCACATCCTACCAGACCTGAG
CACATCACCTGTCCTCTATGGTCAAACACAGCTGCTACAAAGAGCTCAGATC
GCTGATACACTGAAGAAGAAACTGTCCAGCCGTGCTGAGAGAAATGAGCTTC
TGCAGTTGAATATATTACCAGATTTGCAGACGATCATCGCACCAAAGCTCCA
GGCCAAGCAACTCGAGCTCAAGAAACACAAGCTGGCTGACAGCCTAAATGA
GAAGTTGGCCAATCGCCCTGGACCCTTGGAGCTGGTCAGAGAAGGGATCCTG
GAACCAAAGAACAACACGTTGGCAGCCATGGTGCAATCCGTGGATGGGAAC
AATGAACCGTTGAGCGTAGAGGGGGGAGGGGGGGGACACCCCACCTTGTCG
ACATGTGGCTTTTCCGACAGCGAATTCCTGTCTCCCCCAGAGACCCAGAAGA
TCAGCGACTCATCCAGTCCCACTCCTTCCCCACGAGAAGGAAGTGTGGAAGC
TTCGTCTCCTGTCAAGTCCCTCATGTCCCCGCCCACTTTCCCGGGCTCCTTTTC
CGCCATGGCGGCAGGCGCCCAGCAGCACTTTGCACATTCTATGGAGCTGGGA
ACCAGGCTCGGGAAGGCCATGTCCCCAAGCGTGATCCGAAAGAAGCAACAG
AAGCAGCAGAAGTATCGCAAGCTGAGGTACCACGAGTACATCCCCCCGAGC
AAGAACAATGGGAAAGGGGGGAAGACCAACCAGAAGACCCACACCTCGTCC
AAGCCAGAGAGCCCTTACTCGGTGCTCCTCCAGCAGCAGCAGCTGTTCCTGC
AGCTCCAGGTCCTCCAGCAACAGTACCCCAACGGCGTCCTCATGCAGAAACT
TCCCGACATCCTCAAAGGCATCAAGCAGGATGGCTCCTCTTCCTCTGGTGGCA
GGAAGGACAGCAGTGGCACTGGGAAATCTCAGACGAGCCCCTCCGGTGCGG
AAAAGTCCGGGAGCAGTTCCACCCCAGGACTGCCCCAGACGGTGCAGGTGG
AGCAGCCGAACCATCTGAACGCGACCACCATACGCTTCGACGAGCTCAAGGT
GAGCGATCTCAAGACGGCCTGCAAGGAGATGCGACTCATCGTCTCCGGGAAG

AAGGCGGAGCTTGTGGAGAGGCTCCTGGAGCACAACAATGGCTACCTTCCCG
TGTGTGCCCTCCCCGACGGCCAGAGCAAGGACGCCAGGAAATGCTCAGGTGC
CCAGTCCACCGCCTCATTCGACTCCTCCCAGGCCTCTGCCGCTTCCCCCATGT
CCCCCACACTCTCCTCCCCAATCTTCAAATTCCCTCACATCGGGGGCGTGTCC
TCTTCGTCCGTCGTGGACTGCCTTTCTTCCATCTCTCCCCTAGGGGGACCTGCT
ATGGCCCAAGTTTTCCCAGCGTCAAACTTCCAGCAGCAGTTTGACGAAATTGT
TGAGCGACAGAAGAGGAGCTACATCAGTCAGAAGGCACCCAAGACCATTGC
CCCGAGACCCGAGCTGAATGACATGGTGGCCATACGGTTCCCCTGCCTCGAG
CAGAGGGGGGTCAGGGGGGTGGGGGCTCCCAACAACGGCGGGAGGGATGGG
AGATGTCCCCCCGGAGGGGTCCAGGCCTCAAAATCCCTCCCGACCAGTCCCA
AGAACGCCTCCCCCACAGACAGCGCACAGAGCCTTCTCAACGAGCTCATGGA
GAGTGGCGAGGGTGTGGCCGGGGAGGATGTGAAACCCCCGGGATTCGGCGG
GGAGACGCTGACGTCTCAGCCGTCCGGTCTCCAATCGACACGCTTCTCTGAGT
CCCTCGGTCTGACCACACCCAGCCTCAGTGTCATGCACAGTCCATCACCACAC
TCCGTCTATATCCACCAGCAACAGATTCATCATCATCAGCAGCAGCAGCAAC
AGCAGCAATCACAGCAGAGGCTGCACAGGGCGTCCATGCCAGCAGTGCCTG
GCCAAAACCCACTCCAAACTCTTCGCTACGAGCAGCCCTTGATACAGAGATC
GCTGAGCGTCGCTGGGGTGCCTCTGTCCCAACTCTCCACCTCCACCTCCTCCT
CCACTACATCTTACCCTTCCCTTCCTGAGATGGGATCTGGTGGGACGGGCGAC
CTGGGAAAGGCCATGTCCTCCAACGGCCTCCTCCTGGGACAAGATGAGGGTC
TCTCCATGGCTGTAGGCGGAGAGTTAATGGAGATCGAAACCTCTGAGTTCAA
AGACCAGCCGCTCTCAGACATTCTGGACATTTTCCCTCCTGGGAGTAACGAGT
ACAATGCTCACCAGCCACACACCCTCGGATACGACAACAAGGCATTGAGAGT
GGACATGTCTTCATCGGACGACATCATGCTCTCCAGTCACCCGCTCCAACCCT
TTGGCAACAGCCTCAACCACCAGAGCAGGTCGACCTCCGACCTCTGCCTGCG
GGACAACACGAAAAGCAACCTAGGAGGGGGCGGGGGTGGCTATGGAAACAA
TCACATGATCTCCAGCGAGTTTGGGTGGCTCGACCTGACGCTAGACAACATG
GGCACCTTTGGTCTTTCCCCGTCCCCGTCCATTGGCAGTGCAGCTGCGATGAG
TCATTCGAATCCCAACTCCCTGATGCAGGACTCCAACTACATGTACTTCATGG
ACGACAGCTCAGTGCACTCGAAGGGTTCAAACCCGCCCACTGGAGTCAGCGT
CCATCATCACGACGCAACCACCTTCTTAGAACCCGTCCTCAATCCTGCATCTC
ATTTCTTCCCCACATCAGAAGAGGCAACTCTTTTGGAACTTGGCCTTTCCACA
AGCTAACTCATGTTGCATGCTAGAATTGTTACCAGTCCAAAAATAAAAAAAA
TAAAAAATTTCACCTCAAAAATAGATCTAATACCATATGCACTGCAAATCCTT
TTAACCTTTCTGGACCCTCCCATGTCACGTTCAAAAGATTCATGGTGTACTTA
GTGCTTATGTATGTGTGATCCTGTGTCCTGTTATTTTCTGTTTCATTTGCATAT
GCTGTATTTAAAATTTGAACAAATTCTCAATTGTAAAAAAAAAAA

Predicted protein sequence with fragment antibody was raised against underlined;

MSSCEPLSLDWLDEELSASHSVDQRSMNRATVQGELEKRLRCRADRDDLVKKHI
LPDLSTSPVLYGQTQLLQRAQIADTLKKKLSSRAERNELLQLNILPDLQTIIAPKLQ
AKQLELKKHKLADSLNEKLANRPGPLELVREGILEPKNNTLAAMVQSVDGNNEP
LSVEGGGGGHPTLSTCGFSDSEFLSPPETQKISDSSSPTPSPREGSVEASSPVKSLM
SPPTFPGSFSAMAAGAQQHFAHSMELGTRLGKAMSPSVIRKKQQKQQKYRKLR

YHEYIPPSKNNGKGGKTNQKTHTSSKPESPYSVLLQQQQLFLQLQVLQQQYPNG
VLMQKLPDILKGIKQDGSSSSGGRKDSSGTGKSQTSPSGAEKSGSSSTPGLPQTVQ
VEQPNHLNATTIRFDELKVSDLKTACKEMRLIVSGKKAELVERLLEHNNGYLPV
CALPDGQSKDARKCSGAQSTASFDSSQASAASPMSPTLSSPIFKFPHIGGVSSSSV
VDCLSSISPLGGPAMAQVFPASNFQQQFDEIVERQKRSYISQKAPKTIAPRPELND
MVAIRFPCLEQRGVRGVGAPNNGGRDGRCPPGGVQASKSLPTSPKNASPTDSAQ
SLLNELMESGEGVAGEDVKPPGFGGETLTSQPSGLQSTRFSESLGLTTPSLSVMHS
PSPHSVYIHQQQIHHHQQQQQQQQSQQRLHRASMPAVPGQNPLQTLRYEQPLIQ
RSLSVAGVPLSQLSTSTSSSTTSYPSLPEMGSGGTGDLGKAMSSNGLLLGQDEGL
SMAVGGELMEIETSEFKDQPLSDILDIFPPGSNEYNAHQPHTLGYDNKALRVDMS
SSDDIMLSSHPLQPFGNSLNHQSRSTSDLCLRDNTKSNLGGGGGGYGNNHMISSE
FGWLDLTLDNMGTFGLSPSPSIGSAAAMSHSNPNSLMQDSNYMYFMDDSSVHS
KGSNPPTGVSVHHHDATTFLEPVLNPASHFFPTSEEATLLELGLSTS

Sequence for *E. muelleri* Mef2 ortholog from the transcriptome (Pena et al., 2016).

Region cloned for recombinant expression is highlighted in gray. Primer sites are

underlined;

>EmMef2 (comp58604_c0_seq1)
GGTGCACGTGAGATTGTTTATTGGAGAAAACAACACAAGCCAGAAGCAAAA
GCTATTCTTTATTTCATTTTTAGTCTGCTCCACCTTGAATACAGCAGCTAAGGC
GCCAGAAACCATTCTTCTGTCTCATCGTTCTACCACCATATATATAAATACTG
AGAAGGCTGGTCCCTGGAACTGAAACATTATGGGGCGTAAAAAGATAGCAAT
TACACGTATATCAGATGAAAGGAACAGACAGATAACATTTAGTAAGCGTAAA
GCTGGGCTACTGAAGAAAGCTTACGAGCTGAGCATCTTATGTGATGTTGAGA
TAGCTGTGATCATGATCACGAGCAACATGTACCAGTACGCCAGCTCAAATAT
GAACTCAATTCTCATTCGCTACACTGACTTCAAAGATCCTGACGAAAGCAAG
ACTAATGCTGATATACTGGAGGACATAACCAAGAGAGATAAAGGCTCTCAGC
CAGATGACTCAGGGGATGAGGAGGAGGAGACTACCAGTGCCCCTCAGAGCTT
CCTTCTCACTCCCAGAACCCAAGCCCACCATAACAAGCTTGAGGATGATTTTG
AGCGTCTCATACGACACAACCCAGTTCCTCCATCTCCAATGGTACCATCCCCT
CTTAGCTCCAAGGCGCCGGAAGCCATGCCTGTGAGGATTCCAGTCAATCATT
CTCCCAATCCTGTTCATTCCCAATTGGAGCACACCACTGGTCCTTCTTCAGTG
TCCAGTACCAGCAGCATGTTGACACCACCAAACTCCAGTGAATCGACAGTGG
GAAGTCCCTCTGTGCTATCCAAGTCCCCAGGCAGCATGCACCCACCTCAGGG
GAACCCTGCGAGGCTAAGGAAGGTAGGAAATAACACCATCAAGCTTCACCC
ACCCGGCAGTGGACGTAACTACATCACCCTGGAGCCACAAAGTGATGCTCAG
GGGAAGAAGCCCTCCACCCAGTCGCTGAACGGGGAGGGGGAGGAAATAGTT
CTCACCCAGGGGTCAGGTGGAGATGGAGGGCTGGCAGCCAAAGGAGGAGGT
GGGGGAGGGAACAAACCTCAGCTAAGAGTCATGATCCCCAATCAGAAAGTG
TTTGGACCCAAAGGAACGTCACCTCCACACACCGAAGGAGGCACTCACCCAA
CTGCCTCTATTGCCACAACAGACACCAGCTTGACCACGCCCATCATGTCCCTG
GTAACGCCCAGCCTCCTGGGGGGCAACCTGTTCTCCAGTATTATGGGAGGGG

AGTTCCCTTTCAACTCGGCCACAGGGCCGGGCAGTGAGATGCACTCTGCCCTT
GTTGCCTTCCCGGTCAGCATCCAGCCAACAAGTGGAGCAGGGTCCAATTCCA
CAGCTGGGAACATCATCCTTCAGGCCCAGAATATGGGTCAACCTTTTTTACTT
ACGCCTAGCTATGACCGCCAGAACTCTGTCTACACGTCTCAAGTGCAGCTTCC
GGCCAACACGTTTGGCGCCATCAGCCCGGGGTCCCGAGATGTTGAGCAGCTG
AAGATGCATTACGAGAAGATACAGCAGCACTTGCTGCTGTCCCAAGCCCTGC
AGAGCGCCCAGACCAGTACGGCGATGGCAGAAGCAGGCCACATGGGCAGAG
GGGAGGAGGAGCCTGAAACGCAACTAGCATCGCAACCATCACAGTTCTTAAA
TTCTGATGTGATGATGAGTTCGCAGACAAAAGAGCCTCTTCCTTCCATCACTG
TTGAATCTGATGCACCACCGCCTTCTAAGAAGCAGCGAAGAAGACCGTCGTC
TGATACAGCAGTGTGACTGTGTGTGTGGTATGCGTGTATGTGTGCACTGACAC
ACCATCAACACTCGATCATTTGTTATGGTGTAGTTGTTATAGATGGAAGTCAA
CTGAATGTTTGAGCACTTTTATATTTCCTAAATACAGAGAAAAAAA

Predicted protein sequence, with fragment expressed underlined;

MGRKKIAITRISDERNRQITFSKRKAGLLKKAYELSILCDVEIAVIMITSNKKLYQY
ASSNMNSILIRYTDFKDPDESKTNADILEDITKRDKGSQPDDSGDEEEETTSAPQS
FLLTPRTQAHHNKLEDDFERLIRHNPVPPSPMVPSPLSSKAPEAMPVRIPVNHSPN
PVHSQLEHTTGPSSVSSTSSMLTPPNSSESTVGSPSVLSKSPGSMHPPQGNPARLR
KVGNNTIKLHPPGSGRNYITLEPQSDAQGKKPSTQSLNGEGEEIVLTQGSGGDGG
LAAKGGGGGGNKPQLRVMIPNQKVFGPKGTSPPHTEGGTHPTASIATTDTSLTTP
IMSLVTPSLLGGNLFSSIMGGEFPFNSATGPGSEMHSALVAFPVSIQPTSGAGSNST
AGNIILQAQNMGQPFLLTPSYDRQNSVYTSQVQLPANTFGAISPGSRDVEQLKMH
YEKIQQHLLLSQALQSAQTSTAMAEAGHMGRGEEPETQLASQPSQFLNSDVMM
SSQTKEPLPSITVESDAPPPSKKQRRRPSSDTAV

Sequence for *E. muelleri* SRF ortholog from the transcriptome (Pena et al., 2016). Region

cloned for recombinant expression is highlighted in gray. Primer sites are underlined;

>EmSRF (comp29338_c0_seq1)
AAATCTATGCAATAAAGAGAAGTGAACAAGGGCTTTCCATACAAGGTAATTC
CTGCAAACCTCGGAGTCATATAAGCATGAGCGAAAACGGAAAGTCGCAGTCA
CGTACAAACTTCGCGAGTGCGAAGAACAAGCCAACCGTCTCGGCTTCTAAAA
CCTCACAGAAGTTCAGGTCTGCTGGTCAGCCTGCTGGTCAAACTTCTTCAAGT
ATGCTCGGAGAAAGATACAGCCCCAACCCTCAAGAGTCAACAACCGACCCTT
TTGTCCCAGGAACCCAGTACCTTCCCCACAAGCGTAAAATGGATGATAACGA
ACGCTCAAGCGTTAGCGACAACGACGACTCGGTACAGTCGAACGACGAAAA
GCCAAAGCCTGCTCCCGGCAAAAAGACCCGCGGTCGTGTCAAGATCCAAATG
GAATACATCCAGAACAAGCTTCGCAGATACACAACGTTCTCGAAGAGAAAGT
CAGGAATCATGAAGAAGGCCTATGAACTCAGTACTCTTACAGGAACGCAAGT
CATGCTTCTCGTTGCCTCAGAGACCGGGCACGTCTACACCTTTGCAACACCCA
AGCTCCAGCCCATGATTACGTCAGAAGCCGGCAAGGCGCTCATACAGACTTG
CCTTCACAGCCCTGACCCGCCCACCAGTGTGGTCAACCCCGTGATGGAGTAC

GACATGCGCATGAATGTTTCCGGTTACGAAGAAACCGATCTCGGATACGCCG
TGAACGACGAAGATTTCACCACACACGGAATGGTGTCTGTGTGCTCCTCTGG
CAGCATGCCCATCATGAGCAGTCAGGGTATCGTCACCATCCCCCAGGGACTG
ATGCAGATGCCCTTCTCCGGCCATGACACAATGACAACTCACGCCATCATGG
CCCAGACCCATCCAATGCACGTCCAGACCCTGGCCTCTGCCTCCCAGAACCTC
TCGCCCCATGCCTCACCCCCGCCAAGCTACTCCCCACCGCGGACCTACACAG
CCACTCCCTCTTCCTACCCGGGGAGCCCGGGACCTGTGTACTCTCAGGCCTCC
CAACTGCCTCATCAGTCCGTGATGATTGACGACCTTGGCTCTCCCAACCACAT
GGGAGGGAGCCCACACCTGGGCCCCATGGAGCACTATGACAGGAGCCCAAG
CCACAGCCCCATCCAGAGCAGATACAGTCCTCATGGGTACTCCACTGGTAGT
CCTATGACTGGACACTCTCCCATGAGGCACATGTAAACTGCCCTCTCCTGCCC
TCTTTTGGATGTGTCGTGTCTTCCTTGAGAGCTTCTTCTACCCCACCACACCTC
ACTGTGTTTCTTGTTCAAAAAGGCCTAAGACTTTGTGTGTGTCTGAACGTTTG
TTACAACCTCGAGCTGGTCTCGCAGGGCTTTTGCTGTGCGTTCTGTTTTGTACT
GTTTCACTGCTTGCACAGTTTGTTGCAAACATTTACTGTGTATAAACCCTTCCC
CCTCACACGCACACAGCAAACCCCCCCCCCCTCCCACCTCATTTTAGGTCAAC
CTAGCAGCTGGTCTGTTAAGGTTTTTTTTTATTATTAAACTTTAAAAACAAA
AAAAAA

Predicted protein sequence, with fragment expressed underlined;

IYAIKRSEQGLSIQGNSCKPRSHISMSENGKSQSRTNFASAKNKPTVSASKTSQKF
RSAGQPAGQTSSSMLGERYSPNPQESTTDPFVPGTQYLPHKRKMDDNERSSVSD
NDDSVQSNDEKPKPAPGKKTRGRVKIQMEYIQNKLRRYTTFSKRKSGIMKKAYE
LSTLTGTQVMLLVASETGHVYTFATPKLQPMITSEAGKALIQTCLHSPDPPTSVV
NPVMEYDMRMNVSGYEETDLGYAVNDEDFTTHGMVSVCSSGSMPIMSSQGIVT
IPQGLMQMPFSGHDTMTTHAIMAQTHPMHVQTLASASQNLSPHASPPPSYSPPRT
YTATPSSYPGSPGPVYSQASQLPHQSVMIDDLGSPNHMGGSPHLGPMEHYDRSPS
HSPIQSRYSPHGYSTGSPMTGHSPMRHM

Nematostella vectensis Orthologs

Nematostella vectensis ortholog sequences used for *in situ* hybridization probes in gray. Primer sites are underined. Sequences retrieved from JGI *Nematostella vectensis* v1.0 genome (Putnam et al. 2007);

>NvSRF - fgenesh1_pg.scaffold_52000005
ATGCAGTATTCGACACCGTCACAGGTTGTTTTAGAGGGAGCTGGGATTTCAG
AGCAGAGTGAGTCATTTCTCTCTAGTGAAATGGCCGGGGATTCCATGAAACG
ACCTCTCGAGAGCGACGAAGACGATGATGATGGTGCTAGCCCTGTATCGGAC
CAAAAACCCAAGAAAAAAACTCGGGGAAGAGTAAAAATTGAAATGAAGTTT
ATCTCCAATAAACTCAGACGGTATACAACATTCAGCAAAAGAAAGACGGGG
ATTATGAAGAAGGCATATGAGCTTAGCACACTCACGGGGACACAAGTGATGT
TGCTTGTAGCCTCTGAAACAGGCCATGTGTACACATTTGCAACTCGCAAACTA
CAACCCATGATCACGTCTGAAAGTGGCAAAGCACTGATCCAAACTTGTCTCA
ACTCTCCCGATCCTCCAGTCTCGCAGATTCCAAACCCTGATCAGAGAATGTCG
GCAACTGGTTACGAAGAAACTGATCTCACCTATACCGTCAGTGAAAACGAAA
CGGATAAAAAAAAACTGCCCAAAATTTGATTCACAAATCTCTATAACAGTAGT
AATATCAGTAGAAATTTGTATAAAGGACAGGGGAGGAATGTTTACAGCCCAG
CAAATTGAGACCGGACAACAGATTGGAGGCATCAACAATGCTACCATGACAG
GGATTACCGCTATGTCTGCCTCAGGCCACACTTTCCCCATAACAACCTACATA
CCACACCAGGGCAATAGTAAACCCGGACAGCAGTCCTCATATTCCGTTCAAG
CCATGCCAGGGGGCGGGGCATTTACGACGATATTCACACCAGGTTCTAACCT
GGGTGGGACACCTATACAGTTGGCACAGAACCTGTCAGGGCAGCACGGTGTG
CAGATGTTGGCTCAACTCCAAAGAGGTCAAACACAAACCACCACAAGCCAG
ACAAATGTTGGGACCACAGGTCAGCCTTCCACAGTACAAGTCCAGATTGGTA
CAGATGGACAAATGCACACCCAGGAATCTGTAGAGCATTCATCAACCTCACA
GGCGACTACTATGCAGTCTCTTGGAGCTCTTATGGTACCAATTGCCACTCATC
AGGGGGAAGGTCACGTTGTTTCACTGGCCAACGTGGTGCCATCATCTATGAT
GCTGACTACACAATCTGGCCAGATTCCAGTCATGTACTACACAGGACCTGTAT
CAAACATTAACGACAATGAACACCAAGGAACTCAACATGATAGTGGTGAGGT
GTCGCAGCAGGCCATACAGAGTGGCTTGTCACTGTCAACTGTTCATGTTCAGC
ACGACATGGCTCAAGGGTATCATAGTGTGGTTACTGAAGCTAGCGGTAGTCA
GGCGGCTGATGAGGTTCATAATATAGTGAGTGAGGCCTCCATAGGGTCCACT
AATGGAGGCTCCCCCATGAAGGGCGATGTTCCGGATGCGGATAATCACACTG
AAGTGTAA

>NvFoxL-like - fgenesh1_pg.scaffold_11000135
ATGTCTGCCACTACATTGGACACCGAGCTGCACAACCACGATACTGACGTAA
AGAAAGAAGATGGAAGTGCGAGTCCAACGGATTGTATCAAAGCCGAAGGCA
AGGATACTTCTAAAGACCCGAATGTCAAACCTCCGTACTCATATGTCGCGCTC
ATCGCGATGGCTATCCGAGAATCTCCCGAGAAGAGGTTGACCCTGAATGGAA
TCTACCAGTATATCATCAGCAAGTTTCCGTACTATGAGAAGAATAAAAAAGG

ATGGCAAAATTCAATCAGACACAACCTATCTTTGAATGAGTGCTTCATAAAA
GTGCCCCGCGAAGGTGGCGGCGAGAGAAAGGGTAACTACTGGACCCTAGAT
CCTGCATGCGAAGATATGTTTGAGAAGGGAAATTACAGGAGACGGCGACGC
ATGAAGAGGCCATTCCGTCAGCCAAACCTGCAACCCAACAACGGTCTGATCA
CCGGAGATCCACGTGCAATGACATACAACTACATCCAACCCAAGTACACGAC
ATACAACCAAGCGCAAAGCGTGGCTGCGGCGGGAAGATGGGGAGCTATGCC
GAGCGCAGGACCCCTGTCATACTCGTGCAATCCACCATCTCCACGCGTACCTC
CTGTATACCCGTACATGAACATGGGCTCTGCAGTGCCTGTCAGTACCTACACG
GGTACGCAATACTCCACACAAATACAGAACCCCGTCAATAACCAGTGCGGGT
ACGGGGCAGTAGCGATGTCAAACGTAGCGTGCAGGAGTCGACCGGCTGAAC
ATAGTCCAATGCACCATTACCCTTATTGGAGTCAAGACAAACATGTGTACGA
TGTACCTCCAAGGTCGTAG

>NvMRTF - estExt_fgenesh1_pg.C_4510003
ATGTATCCGCTGCCTTGCCCTGAGCGAAAGCGAAACAGTCATGAAATTTGCC
CAGATTTGAACACGGAGATTATTACCGAAATCGGAGAACCTCGGAAACGGTT
GCTTTTTGTAATTTTAGCGGCAATGACAGCCCCCGGTTTGCTGTCTCAAAAGT
CTAAACTCGAGCGGGCAAAGACTGGAGATCTACTACAAAAAAAGATTCGAGT
TCGTCCAAATAGAGCACAGCTTGTACAAAGACACATTCTTGATGACACCTCT
GTTGGTGTTGACCCCTCACTGATTGCAAAGCAGATCCAGCTGAAAAGGAAAA
AGTTGGAGGATGATTTGAATGACAAGCTCCTTGCAAGACCAGGTCCTTTGGA
GTTAGTGAAAGAGAACATTTTAGAGGCTGGAACTGCAGTAGGGCAAGCTGTC
AAGGAGGGAGAAGTTGATTTTACGGATACAACCAAATCTGCCCTCTTACAGC
CAATTTCCCCTGACTCTGAAAGCTCTCCTATTCCATCGCCTGATACCATTCCG
CAAGCTCCCGTTGCTGCTGCAAAAACAGTGTATGAACCATGCATGGGTCAGA
ACTCAGTTTTACAAGCTGTTTCGCAATTGCAAAAGTTGTCAGAAGGAACAAC
CATTCCTACTGTGTCAGAGGCTCAAGGTGTTAAGAAGGAAAGGAGAAAGAA
GGCGGCAAAACCGAAATTTAAAAAGTATAAATATCATGAATATAGGCCTCCC
AATGGGGAGGTTGAGAAGAGCAGTTTGCCGATGGACTCGCCCTATGCACTTA
TGTTACAACAGCAGCAGCTATATTTACAGCTACAGGTGTTATATCAGAACTAT
CCTTGTCAGTTTGTTGGGTTACCCTCTATTCCAGAGAATTCTACTAAGAACAC
TACCTCTAATAATAATAATAATGAGGAAAAACCAGTAAAGATTGAAGATATG
CGGGTTGTTGATATGCGTAAGGAACTAAAACTACGTGGACTTCCAGTGTCTG
GTTCAAAGACTGACTTGATTGAGAGGCTAAAGGCTTCTAGTGAAGAATCTGC
AGTGTCGTCCCAAATACTTGTATCTTCTAGTAGTCCTAGCATTATGGCAACTT
CTGGTTCAGTGAGTTACTCAGATGCACCTATTAACGTCTCTTCTGCAATGACA
AGTCACGGTCAGCTTTCAAGGTCAAACTCATTACCACTAGAAAACCCACACG
TACAACAACTCCAGATGCAACTGATAGCTAATAACCAAAAGTTGAATCAGCA
ATACTCTACCATGCCAGAGGAGCTGCAAAAGCAGTTGCAACAACTACAGTAC
CTTAACCTCCAGATGCAGCTACAACGGCTGAACGTTCAGCAGCCACAAGTGA
CCTCTGTCCAGACCACTTCCCCCATGCAGCAACCAGTCATGCTGAGCACCCA
ACAGATGCCGTCACCCAACACAAGCATCAAACAAGAGCCAGAGTCACCCGA
CACCTGTATATTCTCACAGCAGCCACCGCCACAGCCTGCCATAAAGAAGGTG
GCATCGTCACCTCAGTTCTCTTACAACCAGACGCCTCTCTTTGAACAATCGCA
AAGTTATGAAGAGATGAATTTCCACTCACCAGAAAGTCCAGCTTCAGGGCTT

GTTCTTCTTCAAGCTGAGGCAAATAGACTTAATCATAGTCCAAGCCACAGTG
AGCAGGATTTGCGGCAAATTGAGAGCACTGATTTTAGCATGGGTTGGAGCCC
TAAGTCACATCAGTCACAGGATGTGCCTTCTCCAAATAGCACCTTTATGGTCA
CTACACAGGCTGATGCACAGGCAAGGTTGCTGGATGGTGCAGGTTTTATGCA
TGCCAAGCCTAAGATGGAGTCTATGCAGAGATCGTATTCAAACTCAGAAAGG
AGTCAAGTGGAGGATGGCAAAACCGCATTGTCAGGAATAACAATGGAGGCG
AAACCAAGATCTAATTCCGAGCCACCGCAACCATTCAGCCATAAACGATCAT
CATCACTGCCATCTGGGGTGTTTTTTGTTGATCATATTCAGCCACCTCCGAGC
TACGAGGCGCATATGGCGGGCTTGATGCAGCGTAAAGTTGGACCAGAGTATT
CATCACTGCAGCAACAGCATCTACAACAACAGCTGCAGCAACAACAACTTCA
GCAACAACAGCAATTACATCACCAACAACAGCAACAGCAGCAACTTGCAAA
GAGTGATGACACTGATATGGACACATATCAAGAGCAGGAAATCACTCAGGA
GCTACAAAGGGCAATGATGAAACAGCAGGTTGGACTAGATCATGATGAAATT
CTAGAGATACTTGGTGCTTCCATAAGCCCAACATCAGAAGCAAAGGTGCAAA
CCTCCCTCGGAAACCAAGTCACAACCAGCACAGCAATTGCCAATCAAATGTC
GCCACACAATCCTATGACGAACCACCATCACCTGCCCAACTTACAGATCCCC
AAATCCCCTAGCACTGGATTCCTGGGGACCCACATTTTGCAGAATCAACCAA
TTCAAGGACGGCTCTCTAAAAGCTGTGAGGATGTAGCTGGGGTCAACCTAAA
TTCCAATAAGAACAGTATGCAGATATGCAATGATGGAAGTTTCCCGGACTTT
GAAGCCATGATTATGAGTCCAAGCTCGCCGATGAAAATAGACAATGATAATG
ATTACCAGGGTATTATGATGCACCCTACAAATAGCATCCCAATTCCTGGGTCT
AAAAATGATAGCCTTAGCTGGCTGGACTTGAACAATTCTCCTATCATCACTAG
TACATCTCCAGGATCTCATACGGATGTGAACTATGCCACAAGGGGTACACCG
CCCGCGTCCTTGTATGACACATCGCCCAATCTCTCAAGCGAACATTTTCCTAT
GTCCTTGTTTGAGTTGGATGGGGGATCTGGGCATCTGCCACATGATTTCCCAG
AGGCCATGGATTTCTGTGTATAATGACAAGGTGGTCCTTTTTGTTATCAAAAA
GTTGTGGTAAATCTTAGGAAGTATAGCTTTATTTGTGTAGTGTATTTTCTGGTT
TCTTTTTCGTTTTTCAAATGTATTTAGCGGCTCATGCACCCAAATGAGTATGA
GTAGGGAAAAATTAAGGTTAACAGTGTCATGCATTTGATAGGTTTTTTTCTCT
GGGGTTATTCAAGTCTAAATTTTCGATGTTTATTGTTTGTTTTTAGGGTGTTTG
GTGAATTGCAGTTACTTAAACAATTTTGTCCTGTTTATCCTAAAGTTTTATTTT
TTACTATTGCACTGTTTCAACAACTCTAATGTCAGCAAGTTTATGACCTGAAT
CACTTTCCATTTTTATTTTGGTAGTCATTAAGGTGTCTTTGATGTTATATTATT
TTGGTCCCTTTTACAGGCACAGGTGAGAAATCGCAGACAACATCTGTACTCTA
AGCAGAAGCAAGCACCTATTGTTATAACTAGGCCACCAACCACCATTCTAAT
TAATTTGGTTTAAATTGTGTAAAAAAATTAGAACTGTGTTTTTGTGCTTCAAT
AACACAGGTGGTTT

>NvDach - fgenesh1_pg.scaffold_85000031
ATGGAGTCGCCTACTGCAGTGTACTCGCCTCCTCCTCACCATCCACAAACTCC
ACAAACTTCTGACTACAGCTTCATCGAGCACGACACACCTTCGTTACCCCTCG
GAAAAGAGTACAAGCTAAAGACAGTCACCGTGAATGGCATTGATATTGCCGC
GTTTAACGTCGATGGCGAAGACTTGTTGTGTTTCCCGCAAGTCTATGAATACT
TTCTCAAAGATCTGGTATCTGGAATGCACACAGTGTACACGAAACTCAAGCG
CATGAATATCCAGGGAAGGAATTGTAACGTTGAGCAAGTAAGAATGATGCGA

AGTGTTGGAGCAATCGGACAAGTGGTGAATCGATGCAAGCTCATCTCCAAAG
AAGACTTTAATAAAATCTACGAAGACTGCATTCTCTATAGGTATGCAAACAT
CACTATCTCGTACTCACCAAAACCCCACGAATTCATCCAATATCCTTAA

>NvHAND1 - fgenesh1_pg.scaffold_80000047
GAACTGACTTGATCAGCGCTGCTGAATCGCGCTGAACGGTGGCGCAACTGAA
CGGATAGCGTGTTCAAGCTCGAGAGAAAACACAAGAGAGTGCTAGTCTGGG
ATAGAGTTTAAGCCCGCTATCAAGATTTTGACAGGCCCTTGTAAGAATTCTTC
ATTATGTCAGATCATGAGAAGAGCCCATGCAAAAGCGAACCATCCGAACCCG
AAATCACAGAAGTCACTGTGATATCCAGCGAAGATGAGCCTTCCGCGGGGAA
TAAGCGCAAAGCTCGGCCGATCAAAACAACGACGAGTAAGAAAGAGAGGCG
ACGCACAGAAAACATCAACGCAGCCTTTGCGGAGTTGCGCAAACACATCCCT
AACGTACCATCGGACACCAAGTTGTCCAAGATTAAAACACTCAAGTTAGCAA
TGAGCTACATACATCATCTTGAGCTGCAGCTCTCCGGTGAGGAGAGTAGAGT
GGTTATTGTGAAACATGTAACACCGAGCGAACCTCAACCGGTGATCCGCACA
AGAGAGCGAGAACCGAGTATAGAGTACGATCTTCCATCGAGTCCTGAAAGAG
CTTACGAGGAGGTGGATGAGCCGCGCTCTGGTCGCAGGAGTAGTAGGACCGG
ATGGCCTCAGCATGTATGGGCGCTGGAGTTAGTCCACGGGAATAAAAAACAA
AGTAAAACCACGATGGCTAGACACCAAATCGTCACCTGAACTCCCGGAAAGC
CTATAACTTTGGCGTCAAATTGGGAAGAAGGCAAAGAGCCATTTTATTCCGA
GAAGAACTCTTTCTACGACAAACCAAGGGAAACTCCTTGGAACGGCGTGATA
GTGCAAGCATGCCTGCA

>NvHAND2 - estExt_GenewiseH_1.C_800124
TGAAGACCAAGGGCAAACTTCCGAGCTAGATTCCCCAGAGCTGCCTGATACG
CCGAAAAAACGCTACACTGCAAACCGCAAAGAGAGAAAACGCACTCAAACT
ATGAACACTGCCTTTGAGGATCTTAGAAACCATATTCCCAATGTTCCACCGGA
CACGAAGCTATCTAAAATCAAAACGCTTCGACTAGCGATTAGCTACATTCGA
TACCTAATGGACATCTTGGAAGAGAGCAAAGATGGTAAACCAAGAGTGCGTA
GGAACTTTGTTGTAGAGATGGCTTTGCAGAGCGATATGAAAGAGAAAAGAAA
GCGGGAGCAATCGAGTGTGGAGCTAGCGCCGCGTAAGCGAGGAAGGACGGG
GTGGCCCCAACAGGTCTGGGCGATGGAGCTGCGGCAGTGATAGCCACATTCC
AACCGGTTTAGCCTGTGTTCAAAGTGGTCAGTGGGAATTGAACGCCAAGTGT
AACTGCTACCTGGTTGCACCACAGTTCGTACCATCAAGAGAGACCAGAGAGA
TATGAACACTGGTTTCCAATACATCGGTGGATCACCTAGAGAGAGAGGATTG
TCATGTGTACCCAAAGTACCACCACCAATGGTAAAACGACCACCTCAAACAA
CTTAGCTGATGGTTGCAAGGGAAATGCAACTAGTATATGGGTGACTAATTGG
ATATTCTTTCCTGGTATTGTTCAAGAAACCTTCAGTTTCTAGAGTTTGTCCTCG
TGCAAGGAAGGGTTGACATTGTTACAAACCACCAAAGTCAGTAAAGCAGTCT
GAAATCTACCATCCAATTATACTTGATATTGTTTAACAGTGGGAATAGTTTGG
ATGATTTGGTCGATGGTGTATATGTATGGCGTGTAAATAATCTCAGAAATAG
AAATGGAAGAGGAGTTTTATTTCTTGGAAGAAAATGGATATGGAAATATCGT
TAAACATGCAGCATTCACAGCTCAAGCTTGCGTAGACCAATAAAGAGAAAGA
AGAGTCTATATAAATACCTCCTAATTATTAGCTGAAAAAGTAATTCCAGCACT
ACACCGTGGTAACAATTTGAACTTTGAAAAAAAATGTTTTTAAAATTAATCA

ATGTCAAGCTCATATGCTTGCAAATTACAGTGTGATTTGGTACCAGAAAGGTC
CTCGTGCCGAGCAGAGATGTACCAAAGCCATACAAGCTATATACGTCAGATA
TACCATGGGCCGTGAGTATGGGGAAACTGAGGGTGTTAGGCTCCCCGCGCAT
GGCAAACTTTTAAATACATTTTTATTATTCAGCCCCCTTACCCCTGGATAGGA
GATGAGGAGATATAAGAAGGGAGGAGAAGGAGTAGGAAATAAAAAACAGA
TTTATAAAGAGGAAAGATAGATGAGATATTTAATTAAGG

>NvHAND3 - fgenesh1_pg.scaffold_14000163
ATGCCGCGTTCATTTCTCGTCAAACGAGGGAAAAACGAGGAGGAGATAGTTC
CAGACGGACAGCAGAATGACGTTAAAGTGAAGACAGAAGTTCTTATAGAAG
ATGCCGAGAGACACGCAGCACCAACAGCCAAGAATTGGTATATCAAGTATCA
CCCAGCCGTATCTCACCTCATCCCAGCCAAGCGCTGCGACATTCTGCAACAC
GCCAATGGGGGGTCTTGTTACCTCTGCAGCTGCCCCTACAGACCCCTTCCACA
CACCACGCCCAGCGAGGGGTGTATTAAATATGCACCAGGGGTGCCAATGGCA
GTTCATGTTCAGGACACTAATGGTAATGTTTGCTATTGCAGCATGTGTCAACA
CAAGGTTGCACAACAAGTTGCTTGCAATTGTCCTAGTTGCTTGCAACTCAGAC
ATTCCATGGTGACCCGGAATATACTATTGGAACAACATCAGGTTGCTAAAGC
ACCAATGTGTTGCAGTGTAGTGCACTGCAATCAGGCAATCGAGTTGCAACCA
ACATACCATCCCCTCTGTCACTGCGAGCAATGTGCTCAGAGGCAGAACATTA
TAACAAAGGAGACAGGAGCTCATGTCTATCATGTTCATAATAGAACTCATGT
ACATATTTCATCAGAGAGTTTTAGTCGAACAGAGGAGGGAAAACCTGATAAT
AAACTCAATGGGGAGGTGGACAGAAATGCGAATATAACTAACGCTACATTTG
GTAATTCGGTTAAAGATCATGACACAGCTAAAGAAAGACTGAAAAGAAGAG
TAATGCAGGATAATTCTGGGGAAAAACGGTTCAAACAGGATAACATAAATAA
TGTTAATATGGAAGAAGAGCTGGACTCAAAACCAGAGAGGGTCGCTACAAA
GGATAGTACAAATGAAAATGAGAAAGATGCATCTCTAAAAATAGAAGGAGT
TCTTGTGCAGGATGAACATGAAAGTGTTGCAGATGATGAAGAAATCGATGTT
TGTGAGGAAATTAAAACAAGTCCTGCTGGAAAAAGTGTAGAAACAAGTTTCG
AAAATAAATCTTGTCGTTCTGAGGCTAGTTCTCCTCTAAGCACAGAAACTGAA
AAATCTGTGATTAAAGCAAGGAGGGGGAGGGGAGGAAGAGGACGTAGATAC
AATACAAGGCATGTCAACTCAAAAACTAAATCCTACGACTCAGACTTTGTAA
ACCCTACAGACAGCGAATGGAAACAGGAAAAAGATGTATGTGGTGAGGTGT
CGAAAAATCGCCAGAAAACTAAACTCAACAGGCTTCTTGCTAATGAGCACGA
GCGGCGCAGAGTGGCTCAGTTGAACGGTGCTTACCAAGACTTGAGGCAACTA
ATTCCAGGCTATCAATGTGATACTAAACTTCCAAAAATCAAAATCCTTAGATA
TGCTATCAACTACATAGCACACTTAGATAATATATTGTCTG

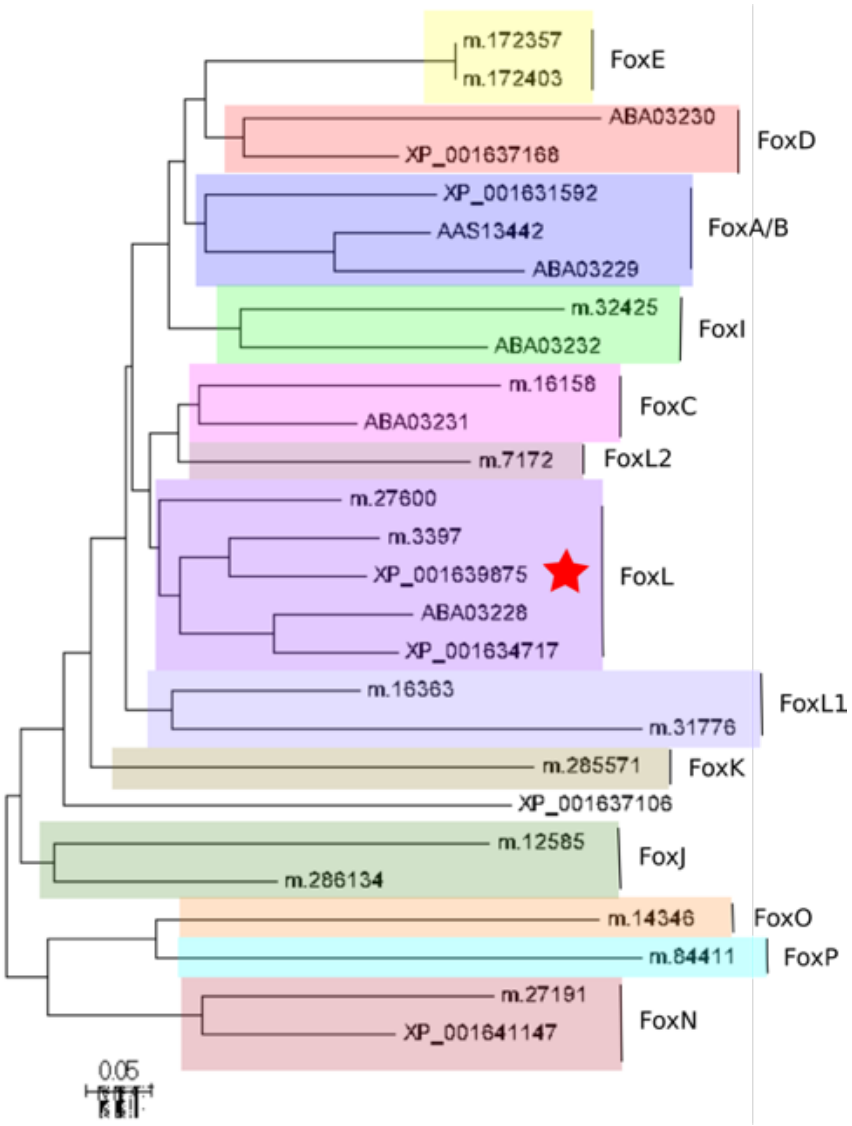

Neighbor joining tree of *N. vectensis* and *E. muelleri* Forkhead proteins. Subfamily names based on reciprocal BLAST searching and alignment with annotated orthologs from other animals. Red star is protein named NvFoxL-like in this document.